Development of novel Reynolds-averaged Navier–Stokes turbulence models based on Lie symmetry constraints

Zur Erlangung des akademischen Grades Doktor-Ingenieur (Dr.-Ing.)
Genehmigte Dissertation von Dario Klingenberg aus Bergisch-Gladbach
Tag der Einreichung: 18.05.22, Tag der Prüfung: 24.08.22

1. Gutachten: Prof. Dr.-Ing. M. Oberlack
2. Gutachten: Prof. Dr. rer. nat. A. Sadiki
Darmstadt, Technische Universität Darmstadt

TECHNISCHE UNIVERSITÄT DARMSTADT

Fachbereich Maschinenbau
Fachgebiet für Strömungsdynamik

Development of novel Reynolds-averaged Navier–Stokes turbulence models based on Lie symmetry constraints

Genehmigte Dissertation von Dario Klingenberg

Tag der Einreichung: 18.05.22
Tag der Prüfung: 24.08.22

Darmstadt, Technische Universität Darmstadt

for Helen

Erklärungen laut Promotionsordnung

§ 8 Abs. 1 lit. c PromO

Ich versichere hiermit, dass die elektronische Version meiner Dissertation mit der schriftlichen Version übereinstimmt.

§ 8 Abs. 1 lit. d PromO

Ich versichere hiermit, dass zu einem vorherigen Zeitpunkt noch keine Promotion versucht wurde. In diesem Fall sind nähere Angaben über Zeitpunkt, Hochschule, Dissertationsthema und Ergebnis dieses Versuchs mitzuteilen.

§ 9 Abs. 1 PromO

Ich versichere hiermit, dass die vorliegende Dissertation selbstständig und nur unter Verwendung der angegebenen Quellen verfasst wurde.

§ 9 Abs. 2 PromO

Die Arbeit hat bisher noch nicht zu Prüfungszwecken gedient.

Darmstadt, 18.05.22

D. Klingenberg

Abstract

In the present work, the problem of RANS (Reynolds-Averaged Navier–Stokes) turbulence modeling is investigated from a novel angle by considering recently discovered constraints arising from Lie symmetry analysis. In this context, symmetries are defined as variable transformations that leave invariant a given equation. For equations describing physical phenomena, it is usually observed that their symmetries correspond to physical principles encoded in the equations. The key idea behind using symmetry methods for modeling tasks is that the physical principles encoded in an exact equation should also be present in a model for these equations. Lie symmetry theory establishes a mathematical framework to formalize this notion.

The symmetries that govern turbulence fall into two main categories: Classical symmetries, which are present in the Navier–Stokes equations as well as in all statistical descriptions of turbulence, and statistical symmetries, which are found exclusively in statistical descriptions of turbulence and have no counterpart in the unaveraged Navier–Stokes equations. Even though the explicit use of symmetry methods in turbulence modeling is not yet prevalent, many well-established constraints imposed on turbulence models to prevent physically unreasonable behavior actually stem from symmetry arguments. This has led to a situation where the constraints implied by classical symmetries, which correspond to fundamental principles found throughout classical mechanics, have generally been taken into account when constructing turbulence models since the 1970s. Roughly speaking, two-equation eddy viscosity models are the simplest class of models to fulfill all of them. Statistical symmetries, on the other hand, are connected to special properties of turbulent statistics, and are, therefore, not as intuitive as the classical symmetries. As a result, they have so far been overlooked in turbulence modeling.

The main goal of the present work is to devise a turbulence model while taking these statistical symmetries into account. This task turns out to be challenging because the combined set of classical and statistical symmetries imposes considerable restrictions on the possible form of the model equations. To overcome this challenge, a formal modeling algorithm is adapted and applied to turbulence modeling. Its results hint at the necessity for auxiliary velocity-like and pressure-like variables. With these model variables, possible model skeletons, both for an eddy-viscosity type model and for a Reynolds stress model, are developed. Subsequently, these simple base models are evolved into full turbulence models by applying them to canonical flows. Due to the complexity of the resulting Reynolds stress model, the emphasis is placed on developing a modified version of the k-ε-model that fulfills the statistical symmetries. This new model is calibrated against a wide range of canonical flows, where it performs at least equally well or better than the standard k-ε-model.

Furthermore, the implementation of the standard k-ω-model in the in-house DG (Discontinuous Galerkin) solver BoSSS (Bounded Support Spectral Solver) is presented. Additionally, a special-purpose solver is developed that allows efficient numerical calculations with the modified k-ε-model for simple flows. The obtained results match well with experimental data.

Zusammenfassung

In der vorliegenden Arbeit wird das Problem der Turbulenzmodellierung basierend auf den reynoldsgemittelten Navier-Stokes-Gleichungen aus einem neuen Blickwinkel untersucht, indem kürzlich entdeckte Bedingungen, die aus einer Lie-Symmetrie-Analyse hervorgehen, in Betracht gezogen werden. In diesem Zusammenhang sind Symmetrien definiert als Variablentransformationen, die eine gegebene Gleichung invariant lassen. Bei Gleichungen, die physikalische Phänomene beschreiben, stellt man oftmals fest, dass ihre Symmetrien in die Gleichungen eingebettete physikalische Prinzipien abbilden. Die zentrale Idee hinter der Verwendung von Symmetriemethoden bei Modellierungsaufgaben besteht darin, dass die physikalischen Prinzipien, die in die exakte Gleichung eingebettet sind, auch in einem Modell für diese Gleichungen vorhanden sein sollten. Die Theorie der Lie-Symmetrien bildet den notwendigen mathematischen Rahmen, um diese Idee zu formalisieren.

Die Symmetrien, die für die Turbulenz bedeutsam sind, fallen in zwei Hauptkategorien: Klassische Symmetrien, die sowohl in den Navier-Stokes-Gleichungen als auch in allen statistischen Beschreibungen von Turbulenz vorhanden sind, und statistische Symmetrien, die ausschließlich in statistischen Beschreibungen von Turbulenz zu finden sind und keine Entsprechung in den ungemittelten Navier-Stokes-Gleichungen haben. Obwohl die ausdrückliche Verwendung von Symmetriemethoden in der Turbulenzmodellierung noch keine vorherrschende Rolle einnimmt, basieren viele in ihrer Anwendung auf Turbulenzmodelle etablierte Bedingungen, die unphysikalisches Modellverhalten verhindern sollen, auf Symmetrieargumenten. Dies dazu geführt, dass die Bedingungen, die aus den klassischen Symmetrien hervorgehen und Grundprinzipien der klassischen Mechanik abbilden, etwa seit den 1970er-Jahren bei der Turbulenzmodellentwicklung in Betracht gezogen werden. Grob gesagt sind Zweigleichungs-Wirbelviskositätsmodelle die einfachste Modellklasse, die alle klassischen Symmetrien erfüllt. Andererseits stehen die statistischen Symmetrien in Verbindung mit speziellen statistischen Eigenschaften der Turbulenz, was sie weniger intuitiv macht als die klassischen Symmetrien. Aus diesem Grund wurden sie bisher in der Turbulenzmodellierung übersehen.

Das Hauptziel der vorliegenden Arbeit ist es, ein Turbulenzmodell unter Betrachtung der statistischen Symmetrien zu entwickeln. Diese Aufgabe erweist sich als Herausforderung, da aus der Kombination von klassischen und statistischen Symmetrien starke Einschränkungen an mögliche Modellgleichungen hervorgehen. Um diese Herausforderung zu überwinden, wird ein formaler Modellierungsalgorithmus an das Problem der Turbulenzmodellierung angepasst und darauf angewendet. Die Ergebnisse weisen auf die Notwendigkeit von geschwindigkeitsartigen und druckartigen Hilfsvariablen hin. Mit diesen Modellvariablen werden mögliche Modellskelette sowohl für ein Wirbelviskositätsmodell als auch für ein Reynoldsspannungsmodell entwickelt. Anschließend werden diese einfachen Grundmodelle zu vollwertigen Turbulenzmodellen weiterentwickelt, indem sie auf kanonische Strömungen angewendet werden. Aufgrund der hohen

Komplexität des entstehenden Reynoldsspannungsmodells wird der Fokus auf die Entwicklung einer modifizierten Version des k-ε-Modells gelegt, das so angepasst wird, dass es die statistischen Symmetrien erfüllt. Dieses neue Modell wird anhand einer Reihe kanonischer Strömungen kalibriert, wobei es stets entweder gleich gut oder besser abschneidet als das Standard-k-ε-Modell.

Außerdem wird die Implementierung des Standard-k-ω-Modells im institutseigenen DG (Diskontinuierliche Galerkin) Löser BoSSS (Bounded Support Spectral Solver) präsentiert. Zudem wird ein Speziallöser entwickelt, der effiziente numerische Berechnungen mit dem neuen Modell für einfache Strömungen erlaubt. Die damit berechneten Ergebnisse stimmen gut mit experimentellen Daten überein.

Acknowledgements

This thesis is the result of my work at the Chair of Fluid Dynamics during the last four and a half years. Here, I would like to use the opportunity to express my gratitude to everyone who has contributed to and made possible the completion of this work.

First and foremost, I would like to thank Prof. Martin Oberlack for the supervision and the many interesting and productive discussions without which this work would not have been possible.

I would also like to thank Prof. Amsini Sadiki for agreeing to co-referee this thesis.

Furthermore, I am grateful to Dr. Florian Kummer for his help with numerical questions in general and the BoSSS code in particular, and to Prof. Wang, who assisted with the teaching aspects of my work at the Chair of Fluid Dynamics, in particular with the tasks associated with my role as the lecture assistant to the statics (TM1) lecture. I will also keenly remember the support in all administrative questions provided by Ruth Völker.

As already mentioned above, I am very happy to have had the opportunity to take part in the statics lecture as an exercise lecturer, which was not only a marvelous experience in itself, but also entailed interesting work with Markus Geisenhofer, Lauritz Beck, Matthias Rieckmann, and our student assistants Pascal Cabos, Patrick Steinberg, Paul Hollmann, Elisabeth Decker as well as the student tutors. I really enjoyed working with all of you!

A special thanks also goes out to all colleagues at the Chair of Fluid Dynamics, who I have tremendously enjoyed working with, even though the pandemic somewhat limited personal interactions in the later part of my work. In particular, I would like to mention my office mates Yi Zhang, Julian Heß, Maurits Silvis, Juan Gutiérrez, Felician Putz, Luca Sarno and Judith Kahle. Furthermore, Tim Gebler, Alparslan Yalçın and Dominik Plümacher, with whom I had many fruitful discussions in the break room and after work, and Benjamin Deußen, with whom I organized many informal get-togethers of the group, should also be mentioned explicitly.

I was lucky to co-supervise three student's theses, by Jonathan Laux, Jan Schäfer and Nils Benedikt, whose works' high quality and usefulness for my research should be apparent from the fact that all of them are cited in this thesis.

The quality of this work has been greatly improved by the excellent feedback from Nils Benedikt, Benjamin Deußen, Tim Gebler, Markus Geisenhofer, Simon Görtz, Helen Grohme, Florian Kummer, Felician Putz, Matthias Rieckmann, Martin Smuda, Alparslan Yalçın and Yi Zhang, for which I am very grateful.

I would also like to thank the Graduate School of Excellence Computational Engineering for providing me with a scholarship for the first three years of my time working on this thesis, and the interdisciplinary contacts resulting from my membership and my work in the students' committee. I would like to mention the staff made up by Markus Lazanowski, Melanie Gattermayer, Christian Schmitt and Carina Schuster for their support in all GSC-related questions, and my colleagues in the students' committee, Mona Fuhrländer, Idoia Cortes Garcia and Christine Herter.

Finally, it goes without saying that this work would not have been possible without the support from my friends and family.

The work of Dario Klingenberg was supported by the Excellence Initiative of the German Federal and State Governments and the Graduate School of Excellence Computational Engineering at Technical University Darmstadt and by the Deutsche Forschungsgemeinschaft (DFG, German Research Foundation) - Project number OB 96/54-1.

Contents

List of Figures

List of Tables

List of symbols

$\overline{(\cdot)}$	mean quantity
$(\cdot)^*$	transformed variable
a	symmetry group parameter
α	model constant (standard and modified k-ω-model, ω-equation production term, standard value $5/9$)
α^*	model constant (standard and modified k-ω-model, k-equation production term, standard value 1)
α^{**}	model constant (modified k-ω-model, ω-equation production term)
β	model constant (standard and modified k-ω-model, ω-equation dissipation term, standard value $3/40$)
β^*	model constant (standard and modified k-ω-model, k-equation dissipation term, standard value 0.09)
β^{**}	model constant (modified k-ω-model, $\hat{\omega}$-equation dissipation term)
C_{b1}	model constant (Spalart–Allmaras model, standard value 0.1355)
C_{b2}	model constant (Spalart–Allmaras model, standard value 0.622)
$C_{\varepsilon,1}$	model constant (standard and modified k-ε-model, ε-equation production term, standard value 1.44)
$C_{\varepsilon,2}$	model constant (standard and modified k-ε-model, ε-equation dissipation term, standard value 1.92)
$\hat{C}_{\varepsilon,1}$	model constant (modified k-ε-model, $\hat{\varepsilon}$-equation production term, standard value 1.42)
$\hat{C}_{\varepsilon,2}$	model constant (modified k-ε-model, $\hat{\varepsilon}$-equation dissipation term, standard value 1.92)
C_μ	model constant (standard and modified k-ε-model, Boussinesq approximation, standard value 0.09)
C_ω	model constant (standard and modified k-ω-model, Boussinesq approximation, standard value 1)
c	constant of integration
C_R	Rotta constant
$\hat{c}_R$	model constant (modified Reynolds stress model, $\hat{R}_{ij}$-equation diffusion term)
c_ε	model constant (modified Reynolds stress model, ε-equation diffusion term)

$\hat{c}_\varepsilon$	model constant (modified Reynolds stress model, $\hat{\varepsilon}$-equation diffusion term)
C_{w1}	model constant (Spalart–Allmaras model, standard value $C_{b1}/\kappa^2 + (1 + C_{b2})/\sigma$)
δ_{ij}	Kronecker delta
Δt	time step size
dy/dx	total derivative of y with respect to x
$\mathcal{D}y/\mathcal{D}x$	total derivative of y with respect to x (in the context of jet notation)
Dy/Dx	material derivative of y with respect to x
$\hat{D}y/\hat{D}x$	material derivative of y with respect to x using auxiliary velocity field $\hat{U}_i$
$\partial y/\partial x$	partial derivative of y with respect to x
$y_{,x}$	partial derivative of y with respect to x (jet notation)
D_{ijk}	diffusion terms appearing in the Reynolds-stress equation
d	distance from the wall (used in the Spalart–Allmaras model)
ϵ_{ijk}	Levi-Civita permutation symbol
ε	turbulent dissipation rate
$\hat{\varepsilon}$	auxiliary turbulent dissipation rate
η	similarity variable
η_i	infinitesimal (dependent variable)
$\tilde{\varepsilon}$	similarity variable (turbulent dissipation)
$\tilde{\hat{\varepsilon}}$	similarity variable (auxiliary turbulent dissipation)
f_{t1}	function appearing in the Spalart–Allmaras model
f_{t2}	function appearing in the Spalart–Allmaras model
f_{v1}	function appearing in the Spalart–Allmaras model
f_w	function appearing in the Spalart–Allmaras model
γ	model constant (modified k-ε-model, $\hat{\varepsilon}$-equation production term, standard value 0.05)
γ^*	model constant (modified k-ω-model, $\hat{\omega}$-equation production term)
Γ	domain boundary
h	grid cell size
H	velocity moment based on instantaneous values
I	turbulent intensity
ι	model constant (modified k-ε-model, auxiliary momentum equation diffusion term, standard value 2)
κ	von Kármán constant
$\tilde{k}$	similarity variable (turbulent kinetic energy)
k	turbulent kinetic energy
L_m	mixing length
m	polynomial degree
$\mathcal{N}_i$	ith component of the Navier–Stokes momentum equation

$\mathcal{N}_i'$	ith component of the fluctuation Navier–Stokes momentum equation
Ω	domain size
ω	specific turbulent dissipation rate
$\hat{\omega}$	auxiliary specific turbulent dissipation rate
$\tilde{\omega}$	transformed specific turbulent dissipation rate
O	Landau symbol
$\bar{P}$	mean pressure (divided by density)
P	pressure (divided by density)
$\hat{P}$	auxiliary pressure-like field
p	fluctuation pressure (divided by density)
Π	pressure-strain correlation
ϕ	trial function
$\boldsymbol{Q}^{[\alpha]}$	rotation matrix along x_α-axis
$\mathbb{R}$	the set of all real numbers
r	residual
R	velocity moment based on fluctuation values. In particular, R_{ij} is also known as the Reynolds stress tensor
$\hat{R}_{ij}$	Auxiliary Reynolds stress tensor-like field.
σ^{**}	model constant (modified k-ω-model, $\hat{\omega}$-equation diffusion term)
σ	model constant (standard and modified k-ω-model, ω-equation diffusion term, standard value 0.5)
$\hat{\sigma}_\varepsilon$	model constant (modified k-ε-model, $\hat{\varepsilon}$-equation diffusion term, standard value 1.25)
σ_ε	model constant (standard and modified k-ε-model, ε-equation diffusion term, standard value 1.3)
σ^*	model constant (standard and modified k-ω-model, k-equation diffusion term, standard value 0.5)
σ_k	model constant (standard and modified k-ε-model, k-equation diffusion term, standard value 1, modified value 0.91)
$\tilde{\sigma}$	model constant (Spalart–Allmaras model, standard value $2/3$)
S_{ij}	ij-component of the symmetric part of the velocity gradient
S	source term
$\tilde{S}$	scalar norm of the velocity gradient used in the production term in the Spalart–Allmaras model
t	temporal coordinate
T	global symmetry transformation
$\bar{U}$	mean velocity
U	velocity
$\hat{U}$	auxiliary velocity-like field
u	fluctuation velocity
u_τ	wall friction velocity
$\tilde{u}$	similarity variable (mean streamwise velocity)

$\tilde{\hat{u}}$	similarity variable (mean streamwise auxiliary velocity)
ν	kinematic viscosity
$\tilde{\nu}$	auxiliary turbulent viscosity-like variable (Spalart–Allmaras model)
ν_t	turbulent viscosity (eddy viscosity)
v	test function
$\tilde{v}$	similarity variable (mean cross-stream velocity)
$\tilde{\hat{v}}$	similarity variable (mean cross-stream auxiliary velocity)
$\tilde{V}$	similarity variable (mean cross-stream velocity-like function)
$\tilde{\hat{V}}$	similarity variable (mean cross-stream auxiliary velocity-like function)
W_{ij}	ij-component of the antisymmetric part of the velocity gradient
X	infinitesimal generator
$X^{(n)}$	nth prolonged infinitesimal generator
x	spatial coordinate
ξ_i	infinitesimal
ξ	transformed similarity variable
z	dependent coordinate

List of Abbreviations

AMR adaptive mesh refinement

BDF backward differentiation formula

BLAS basic linear algebra subprograms

BoSSS Bounded Support Spectral Solver

BVP boundary value problem

CAS computer algebra system

CFD computational fluid dynamics

DAE differential-algebraic equation

DG Diskontinuierliche Galerkin

DG Discontinuous Galerkin

DNS direct numerical simulation

EARSM explicit algebraic Reynolds stress model

EOC experimental order of convergence

EVM Eddy-viscosity model

FDS Finite Differencing Scheme

FEM Finite Element Method

FVM Finite Volume Method

IVP initial value problem

LAPACK linear algebra package

LES large-eddy simulation

LMN Lundgren–Monin–Novikov

MPI message-passing interface

NLEVM nonlinear Eddy-viscosity model

ODE ordinary differential equation

PDE partial differential equation

PDF probability-density function

RANS Reynolds-Averaged Navier–Stokes

RDT rapid distortion theory

RSM Reynolds stress model

SIMPLE semi-implicit method for pressure-linked equation

SIP symmetric interior penalty

SST shear-stress transport

1. Introduction to Turbulence

From our everyday experience, we know that air, water and other fluids can flow in a very organized and calm manner under certain circumstances, but that this state, which is known as laminar flow, is fragile. Often, a small change, such as a slight increase in flow velocity or the presence of perturbations, can lead to the flow suddenly becoming irregular and chaotic. This phenomenon of turbulent flow is ubiquitous in natural and technical fluid systems. The presence of turbulence can alter the behavior of systems decisively and often leads to unwanted effects. For instance, turbulence affects atmospheric flows, and, thus, global and local weather phenomena, the flow around cars and airplanes, and it should be prevented in our cardiovascular systems, which constrains the design of heart implants (e.g. Moin and Kim, 1997; Pietrasanta et al., 2022).

Despite the high practical relevance arising from this, the chaotic nature of turbulence still prohibits a universally accurate and efficient treatment. One of the earliest systematic studies of turbulence was conducted by Reynolds (1883), who carried out a now famous experiment of water flow in a transparent pipe in the middle of which he injected dye. By visually observing whether the stream of dye remained concentrated in the center of the pipe or spread across the entire pipe cross-section, he was able to distinguish between laminar and turbulent flow, and to develop heuristics to determine when the flow transitions from laminar to turbulent state.

The best known quantitative model describing laminar and turbulent incompressible flow are the Navier–Stokes equations, which directly result from the axioms of mass and momentum conservation and read

$$\frac{\partial U_i}{\partial x_i} = 0, \tag{1.1}$$

$$\mathcal{N}_i = \frac{\partial U_i}{\partial t} + U_j \frac{\partial U_i}{\partial x_j} + \frac{\partial P}{\partial x_i} - \nu \frac{\partial^2 U_i}{\partial x_j \partial x_j} = 0, \tag{1.2}$$

where t and x_i stand for the temporal and spatial coordinates, respectively, U_i represents the velocity, P is the pressure divided by the density and ν denotes the kinematic viscosity. Here and in the following, the Einstein summation convention of repeated indices is implied. Equations (1.1) and (1.2) are notorious for their mathematical complexity, and except for some laminar flows with simple geometries, they cannot be solved analytically. Resorting to the numerical solution of Eqs. (1.1) and (1.2) is possible, but such DNS (direct numerical simulation) quickly becomes unfeasible due to the tendency of turbulence to generate small structures, resolving which often requires a prohibitively fine numerical resolution in time and space. Moin and Kim (1997) estimated that calculating a single second of aircraft flight would take several thousand years on the fastest computers of that time. Even though computational power has increased since then, DNS calculations of such technical applications can still require years or decades of runtime depending on the flow problem. Clearly, this is not feasible in industrial applications, but note that DNS is a valuable tool in turbulence research, where calculating canonical flows with simple geometries can yield important insights into the physics of turbulence.

In many applications, however, one is not interested in the stochastic fluctuations of velocity and pressure, but only in their mean values. Therefore, a natural idea is to solve for these mean quantities directly. An equation for the mean velocity and mean pressure can be obtained by averaging Eqs. (1.1) and (1.2), resulting in

$$\frac{\partial \bar{U}_i}{\partial x_i} = 0, \tag{1.3}$$

$$\overline{\mathcal{N}_i} = \frac{\partial \bar{U}_i}{\partial t} + \frac{\partial H_{ij}^{(0)}}{\partial x_j} + \frac{\partial \bar{P}}{\partial x_i} - \nu \frac{\partial^2 \bar{U}_i}{\partial x_j \partial x_j} = 0, \tag{1.4}$$

where the bar denotes averaging, and $H_{ij}^{(0)} = \overline{U_i U_j}$. The superscript (0) indicates that both velocities are evaluated at the same point in space, which is discussed further in Section 3.1. Reynolds (1895) suggested decomposing velocity and pressure into a mean and a fluctuation value, which we denote using lowercase letters, i.e.

$$U_i = \bar{U}_i + u_i, \quad P = \bar{P} + p, \tag{1.5}$$

which, inserted into (1.4), then yields

$$\overline{\mathcal{N}_i} = \frac{\partial \bar{U}_i}{\partial t} + \bar{U}_j \frac{\partial \bar{U}_i}{\partial x_j} + \frac{\partial \bar{P}}{\partial x_i} - \nu \frac{\partial^2 \bar{U}_i}{\partial x_j \partial x_j} + \frac{\partial R_{ij}^{(0)}}{\partial x_j} = 0. \tag{1.6}$$

The mathematical rules of averaging needed to obtain Eq. (1.6) are presented more extensively in Section 3.1.1. Here, it must be noted that the average of a fluctuation value is zero, but this is not necessarily true for the product of two fluctuating values. This gives rise to $R_{ij}^{(0)} = \overline{u_i u_j}$, the so-called Reynolds stress tensor. A comparison of the averaged system (1.3) and (1.6), known as the RANS (Reynolds-Averaged Navier–Stokes) equations, with the original Navier–Stokes equations (1.1) and (1.2) reveals that the equations are structurally similar, with the only difference being the additional unknown term $R_{ij}^{(0)}$ in Eq. (1.6). This situation, where the number of unknowns is larger than the number of equations, is known as the closure problem of turbulence. To overcome it, empirical closure relations for the unknown terms have to be established, a process referred to as turbulence modeling. Numerous turbulence models of different complexity have been proposed, and the most important ideas to the present work are discussed in Section 3.4.

Note that a compromise between DNS and RANS is provided by LES (large-eddy simulation). It relies on the insight that on the one hand, in DNS, as discussed above, the smallest turbulent structures are the main problem, but, on the other hand, in RANS, issues in model accuracy are often caused by the largest turbulent structures. These large structures usually depend on the problem-specific geometry and are, therefore, difficult to model in a universal way. The main idea of LES is, therefore, to resolve only the large scales, and to account for the small turbulent scales using model terms. However, since LES calculations can still take weeks or months depending on the problem, they have so far not been able to replace RANS, where a typical calculation only takes hours or days, and the results, depending on the problem, are often good enough. Therefore, the need for accurate and reliable RANS models still remains, which motivates the present work.

1.1. Motivation for the Use of Symmetries in Turbulence

A fundamental guiding concept used in this work is that of symmetries. Even though the use of the mathematical theory of Lie symmetries, which is discussed in Chapter 2, is not widespread in turbulence research, the intuition behind symmetries is simple and well-known in the field. In fact, the successful application of symmetries in physics predates the mathematical developments by Sophus Lie in the 19th century, and many fundamental ideas in fluid mechanics are essentially symmetry arguments. As an early example for ingenious use of symmetry arguments, we may turn to an anecdote discussed by Mach (1883) about Christian Huygens analyzing an early and flawed theory of collisions by René Descartes. Among other postulates, Descartes asserted that in elastic collisions, the absolute value of what is now called the momentum vector is conserved. Today we know that this is correct for the one-dimensional case, but not for higher dimensions and that indeed each component of the momentum vector is conserved individually. Christian Huygens discovered an elegant argument to show this. He proposed a thought experiment in which the collision takes place on a boat moving linearly at constant velocity, and is observed by someone on the boat and by someone else at the shore. Huygens's crucial insight was that the movement of the boat, as long as it moves at a constant velocity, does not have any effect on the collision experiment. Today, this principle is known as Galilean invariance. As a result, both the observer on the boat and the observer on land should be able to use the same formula to get the correct results for their respective frame of reference, even though all appearing velocities are shifted. It is straightforward to see that this does not work when using the absolute value of the momentum vector, which disproves Descartes's initial proposal. Huygens's key insight—that invariance principles observed in reality must manifest themselves in the equations—is an important foundational principle for the present work.

To a certain extent, this insight is naturally applied in turbulence modeling in the form of invariant modeling (Donaldson and Rosenbaum, 1968). Invariant modeling is based on the principle that the equations of any universal turbulence model must be (i) dimensionally correct, (ii) in correct tensorial formulation, (iii) Galilean invariant, and (iv) fulfill all relevant conservation laws. Points (i)–(iii) can be directly connected to symmetry theory. Dimensional correctness is equivalent to the principle that equations must not depend on the unit system used. In other words, it must be possible to change the unit system—which is the same as rescaling all appearing variables in a certain way—while leaving the equations invariant. Correct tensorial formulation ensures that the equations are not affected by the orientation of the coordinate system, i.e. that they are invariant under a rotation of the coordinate system, and Galilean invariance has already been discussed in the above example of momentum conservation. In a certain sense, point (iv) is also linked to symmetries via Noether's theorem (Noether, 1918), but since this connection is more subtle than for the first three points, we do not discuss it in more detail here.

There are additional, less obvious examples for symmetry arguments giving rise to well-known results in fluid mechanics. As is discussed in Section 3.3, the concept of self-similarity, which is crucial for quantitatively describing boundary layer flows and many free-stream flows such as jets, wakes and mixing layers, is intimately connected with the scaling symmetries of the governing equations (Sadeghi et al., 2018). Moreover, turbulent scaling laws, i.e. special-case solutions, can usually be constructed using symmetries, the most famous example probably being the logarithmic law of the wall (Oberlack, 2001; Oberlack et al., 2022).

In recent years, applying the mathematical framework of Lie symmetries in turbulence modeling has been gaining significant traction. An early example is the contribution by Oberlack (1997), who applied symmetry methods in the context of LES models. Popovich and Bihlo (2012) made use of symmetries to systematically generate invariant models for meteorological problems, though their method is general enough to be applied to other modeling challenges as well. Later, Bihlo and Bluman (2013) further developed this method by also incorporating constraints arising from conservation laws. Schaefer-Rolffs et al. (2015) presented a scale invariance criterion for LES and subsequently applied it to geophysical flows in Schaefer-Rolffs (2019). Therein, it was highlighted that some scaling symmetries, unlike symmetries which are connected to conservation laws and therefore generally accounted for in models and numerical schemes, are frequently overlooked. All of these works, however, only take into account the symmetries of the Navier–Stokes equations (1.1) and (1.2). The main new development of the present work is the inclusion of additional symmetry constraints which arise when analyzing a statistical representation of turbulence. These symmetries are further discussed in Section 3.2.

1.2. The Role of Numerics in Turbulence

As has probably become clear in the beginning of the introduction, numerical methods play a central role in turbulence research. This is particularly true for the development of RANS models, because one not only relies on numerical data to design the model, but applying the model to moderately complicated flows also requires the numerical solution of its equations.

In this work, we use the open-source code framework BoSSS (Bounded Support Spectral Solver) (Kummer and Oberlack, 2013), which is under active development at the Chair of Fluid Dynamics at TU Darmstadt, and, notably, uses a DG (Discontinuous Galerkin) discretization in space. It is implemented in the object-oriented and easy-to-use programming language C#, which at the same time offers high performance. For the most performance-critical parts such as the linear equation solver, BoSSS relies on well-established external packages such as BLAS (basic linear algebra subprograms) and LAPACK (linear algebra package). It can also run in parallel by using the MPI (message-passing interface) standard, which, in conjunction with the relative simplicity of the language makes it possible to use BoSSS for a wide range of tasks, from simple prototyping to calculations on high-performance supercomputers. In recent years, many different physical problems have been investigated using BoSSS, including incompressible flows with the SIMPLE (semi-implicit method for pressure-linked equation) method (Klein et al., 2013; Klein et al., 2015), compressible flows (Müller et al., 2016; Geisenhofer et al., 2019), multiphase flows (Kummer, 2016; Gründing et al., 2020), and, perhaps most similar to the problem discussed in this work, viscoelastic flows (Kikker and Kummer, 2018) and combustion problems (Gutiérrez-Jorquera and Kummer, 2021). The present work, in a sense, is an outlier in that the main focus here is not the development or improvement of new numerical methods and techniques, but on applying the already existing methods to a new physical problem.

Within the present work, both a well-established and a newly developed turbulence model have been implemented in BoSSS. However, the numerical solution of the new model, which significantly differs from previously existing models and for which no reasonable model parameters were known, turned out to be too difficult to be feasible. Therefore, a special-purpose solver for a simplified version of the new model was also developed and implemented in the programming language Python (Python Software Foundation, 2016). For this solver, a simple FDS (Finite Differencing Scheme) discretization was chosen and found to be sufficient.

1.3. Outline of This Work

This work is structured as follows: In Chapter 2, we introduce the concept of Lie symmetries more formally and discuss the mathematical background necessary for the later sections. In Chapter 3, the relevant ideas from turbulence research are presented. We show different statistical descriptions of turbulence in Section 3.1, the significance of Lie symmetries governing turbulence in Section 3.2, and discuss how Lie symmetries can be used to find turbulent scaling laws in Section 3.3. A non-exhaustive review of existing turbulence models follows in Section 3.4, and their application to self-similar flows is the topic of Section 3.5.

Chapter 4 discusses the main numerical developments of the present work and introduces the necessary theoretical background. The DG method, which is employed by BoSSS for spatial discretization, is presented in Section 4.1, and a discussion of the temporal discretization follows in Section 4.2. In Section 4.3, the implementation of the classical k-ω-model in BoSSS, the challenges arising in the process and some numerical results are presented. A discussion of simpler special-purpose numerical solvers is found in Section 4.4, which became necessary to efficiently obtain results for the newly developed turbulence models.

Having established all of these foundations, the main results are then presented in Chapter 5. First, a formal and algorithmic approach for finding turbulence models is employed in Section 5.1, the results of which suggest some useful modifications to existing turbulence models. This idea is further detailed in Section 5.2, where modified versions of the classical k-ε-model, the classical k-ω-model and RSMs (Reynolds stress models) are developed and applied to canonical flows. The gained insights are used to calibrate the model constants appearing in the modified k-ε-model. Finally, the numerical implementation of the novel k-ε-model and numerical results are discussed in Section 5.3. We close with a conclusion in Chapter 6.

2. Lie Point Symmetries

Most people are intuitively familiar with the concept of symmetries as special properties of certain geometric objects. More precisely, symmetries can be defined as transformations, e.g. rotation, that leave said object, e.g. a sphere, unchanged. This concept can be extended to algebraic and differential equations, where it has proven useful not only as a mathematical tool, but also as a concept to better understand physics. For a deeper introduction into the subject, the interested reader is referred to Bluman and Anco (2002) and Bluman et al. (2010), on which the following discussion is based.

In the present context, a symmetry is defined as a variable transformation

$$T : \boldsymbol{x}^* = \boldsymbol{\phi}(\boldsymbol{x}, a) \tag{2.1}$$

that leaves an equation $\boldsymbol{F}$ depending on the vector of variables $\boldsymbol{x}$ invariant, i.e.

$$\boldsymbol{F}(\boldsymbol{x}) = 0 \quad \Leftrightarrow \quad \boldsymbol{F}(\boldsymbol{x}^*) = 0. \tag{2.2}$$

Therein, $a \in \mathbb{R}$ is an arbitrary constant referred to as the group parameter. Within the scope of this work, we can always assume that this symmetry admits group properties and that, furthermore, it is a Lie group as defined in Appendix A.1. With these prerequisites, it is possible without loss of generality to write $\boldsymbol{\phi}$ in such a way that $a = 0$ is the identity element, i.e.

$$\boldsymbol{x}^* = \boldsymbol{\phi}(\boldsymbol{x}, a = 0) = \boldsymbol{x}, \tag{2.3}$$

and that the composition operation is addition,

$$\boldsymbol{\phi}(\boldsymbol{\phi}(\boldsymbol{x}; a_1); a_2) = \boldsymbol{\phi}(\boldsymbol{x}; a_1 + a_2). \tag{2.4}$$

Under these assumptions, we can expand (2.1) as a Taylor series around $a = 0$, leading to

$$x_i^* = \phi_i(\boldsymbol{x}, a = 0) + a \left.\frac{\partial \phi_i}{\partial a}\right|_{a=0} + O(a^2) \tag{2.5}$$

$$= x_i + a \left.\frac{\partial \phi_i}{\partial a}\right|_{a=0} + O(a^2). \tag{2.6}$$

A crucial result of Lie group theory is Lie's first theorem, which states that the term linear in a in Eq. (2.6) is sufficient to uniquely define the entire action of the transformation (2.1). This insight naturally motivates the definition of the infinitesimal generator

$$X = \xi_i \frac{\partial}{\partial x_i}, \tag{2.7}$$

where the infinitesimals ξ_i are given by

$$\xi_i = \left.\frac{\partial \phi_i}{\partial a}\right|_{a=0}. \tag{2.8}$$

Then, instead of using the global form of the symmetry as given by Eq. (2.2), we can equivalently state that $\boldsymbol{F}$ is invariant under a symmetry with infinitesimal generator X if

$$X\boldsymbol{F}|_{\boldsymbol{F}=0} = 0. \tag{2.9}$$

So far, strictly speaking, we have only considered algebraic equations. However, the extension to differential equations is straightforward. The main idea is to, for the most part, treat derivatives as new variables that are completely unrelated to the other dependent and independent variables. From this perspective, a differential equation is nothing but an algebraic equation with many dependent variables. The only question we must address is how the derivatives transform under a given symmetry, and it is exclusively in this context that the connection between derivatives and the original dependent and independent variables is important. In concrete terms, we now distinguish among the arguments of $\boldsymbol{F}$ between independent variables $\boldsymbol{x}$, dependent variables $\boldsymbol{z}$, and the derivatives $\boldsymbol{z}_{,x_1}; \cdots ; \boldsymbol{z}_{,x_n}$, and assume that the transformations

$$T : \boldsymbol{x}^* = \boldsymbol{\phi}(\boldsymbol{x}, \boldsymbol{z}, a), \quad \boldsymbol{z}^* = \boldsymbol{\psi}(\boldsymbol{x}, \boldsymbol{z}, a) \tag{2.10}$$

are given. Note that the notation of writing derivation in the index, which is known as jet notation, serves to highlight that unless explicitly stated otherwise, we treat these derivatives as new variables without any connection to $\boldsymbol{x}$ and $\boldsymbol{z}$. Equivalently, we can express the transformation (2.10) using its infinitesimal generator

$$X = \xi_i \frac{\partial}{\partial x_i} + \eta_i \frac{\partial}{\partial z_i}, \tag{2.11}$$

where

$$\eta_i = \left.\frac{\partial \psi_i}{\partial a}\right|_{a=0}. \tag{2.12}$$

The effect of the transformation (2.10) on the first derivatives can then be calculated using

$$z^*_{i,x_j} = \psi_{i,x_j} = \frac{\mathcal{D}\psi_i}{\mathcal{D}x_k}[\boldsymbol{A}^{-1}]_{kj}, \tag{2.13}$$

where $\boldsymbol{A}^{-1}$ is the inverse of the Jacobian matrix

$$A_{ij} = \frac{\mathcal{D}\phi_i}{\mathcal{D}x_j}, \tag{2.14}$$

with the total differentiation operator

$$\frac{\mathcal{D}}{\mathcal{D}x_i} = \frac{\partial}{\partial x_i} + z_{k,i}\frac{\partial}{\partial z_k} + \cdots . \tag{2.15}$$

In Eq. (2.13) and in the following, the index ij after a matrix refers to its element in the ith row and jth column. Also note that we denote vectors and matrices using bold letters, and their elements using the same letter in non-boldface.

It can be shown that Eq. (2.13) follows from the chain rule of differentiation if we do take the connection between derivatives $\boldsymbol{z}_{,x_1}; \cdots ; \boldsymbol{z}_{,x_n}$ and original dependent variables $\boldsymbol{z}$ and independent variables $\boldsymbol{x}$ into account. The action on higher-order derivatives can be inferred by recursively applying (2.13),

$$z^*_{i,x_{m_1}\cdots x_{m_{p-1}}x_j} = \psi_{i,x_{m_1}\cdots x_{m_{p-1}}x_j} = \frac{\mathcal{D}\psi_{i,x_{m_1}\cdots x_{m_{p-1}}}}{\mathcal{D}x_k}[\boldsymbol{A}^{-1}]_{kj}, \tag{2.16}$$

where we assume that there are p independent variables. In practice, this method of extending symmetries to act on derivatives can quickly become cumbersome. A simpler method is often to use the infinitesimal generators, which, when extended to also include derivatives, are referred to as prolonged operators. Again using the chain rule of differentiation, the nth prolonged operator can be calculated to be

$$X^{(n)} = \xi_i \frac{\partial}{\partial x_i} + \eta_i \frac{\partial}{\partial z_i} \underbrace{+ \eta_{i;x_{j_1}} \frac{\partial}{\partial z_{i,x_{j_1}}} + \eta_{i;x_{j_1};x_{j_2}} \frac{\partial}{\partial z_{i,x_{j_1}x_{j_2}}} + \cdots}_{n \text{ terms}}, \tag{2.17}$$

where

$$\eta_{i;x_{j_1}\dots x_{j_s}} = \frac{\mathcal{D}\eta_{i;x_{j_1}\dots x_{j_{s-1}}}}{\mathcal{D}x_{j_s}} - \sum_{m=1}^{s-1} z_{i,x_{j_1}\dots x_{j_{s-1}}x_{j_m}} \frac{\mathcal{D}\xi_{j_m}}{\mathcal{D}x_{j_s}}. \tag{2.18}$$

For the purposes of the present work, this method of calculating prolongations suffices because we usually restrict ourselves to first derivatives, however, if higher derivatives are to be taken into account, using the characteristic (or evolutionary) form of symmetries is often more efficient. The main idea is that instead of using Eq. (2.11), the form

$$\hat{X} = \hat{\eta}_i \frac{\partial}{\partial z_i} \tag{2.19}$$

is used, where, crucially, , unlike ξ_i and η_i in Eq. (2.11), $\hat{\eta}_i$ is allowed to depend on derivatives. In concrete terms, $\hat{\eta}_i$ is given by

$$\hat{\eta}_i = \eta_i - \xi_j z_{i,x_j}. \tag{2.20}$$

Then, the prolongations simply follow from application of the total derivative,

$$\hat{X}^{(n)} = \hat{X} + \frac{\mathcal{D}\hat{\eta}_i}{\mathcal{D}x_j}\frac{\partial}{\partial z_{i,x_j}} + \cdots . \tag{2.21}$$

To make the preceding discussion clearer, we now discuss as an example the Euler momentum equation, i.e. (1.2) with $\nu = 0$, which, written in jet notation, reads

$$F_i = U_{i,t} + U_j U_{i,x_j} + P_{,x_i} = 0, \tag{2.22}$$

and the transformation

$$T_{\mathrm{Sc},I}: \quad t^* = t, \;\; x_i^* = x_i e^{a_{\mathrm{Sc},I}}, \;\; U_i^* = U_i e^{a_{\mathrm{Sc},I}}, \;\; P^* = P e^{2a_{\mathrm{Sc},I}}, \tag{2.23}$$

is considered as an example. Observe that writing the scaling factor in exponential form ensures that conditions (2.3) and (2.4) are fulfilled. We now show that (2.23) is a symmetry of (2.22). To this end, we first have to establish how the derivatives appearing in (2.22) transform under (2.23). In order to apply (2.13), we first calculate the matrix $\boldsymbol{A}$ using (2.14). Assuming the two-dimensional case, we use

$$\boldsymbol{x}^* = \begin{bmatrix} x_1^* \\ x_2^* \\ t^* \end{bmatrix} = \begin{bmatrix} \phi_1 \\ \phi_2 \\ \phi_3 \end{bmatrix} = \begin{bmatrix} x_1 e^{a_{\mathrm{Sc},I}} \\ x_2 e^{a_{\mathrm{Sc},I}} \\ t \end{bmatrix} , \tag{2.24}$$

and

$$\boldsymbol{z}^* = \begin{bmatrix} U_1^* \\ U_2^* \\ P^* \end{bmatrix} = \begin{bmatrix} \psi_1 \\ \psi_2 \\ \psi_3 \end{bmatrix} = \begin{bmatrix} U_1 e^{a_{\mathrm{Sc},I}} \\ U_2 e^{a_{\mathrm{Sc},I}} \\ P e^{2a_{\mathrm{Sc},I}} \end{bmatrix} . \tag{2.25}$$

Then, for the transformation (2.23), $\boldsymbol{A}$ becomes

$$\begin{aligned} A_{ij} &= \begin{bmatrix} \frac{\mathcal{D}\phi_1}{\mathcal{D}x_1} & \frac{\mathcal{D}\phi_1}{\mathcal{D}x_2} & \frac{\mathcal{D}\phi_1}{\mathcal{D}t} \\ \frac{\mathcal{D}\phi_2}{\mathcal{D}x_1} & \frac{\mathcal{D}\phi_2}{\mathcal{D}x_2} & \frac{\mathcal{D}\phi_2}{\mathcal{D}t} \\ \frac{\mathcal{D}\phi_3}{\mathcal{D}x_1} & \frac{\mathcal{D}\phi_3}{\mathcal{D}x_2} & \frac{\mathcal{D}\phi_3}{\mathcal{D}t} \end{bmatrix}_{ij} = \begin{bmatrix} \frac{\mathcal{D}\left(x_1 e^{a_{\mathrm{Sc},I}}\right)}{\mathcal{D}x_1} & \frac{\mathcal{D}\left(x_1 e^{a_{\mathrm{Sc},I}}\right)}{\mathcal{D}x_2} & \frac{\mathcal{D}\left(x_1 e^{a_{\mathrm{Sc},I}}\right)}{\mathcal{D}t} \\ \frac{\mathcal{D}\left(x_2 e^{a_{\mathrm{Sc},I}}\right)}{\mathcal{D}x_1} & \frac{\mathcal{D}\left(x_2 e^{a_{\mathrm{Sc},I}}\right)}{\mathcal{D}x_2} & \frac{\mathcal{D}\left(x_2 e^{a_{\mathrm{Sc},I}}\right)}{\mathcal{D}t} \\ \frac{\mathcal{D}t}{\mathcal{D}x_1} & \frac{\mathcal{D}t}{\mathcal{D}x_2} & \frac{\mathcal{D}t}{\mathcal{D}t} \end{bmatrix}_{ij} \\ &= \begin{bmatrix} e^{a_{\mathrm{Sc},I}} & 0 & 0 \\ 0 & e^{a_{\mathrm{Sc},I}} & 0 \\ 0 & 0 & 1 \end{bmatrix}_{ij} . \end{aligned} \tag{2.26}$$

The inverse of A_{ij} is easy to calculate and reads

$$[\boldsymbol{A}^{-1}]_{ij} = \begin{bmatrix} e^{-a_{\mathrm{Sc},I}} & 0 & 0 \\ 0 & e^{-a_{\mathrm{Sc},I}} & 0 \\ 0 & 0 & 1 \end{bmatrix}_{ij} . \tag{2.27}$$

Next, we turn to the matrix $\mathcal{D}\psi_i/\mathcal{D}x_j$ appearing in Eq. (2.13). Here, the definition of the total derivative (2.15) becomes important, and, for example,

$$\begin{aligned} \frac{\mathcal{D}\psi_1}{\mathcal{D}x_2} &= \frac{\mathcal{D}\left(U_1 e^{a_{\mathrm{Sc},I}}\right)}{\mathcal{D}x_2} = e^{a_{\mathrm{Sc},I}} \frac{\mathcal{D}U_1}{\mathcal{D}x_2} \\ &= e^{a_{\mathrm{Sc},I}} \left(\cancel{\frac{\partial U_1}{\partial x_2}} + U_{1,x_2} \frac{\partial U_1}{\partial U_1} + U_{2,x_2} \cancel{\frac{\partial U_1}{\partial U_2}} + \cdots \right) = e^{a_{\mathrm{Sc},I}} U_{1,x_2} . \end{aligned} \tag{2.28}$$

Hopefully, this example also makes the use of jet notation clearer. In particular, note that the fact that e.g. $\partial U_1/\partial x_2 = 0$, which we have used above, only implies that the expression U_1 does not contain the expression x_2. If we wanted to express a vanishing $(1,2)$-component of the velocity gradient in the current setting, we would have to write $U_{1,x_2} = 0$. Repeating the calculation detailed in (2.28) for all components yields

$$\frac{\mathcal{D}\psi_i}{\mathcal{D}x_j} = \begin{bmatrix} U_{1,x_1} e^{a_{\mathrm{Sc},I}} & U_{1,x_2} e^{a_{\mathrm{Sc},I}} & U_{1,t} e^{a_{\mathrm{Sc},I}} \\ U_{2,x_1} e^{a_{\mathrm{Sc},I}} & U_{2,x_2} e^{a_{\mathrm{Sc},I}} & U_{2,t} e^{a_{\mathrm{Sc},I}} \\ P_{,x_1} e^{2a_{\mathrm{Sc},I}} & P_{,x_2} e^{2a_{\mathrm{Sc},I}} & P_{,t} e^{2a_{\mathrm{Sc},I}} \end{bmatrix}_{ij} . \tag{2.29}$$

We now invoke Eq. (2.13) with the results from Eqs. (2.27) and (2.29) to obtain

$$\begin{aligned}
\begin{bmatrix} U^*_{1,x_1^*} & U^*_{1,x_2^*} & U^*_{1,t^*} \\ U^*_{2,x_1^*} & U^*_{2,x_2^*} & U^*_{2,t^*} \\ P^*_{,x_1^*} & P^*_{,x_2^*} & P^*_{,t^*} \end{bmatrix} &= \begin{bmatrix} U_{1,x_1} e^{a_{\mathrm{Sc},I}} & U_{1,x_2} e^{a_{\mathrm{Sc},I}} & U_{1,t} e^{a_{\mathrm{Sc},I}} \\ U_{2,x_1} e^{a_{\mathrm{Sc},I}} & U_{2,x_2} e^{a_{\mathrm{Sc},I}} & U_{2,t} e^{a_{\mathrm{Sc},I}} \\ P_{,x_1} e^{2a_{\mathrm{Sc},I}} & P_{,x_2} e^{2a_{\mathrm{Sc},I}} & P_{,t} e^{2a_{\mathrm{Sc},I}} \end{bmatrix} \begin{bmatrix} e^{-a_{\mathrm{Sc},I}} & 0 & 0 \\ 0 & e^{-a_{\mathrm{Sc},I}} & 0 \\ 0 & 0 & 1 \end{bmatrix} \\
&= \begin{bmatrix} U_{1,x_1} & U_{1,x_2} & U_{1,t} e^{a_{\mathrm{Sc},I}} \\ U_{2,x_1} & U_{2,x_2} & U_{2,t} e^{a_{\mathrm{Sc},I}} \\ P_{,x_1} e^{a_{\mathrm{Sc},I}} & P_{,x_2} e^{a_{\mathrm{Sc},I}} & P_{,t} e^{2a_{\mathrm{Sc},I}} \end{bmatrix}, \qquad (2.30)
\end{aligned}$$

which we can finally insert into (2.22), leading to

$$U^*_{i,t^*} + U^*_j U^*_{i,x_j^*} + P^*_{,x_i^*} = 0 \quad \Leftrightarrow \quad U_{i,t} e^{a_{\mathrm{Sc},I}} + U_j e^{a_{\mathrm{Sc},I}} U_{i,x_j} + P_{,x_i} e^{a_{\mathrm{Sc},I}} = 0. \qquad (2.31)$$

Since $e^{a_{\mathrm{Sc},I}}$ can be canceled, we conclude that (2.23) is indeed a symmetry of (2.22).

The above analysis usually becomes easier if we work with the infinitesimal generator of (2.23). Employing (2.8) and (2.12), we obtain

$$\begin{aligned}
\xi_t &= \left.\frac{\partial t^*}{\partial a_{\mathrm{Sc},I}}\right|_{a_{\mathrm{Sc},I}=0} = 0, \\
\xi_{x_i} &= \left.\frac{\partial x_i^*}{\partial a_{\mathrm{Sc},I}}\right|_{a_{\mathrm{Sc},I}=0} = \left[x_i e^{a_{\mathrm{Sc},I}}\right]_{a_{\mathrm{Sc},I}=0} = x_i, \\
\eta_{U_i} &= \left.\frac{\partial U_i^*}{\partial a_{\mathrm{Sc},I}}\right|_{a_{\mathrm{Sc},I}=0} = \left[U_i e^{a_{\mathrm{Sc},I}}\right]_{a_{\mathrm{Sc},I}=0} = U_i, \\
\eta_P &= \left.\frac{\partial P^*}{\partial a_{\mathrm{Sc},I}}\right|_{a_{\mathrm{Sc},I}=0} = \left[2P e^{2a_{\mathrm{Sc},I}}\right]_{a_{\mathrm{Sc},I}=0} = 2P, \qquad (2.32)
\end{aligned}$$

which, using (2.11), leads to the infinitesimal generator

$$X_{\mathrm{Sc},I} = \xi_t \frac{\partial}{\partial t} + \xi_{x_i}\frac{\partial}{\partial x_i} + \eta_{U_i}\frac{\partial}{\partial U_i} + \eta_P \frac{\partial}{\partial P} = x_i \frac{\partial}{\partial x_i} + U_i \frac{\partial}{\partial U_i} + 2P\frac{\partial}{\partial P}. \qquad (2.33)$$

We can now use (2.17) together with (2.18) to infer the action of (2.33) on the derivatives appearing in (2.22), i.e. $U_{i,t}$, U_{i,x_j} and $P_{,x_i}$. Using (2.18), we obtain

$$\eta_{U_i;t} = \frac{\mathcal{D}\eta_{U_i}}{\mathcal{D}t} - U_{i,t}\cancel{\frac{\mathcal{D}\xi_t}{\mathcal{D}t}} - U_{i,x_k}\cancel{\frac{\mathcal{D}\xi_{x_k}}{\mathcal{D}t}} = \cancel{\frac{\partial U_i}{\partial t}} + U_{k,t}\frac{\partial U_i}{\partial U_k} + P_{,t}\cancel{\frac{\partial \eta_{U_i}}{\partial P}} = U_{k,t}\delta_{ik}, = U_{i,t}, \qquad (2.34)$$

$$\begin{aligned}
\eta_{U_i;x_j} &= \frac{\mathcal{D}\eta_{U_i}}{\mathcal{D}x_j} - U_{i,t}\cancel{\frac{\mathcal{D}\xi_t}{\mathcal{D}x_j}} - U_{i,x_k}\frac{\mathcal{D}\xi_{x_k}}{\mathcal{D}x_j} = \cancel{\frac{\partial U_i}{\partial x_j}} + U_{k,x_j}\frac{\partial U_i}{\partial U_k} + P_{,x_j}\cancel{\frac{\partial U_i}{\partial P}} - U_{i,x_k}\frac{\partial x_k}{\partial x_j} \\
&= U_{k,x_j}\delta_{ik} - U_{i,x_k}\delta_{jk} = U_{i,x_j} - U_{i,x_j} = 0, \qquad (2.35) \\
\eta_{P;x_i} &= \frac{\mathcal{D}\eta_P}{\mathcal{D}x_i} - P_{,t}\cancel{\frac{\mathcal{D}\xi_t}{\mathcal{D}x_i}} - P_{,x_k}\frac{\mathcal{D}\xi_{x_k}}{\mathcal{D}x_i} = 2\cancel{\frac{\partial P}{\partial x_j}} + U_{k,x_i}2\cancel{\frac{\partial P}{\partial U_k}} + P_{,x_i}2\frac{\partial P}{\partial P} - P_{,x_k}\delta_{ik} \\
&= 2P_{,x_i} - P_{,x_i} = P_{,x_i}, \qquad (2.36)
\end{aligned}$$

where

$$\delta_{ij} = \begin{cases} 1 & \text{for } i = j \\ 0 & \text{for } i \neq j \end{cases} \qquad (2.37)$$

denotes the Kronecker delta. Putting everything together, we can then obtain the first prolongation according to Eq. (2.17)

$$\begin{aligned} X^{(1)}_{\mathrm{Sc},I} &= x_i \frac{\partial}{\partial x_i} + U_i \frac{\partial}{\partial U_i} + 2P \frac{\partial}{\partial P} + \eta_{U_i;t} \frac{\partial}{\partial U_{i,t}} + \eta_{U_i;x_j} \frac{\partial}{\partial U_{i,x_j}} + \eta_{P;x_i} \frac{\partial}{\partial P_{,x_i}} \\ &= x_i \frac{\partial}{\partial x_i} + U_i \frac{\partial}{\partial U_i} + 2P \frac{\partial}{\partial P} + U_{i,t} \frac{\partial}{\partial U_{i,t}} + P_{,x_i} \frac{\partial}{\partial P_{,x_i}}, \end{aligned} \tag{2.38}$$

where we have omitted the action on $P_{,t}$ because this variable does not occur in (2.22). Using

$$\begin{aligned} XF_i &= X^{(1)}_{\mathrm{Sc},I}(U_{i,t} + U_j U_{i,x_j} + P_{,x_i}) \\ &= X^{(1)}_{\mathrm{Sc},I} U_{i,t} + X^{(1)}_{\mathrm{Sc},I}(U_j U_{i,x_j}) + X^{(1)}_{\mathrm{Sc},I} P_{,x_i} \\ &= X^{(1)}_{\mathrm{Sc},I} U_{i,t} + U_j \cancel{X^{(1)}_{\mathrm{Sc},I} U_{i,x_j}} + U_{i,x_j} X^{(1)}_{\mathrm{Sc},I} U_j + X^{(1)}_{\mathrm{Sc},I} P_{,x_i} \\ &= U_{k,t} \frac{\partial U_{i,t}}{\partial U_{k,t}} + U_{i,x_j} U_k \frac{\partial U_j}{\partial U_k} + P_{,x_k} \frac{\partial P_{,x_i}}{\partial P_{,x_k}} \\ &= U_{k,t}\delta_{ik} + U_{i,x_j} U_k \delta_{ik} + P_{,x_k}\delta_{ik} \\ &= U_{i,t} + U_j U_{i,x_j} + P_{,x_i}, \end{aligned} \tag{2.39}$$

we can then insert into Eq. (2.9),

$$X^{(1)}_{\mathrm{Sc},I} F_i|_{F_i=0} = \left[U_{i,t} + U_j U_{i,x_j} + P_{,x_i}\right]_{U_{i,t}+U_j U_{i,x_j}+P_{,x_i}=0} = 0, \tag{2.40}$$

which confirms that (2.38) is indeed a symmetry of (2.22).

Without going into much detail, we note that the theory introduced here also allows one to algorithmically calculate the symmetries of any given equation. This is accomplished by assuming a general form of X, calculating the prolongation as needed following (2.17), inserting into (2.9) and solving the arising PDE (partial differential equation) system for the infinitesimals ξ_i and η_i. Depending on the problem, such a calculation can require significant effort when done manually, but in recent years, the advent of CASs (computer algebra systems) has greatly simplified the use of symmetry methods. It must be emphasized that there is no need to rely on educated guesses to obtain symmetries such as Eq. (2.33), but that they can be calculated algorithmically from the respective equation, i.e. (2.22) in the above example. In the present work, this aspect of symmetry theory only plays a minor role, because we are concerned with equations that have already been thoroughly studied and whose symmetries are, therefore, already known.

Conversely, an analogous line of reasoning also allows constructing equations that are invariant under a certain symmetry or a set of symmetries. This problem is also known as the inverse problem of group classification. To solve it, one assumes a general form of $\boldsymbol{F}$ and solves the PDE system arising from (2.9) to obtain a constrained form for $\boldsymbol{F}$ that is guaranteed to be invariant under the selected symmetry or symmetries. This method for constructing equations based on symmetries is crucial to the present work because it lies at the heart of the discussion in Section 5.1, where it is also discussed in more detail.

An alternative approach for finding equations that are invariant under a certain set of symmetries is provided by the method of moving frames pioneered by Olver (2000). Unlike the method described in the previous paragraph, the method of moving frames operates on the level of global transformations (2.10). The main idea is that given some symmetry, or some combination of multiple symmetries, i.e. a so-called multi-parameter group, one sets the $\boldsymbol{x}^*$ and $\boldsymbol{z}^*$ to some convenient fixed value (usually 0 or 1) and solves the arising equation system for the group parameter(s). Then, one calculates the transformed derivatives and inserts the results for the group parameters to obtain the differential invariants. As an example, consider the multi-parameter group consisting of a translation in time and a scaling in space and time

$$t^* = a_{\mathrm{Sc},II} t + a_T, \quad x^* = a_{\mathrm{Sc},I} x, \quad z^* = \frac{a_{\mathrm{Sc},I}}{a_{\mathrm{Sc},II}} z, \tag{2.41}$$

where t and x are the independent coordinates, and z is the dependent coordinate. Setting $t^* = 0$ and $x^* = z^* = 1$, i.e.

$$t^* = a_{\mathrm{Sc},II} t + a_T = 0, \quad x^* = a_{\mathrm{Sc},I} x = 1, \quad z^* = \frac{a_{\mathrm{Sc},I}}{a_{\mathrm{Sc},II}} z = 1, \tag{2.42}$$

then yields

$$a_T = -\frac{zt}{x}, \quad a_{\mathrm{Sc},II} = \frac{z}{x}, \quad a_{\mathrm{Sc},I} = \frac{1}{x}. \tag{2.43}$$

The transformed derivatives read

$$z_x^* = \frac{\partial z^*}{\partial x^*} = \frac{1}{a_{\mathrm{Sc},II}} \frac{\partial z}{\partial x} = \frac{x z_x}{z}, \tag{2.44}$$

$$z_t^* = \frac{\partial z^*}{\partial t^*} = \frac{a_{\mathrm{Sc},I}}{a_{\mathrm{Sc},II}^2} \frac{\partial z}{\partial t} = \frac{x z_t}{z^2}, \tag{2.45}$$

which gives rise to the differential invariants $x z_x / z$ and $x z_t / z^2$. Note that a deeper explanation of why this method works requires considerable understanding in differential geometry and is hence beyond the scope of this discussion. The interested reader is referred to Olver (2000) for more details. A crucial observation is that whereas the method based on infinitesimal generators gives rise to a linear PDE system from which to calculate the invariants, the moving frames method requires the solution of a nonlinear algebraic equation system, i.e. (2.42) in the above example. This system has to be solved fully coupled, which can be complicated depending on the problem. Since the infinitesimal-based method allows for a decoupled solution of the linear PDE system, it was found to work better for our present purposes.

This concludes the short discussion of the mathematical prerequisites. We are now equipped to apply Lie symmetry theory to the equations governing fluid mechanics, which we address in Section 3.2.

3. Turbulence Theory and Modeling

In this chapter, the relevant ideas from turbulence research that the present work builds upon are introduced. In particular, we first establish the statistical framework in which turbulence is described, then discuss the Lie symmetries of the governing equations in this setting and some turbulent scaling laws that can be derived from them, and give a short introduction to RANS turbulence modeling. The application of turbulence models to a class of simple self-similar flows is also shown.

3.1. Statistical Moment Description of Turbulence

Generally, a natural way to describe stochastic processes is in terms of their statistical moments. In turbulence, this is the most common framework in which flow statistics are investigated. Differences arise from the choice of the statistical moments in which to write the equations, and we discuss several choices in the following. Note that there are other statistical descriptions of turbulence such as the LMN (Lundgren–Monin–Novikov) hierarchy based on PDFs (probability-density functions) (Lundgren, 1967) or on characteristic functionals (Hopf, 1952), but since these approaches are only tangentially relevant to the present work, we do not discuss them further here. For a discussion of Lie symmetries in these settings, we refer to Waclawczyk et al. (2014).

3.1.1. The Mathematical Rules of Averaging

The averaging operation we have used without much discussion in deriving (1.3), (1.4) and (1.6) is now discussed in more detail following Pope (2000). We denote the flow velocity at some point in space and time with U_i, and assume that the same flow experiment is repeated many times. If the velocity in the nth realization of the experiment is denoted by $U_i^{(n)}$, this allows defining the average as

$$\bar{U}_i = \lim_{N\to\infty} \frac{1}{N} \sum_{n=1}^{N} U_i^{(n)}, \tag{3.1}$$

where N is the number of repetitions. In a turbulent flow, generally, all $U_i^{(n)}$ are independent random variables.

From (3.1), some properties of the averaging operation can be inferred. First, averaging is idempotent, which means that repeatedly applying it to an already averaged property has no effect, i.e. $\bar{\bar{U}}_i = \bar{U}_i$. Second, since averaging is essentially a summation, it is linear, i.e.

$\overline{aU_i + bU_j} = a\bar{U}_i + b\bar{U}_j$ for any constants a and b. By the same token, it also commutates with derivation, i.e.

$$\overline{\left(\frac{\partial U_i}{\partial t}\right)} = \frac{\partial \bar{U}_i}{\partial t}.$$

By averaging the decomposition of velocity and pressure (though this obviously works for any statistical variable) given by Eq. (1.5) and using idempotence, it can also be seen that the average of a fluctuating value vanishes, i.e. $\bar{u}_i = 0$. Intuitively, this makes sense because u_i fluctuates around the mean value, so that positive and negative contributions cancel out on average. However, this is not generally true for the average of the product of two fluctuating variables. This might seem counterintuitive at first, but becomes obvious if one considers the case where a fluctuating variable is squared before the average is taken. Clearly, the square is always positive, so that positive and negative contributions are no longer in balance. This also extends to the general case of averages of the product of two possibly different fluctuating variables provided that the two variables are correlated, which is generally the case in the context of turbulence.

3.1.2. One-Point Moment Description

For the unknown terms in (1.4) and (1.6), exact equations can be derived. It was probably Chou (1945) who first derived the equation for the unknown Reynolds stress tensor $R_{ij}^{(0)}$ appearing in (1.6). Using the momentum equation for the fluctuating velocity,

$$\mathcal{N}_i' = \mathcal{N}_i - \overline{\mathcal{N}_i} = \frac{\partial u_i}{\partial t} + U_j \frac{\partial U_i}{\partial x_j} - \bar{U}_j \frac{\partial \bar{U}_i}{\partial x_j} - \frac{\partial R_{ij}^{(0)}}{\partial x_j} + \frac{\partial p}{\partial x_i} - \nu \frac{\partial^2 u_i}{\partial x_j \partial x_j} = 0, \tag{3.2}$$

and evaluating the expression

$$\overline{u_i \mathcal{N}_j' + u_j \mathcal{N}_i'} = 0$$

while using the rules discussed in Section 3.1.1 leads to a transport equation for the Reynolds stress tensor,

$$\frac{\partial R_{ij}^{(0)}}{\partial t} + \bar{U}_k \frac{\partial R_{ij}^{(0)}}{\partial x_k} + R_{ik}^{(0)} \frac{\partial \bar{U}_j}{\partial x_k} + R_{jk}^{(0)} \frac{\partial \bar{U}_i}{\partial x_k} - \overline{p\left(\frac{\partial u_i}{\partial x_j} + \frac{\partial u_j}{\partial x_i}\right)}^{(0)} + 2\nu \overline{\frac{\partial u_i}{\partial x_k}\frac{\partial u_j}{\partial x_k}}^{(0)}$$
$$+ \frac{\partial}{\partial x_k}\left(R_{ijk}^{(0)} + \overline{(\delta_{jk} u_i + \delta_{ik} u_j) p}^{(0)} - \nu \frac{\partial R_{ij}^{(0)}}{\partial x_k}\right) = 0, \tag{3.3}$$

where the Kronecker delta defined by Eq. (2.37) appears again. The superscript "(0)" indicates that the respective property is a one-point moment, in contrast to multipoint moments to be discussed in Section 3.1.3. In analogy to $R_{ij}^{(0)}$, the triple correlation $R_{ijk}^{(0)}$ equals $\overline{u_i u_j u_k}$. No additional physical information is employed in deriving Eq. (3.3), so that, obviously, this does not solve the closure problem of turbulence, because new unknown correlations appear in (3.3). However, we note that since it is possible to obtain transport equations for these unknown quantities (which again contain further unknown correlations), turbulent statistics can be fully described using this infinite hierarchy of equations.

Thanks to the intuitive interpretation of $R_{ij}^{(0)}$ as an additional turbulent stress tensor, the framework given by (1.3), (1.6) and (3.3) and infinitely many additional equations is the most commonly used one in turbulence modeling. However, a major drawback is the complicated form of the arising equations, as evidenced by (3.3). Oberlack and Rosteck (2010) and Rosteck and Oberlack (2011) put forward the idea to omit the Reynolds decomposition given by Eq. (1.5), and to treat the moment based on instantaneous velocities $H_{ij}^{(0)}$ in (1.4) as a single unknown variable. Then, in an analogous fashion to the derivation of (3.3), a transport equation for $H_{ij}^{(0)}$ can be derived. This time, we evaluate

$$\overline{U_i \mathcal{N}_j + U_j \mathcal{N}_i} = 0,$$

leading to

$$\frac{\partial H_{ij}^{(0)}}{\partial t} + \frac{\partial H_{ijk}^{(0)}}{\partial x_k} + \frac{\partial \overline{PU_i}^{(0)}}{\partial x_j} + \frac{\partial \overline{PU_j}^{(0)}}{\partial x_i} - \overline{P\left(\frac{\partial U_i}{\partial x_j} + \frac{\partial U_j}{\partial x_i}\right)}^{(0)}$$
$$- \nu \frac{\partial^2 H_{ij}^{(0)}}{\partial x_k \partial x_k} + 2\nu \overline{\frac{\partial U_i}{\partial x_k}\frac{\partial U_j}{\partial x_k}}^{(0)} = 0, \tag{3.4}$$

where again, the averaging rules shown in Section 3.1.1 are applied. Here, the triple correlation $H_{ijk}^{(0)}$ is a compact notation for $\overline{U_i U_j U_k}$. Evidently, this equation is simpler than (3.3) in the sense that it has fewer terms and, crucially, it is linear. This linearity is also present in the infinite hierarchy of equations that would arise from successively deriving equations for the unknown quantities in (3.4). Obviously, since (3.3) and (3.4) are mathematically equivalent, the complexity of Eq. (3.3) is, in a sense, still present in (3.4), but it is hidden inside the variables appearing in (3.4). Thus, the relative simplicity of Eq. (3.4) comes at the cost of it being written in terms of more complicated variables that are more difficult to interpret intuitively. Therefore, it strongly depends on the context whether fluctuation moments or instantaneous moments are more useful.

3.1.3. Multipoint Moment Description

An even simpler equation system can be found by considering multipoint moments. While one-point moments such as $R_{ij}^{(0)} = \overline{u_i u_j}$ are formed by evaluating u_i and u_j at the same spatial location, multipoint moments are more general, because they are defined by evaluating u_i and u_j at different points in space. This comes at the cost of increasing the number of independent variables, because on top of the three spatial coordinates, the distance vectors between the points of evaluation appear as additional variables.

Considering first the fluctuation moment approach, a transport equation for $R_{ij} = \overline{u_i(\boldsymbol{x}) u_j(\boldsymbol{y})}$ is obtained by evaluating

$$\overline{\mathcal{N}_i'(\boldsymbol{x}) u_j(\boldsymbol{y}) + \mathcal{N}_j'(\boldsymbol{y}) u_i(\boldsymbol{x})} = 0,$$

and, using the averaging rules as discussed in Section 3.1.1, reads

$$\frac{\partial R_{ij}}{\partial t} + \bar{U}_k \frac{\partial R_{ij}}{\partial x_k} + \bar{U}_k \frac{\partial R_{ij}}{\partial y_k} + R_{ik} \frac{\partial \bar{U}_j}{\partial y_k} + R_{kj} \frac{\partial \bar{U}_i}{\partial x_k}$$
$$+ \frac{\partial \overline{p u_j}}{\partial x_i} + \frac{\partial \overline{u_i p}}{\partial y_j} - \nu \frac{\partial^2 R_{ij}}{\partial x_k \partial x_k} - \nu \frac{\partial^2 R_{ij}}{\partial y_k \partial y_k} + \frac{\partial R_{(ik)j}}{\partial x_k} + \frac{\partial R_{i(jk)}}{\partial y_k} = 0, \tag{3.5}$$

where we have used the notation introduced by Rotta (1975), which uses parentheses in the index to indicate that the corresponding velocities are evaluated at the same point in space, e.g. $R_{(ik)j} = \overline{u_i(\boldsymbol{x})u_k(\boldsymbol{x})u_j(\boldsymbol{y})}$, and assumes $R_{ij\cdots} = \overline{u_i(\boldsymbol{x})u_j(\boldsymbol{y})\cdots}$ otherwise. In (3.5), the only unknown term is the triple correlation of the form $R_{(ik)j} = \overline{u_i(\boldsymbol{x})u_k(\boldsymbol{x})u_j(\boldsymbol{y})}$. Note that the pressure-velocity correlations $\overline{pu_j}$ and $\overline{u_ip}$ are not new unknown terms because for them, a Poisson equation can be derived.

Similarly, a transport equation for the instantaneous two-point moment H_{ij} is obtained by considering

$$\overline{\mathcal{N}_i(\boldsymbol{x})U_j(\boldsymbol{y}) + \mathcal{N}_j(\boldsymbol{y})U_i(\boldsymbol{x})} = 0,$$

leading to the concise equation (Oberlack and Rosteck, 2010)

$$\frac{\partial H_{ij}}{\partial t} + \frac{\partial H_{(ik)j}}{\partial x_k} + \frac{\partial H_{i(jk)}}{\partial y_k} + \frac{\partial \overline{PU_j}}{\partial x_i} + \frac{\partial \overline{U_iP}}{\partial y_j} - \nu \frac{\partial^2 H_{ij}}{\partial x_k \partial x_k} - \nu \frac{\partial^2 H_{ij}}{\partial y_k \partial y_k} = 0, \tag{3.6}$$

where we once again have to invoke the averaging rules as presented in Section 3.1.1. In fact, this equation is so structurally simple that it becomes straightforward to generalize it to arbitrary moments, allowing for mathematical insights to be discussed in Section 3.2 (Rosteck, 2013). The only trade-off is that the statistical moments appearing in it are a bit more complicated to interpret intuitively compared to the central one-point moments appearing in the classical approach.

In the remainder of the present work, we only rely on the instantaneous one-point approach given by (3.4) and the classical fluctuation one-point approach given by (3.3). Since both of these approaches are mathematically equivalent, it is easily possible to switch between the two as needed. Note that since we only consider one-point moments from now on, we omit the superscript (0).

3.2. Lie Symmetries and Turbulence

As has been discussed in Chapter 2, the symmetries of any given equation can be calculated algorithmically. For the incompressible Navier–Stokes equations (1.1) and (1.2), this calculation was first carried out by Bytev (1972). For the case of vanishing viscosity ($\nu = 0$), the symmetries of Eqs. (1.1) and (1.2) read

$$\begin{aligned}
&T_t: && t^* = t + a_T, && x_i^* = x_i, \\
& && U_i^* = U_i, && P^* = P; && (3.7)\\
&T_{\text{rot}_\alpha}: && t^* = t, && x_i^* = x_j Q_{ij}^{[\alpha]}, \\
& && U_i^* = U_j Q_{ij}^{[\alpha]}, && P^* = P; && (3.8)\\
&T_{\text{Gal}_i}: && t^* = t, && x_i^* = x_i + f_{\text{Gal}_i}(t), \\
& && U_i^* = U_i + f'_{\text{Gal}_i}(t), && P^* = P - x_j f''_{\text{Gal}_j}(t); && (3.9)\\
&T_P: && t^* = t, && x_i^* = x_i, \\
& && U_i^* = U_i, && P^* = P + f_P(t); && (3.10)
\end{aligned}$$

$$
\begin{aligned}
T_{\mathrm{Sc},I}: \quad & t^* = t, & x_i^* &= x_i e^{a_{\mathrm{Sc},I}}, \\
& U_i^* = U_i e^{a_{\mathrm{Sc},I}}, & P^* &= P e^{2a_{\mathrm{Sc},I}}; \qquad (3.11)\\
T_{\mathrm{Sc},II}: \quad & t^* = t e^{a_{\mathrm{Sc},II}}, & x_i^* &= x_i, \\
& U_i^* = U_i e^{-a_{\mathrm{Sc},II}}, & P^* &= P e^{-2a_{\mathrm{Sc},II}}; \qquad (3.12)
\end{aligned}
$$

where the constant rotational matrices $\boldsymbol{Q}^{[\alpha]}$ are given by

$$
\boldsymbol{Q}^{[1]} = \begin{pmatrix} 1 & 0 & 0 \\ 0 & \cos a_{\mathrm{rot}_1} & -\sin a_{\mathrm{rot}_1} \\ 0 & \sin a_{\mathrm{rot}_1} & \cos a_{\mathrm{rot}_1} \end{pmatrix}; \tag{3.13}
$$

$$
\boldsymbol{Q}^{[2]} = \begin{pmatrix} \cos a_{\mathrm{rot}_2} & 0 & -\sin a_{\mathrm{rot}_2} \\ 0 & 1 & 0 \\ \sin a_{\mathrm{rot}_2} & 0 & \cos a_{\mathrm{rot}_2} \end{pmatrix}; \tag{3.14}
$$

$$
\boldsymbol{Q}^{[3]} = \begin{pmatrix} \cos a_{\mathrm{rot}_3} & \sin a_{\mathrm{rot}_3} & 0 \\ -\sin a_{\mathrm{rot}_3} & \cos a_{\mathrm{rot}_3} & 0 \\ 0 & 0 & 1 \end{pmatrix}, \tag{3.15}
$$

respectively. Therein, the a_i stand for arbitrary real-valued constants, and $f_P(t)$ and $f_{\mathrm{Gal}_i}(t)$ are free time-dependent functions. Notice that in (3.11) and (3.12), we write the scaling factor in exponential form to ensure that (2.3) and (2.4) are fulfilled.

In the viscous case (i.e. $\nu \neq 0$), due to the appearance of the kinematic viscosity, further discussion is necessary. We view the viscosity as an externally imposed constant which, therefore, cannot be affected by any of the symmetries (3.7)–(3.12). Note that by contrast, additional field variables one might consider, such as the temperature or the scalar variables introduced by turbulence models discussed in Section 3.4.1, could be transformed by these symmetries. Therefore, the presence of ν has an important implication for the scaling symmetries (3.11) and (3.12), which can be observed by inserting them into Eq. (1.2),

$$
\left(\frac{\partial U_i^*}{\partial t^*} + U_j^* \frac{\partial U_i^*}{\partial x_j^*} + \frac{\partial P^*}{\partial x_i^*} \right) e^{-a_{\mathrm{Sc},I} + 2a_{\mathrm{Sc},II}} - \nu \frac{\partial^2 U_i^*}{\partial x_j^* \partial x_j^*} e^{a_{\mathrm{Sc},I} + a_{\mathrm{Sc},II}} = 0, \tag{3.16}
$$

where Eq. (2.13) is employed to infer the transformation behavior of the appearing derivatives. Apparently, the viscous term scales differently than the three others. In order for the e-terms to cancel, their exponents have to match, leading to the symmetry-breaking constraint $2a_{\mathrm{Sc},I} = a_{\mathrm{Sc},II}$. In other words, (3.11) and (3.12) combine to a single scaling symmetry

$$
T_{\mathrm{Sc,ns}}: \quad t^* = t e^{2a_{\mathrm{Sc,ns}}}, \quad x_i^* = x_i e^{a_{\mathrm{Sc,ns}}}, \quad U_i^* = U_i e^{-a_{\mathrm{Sc,ns}}}, P^* = P e^{-2a_{\mathrm{Sc,ns}}}, \tag{3.17}
$$

where we denote the group parameter differently in order to avoid confusion. Evidently, the kinematic viscosity acts as a symmetry-breaking property.

Note that a concept closely related to symmetries is that of equivalence transformations. A notable difference is that equivalence transformations do allow transformations of external parameters such as ν (Bluman et al., 2010).

Equivalently, symmetries (3.7)–(3.12) and (3.17) can also be expressed using their infinitesimal generators, which can be calculated by invoking (2.17), and, using the same naming convention in the indices as before, read

$$X_t = \frac{\partial}{\partial t}, \tag{3.18}$$

$$X_{\mathrm{rot}_\alpha} = \epsilon_{jk\alpha} x_j \frac{\partial}{\partial x_k} + \epsilon_{jk\alpha} U_j \frac{\partial}{\partial U_k}, \tag{3.19}$$

$$X_{\mathrm{Gal}} = f_{\mathrm{Gal}_i}(t) \frac{\partial}{\partial x_i} + f'_{\mathrm{Gal}_i}(t) \frac{\partial}{\partial U_i} - x_i f''_{\mathrm{Gal}_i}(t) \frac{\partial}{\partial P}, \tag{3.20}$$

$$X_P = f_P(t) \frac{\partial}{\partial P}, \tag{3.21}$$

$$X_{\mathrm{Sc},I} = x_i \frac{\partial}{\partial x_i} + U_i \frac{\partial}{\partial U_i} + 2P \frac{\partial}{\partial P}, \tag{3.22}$$

$$X_{\mathrm{Sc},II} = t \frac{\partial}{\partial t} - U_i \frac{\partial}{\partial U_i} - 2P \frac{\partial}{\partial P}, \tag{3.23}$$

$$X_{\mathrm{Sc,ns}} = 2t \frac{\partial}{\partial t} + x_i \frac{\partial}{\partial x_i} - U_i \frac{\partial}{\partial U_i} - 2P \frac{\partial}{\partial P}. \tag{3.24}$$

In (3.19), ϵ_{ijk} stands for the Levi-Civita permutation symbol.

All Navier–Stokes symmetries have fundamental physical implications. The time translation symmetry (3.7) allows arbitrarily shifting the temporal coordinate without affecting the physics of the flow, which makes intuitive sense because there is no absolute origin of time. A similar principle concerning the spatial coordinates is encoded in (3.9) with constant $f_{\mathrm{Gal}_i}(t)$. The rotational symmetry (3.8) implies that the orientation of a physical system in space is not relevant, because rotations by an arbitrary fixed angle do not affect the equations. This symmetry is directly connected to the principle of correct tensor formulation, that is, roughly speaking, a set of mathematical rules that must be observed in tensor calculus to ensure that tensorial expressions do not depend on the orientation of the coordinate system. Note that a_{rot_i} must not depend on time, because time-dependent rotation does affect physics, at least in systems where inertial effects play a role, which is generally the case in fluid mechanics. The Galilean symmetry (3.9) with constant $f'_{\mathrm{Gal}_i}(t)$ is also found throughout classical mechanics, and states that physics are not affected by a linear movement of the entire system at a constant velocity. For incompressible flows, even accelerations are possible, provided that the effect on the pressure field is absorbed by transforming it accordingly. Another symmetry that is specific to incompressible flow is the pressure translation symmetry (3.10), because only pressure differences matter, and, therefore, shifting the absolute value of the pressure by some constant does not have any effect. More precisely, this shifting value only has to be constant in space, but it may change over time, which manifests itself by the appearance of the free function $f_P(t)$. Lastly, the two scaling symmetries (3.11) and (3.12) indicate a particular rescaling of space and time that leaves the equations invariant. We may directly connect this to the principle of dimensional correctness if we realize that changing the system of measurement is an example for such a rescaling, and that equations have to be dimensionally correct precisely because the system of measurement must be arbitrary. On a technical note, the analogy between dimensional correctness and the scaling symmetries (3.11) and (3.12) is not perfect, because the way in which the appearance of external parameters such as ν are handled differs slightly. As has been discussed above, in the context of symmetries, we assume such constants to not be affected by any symmetry transformations, which in turn leads to them acting as symmetry-breaking. On the other hand, ν does have dimensional units, so that its value would change when changing the unit system. As a consequence, its appearance does not lead to the Navier–Stokes equations being considered dimensionally incorrect. Note that both points of view ultimately lead to the same conclusions, and the differences discussed here at most lead to a difference in terminology.

This discussion clearly shows how fundamental the implications of these symmetries are. Indeed, they are so intuitive that it becomes obvious why the mathematical possibilities of symmetry theory are so rarely used exhaustively in fluid mechanics and in turbulence modeling: In many cases, physical understanding and intuition suffice. This may explain why, roughly speaking, all complete turbulence models, i.e. models striving for general applicability without the need for flow-specific a priori assumptions, are in agreement with the Navier–Stokes-symmetries in that they fulfill the symmetries (3.7)–(3.10) and (3.17), and, in the limit $\nu = 0$, also (3.11) and (3.12). Examples of symmetry breaking in turbulence models can most prominently be found in simple, flow-specific models such as the mixing length model to be discussed in Section 3.4. Firstly, this model assumes shear flow and an accordingly oriented coordinate system, which renders its equations in violation of the principle of tensorial correctness, or, in terms of the previously described symmetries, they break the rotational symmetry given by Eq. (3.8). Secondly, the introduction of an external length scale breaks the scaling symmetry in space (3.11) (or (3.17) if we assume the viscous case). Both of these symmetry violations are hence connected with well-known limitations of this model. It must be emphasized that symmetry breaking in turbulence models does not automatically lead to bad and physically unreasonable results, but simply restricts the universality of the model, often in ways already foreseen and accepted by the modeler.

When adopting a statistical description of turbulence as given by (1.3) and (1.4), all symmetries of the unaveraged system, i.e. (3.7)–(3.12) and (3.17), which we also refer to as classical symmetries in this work, are preserved. Averaging commutates with applying any of the symmetry transformations (3.7)–(3.12) and (3.17), which makes it straightforward to calculate the transformation behavior of any statistical moment under any of the symmetries. For example, averaging (3.9) leads to

$$T_{\mathrm{Gal}_i}: \ \ t^* = t, \ \ x_i^* = x_i + f_{\mathrm{Gal}_i}(t), \ \ \bar{U}_i^* = \bar{U}_i + f'_{\mathrm{Gal}_i}(t), \ \ \bar{P}^* = \bar{P} - x_j f''_{\mathrm{Gal}_j}(t). \tag{3.25}$$

To infer the transformation of, say, H_{ij}, we apply (3.9) inside the averaging operator, i.e.

$$\begin{aligned} H_{ij}^* = \overline{U_i^* U_j^*} &= \overline{(U_i + f_{\mathrm{Gal}_i}(t))(U_j + f_{\mathrm{Gal}_j}(t))} \\ &= \overline{U_i U_j} + \bar{U}_i f_{\mathrm{Gal}_j}(t) + \bar{U}_j f_{\mathrm{Gal}_i}(t) + f_{\mathrm{Gal}_i}(t) f_{\mathrm{Gal}_j}(t) \\ &= H_{ij} + \bar{U}_i f_{\mathrm{Gal}_j}(t) + \bar{U}_j f_{\mathrm{Gal}_i}(t) + f_{\mathrm{Gal}_i}(t) f_{\mathrm{Gal}_j}(t). \end{aligned} \tag{3.26}$$

Here, we have used the fact that a group parameter, or in this case, the free function $f_{\mathrm{Gal}_i}(t)$, is externally imposed. As a result, it is deterministic and unaffected by the averaging operation. To summarize, the classical symmetries (3.7)–(3.12) and (3.17) written in averaged variables are given by

$$T_t: \ t^* = t + a_T, \ \ x_i^* = x_i, \ \ \bar{U}_i^* = \bar{U}_i, \ \ \bar{P}^* = \bar{P}, \ \ H_{ij}^* = H_{ij}, \ \ \overline{PU_i}^* = \overline{PU_i}; \tag{3.27}$$

$$\begin{aligned} T_{\mathrm{rot}_\alpha}: \ & t^* = t, \ \ x_i^* = x_j Q_{ij}^{[\alpha]}, \ \ \bar{U}_i{}^* = \bar{U}_j Q_{ij}^{[\alpha]}, \ \ \bar{P}^* = \bar{P}, \\ & H_{ij}{}^* = H_{kl} Q_{ik}^{[\alpha]} Q_{jl}^{[\alpha]}, \ \ \overline{PU_i}^* = \overline{PU_j} Q_{ij}^{[\alpha]}; \end{aligned} \tag{3.28}$$

$$
\begin{aligned}
T_{\mathrm{Gal}_i}:\ & t^* = t,\ \ x_i^* = x_i + f_{\mathrm{Gal}_i}(t),\ \ \bar{U}_i^* = \bar{U}_i + f'_{\mathrm{Gal}_i}(t), \bar{P}^* = \bar{P} - x_j f''_{\mathrm{Gal}_j}(t),\\
& H_{ij}^* = H_{ij} + f'_{\mathrm{Gal}_i}(t)\bar{U}_j + f'_{\mathrm{Gal}_j}(t)\bar{U}_i + f'_{\mathrm{Gal}_i}(t) f'_{\mathrm{Gal}_j}(t)\\
& \overline{PU_i}^* = \overline{PU_i} + \bar{P} f'_{\mathrm{Gal}_i}(t) - \bar{U}_i x_j f''_{\mathrm{Gal}_j}(t) - f'_{\mathrm{Gal}_i}(t) x_j f''_{\mathrm{Gal}_j}(t); && (3.29)\\
T_P:\ & t^* = t,\ \ x_i^* = x_i,\ \ \bar{U}_i^* = \bar{U}_i,\ \ \bar{P}^* = \bar{P} + f_P(t),\\
& H_{ij}^* = H_{ij},\ \ \overline{PU_i}^* = \overline{PU_i} + \bar{U}_i f_P(t); && (3.30)\\
T_{\mathrm{Sc},I}:\ & t^* = t,\ \ x_i^* = x_i e^{a_{\mathrm{Sc},I}},\ \ \bar{U}_i^* = \bar{U}_i e^{a_{\mathrm{Sc},I}},\ \ \bar{P}^* = \bar{P} e^{2a_{\mathrm{Sc},I}},\\
& H_{ij}^* = H_{ij} e^{2a_{\mathrm{Sc},I}},\ \ \overline{PU_i}^* = \overline{PU_i} e^{3a_{\mathrm{Sc},I}}; && (3.31)\\
T_{\mathrm{Sc},II}:\ & t^* = t e^{a_{\mathrm{Sc},II}},\ \ x_i^* = x_i,\ \ \bar{U}_i^* = \bar{U}_i e^{-a_{\mathrm{Sc},II}},\ \ \bar{P}^* = \bar{P} e^{-2a_{\mathrm{Sc},II}},\\
& H_{ij}^* = H_{ij} e^{-2a_{\mathrm{Sc},II}},\ \ \overline{PU_i}^* = \overline{PU_i} e^{-3a_{\mathrm{Sc},II}}; && (3.32)\\
T_{\mathrm{Sc,ns}}:\ & t^* = t e^{2a_{\mathrm{Sc,ns}}},\ \ x_i^* = x_i e^{a_{\mathrm{Sc,ns}}},\ \ \bar{U}_i^* = \bar{U}_i e^{-a_{\mathrm{Sc,ns}}} \bar{P}^* = \bar{P} e^{-2a_{\mathrm{Sc,ns}}},\\
& H_{ij}^* = H_{ij} e^{-2a_{\mathrm{Sc,ns}}},\ \ \overline{PU_i}^* = \overline{PU_i} e^{-3a_{\mathrm{Sc},I}}, && (3.33)
\end{aligned}
$$

or, in infinitesimal form,

$$
\begin{aligned}
X_t &= \frac{\partial}{\partial t}, && (3.34)\\
X_{\mathrm{rot}_\alpha} &= \epsilon_{jk\alpha} x_j \frac{\partial}{\partial x_k} + \epsilon_{jk\alpha} \bar{U}_j \frac{\partial}{\partial \bar{U}_k}\\
&\quad + (\epsilon_{ki\alpha} H_{kj} + \epsilon_{kj\alpha} H_{ik}) \frac{\partial}{\partial H_{ij}} + \epsilon_{jk\alpha} \overline{PU_j} \frac{\partial}{\partial \overline{PU_k}}, && (3.35)\\
X_{\mathrm{Gal}} &= f_{\mathrm{Gal}_i}(t) \frac{\partial}{\partial x_i} + f'_{\mathrm{Gal}_i}(t) \frac{\partial}{\partial \bar{U}_i} - x_i f''_{\mathrm{Gal}_i}(t) \frac{\partial}{\partial \bar{P}}\\
&\quad + \left(f'_{\mathrm{Gal}_i}(t)\bar{U}_j + f'_{\mathrm{Gal}_j}(t)\bar{U}_i\right) \frac{\partial}{\partial H_{ij}}, + \left(f'_{\mathrm{Gal}_i}(t)\bar{P} - \bar{U}_i x_j f''_{\mathrm{Gal}_j}(t)\right) \frac{\partial}{\partial \overline{PU_i}}, && (3.36)\\
X_P &= f_P(t) \frac{\partial}{\partial \bar{P}} + f_P(t) \bar{U}_i \frac{\partial}{\partial \overline{PU_i}}, && (3.37)\\
X_{\mathrm{Sc},I} &= x_i \frac{\partial}{\partial x_i} + \bar{U}_i \frac{\partial}{\partial \bar{U}_i} + 2\bar{P} \frac{\partial}{\partial \bar{P}} + 2H_{ij} \frac{\partial}{\partial H_{ij}} + 3\overline{PU_i} \frac{\partial}{\partial \overline{PU_i}}, && (3.38)\\
X_{\mathrm{Sc},II} &= t \frac{\partial}{\partial t} - \bar{U}_i \frac{\partial}{\partial \bar{U}_i} - 2\bar{P} \frac{\partial}{\partial \bar{P}} - 2H_{ij} \frac{\partial}{\partial H_{ij}} - 3\overline{PU_i} \frac{\partial}{\partial \overline{PU_i}}, && (3.39)\\
X_{\mathrm{Sc,ns}} &= 2t \frac{\partial}{\partial t} + x_i \frac{\partial}{\partial x_i} - \bar{U}_i \frac{\partial}{\partial \bar{U}_i} - 2\bar{P} \frac{\partial}{\partial \bar{P}} - 2H_{ij} \frac{\partial}{\partial H_{ij}} - 3\overline{PU_i} \frac{\partial}{\partial \overline{PU_i}}. && (3.40)
\end{aligned}
$$

Note that there are infinitely many statistical moments, and we have only written out the symmetries for those appearing in the analysis in Section 5.1. The action of any of the above symmetries on other statistical moments can be calculated as shown in the example (3.26) or found in Rosteck (2013). In particular, the actions of (3.27)–(3.33) on the moments based on velocity fluctuations are given by

$$
\begin{aligned}
T_t:\ & t^* = t + a_T,\ \ x_i^* = x_i,\ \ \bar{U}_i^* = \bar{U}_i,\ \ \bar{P}^* = \bar{P},\ \ R_{ij}^* = R_{ij},\ \ \overline{pu_i}^* = \overline{pu_i}; && (3.41)\\
T_{\mathrm{rot}_\alpha}:\ & t^* = t,\ \ x_i^* = x_j Q_{ij}^{[\alpha]},\ \ \bar{U}_i{}^* = \bar{U}_j Q_{ij}^{[\alpha]},\ \ \bar{P}^* = \bar{P},\\
& R_{ij}{}^* = R_{kl} Q_{ik}^{[\alpha]} Q_{jl}^{[\alpha]},\ \ \overline{pu_i}^* = \overline{pu_j} Q_{ij}^{[\alpha]}; && (3.42)
\end{aligned}
$$

$$
\begin{aligned}
T_{\mathrm{Gal}_i}:\ & t^* = t,\ \ x_i^* = x_i + f_{\mathrm{Gal}_i}(t),\ \ \bar{U}_i^* = \bar{U}_i + f'_{\mathrm{Gal}_i}(t), \bar{P}^* = \bar{P} - x_j f''_{\mathrm{Gal}_j}(t),\\
& R_{ij}^* = R_{ij},\ \ \overline{pu_i}^* = \overline{pu_i}; \qquad (3.43)\\
T_P:\ & t^* = t,\ \ x_i^* = x_i,\ \ \bar{U}_i^* = \bar{U}_i,\ \ \bar{P}^* = \bar{P} + f_P(t);\\
& R_{ij}^* = R_{ij},\ \ \overline{pu_i}^* = \overline{pu_i}; \qquad (3.44)\\
T_{\mathrm{Sc},I}:\ & t^* = t,\ \ x_i^* = x_i e^{a_{\mathrm{Sc},I}},\ \ \bar{U}_i^* = \bar{U}_i e^{a_{\mathrm{Sc},I}},\ \ \bar{P}^* = \bar{P} e^{2a_{\mathrm{Sc},I}};\\
& R_{ij}^* = R_{ij} e^{2a_{\mathrm{Sc},I}},\ \ \overline{pu_i}^* = \overline{pu_i} e^{3a_{\mathrm{Sc},I}}; \qquad (3.45)\\
T_{\mathrm{Sc},II}:\ & t^* = t e^{a_{\mathrm{Sc},II}},\ \ x_i^* = x_i,\ \ \bar{U}_i^* = \bar{U}_i e^{-a_{\mathrm{Sc},II}},\ \ \bar{P}^* = \bar{P} e^{-2a_{\mathrm{Sc},II}},\\
& R_{ij}^* = R_{ij} e^{-2a_{\mathrm{Sc},II}},\ \ \overline{pu_i}^* = \overline{pu_i} e^{-3a_{\mathrm{Sc},II}}; \qquad (3.46)\\
T_{\mathrm{Sc,ns}}:\ & t^* = t e^{2a_{\mathrm{Sc,ns}}},\ \ x_i^* = x_i e^{a_{\mathrm{Sc,ns}}},\ \ \bar{U}_i^* = \bar{U}_i e^{-a_{\mathrm{Sc,ns}}} \bar{P}^* = \bar{P} e^{-2a_{\mathrm{Sc,ns}}};\\
& R_{ij}^* = R_{ij} e^{-2a_{\mathrm{Sc,ns}}},\ \ \overline{pu_i}^* = \overline{pu_i} e^{-3a_{\mathrm{Sc,ns}}}, \qquad (3.47)
\end{aligned}
$$

and in infinitesimal form by

$$ X_t = \frac{\partial}{\partial t}, \qquad (3.48) $$

$$
\begin{aligned}
X_{\mathrm{rot}_\alpha} = {} & \epsilon_{jk\alpha} x_j \frac{\partial}{\partial x_k} + \epsilon_{jk\alpha} \bar{U}_j \frac{\partial}{\partial \bar{U}_k}\\
& + (\epsilon_{ki\alpha} R_{kj} + \epsilon_{kj\alpha} R_{ik}) \frac{\partial}{\partial R_{ij}} + \epsilon_{jk\alpha} \overline{pu_j} \frac{\partial}{\partial \overline{pu_k}}, \qquad (3.49)
\end{aligned}
$$

$$ X_{\mathrm{Gal}} = f_{\mathrm{Gal}_i}(t) \frac{\partial}{\partial x_i} + f'_{\mathrm{Gal}_i}(t) \frac{\partial}{\partial \bar{U}_i} - x_i f''_{\mathrm{Gal}_i}(t) \frac{\partial}{\partial \bar{P}}, \qquad (3.50) $$

$$ X_P = f_P(t) \frac{\partial}{\partial \bar{P}}, \qquad (3.51) $$

$$ X_{\mathrm{Sc},I} = x_i \frac{\partial}{\partial x_i} + \bar{U}_i \frac{\partial}{\partial \bar{U}_i} + 2\bar{P} \frac{\partial}{\partial \bar{P}} + 2R_{ij} \frac{\partial}{\partial R_{ij}} + 3\overline{pu_i} \frac{\partial}{\partial \overline{pu_i}}, \qquad (3.52) $$

$$ X_{\mathrm{Sc},II} = t \frac{\partial}{\partial t} - \bar{U}_i \frac{\partial}{\partial \bar{U}_i} - 2\bar{P} \frac{\partial}{\partial \bar{P}} - 2R_{ij} \frac{\partial}{\partial R_{ij}} - 3\overline{pu_i} \frac{\partial}{\partial \overline{pu_i}}, \qquad (3.53) $$

$$ X_{\mathrm{Sc,ns}} = 2t \frac{\partial}{\partial t} + x_i \frac{\partial}{\partial x_i} - \bar{U}_i \frac{\partial}{\partial \bar{U}_i} - 2\bar{P} \frac{\partial}{\partial \bar{P}} - 2R_{ij} \frac{\partial}{\partial R_{ij}} - 3\overline{pu_i} \frac{\partial}{\partial \overline{pu_i}}. \qquad (3.54) $$

So far, the discussion of Lie symmetries in fluid mechanics has revealed little beyond what would already be intuitively known to anyone with a decent understanding of classical physics. However, a seminal result by Oberlack and Rosteck (2010) and Rosteck and Oberlack (2011) is that the averaged system given by (1.3), (1.4) and (3.4) and an infinite hierarchy of equations for the higher moments contains additional symmetries that have no counterpart in the original Navier–Stokes system (1.1) and (1.2). As these symmetries are connected to statistical properties of turbulence, we refer to them as statistical symmetries. They are given by the transformations

$$
\begin{aligned}
T_{\mathrm{Sc,stat}}:\ & t^* = t,\ \ x_i^* = x_i,\ \ \bar{U}_i^* = \bar{U}_i e^{a_{\mathrm{Sc,stat}}},\ \ \bar{P}^* = \bar{P} e^{a_{\mathrm{Sc,stat}}},\\
& H_{ij}^* = H_{ij} e^{a_{\mathrm{Sc,stat}}}, \cdots; \qquad (3.55)\\
T_{\mathrm{Tr,stat},1}:\ & t^* = t,\ \ x_i^* = x_i,\ \ \bar{U}_i^* = \bar{U}_i + a_{\mathrm{Tr,stat},I,i},\ \ \bar{P}^* = \bar{P},\\
& H_{ij}^* = H_{ij}, \cdots; \qquad (3.56)
\end{aligned}
$$

$$T_{\text{Tr,stat},2}: \; t^* = t, \;\; x_i^* = x_i, \;\; \bar{U}_i^* = \bar{U}_i, \;\; \bar{P}^* = \bar{P},$$
$$H_{ij}^* = H_{ij} + a_{\text{Tr,stat},II,ij}, \cdots; \tag{3.57}$$
$$T_{\text{Tr,stat},3}: \; t^* = t, \;\; x_i^* = x_i, \;\; \bar{U}_i^* = \bar{U}_i, \;\; \bar{P}^* = \bar{P},$$
$$H_{ij}^* = H_{ij}, \;\; \overline{PU_i}^* = \overline{PU_i} + a_{\text{Tr,stat},III,i}, \tag{3.58}$$
$$\cdots .$$

Again, we can also express these symmetries in infinitesimal form, leading to

$$X_{\text{Sc,stat}} = \bar{U}_i \frac{\partial}{\partial \bar{U}_i} + \bar{P}\frac{\partial}{\partial \bar{P}} + H_{ij}\frac{\partial}{\partial H_{ij}} + \overline{PU_i}\frac{\partial}{\partial \overline{PU_i}} + \cdots, \tag{3.59}$$
$$X_{\text{Tr,stat},1} = \frac{\partial}{\partial \bar{U}_i}, \tag{3.60}$$
$$X_{\text{Tr,stat},2} = \frac{\partial}{\partial H_{ij}}, \tag{3.61}$$
$$X_{\text{Tr,stat},3} = \frac{\partial}{\partial \overline{PU_i}}, \tag{3.62}$$
$$\cdots .$$

In the instantaneous mean Navier–Stokes equations (1.3) and (1.4), both the statistical scaling symmetry (3.55) and the statistical translations symmetries (3.56)–(3.58) can easily be confirmed to be symmetries.

Inserting the transformation (3.55) into (1.4) leads to

$$\frac{\partial \bar{U}_i^*}{\partial t} e^{-a_{\text{Sc,stat}}} + \frac{\partial H_{ij}^*}{\partial x_j} e^{-a_{\text{Sc,stat}}} + \frac{\partial \bar{P}^*}{\partial x_i} e^{-a_{\text{Sc,stat}}} - \nu \frac{\partial^2 \bar{U}_i^*}{\partial x_j \partial x_j} e^{-a_{\text{Sc,stat}}} = 0. \tag{3.63}$$

Clearly, all terms contain the same factor $e^{-a_{\text{Sc,stat}}}$, which cancels out. This also holds for the infinite hierarchy of equations that can be derived for higher moments, which is most clearly observed when using multipoint moments as discussed in Section 3.1.3. For example, after (3.55) is inserted into (3.6), it reads

$$\frac{\partial H_{ij}^*}{\partial t} e^{-a_{\text{Sc,stat}}} + \frac{\partial H_{(ik)j}^*}{\partial x_k} e^{-a_{\text{Sc,stat}}} + \frac{\partial H_{i(jk)}^*}{\partial y_k} e^{-a_{\text{Sc,stat}}} + \frac{\partial \overline{PU_j}^*}{\partial x_i} e^{-a_{\text{Sc,stat}}} + \frac{\partial \overline{U_i P}^*}{\partial y_j} e^{-a_{\text{Sc,stat}}}$$
$$- \nu \frac{\partial^2 H_{ij}^*}{\partial x_k \partial x_k} e^{-a_{\text{Sc,stat}}} - \nu \frac{\partial^2 H_{ij}^*}{\partial y_k \partial y_k} e^{-a_{\text{Sc,stat}}} = 0, \tag{3.64}$$

where $e^{-a_{\text{Sc,stat}}}$ again cancels out.

Furthermore, all statistical moments in the instantaneous formulation appear under a derivative and can, therefore, be shifted by some arbitrary constant as expressed in the statistical translation symmetries (3.56)–(3.58). For example, inserting (3.56) into (1.4) leads to

$$\frac{\partial (\bar{U}_i^* - a_{\text{Tr,stat},I,i})}{\partial t} + \frac{\partial H_{ij}^*}{\partial x_j} + \frac{\partial \bar{P}^*}{\partial x_i} - \nu \frac{\partial^2 (\bar{U}_i^* - a_{\text{Tr,stat},I,i})}{\partial x_j \partial x_j} =$$
$$\frac{\partial \bar{U}_i^*}{\partial t} - \frac{\partial a_{\text{Tr,stat},I,i}}{\partial t} + \frac{\partial H_{ij}^*}{\partial x_j} + \frac{\partial \bar{P}^*}{\partial x_i} - \nu \frac{\partial^2 \bar{U}_i^*}{\partial x_j \partial x_j} + \nu \frac{\partial^2 a_{\text{Tr,stat},I,i}}{\partial x_j \partial x_j} =$$
$$\frac{\partial \bar{U}_i^*}{\partial t} + \frac{\partial H_{ij}^*}{\partial x_j} + \frac{\partial \bar{P}^*}{\partial x_i} - \nu \frac{\partial^2 \bar{U}_i^*}{\partial x_j \partial x_j} = 0, \tag{3.65}$$

which is obviously equivalent to (1.4). Owing to the simple structure of Eq. (3.6), a generalization to arbitrary moments is possible, which allows verifying that the statistical symmetries (3.55)–(3.58) are symmetries of the entire infinite-dimensional hierarchy of statistical moment equations (Rosteck and Oberlack, 2011). Note that these symmetries can also be found in other statistical descriptions of turbulence, including the one-point moment approach, but also the LMN hierarchy and the Hopf functional approach (Waclawczyk et al., 2014).

In the context of turbulence modeling, it is often useful to write the statistical symmetries in terms of the fluctuating one-point moments, e.g. R_{ij}. The statistical scaling symmetry (3.55) for the fluctuating variables can be inferred from the identities arising from application of the averaging rules. For H_{ij}, it holds that

$$\begin{aligned} H_{ij} = \overline{U_i U_j} &= \overline{(\bar{U}_i + u_i)(\bar{U}_j + u_j)} = \overline{\bar{U}_i \bar{U}_j} + \overline{\bar{U}_i u_j} + \overline{u_i \bar{U}_j} + \overline{u_i u_j} \\ &= \bar{U}_i \bar{U}_j + \bar{U}_i \cancel{\bar{u}_j} + \cancel{\bar{u}_i} \bar{U}_j + \overline{u_i u_j} = \bar{U}_i \bar{U}_j + R_{ij}. \end{aligned} \tag{3.66}$$

Here, we have used the fact that the average of an already averaged value can be omitted, i.e. $\bar{\bar{U}}_i = \bar{U}_i$, and that the average of a fluctuation value vanishes, i.e. $\bar{u}_i = 0$, as has already been discussed in Section 3.1.1. Then, the transformation of R_{ij} under e.g. (3.55) can be found to be

$$R^*_{ij} = H^*_{ij} - \bar{U}^*_i \bar{U}^*_j = H_{ij} e^{a_{\text{Sc,stat}}} - \bar{U}_i \bar{U}_j e^{2a_{\text{Sc,stat}}} = (R_{ij} + \bar{U}_i \bar{U}_j) e^{a_{\text{Sc,stat}}} - \bar{U}_i \bar{U}_j e^{2a_{\text{Sc,stat}}}. \tag{3.67}$$

Similarly, the transformation behavior of all moments under all statistical symmetries can be inferred, but we only write out (3.59)–(3.62) for the moments relevant to the present work,

$$\begin{aligned} T_{\text{Sc,stat}}: \; & t^* = t, \;\; x^*_i = x_i, \;\; \bar{U}^*_i = \bar{U}_i e^{a_{\text{Sc,stat}}}, \;\; \bar{P}^* = \bar{P} e^{a_{\text{Sc,stat}}}, \\ & R^*_{ij} = (R_{ij} + \bar{U}_i \bar{U}_j) e^{a_{\text{Sc,stat}}} - \bar{U}_i \bar{U}_j e^{2a_{\text{Sc,stat}}}, \\ & \overline{u_i p}^* = (\overline{u_i p} + \bar{U}_i \bar{P}) e^{a_{\text{Sc,stat}}} - \bar{U}_i \bar{P} e^{2a_{\text{Sc,stat}}}, \end{aligned} \tag{3.68}$$

and the translation symmetries (3.56)–(3.58) become

$$\begin{aligned} T_{\text{Tr,stat,1}}: \; & t^* = t, \;\; x^*_i = x_i, \;\; \bar{U}^*_i = \bar{U}_i + a_{\text{Tr,stat},I,i}, \;\; \bar{P}^* = \bar{P}, \\ & R^*_{ij} = R_{ij} - \bar{U}_i a_{\text{Tr,stat},I,j} - \bar{U}_j a_{\text{Tr,stat},I,i} - a_{\text{Tr,stat},I,i} a_{\text{Tr,stat},I,j}, \\ & \overline{u_i p}^* = \overline{u_i p} - \bar{P} a_{\text{Tr,stat},I,i}; \end{aligned} \tag{3.69}$$

$$\begin{aligned} T_{\text{Tr,stat,2}}: \; & t^* = t, \;\; x^*_i = x_i, \;\; \bar{U}^*_i = \bar{U}_i, \;\; \bar{P}^* = \bar{P}, \\ & R^*_{ij} = R_{ij} + a_{\text{Tr,stat},II,ij}, \;\; \overline{u_i p}^* = \overline{u_i p}; \end{aligned} \tag{3.70}$$

$$\begin{aligned} T_{\text{Tr,stat,3}}: \; & t^* = t, \;\; x^*_i = x_i, \;\; \bar{U}^*_i = \bar{U}_i, \;\; \bar{P}^* = \bar{P}, \;\; R^*_{ij} = R_{ij}, \\ & \overline{u_i p}^* = \overline{u_i p} + a_{\text{Tr,stat},III,i}. \end{aligned} \tag{3.71}$$

The infinitesimal form of these symmetries is given by

$$X_{\text{Sc,stat}} = \bar{U}_i \frac{\partial}{\partial \bar{U}_i} + \bar{P} \frac{\partial}{\partial \bar{P}} + \left(R_{ij} - \bar{U}_i \bar{U}_j\right) \frac{\partial}{\partial R_{ij}} + \left(\overline{p u_i} - \bar{U}_i \bar{P}\right) \frac{\partial}{\partial \overline{p u_i}}, \tag{3.72}$$

$$X_{\text{Tr,stat},1,i} = \frac{\partial}{\partial \bar{U}_i} - \left(\delta_{ij} \bar{U}_k + \delta_{ik} \bar{U}_j\right) \frac{\partial}{\partial R_{jk}} - \bar{P} \frac{\partial}{\partial \overline{p u_i}}, \tag{3.73}$$

$$X_{\text{Tr,stat},2,ij} = \frac{\partial}{\partial R_{ij}}, \tag{3.74}$$

$$X_{\text{Tr,stat},3,i} = \frac{\partial}{\partial \overline{u_i p}}. \tag{3.75}$$

The physical interpretation of these symmetries is more difficult compared to the classical ones, and apart from the models to be presented later in this work (first published in Klingenberg et al., 2020; Klingenberg and Oberlack, 2022), they have so far not been implemented into turbulence models. While an interpretation in the framework of statistical moments remains difficult, Waclawczyk et al. (2014) were able to establish a connection to intermittency and non-Gaussianity—two frequently observed phenomena of turbulent statistics—by considering the statistical symmetries in the PDF framework. A second important indicator for the physical relevance of these symmetries is found in a number of turbulent scaling laws in whose derivation these symmetries are crucial. An example for such a scaling law is the famous logarithmic law of the wall. This aspect is further discussed in Section 3.3. Therefore, we may expect turbulence models which fulfill not only the classical, but also the statistical symmetries, to be significantly more reliable and general. The development of such models is pursued in Chapter 5.

3.3. Turbulent Scaling Laws

Universal theoretical results are rare in turbulence, but the closest approximation to something of this kind are probably turbulent scaling laws. These usually semi-empirical laws are functional dependencies between statistical flow quantities and coordinates that are observed in certain regions of particular flows. The most prominent example for a turbulent scaling law is certainly the logarithmic law of the wall (or log law for short), which originally is valid in a region close to the wall in parallel shear flows such as channel and pipe flow (Kármán, 1930), but is sometimes also considered applicable to other wall-bounded flows such as boundary layers. A fundamental problem with the log law and other scaling laws is that they cannot be derived from the Navier–Stokes equations or other first principles, which can lead to controversy about the question whether they are valid at all, or if different functional dependencies describe the same flow regions better (Barenblatt, 1993; Barenblatt and Prostokishin, 1993; Barenblatt et al., 2014).

Symmetry theory offers a way to mitigate this issue at least to some degree. Instead of relying purely on guesswork and curve-fits, the concept of invariant solutions of symmetries may be employed to find new scaling laws which can in a second step be calibrated and validated using empirical flow data. As we see in the following subsections, some arbitrariness still remains in the choice of symmetries used to generate the invariant solution and more research and a deeper understanding is needed to make the process rigorous, however, in many cases, intuitive arguments can be made to motivate a particular choice.

Fundamentally, some function $\boldsymbol{z} = \boldsymbol{\Theta}(\boldsymbol{x})$ that is (i) invariant under a (possibly multi-parameter) symmetry generator X and is (ii) a solution of the underlying differential equation is defined to be an invariant solution (Bluman et al., 2010). Provided that the symmetry X is given, then, using the invariance condition (2.9), which can now be written as

$$X(z_i - \Theta_i(\boldsymbol{x}))|_{z_i=\Theta_i(\boldsymbol{x})} = 0, \tag{3.76}$$

or, inserting the definition of the infinitesimal generator (2.11),

$$\xi_j \frac{\partial(z_i - \Theta_i(\boldsymbol{x}))}{\partial x_j}\bigg|_{z_i=\Theta_i(\boldsymbol{x})} + \eta_j \frac{\partial(z_i - \Theta_i(\boldsymbol{x}))}{\partial z_j}\bigg|_{z_i=\Theta_i(\boldsymbol{x})}$$
$$= \xi_j \frac{\partial(-\Theta_i(\boldsymbol{x}))}{\partial x_j}\bigg|_{z_i=\Theta_i(\boldsymbol{x})} + \eta_i = -\xi_j \frac{\partial z_i}{\partial x_j} + \eta_i = 0. \tag{3.77}$$

In other words, we are looking for a solution of the quasilinear PDE

$$\xi_j \frac{\partial z_i}{\partial x_j} = \eta_i, \tag{3.78}$$

which can be found using the method of characteristics. An introduction to this method can be found in John (1978). The main idea is that using the characteristic variable τ, (3.78) can be written as the ODE (ordinary differential equation) system

$$\frac{dx_i}{d\tau} = \xi_i, \quad \frac{dz_i}{d\tau} = \eta_i. \tag{3.79}$$

By eliminating τ, one in turn obtains the system

$$\frac{dx_1}{\xi_1} = \frac{dx_2}{\xi_2} = \cdots = \frac{dx_{[n]}}{\xi_{[n]}} = \frac{dz_1}{\eta_1} = \frac{dz_2}{\eta_2} = \cdots = \frac{dz_{[m]}}{\eta_{[m]}}, \tag{3.80}$$

where n and m are the number of independent and dependent variables, respectively, and brackets denote that the Einstein summation over repeated indices is suppressed. The solutions $\boldsymbol{z} = \boldsymbol{\Theta}(\boldsymbol{x})$ of this system are invariant under the symmetry generator X, and it still has to be ensured that they are also solutions of the given differential equation. In the next subsections, we apply this theory to obtain some turbulent scaling laws.

3.3.1. The Logarithmic Law of the Wall

As an example, we consider how to derive the log law from symmetries, following Oberlack et al. (2022). The symmetry generator is a linear combination of (3.38), (3.39) and (3.59)–(3.61) and reads

$$X = a_{\mathrm{Sc},I} x_i \frac{\partial}{\partial x_i} + ((a_{\mathrm{Sc},I} - a_{\mathrm{Sc},II} + a_{\mathrm{Sc,stat}})\bar{U}_i + a_{\mathrm{Tr,stat},I,1}) \frac{\partial}{\partial \bar{U}_i}$$
$$+ ((2(a_{\mathrm{Sc},I} - a_{\mathrm{Sc},II}) + a_{\mathrm{Sc,stat}})H_{ij} + a_{\mathrm{Tr,stat},II,ij}) \frac{\partial}{\partial H_{ij}} \cdots, \tag{3.81}$$

where we have omitted some variables whose scaling behavior is not relevant to this analysis. The resulting invariant surface condition for the moments and components we are interested in then reads

$$\frac{dx_2}{a_{\mathrm{Sc},I} x_2} = \frac{d\bar{U}_1}{(a_{\mathrm{Sc},I} - a_{\mathrm{Sc},II} + a_{\mathrm{Sc,stat}})\bar{U}_1 + a_{\mathrm{Tr,stat},I,1}}$$
$$= \frac{dH_{[ij]}}{(2(a_{\mathrm{Sc},I} - a_{\mathrm{Sc},II}) + a_{\mathrm{Sc,stat}})H_{[ij]} + a_{\mathrm{Tr,stat},II,[ij]}}$$
$$= \frac{dH_{[i_{\{n\}}]}}{(n(a_{\mathrm{Sc},I} - a_{\mathrm{Sc},II}) + a_{\mathrm{Sc,stat}})H_{[i_{\{n\}}]} + a_{\mathrm{Tr,stat},II,[i_{\{n\}}]}}. \tag{3.82}$$

Here, we have adopted the notation introduced in Rosteck (2013), where

$$H_{i_{\{n\}}} = \underbrace{\overline{U_i U_j \cdots}}_{n \text{ times}} \tag{3.83}$$

denotes the nth instantaneous velocity moment. Evidently, depending on the values of the group parameters in (3.82), both a power law and a logarithmic law would be possible for the mean velocity and the second instantaneous moment. However, if we assume that the presence of the wall enters the problem through the wall friction velocity u_τ, then this velocity scale must act as symmetry-breaking. This leads to the constraint $a_{\mathrm{Sc},I} - a_{\mathrm{Sc},II} + a_{\mathrm{Sc,stat}} = 0$ and, thus, the logarithmic law of the wall

$$\bar{U}_1 = \frac{a_{\mathrm{Tr,stat},I,1}}{a_{\mathrm{Sc},I}} \ln x_2 + C_1, \tag{3.84}$$

where C_1 is a constant of integration. It is an important advantage of this method that this immediately also implies scaling laws for the second and all higher moments. From (3.82), it follows that the second moment must scale as

$$H_{ij} = C_{ij} x_2^{1-\frac{a_{\mathrm{Sc},II}}{a_{\mathrm{Sc},I}}} - \frac{a_{\mathrm{Tr,stat},II,ij}}{a_{\mathrm{Sc},I} - a_{\mathrm{Sc},II}}, \tag{3.85}$$

where C_{ij} are also constants of integration. In general, for the nth velocity moment, we obtain

$$H_{i_{(n)}} = C_{i_{\{n\}}} x_2^{(n-1)\left(1-\frac{a_{\mathrm{Sc},II}}{a_{\mathrm{Sc},I}}\right)} - \frac{a_{\mathrm{Tr,stat},II,i_{\{n\}}}}{(n-1)(a_{\mathrm{Sc},I} - a_{\mathrm{Sc},II})}. \tag{3.86}$$

Evidently, (3.85) is a special case of (3.86). Crucially, the appearing group parameters, which must be fitted to experimental or numerical data, are the same in (3.84) as in (3.85), and they obviously also appear in all scaling laws for higher moments given by (3.86). In concrete terms, this implies that the exponents in Eqs. (3.85) and (3.86) are not independent. Therefore, as we increase the number of statistical moments considered in the fit, the relative freedom introduced by the fitting parameters decreases. As is discussed in Oberlack et al. (2022), the fact that the scaling behavior matches very well with numerical data for the first six statistical moments increases the trustworthiness of this scaling law compared to scaling laws that have not been obtained with symmetry methods and can, therefore, only be compared with a single variable, e.g. the mean velocity. One of the main results of Oberlack et al. (2022) is shown in Fig. 3.1, in which the good agreement of Eq. (3.86) with DNS data in the logarithmic region can be observed. Note that Oberlack et al. (2022) also verify that Eq. (3.84) holds, and the corresponding plot can be found in that publication. Following Marusic et al. (2013), the range of validity for the scaling law is assumed to be $3\mathrm{Re}_\tau^{1/2} < x_2 u_\tau/\nu < 0.15\mathrm{Re}_\tau$, though it appears that the fit could even be extended further to the left.

3.3.2. Core Region Deficit Law

If we consider (3.82) in the central region of a channel flow, the absence of an external symmetry-breaking velocity scale such as u_τ implies that $a_{\mathrm{Sc},I} - a_{\mathrm{Sc},II} + a_{\mathrm{Sc,stat}} \neq 0$. Thus, a

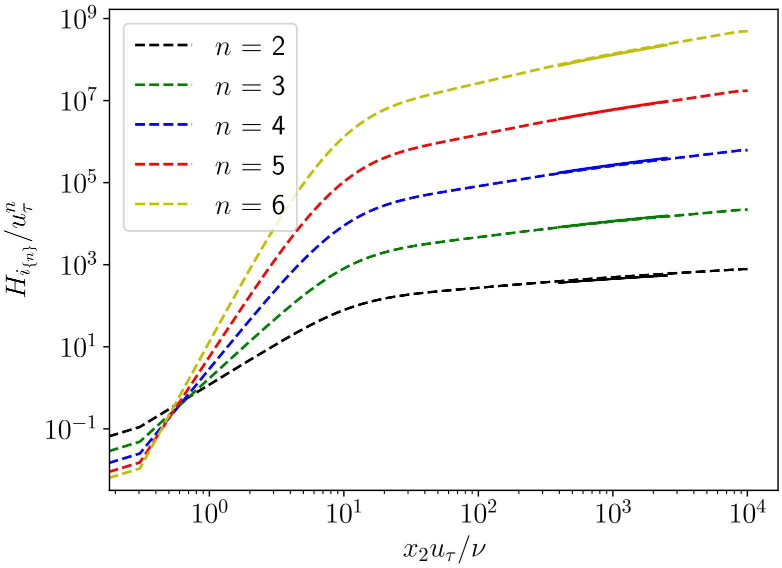

Figure 3.1.: Scaling law given by Eq. (3.86) (solid lines) fitted to numerical Poiseuille flow data (dashed lines; Hoyas et al., 2022). Note that the coordinate system is anchored at the wall, so that the wall is on the left-hand side and the channel center on the right-hand side. The wall-normal coordinate x_2 and the velocity moments are nondimensionalized using the kinematic viscosity ν and the wall friction velocity u_τ. This plot is adapted from Oberlack et al. (2022), and was, like all plots in this work, created using the Python library Matplotlib (Hunter, 2007).

power law for all statistical moments including the first one (i.e. the mean velocity) results,

$$\bar{U}_1 = c_1 x_2^{\frac{a_{\text{Sc},I} - a_{\text{Sc},II} - a_{\text{Sc,stat}}}{a_{\text{Sc},I}}} - \frac{a_{\text{Tr,stat},I,1}}{a_{\text{Sc},I} - a_{\text{Sc},II}}, \tag{3.87}$$

$$H_{ij} = c_{ij} x_2^{\frac{2(a_{\text{Sc},I} - a_{\text{Sc},II}) - a_{\text{Sc,stat}}}{a_{\text{Sc},I}}} - \frac{a_{\text{Tr,stat},II,ij}}{a_{\text{Sc},I} - a_{\text{Sc},II}}, \tag{3.88}$$

$$H_{i_{\{n\}}} = c_{i_{\{n\}}} x_2^{\frac{n(a_{\text{Sc},I} - a_{\text{Sc},II}) - a_{\text{Sc,stat}}}{a_{\text{Sc},I}}} - \frac{a_{\text{Tr,stat},II,i_{\{n\}}}}{a_{\text{Sc},I} - a_{\text{Sc},II}}, \tag{3.89}$$

where we again note that (3.87) and (3.88) are special cases of (3.89), but we write them out for convenience. Note that again, the exponents for arbitrary moments only contain the two free parameters $a_{\text{Sc},II}/a_{\text{Sc},I}$ and $a_{\text{Sc,stat}}/a_{\text{Sc},I}$. Nevertheless, Oberlack et al. (2022) find excellent agreement with DNS data for up to $n = 6$ in a large central region of the flow, as is shown in Fig. 3.2.

Details on the fitting procedure used for obtaining Figs. 3.1 and 3.2 can be found in Laux (2020) and Oberlack et al. (2022).

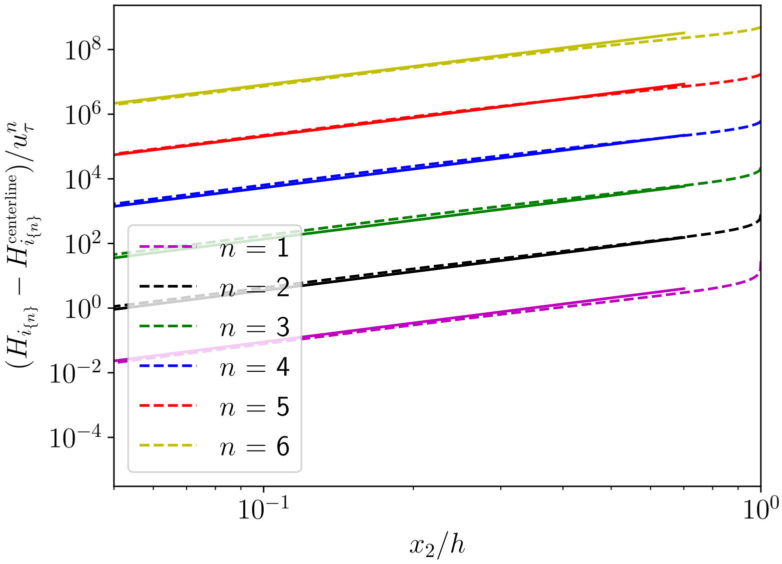

Figure 3.2.: Scaling law given by Eq. (3.89) (solid lines) fitted to numerical Poiseuille flow data (dashed lines; Hoyas et al., 2022). Note that the coordinate system is anchored at the channel center, so that the channel center is on the left-hand side and the wall on the right-hand side, and h stands for the channel half-width. This plot is adapted from Oberlack et al. (2022).

3.3.3. Plane Turbulent Jet Flow

We now turn our attention to self-similar plane jets, where the classical theory, which is further detailed in Section 3.5, can be recovered using invariant solutions, and, more interestingly, a generalized theory can be developed by including additional statistical symmetries.

Classical Scaling Law

We first show how to obtain the classical scaling laws using symmetry methods. By considering the two scaling symmetries $X_{\text{Sc},I}$ and $X_{\text{Sc},II}$ given by Eqs. (3.52) and (3.53), i.e.

$$X = a_{\text{Sc},I} x_i \frac{\partial}{\partial x_i} + (a_{\text{Sc},I} - a_{\text{Sc},II}) \bar{U}_i \frac{\partial}{\partial \bar{U}_i} + 2(a_{\text{Sc},I} - a_{\text{Sc},II}) R_{ij} \frac{\partial}{\partial R_{ij}} \cdots , \tag{3.90}$$

we obtain for the invariant surface condition

$$\frac{dx_1}{a_{\text{Sc},I} x_1} = \frac{dx_2}{a_{\text{Sc},I} x_2} = \frac{d\bar{U}_1}{(a_{\text{Sc},I} - a_{\text{Sc},II}) \bar{U}_1} = \frac{R_{[ij]}}{2(a_{\text{Sc},I} - a_{\text{Sc},II}) R_{[ij]}}, \tag{3.91}$$

where we have omitted moments and components in which we are not interested. Integrating the first part of these equations,

$$\frac{dx_1}{a_{\text{Sc},I} x_1} = \frac{dx_2}{a_{\text{Sc},I} x_2}, \tag{3.92}$$

directly leads to

$$\frac{x_2}{x_1} = c_1. \tag{3.93}$$

The constants of integration, mathematically speaking, are the invariants with respect to the considered symmetries, and, in the context of scaling laws, are referred to as similarity variables. Hence, (3.93) is equivalent to the definition of the classical similarity variable η to be discussed in Section 3.5, where it is given by (3.168). Further, the relation

$$\frac{dx_1}{a_{\text{Sc},I} x_1} = \frac{d\bar{U}_1}{(a_{\text{Sc},I} - a_{\text{Sc},II})\bar{U}_1}, \tag{3.94}$$

can be integrated to read

$$\bar{U}_1 = c_{2_1} x_1^{1 - \frac{a_{\text{Sc},II}}{a_{\text{Sc},I}}}. \tag{3.95}$$

This is equivalent to the classical result given by (3.169), where, as is also shown in Section 3.5, the exponent $1 - a_{\text{Sc},II}/a_{\text{Sc},I}$ can be constrained to $-1/2$. Last, for the Reynolds stresses, we have

$$\frac{dx_1}{a_{\text{Sc},I} x_1} = \frac{dR_{[ij]}}{2(a_{\text{Sc},I} - a_{\text{Sc},II})R_{[ij]}}, \tag{3.96}$$

where the square brackets again indicate that the Einstein summation convention is suppressed. Integration of (3.96) leads to

$$R_{ij} = c_{3_{ij}} x_1^{\frac{2(a_{\text{Sc},I} - a_{\text{Sc},II})}{a_{\text{Sc},I}}}. \tag{3.97}$$

As the exponent in Eq. (3.97) is fixed to be twice as large as the exponent in Eq. (3.95), this is also equivalent to the classical proposition.

However, many publications have found that this classical theory for jets, which can similarly also be applied to other free shear flows, does not always agree well with data, especially for second and higher moments (e.g. George, 1989; Johansson et al., 2003; Uddin and Pollard, 2007). This is often explained by small differences in the experimental or numerical setup, e.g. in the inlet profiles. Having derived these scaling laws from symmetries, a generalization to cover more setups is straightforward, because it simply requires taking into account more symmetries in the first step given by Eq. (3.90). This is discussed in the next section.

Generalized Jet Scaling Law

We now show that by including additional symmetries, we can generalize the classical results to potentially cover more experimental and numerical jet setups. The subsequent analysis is more conveniently conducted in the H-Formulation, but we convert the results back into the more commonly used R-Formulation.

In addition to the two classical scaling symmetries (3.38) and (3.39), we now also consider the statistical scaling symmetry (3.59) and the statistical translation symmetries (3.60) and (3.61). In concrete terms, instead of (3.90), we use

$$\begin{aligned} X = {} & a_{\text{Sc},I} x_i \frac{\partial}{\partial x_i} + \left((a_{\text{Sc},I} - a_{\text{Sc},II} + a_{\text{Sc,stat}}) \bar{U}_i + a_{\text{Tr,stat},I,i} \right) \frac{\partial}{\partial \bar{U}_i} \\ & + \left((2\,(a_{\text{Sc},I} - a_{\text{Sc},II}) + a_{\text{Sc,stat}}) \, H_{ij} + a_{\text{Tr,stat},II,ij} \right) \frac{\partial}{\partial H_{ij}} \cdots . \end{aligned} \tag{3.98}$$

As a result, instead of (3.91), we now obtain the invariant surface condition

$$\frac{dx_1}{a_{\text{Sc},I}x_1} = \frac{dx_2}{a_{\text{Sc},I}x_2} = \frac{d\bar{U}_1}{\left(a_{\text{Sc},I} - a_{\text{Sc},II} + a_{\text{Sc,stat}}\right)\bar{U}_1 + a_{\text{Tr,stat},I,1}}$$
$$= \frac{H_{[ij]}}{\left(2\left(a_{\text{Sc},I} - a_{\text{Sc},II}\right) + a_{\text{Sc,stat}}\right)H_{[ij]} + a_{\text{Tr,stat},II,[ij]}}. \tag{3.99}$$

Clearly, the similarity variable as given by (3.93) can again be obtained from the first identity in (3.99). However, for the mean velocity, integrating

$$\frac{dx_1}{a_{\text{Sc},I}x_1} = \frac{d\bar{U}_1}{\left(a_{\text{Sc},I} - a_{\text{Sc},II} + a_{\text{Sc,stat}}\right)\bar{U}_1 + a_{\text{Tr,stat},I,1}} \tag{3.100}$$

leads to the more general result

$$\bar{U}_1 = c_{2_1} x_1^{\frac{a_{\text{Sc},I} - a_{\text{Sc},II} + a_{\text{Sc,stat}}}{a_{\text{Sc},I}}} - \frac{a_{\text{Tr,stat},I,1}}{a_{\text{Sc},I} - a_{\text{Sc},II} + a_{\text{Sc,stat}}}. \tag{3.101}$$

Evidently, Eq. (3.95) constitutes the special case of $a_{\text{Sc,stat}} = a_{\text{Tr,stat},I,1} = 0$. Last, for the second instantaneous velocity moments, we integrate

$$\frac{dx_1}{a_{\text{Sc},I}x_1} = \frac{H_{[ij]}}{\left(2\left(a_{\text{Sc},I} - a_{\text{Sc},II}\right) + a_{\text{Sc,stat}}\right)H_{[ij]} + a_{\text{Tr,stat},II,[ij]}}. \tag{3.102}$$

which yields

$$H_{ij} = c_{3_{ij}} x_1^{\frac{2(a_{\text{Sc},I} - a_{\text{Sc},II}) + a_{\text{Sc,stat}}}{a_{\text{Sc},I}}} - \frac{a_{\text{Tr,stat},II,ij}}{2\left(a_{\text{Sc},I} - a_{\text{Sc},II}\right) + a_{\text{Sc,stat}}}, \tag{3.103}$$

or, in R-Formulation,

$$\begin{aligned} R_{ij} &= c_{3_{ij}} x_1^{\frac{2(a_{\text{Sc},I} - a_{\text{Sc},II}) + a_{\text{Sc,stat}}}{a_{\text{Sc},I}}} - c_{2_i} c_{2_j} x_1^{2\frac{a_{\text{Sc},I} - a_{\text{Sc},II} + a_{\text{Sc,stat}}}{a_{\text{Sc},I}}} \\ &+ \left(c_{2_i} \frac{a_{\text{Tr,stat},I,j}}{a_{\text{Sc},I} - a_{\text{Sc},II} + a_{\text{Sc,stat}}} + c_{2_j} \frac{a_{\text{Tr,stat},I,i}}{a_{\text{Sc},I} - a_{\text{Sc},II} + a_{\text{Sc,stat}}} \right) x_1^{\frac{a_{\text{Sc},I} - a_{\text{Sc},II} + a_{\text{Sc,stat}}}{a_{\text{Sc},I}}} \\ &- \frac{a_{\text{Tr,stat},I,i} a_{\text{Tr,stat},I,j}}{2(a_{\text{Sc},I} - a_{\text{Sc},II} + a_{\text{Sc,stat}})} - \frac{a_{\text{Tr,stat},II,ij}}{2\left(a_{\text{Sc},I} - a_{\text{Sc},II}\right) + a_{\text{Sc,stat}}}. \end{aligned} \tag{3.104}$$

We note again that from (3.104), Eq. (3.97) can be recovered by setting $a_{\text{Sc,stat}} = a_{\text{Tr,stat},I,1} = a_{\text{Tr,stat},II,ij} = 0$.

Apparently, the scaling law for the mean velocity (3.101) is slightly generalized compared to (3.95) by now allowing some constant to be added to the mean velocity profile. For the classical jet, such a constant would naturally be zero, as the velocity has to vanish for large x_1 and x_2, but for jets with coflow, the constant would be important. Even for the classical jet, however, the scaling law for the Reynolds stresses takes an interesting form. The second term captures the classical behavior, while the first term introduces additional freedom to account for e.g. a sensitivity on initial conditions. The third term vanishes in the absence of a coflow, and in the presence of a coflow, only affects components in the first row and column of the Reynolds stress tensor. Eventually, one of the terms will dominate, but if the exponents take values close to each other, such a classical self-similar behavior is only observed very far downstream, which is indeed often found in experiments (see e.g. Wygnanski and Fiedler, 1969). Using the H-Formulation, self-similarity would be observed much earlier. So far, this behavior has not been confirmed by experiments or simulations, but these results motivate further research into this.

3.4. Turbulence Models

The usefulness of all known exact statistical descriptions of turbulence is limited by the closure problem, i.e. such descriptions cannot in general be used to calculate solutions because the number of unknowns always exceeds the number of equations. In order to obtain results, e.g. in a numerical simulation, it is necessary to break the infinite hierarchy at some point and to introduce empirical closure relations for the unknown terms on that level. Usually, turbulence models are based on the statistical one-point fluctuation moment description introduced in Section 3.1.2, but other approaches based on two-point moments (e.g. Oberlack and Peters, 1993) or on PDFs (e.g. Pope, 1994; Pope, 2011) also exist, though a discussion of such models is beyond the scope of the present work.

The most widely used turbulence models introduce a model for R_{ij} in the mean momentum equation (1.6), i.e. they use

$$\frac{D\bar{U}_i}{Dt} = \frac{\partial \bar{U}_i}{\partial t} + \bar{U}_j \frac{\partial \bar{U}_i}{\partial x_j} = -\frac{\partial \bar{P}}{\partial x_i} + \nu \frac{\partial^2 \bar{U}_i}{\partial x_j \partial x_j} - \frac{\partial \tilde{R}_{ij}}{\partial x_j}, \tag{3.105}$$

where we denote the model term for the Reynolds stress tensor with $\tilde{R}_{ij}$ to highlight the distinction from the exact expression, and $D\bar{U}_i/Dt$ denotes the material derivative. Since this term is interpreted as an additional stress, and, therefore, modeled in analogy to the molecular stress, such models are also referred to as EVMs (Eddy-viscosity models). These model are discussed in more detail in Section 3.4.1.

Models that introduce modeling assumptions one level higher, i.e. for the unknown terms in (3.3), are known as RSMs. Typical modeling assumptions used in models of this class are discussed in Section 3.4.2.

In principle, it would be possible to retain (3.3) exactly and only introduce model assumptions in the equations of the unclosed terms appearing therein. However, due to the fast increase of the number of unknown terms, this is not practically feasible.

In the following review, we mostly restrict ourselves to models that are relevant to the present work. For a broader review, the reader is referred to the article by Leschziner and Drikakis (2002) and the textbooks by Wilcox (1994) and Pope (2000).

3.4.1. Eddy-Viscosity Models

A fundamental idea used for first-order closure was introduced by Boussinesq (1877), who suggested modeling the Reynolds stress tensor in analogy to the molecular stress, leading to

$$\tilde{R}_{ij} = -\nu_t \left(\frac{\partial \bar{U}_i}{\partial x_j} + \frac{\partial \bar{U}_j}{\partial x_i} \right) + \frac{2}{3} k \delta_{ij}. \tag{3.106}$$

This so-called Boussinesq approximation reduces the task of modeling the six independent components of R_{ij} to modeling the turbulent viscosity, or eddy viscosity, ν_t and the turbulent kinetic energy k. One of the simplest models for ν_t is the Prandtl mixing length model (Prandtl, 1925), which is designed for simple, statistically planar shear flows. By assumption, the fluid primarily flows along the x_1-direction and is sheared mainly along the x_2-direction, so that the second right-hand side term in (3.106) either vanishes exactly or can be neglected when inserted into the mean momentum equation (3.105). Then, further invoking an analogy between Reynolds stresses and molecular stresses, Prandtl (1925) makes dimensional arguments to reformulate ν_t in terms of a mixing length L_m,

$$\nu_t = L_m^2 \left| \frac{\partial \bar{U}_1}{\partial x_2} \right|. \tag{3.107}$$

This model works well for simple shear flows, provided that a suitable value for the mixing length is chosen. Unfortunately, it is not possible to know this value a priori, so that this model has to be calibrated for every new flow it is applied to. Some authors refer to such a model as incomplete (Wilcox, 1994). For many canonical flows, where an appropriate value for L_m is already known, this model is nevertheless popular due to its simplicity. Improved versions of the mixing length model were suggested by Smith and Cebeci (1967) and Baldwin and Lomax (1978).

The special-purpose nature of this simple model, which is also observed in other algebraic models, can readily be understood by analyzing it through the lens of Lie symmetries. Notably, Eq. (3.107) breaks the rotational symmetry (3.28) and the scaling symmetry in space (3.31). To observe the breaking of the rotational symmetry, we have to establish how ν_t, L_m and the velocity gradient $\partial \bar{U}_i / \partial x_j$ transform under it. Since ν_t and L_m are scalars, it is clear that they are not affected by a rotation of the coordinate system. The transformation of the velocity gradient under rotation can be calculated from Eq. (3.28) using Eq. (2.13) and reads

$$\frac{\partial \bar{U}_i^*}{\partial x_j^*} = \frac{\partial \bar{U}_k}{\partial x_l} Q_{ik}^{[\alpha]} Q_{jl}^{[\alpha]}. \tag{3.108}$$

For example, assuming $\alpha = 3$, insertion into (3.107) then leads to

$${\nu_t}^* = {L_m^*}^2 \left| \frac{\partial \bar{U}_2^*}{\partial x_1^*} \right|, \tag{3.109}$$

which is obviously not the same as Eq. (3.107). Evidently, Eq. (3.107) breaks the rotational symmetry because of the restriction to shear flows, and the associated fixed choice of the coordinate system orientation. The practical implication of this somewhat technical discussion is that it is unclear how to apply (3.107) to general flows, because then, it would not be obvious which component of the velocity gradient to use.

The breaking of the scaling symmetry in space can best be observed if we insert (3.107) into (3.106), which, due to the abovementioned restriction to shear flows only makes sense for the $(1, 2)$-component and leads to

$$\tilde{R}_{12} = -L_m^2 \left| \frac{\partial \bar{U}_1}{\partial x_2} \right| \frac{\partial \bar{U}_1}{\partial x_2}. \tag{3.110}$$

As has been discussed in Section 3.2 in the context of the kinematic viscosity, an externally imposed variable such as L_m cannot be affected by any of the symmetries. Thus, inserting the scaling symmetry in space (3.31) into (3.110) yields

$$\tilde{R}_{12}^* e^{-2a_{\mathrm{Sc},I}} = -{L_m^*}^2 \left| \frac{\partial \bar{U}_1^*}{\partial x_2^*} \right| \frac{\partial \bar{U}_1^*}{\partial x_2^*}. \tag{3.111}$$

Since the $e^{-2a_{\text{Sc},I}}$ cannot be cancelled, it is clear that (3.110) breaks the scaling symmetry (3.31). This symmetry breaking due to the appearance of an external dimensional scale L_m is intimately connected with the observation that the appropriate value for L_m differs in every flow.

Interestingly, one of the perhaps most widely used turbulence models, the Spalart–Allmaras model (Spalart and Allmaras, 1992), is also incomplete. Its focus on shear flows already manifests itself in the model for $\tilde{R}_{ij}$, for which it uses Eq. (3.106) but without the k-term, because, as discussed above, this term is not important in such flows. The modeling efforts are entirely focused on ν_t, which is formulated in terms of an auxiliary variable $\tilde{\nu}$, whose entirely empirical transport equation reads

$$\begin{aligned}\frac{D\tilde{\nu}}{Dt} &= C_{b1}(1-f_{t2})\tilde{S}\tilde{\nu} - \left(C_{w1}f_w - \frac{C_{b1}}{\kappa^2}f_{t2}\right)\left(\frac{\tilde{\nu}}{d}\right)^2 \\ &+ \frac{1}{\tilde{\sigma}}\left(\frac{\partial}{\partial x_j}\left((\nu+\tilde{\nu})\frac{\partial\tilde{\nu}}{\partial x_j}\right) + C_{b2}\frac{\partial\tilde{\nu}}{\partial x_j}\frac{\partial\tilde{\nu}}{\partial x_j}\right) + f_{t1}\frac{\partial^2(\bar{U}_i\bar{U}_i)}{\partial x_j\partial x_j}.\end{aligned} \tag{3.112}$$

Therein,

$$\tilde{\nu} = \frac{\nu_t}{f_{v1}}, \quad \tilde{S} = 2\sqrt{\left(\frac{\partial\bar{U}_i}{\partial x_j} - \frac{\partial\bar{U}_j}{\partial x_i}\right)\left(\frac{\partial\bar{U}_i}{\partial x_j} - \frac{\partial\bar{U}_j}{\partial x_i}\right)} + \frac{\tilde{\nu}}{\kappa^2 d^2}f_{t2}, \tag{3.113}$$

where κ is the von Kármán constant, d the distance from the wall, all C_i are empirical model constants and the f_i are empirical functions whose form can be found in Spalart and Allmaras (1992). Without going into further detail, the specialized nature of this model should already be apparent. As is made clear in the original publication, the main goal of this model is to yield good results in shear flows with minimal computational effort, while sacrificing general validity of the model. From an industrial perspective, this makes the model attractive, especially in fields such as airplane engineering, where only a few particular flow types are of interest. Therefore, it should not be surprising that the Spalart–Allmaras model does not fulfill all classical symmetries, and, in particular, breaks the scaling symmetry in space (3.31) due to the appearance of the dimensional property d. This again shows that symmetry breaking does not allow any conclusions about the usefulness of a model, but only about its generality.

Nevertheless, there are many practical flow problems that are not well-investigated, and for which no special-purpose turbulence model is available. Therefore, in order to overcome the limitations associated with such relatively simple models and to obtain a complete model, i.e. a model that can reasonably be expected to generalize to flows without any a priori calibration, it is necessary to find more sophisticated and robust ways to calculate k and ν_t. Since k is defined as $\tilde{R}_{ii}/2$, an exact but unclosed equation for it can be obtained by contracting the indices in (3.3). In order to form dimensionally correct expressions from which to obtain ν_t, a transport equation for a second scale-providing variable has to be formulated as well. Two-equation models are primarily different in this choice. In contrast to algebraic models such as the mixing length model, which introduce almost no computational overhead compared to a laminar flow simulation, two-equation models do require moderately more computational effort. The probably most well-known turbulence model is the k-ε-model (Jones and Launder, 1972), which employs the turbulent dissipation ε as the second variable. Dimensional arguments then lead to

$$\nu_t = C_\mu\frac{k^2}{\varepsilon}, \tag{3.114}$$

where C_μ is a dimensionless model parameter. In the exact equation for k, the production term appears in closed form, and dissipation and two other unknown correlations that are generally interpreted as diffusion terms have to modeled. Since the k-ε-model already contains the dissipation as the second model variable, this term is taken care of. The diffusion is then modeled using a gradient-diffusion hypothesis, leading to

$$\frac{Dk}{Dt} = -\tilde{R}_{ij}\frac{\partial \bar{U}_i}{\partial x_j} - \varepsilon + \frac{\partial}{\partial x_j}\left(\left(\nu + \frac{\nu_t}{\sigma_k}\right)\frac{\partial k}{\partial x_j}\right). \tag{3.115}$$

Even though an exact equation for ε can be derived, it did not prove useful as a starting point from which to develop its model equation. Two reasons are typically invoked for this: First, the exact ε-equation is very complicated, with many unknown and difficult to measure terms, and, second, the ε appearing in the k-ε-model primarily acts as a scale-providing variable that is best interpreted as the energy flow rate of the turbulent cascade, and as such is determined by large-scale motion. On the other hand, the exact equation for ε is closely related to viscous effects that are only relevant for small-scale motion (Pope, 2000). Therefore, a purely empirical equation whose structure is based on the k-equation (3.115),

$$\frac{D\varepsilon}{Dt} = -C_{\varepsilon,1}\frac{\varepsilon}{k}\tilde{R}_{ij}\frac{\partial \bar{U}_i}{\partial x_j} - C_{\varepsilon,2}\frac{\varepsilon^2}{k} + \frac{\partial}{\partial x_j}\left(\left(\nu + \frac{\nu_t}{\sigma_\varepsilon}\right)\frac{\partial \varepsilon}{\partial x_j}\right), \tag{3.116}$$

is used. The appearing model parameters $C_{\varepsilon,1}, C_{\varepsilon,2}$ and σ_ε (together with the parameters C_μ and σ_k) offer enough flexibility to calibrate this model against a wide range of canonical flows, resulting in a model that can be expected to yield reasonably accurate results for many simple and moderately complex flows, though it must be mentioned that the generality of this model is still restricted by factors unrelated to the classical symmetries (3.27)–(3.33). The arguments used in the calibration process are discussed in Section 3.4.1.

Another popular choice for the second scale-providing variable is the turbulent dissipation rate ω. Two-equation models were thus formulated as early as Kolmogorov (1942) and later by Saffmann (1970) and Launder and Spalding (1972). However, when talking about the standard k-ω-model, one today typically refers to the work of Wilcox (1988) and Wilcox (2007). Using analogous arguments as those leading to the k-ε-model, the k-ω-model reads

$$\nu_t = C_\omega \frac{k}{\omega}, \tag{3.117}$$

$$\frac{Dk}{Dt} = -\alpha^* \tilde{R}_{ij}\frac{\partial \bar{U}_i}{\partial x_j} - \beta^* k\omega + \frac{\partial}{\partial x_j}\left((\nu + \nu_t\sigma^*)\frac{\partial k}{\partial x_j}\right), \tag{3.118}$$

$$\frac{D\omega}{Dt} = -\alpha\frac{\omega}{k}\tilde{R}_{ij}\frac{\partial \bar{U}_i}{\partial x_j} - \beta\omega^2 + \frac{\partial}{\partial x_j}\left((\nu + \nu_t\sigma)\frac{\partial \omega}{\partial x_j}\right), \tag{3.119}$$

where again, a model calibration is possible using the free constants $\alpha, \beta, \sigma, \beta^*$ and σ^*. Note that the model constants C_ω and α^* are equal to unity and, therefore, usually not introduced in the literature. The reason why we introduce them here lies in their relevance to the numerical solution method discussed in Section 4.3.3.

Generally speaking, the choice of the second scale-providing variable matters relatively little, which also helps explain why other two-equation models that have been proposed have not seen widespread adoption. Since, for example, ω can be expressed in terms of k and ε, Eq. (3.119) can be turned into a transport equation for ε that only differs slightly from Eq. (3.116). The main difference is that the diffusion term gives rise to an additional so-called cross-diffusion term. Note, however, that this term can be crucial in some situations, for example in free shear flows, where it ensures that the results of the k-ε-model, unlike those of the k-ω-model, do not depend on the arbitrary free-stream boundary conditions. In fact, in an effort to obtain a model that combines the advantages of the k-ε-model and the k-ω-model, Menter (1994) proposed his k-ω SST (shear-stress transport) model, which is a k-ω-model that uses such cross-diffusion terms in conjunction with an adaptation of the model parameters to blend between k-ω-model behavior and k-ε-model behavior depending on the circumstances. Another difference between the k-ε-model and the k-ω-model lies in the behavior of the second scale-providing variable in the vicinity of solid boundaries. Here, ε behaves more reasonably than ω, which becomes singular close to walls. However, since typically the near-wall region is not resolved, but calculated using wall-functions, this is not as big an issue in practice as it might seem at first glance. Boundary conditions for ω in the context of high-order codes are discussed in Section 4.3.

Historically, each new generation of turbulence models fulfilled more symmetries than the previous one, with two-equation models being the first class to fulfill all classical symmetries given by (3.27)–(3.32) (the last two of which combine to (3.33) in the viscous case), which is deeply connected to their completeness. Interestingly, the perhaps most prominent shortcoming of linear EVMs—their inability to predict rotating or high streamline curvature flows accurately (Hirai et al., 1988; Rubinstein and Zhou, 2004)—is also connected to symmetries. Here, however, the issue arises from Eq. (3.106) admitting too many symmetries (Oberlack, 2000), because its right-hand side is invariant under a time-dependent rotation of the system, i.e. (3.28) with time-dependent a_{rot_α}. Whereas this property, which is also known as objectivity, makes sense for the molecular stress tensor, it does not apply to Reynolds stresses, because they are affected by inertial effects. The simplest way to overcome this issue is by extending (3.106) with additional terms that include not only the symmetric, but also the antisymmetric part of the velocity gradient. Such NLEVMs (nonlinear Eddy-viscosity models) replace Eq. (3.106) with an equation of the form

$$\tilde{R}_{ij} = \frac{2}{3} k \delta_{ij} + \sum_k F_{ij}^k, \tag{3.120}$$

where the F_{ij}^k are functions of tensor products of the symmetric part of the velocity gradient S_{ij} given by

$$S_{ij} = \frac{1}{2}\left(\frac{\partial \bar{U}_i}{\partial x_j} + \frac{\partial \bar{U}_j}{\partial x_i}\right) \tag{3.121}$$

and the antisymmetric part of the velocity gradient W_{ij}

$$W_{ij} = \frac{1}{2}\left(\frac{\partial \bar{U}_i}{\partial x_j} - \frac{\partial \bar{U}_j}{\partial x_i}\right). \tag{3.122}$$

Obviously, Eq. (3.106) is a special case of Eq. (3.120), which only uses $F_{ij}^1 = 2S_{ij}$. Crucially, unlike S_{ij}, W_{ij} is sensitive to a time-dependent rotation of the system. This means that in contrast to Eq. (3.106), Eq. (3.120) can be formulated such that the effect of system rotation on the Reynolds stresses $\tilde{R}_{ij}$ is properly incorporated into the model. Note that by virtue of the Cayley-Hamilton theorem, it can be shown that there are only ten independent symmetric tensor products that could appear in (3.120), though NLEVMs rarely use more than six terms. Interestingly, (3.120) can also be obtained by invoking a number of simplifying approximations to RSMs. Models arising from such arguments are also known as EARSMs (explicit algebraic Reynolds stress models) and are further discussed in Section 3.4.3.

Examples for NLEVMs and EARSMs include those developed in Shih and Zhu (1993), Wallin and Johansson (2000), Yoshizawa (1984), Gatski and Speziale (1993), Rubinstein and Barton (1990), and Craft et al. (1996). Like the class of RSMs discussed in Section 3.4.2, these models are in complete agreement with the classical symmetries (3.27)–(3.33).

Calibration of Two-Equation Eddy-Viscosity Models

We now address the question of how to assign appropriate values to the model parameters appearing in Eqs. (3.114)–(3.119). As is discussed in the textbooks by Wilcox (1994) and Pope (2000), most two-equation models follow more or less the same systematic approach. In the following, the primary focus lies on the k-ε-model.

Homogeneous Turbulence First, the arguably simplest nontrivial turbulent flow case is considered. In homogeneous turbulence, by assumption, all spatial gradients vanish, so that Eqs. (3.115) and (3.116) simplify to

$$\frac{dk}{dt} = -\varepsilon, \tag{3.123}$$

$$\frac{d\varepsilon}{dt} = -C_{\varepsilon,2}\frac{\varepsilon^2}{k}, \tag{3.124}$$

whose solution reads

$$k(t) \propto t^{\frac{1}{1-C_{\varepsilon,2}}}, \;\; \varepsilon(t) \propto t^{\frac{C_{\varepsilon,2}}{1-C_{\varepsilon,2}}}. \tag{3.125}$$

Due to the absence of mean velocity gradients, we expect k and ε to decay over time. Such homogeneous, isotropic turbulence is difficult to study experimentally, but, due to its significance for turbulence model calibration, the exponent of k in (3.125) has been determined to lie in the range from -1.15 to -1.45 (Pope, 2000), though the standard choice of $C_{\varepsilon,2} = 1.92$ leads to an exponent slightly below this observed range. For the k-ω-model, analogous arguments lead to the constraint that the ratio β^*/β must be around 1.2 (Wilcox, 1994).

Homogeneous Shear Turbulence Having thus constrained the dissipation term in the ε-equation, the next step is to fix the relative magnitude of the production term. This is accomplished by considering homogeneous shear turbulence. Like in homogeneous turbulence, the spatial gradients of k and ε vanish, but one component of the velocity gradient takes a nonzero value of $2S_{12}$. The model equations then read

$$\frac{dk}{dt} = 4C_\mu\frac{k^2}{\varepsilon}S_{12}^2 - \varepsilon, \tag{3.126}$$

$$\frac{d\varepsilon}{dt} = 4C_{\varepsilon,1}C_\mu k S_{12}^2 - C_{\varepsilon,2}\frac{\varepsilon^2}{k}, \tag{3.127}$$

from which the temporal evolution of the ratio k/ε can be determined to be

$$\frac{d}{dt}\left(\frac{k}{\varepsilon}\right) = \frac{dk}{dt}\frac{1}{\varepsilon} - \frac{d\varepsilon}{dt}\frac{k}{\varepsilon^2} = 4C_\mu S_{12}^2 \frac{k^2}{\varepsilon^2}(1 - C_{\varepsilon,1}) - (1 - C_{\varepsilon,2}). \tag{3.128}$$

For large times, experimental data suggests an exponential growth according to

$$k = k_0 e^{\lambda_k t}, \tag{3.129}$$

$$\varepsilon = \varepsilon_0 e^{\lambda_\varepsilon t}, \tag{3.130}$$

which, inserted into (3.126) and (3.127), leads to the relation

$$S^2 \frac{k_0^2}{\varepsilon_0^2} = \frac{1}{C_\mu} \frac{C_{\varepsilon,2} - 1}{C_{\varepsilon,1} - 1}, \tag{3.131}$$

and the constraint that all exponents must be the same, i.e. $\lambda = \lambda_k = \lambda_\varepsilon$. From this, λ can be determined to be

$$\lambda = S_{12} \sqrt{C_\mu \frac{C_{\varepsilon,1} - 1}{C_{\varepsilon,2} - 1}} \left(\frac{C_{\varepsilon,2} - 1}{C_{\varepsilon,1} - 1} - 1 \right). \tag{3.132}$$

During this exponential growth of k and ε, in the limit of large times, the ratio k/ε and the ratio of production to dissipation $4C_\mu S_{12}^2 k^2/\varepsilon^2$ eventually becomes constant, with the latter assuming a value around 1.7 (e.g. Pope, 2000). This leads to a vanishing left-hand side of Eq. (3.128), so that the ratio $4C_\mu S_{12}^2 k^2/\varepsilon^2$ is determined by $C_{\varepsilon,1}$ and $C_{\varepsilon,2}$. Note that inserting the standard value of $C_{\varepsilon,1} = 1.44$ into (3.128) yields a significantly higher ratio of production to dissipation of approximately 2.1 (Pope, 2000). According to Wilcox (1994), the standard k-ω-model does not invoke this test case and instead determines α from the log layer, which we consider next.

The Log Region Turning again to the k-ε-model, we assume parallel channel flow along the x_1-direction, with x_2 denoting the wall-normal coordinate. Further, we assume viscous effects to be negligible. Then, the mean momentum equation (3.105) simplifies to

$$0 = \frac{\partial}{\partial x_2}\left(\nu_t \frac{\partial \bar{U}_1}{\partial x_2} \right), \tag{3.133}$$

and the equations for k and ε become

$$0 = C_\mu \frac{k^2}{\varepsilon} \left(\frac{\partial \bar{U}_1}{\partial x_2} \right)^2 - \varepsilon + \frac{\partial}{\partial x_2}\left(\frac{\nu_t}{\sigma_k} \frac{\partial k}{\partial x_2} \right), \tag{3.134}$$

$$0 = C_{\varepsilon,1} C_\mu k \left(\frac{\partial \bar{U}_1}{\partial x_2} \right)^2 - C_{\varepsilon,2} \frac{\varepsilon^2}{k} + \frac{\partial}{\partial x_2}\left(\frac{\nu_t}{\sigma_\varepsilon} \frac{\partial \varepsilon}{\partial x_2} \right). \tag{3.135}$$

To find a solution of Eqs. (3.133)–(3.135), we insert the famous logarithmic law for the velocity and make a power-law ansatz for k and ε using ν and the wall friction velocity u_τ for nondimensionalization

$$\bar{U}_1 = \frac{u_\tau}{\kappa} \ln x_{2+} + B, \quad k = C_k {u_\tau}^2 x_{2+}^{n_k}, \quad \varepsilon = C_\varepsilon \frac{{u_\tau}^4}{\nu} x_{2+}^{n_\varepsilon}, \tag{3.136}$$

where $x_{2+} = x_2 u_\tau/\nu$, and κ is the famous von Kármán constant. Insertion of this ansatz into (3.133) leads to the constraint $2n_k - n_\varepsilon = 1$. At the same time, the requirement that the scaling exponents of the production and dissipation terms in Eq. (3.134) must match yields $n_k - n_\varepsilon = 1$. In order for these two constraints to be fulfilled simultaneously, $n_k = 0$ and $n_\varepsilon = -1$ must hold. Indeed, k is usually assumed to be constant in the log layer. Further inspection of Eq. (3.134) also reveals that due to the constancy of k, the diffusion term vanishes, so that production and dissipation are in balance. Using this equality leads to the classical result that

$$\varepsilon = \frac{{u_\tau}^3}{\kappa x_2}, \tag{3.137}$$

or, equivalently, $C_\varepsilon = 1/\kappa$, so that the k-equation gives the relation

$$k = \frac{{u_\tau}^2}{\sqrt{C_\mu}}, \tag{3.138}$$

which, inserted into the ε-equation, then yields

$$\sigma_\varepsilon = \frac{\kappa^2}{\sqrt{C_\mu}(C_{\varepsilon,2} - C_{\varepsilon,1})}. \tag{3.139}$$

Additionally, the ratio of $\tilde{R}_{12}$ and k, by virtue of the Boussinesq approximation (3.106) together with (3.114), (3.137) and (3.138), can be shown to be

$$\frac{\tilde{R}_{12}}{k} = \sqrt{C_\mu}. \tag{3.140}$$

Experimental data implies that this ratio is around 0.3, leading to the choice of $C_\mu = 0.09$. With all variables of the right-hand side of Eq. (3.139) thus known, this equation can be used to yield $\sigma_\varepsilon = 1.3$. The only remaining model parameter σ_k is set to unity in the standard model.

For the k-ω-model, the analog of (3.140) constrains β^* to 0.09, and the analog of (3.139) is used to set α to $5/9$. This choice of α requires a value for σ, which Wilcox (1994) infers from a numerical investigation of the defect region of a boundary layer flow. In conclusion, the model parameters of the standard k-ε-model are (Jones and Launder, 1972)

$$C_\mu = 0.09, \quad \sigma_k = 1.0, \quad C_{\varepsilon,1} = 1.44, \quad C_{\varepsilon,2} = 1.92, \quad \sigma_\varepsilon = 1.3, \tag{3.141}$$

and for the standard k-ω-model (Wilcox, 1988)

$$C_\omega = 1.0, \quad \alpha^* = 1.0, \quad \beta^* = 0.09, \quad \sigma^* = 0.5, \quad \alpha = 5/9, \quad \beta = 3/40, \quad \sigma = 0.5. \tag{3.142}$$

This concludes the discussion of common canonical flows used for the calibration of model parameters in EVMs. As we see in Section 5.2.1, the range of flows that can be used to set the model parameters is somewhat narrow compared to the models to be developed in Chapter 5.

Modifications for Increased Numerical Stability

As things stand, the equations of the k-ε-model and the k-ω-model are notorious for their associated numerical difficulties. In the context of classical numerical schemes, which tend to use an FVM (Finite Volume Method) discretization associated with a high numerical diffusion, this issue usually manifests itself less strongly. Moreover, such implementations typically rely on a segregated solution approach, so that even in the worst case, convergence will usually be accomplished, though possibly slow.

Even in such traditional solvers, one minor tweak is often used that concerns some of the source terms in the equations for the turbulent scalars, which can have an adverse effect on the diagonal dominance of the matrix. Therefore, in the context of steady-state calculations, for example, the dissipation term in the k-equation is often multiplied with the ratio of k^{n+1}/k^n, where k^n denotes the value from the current iteration, and k^{n+1} that from the previous one (Schäfer, 2006). Obviously, in the limit of a stationary solution, $k^n = k^{n+1}$, so that this modification does not affect the final result.

In the context of higher-order schemes such as the DG method to be discussed in Section 4.1, however, numerical problems manifest themselves so strongly as to require further consideration. Much of the pioneering work on this has been carried out in the context of the k-ω-model (Bassi et al., 2005; Bassi et al., 2014), but the results can be applied to other two-equation models as well (e.g. Tiberga et al., 2020). One important problem results from the fact that ω appears in the denominator in Eqs. (3.117)–(3.119). In theory, this is not an issue, because ω has to be strictly positive. However, in the context of high-order numerical schemes, it is common for an intermediate solution to contain areas where ω becomes zero or negative, often near walls. Without special treatment, such areas will obviously lead to immediate numerical problems and inhibit further convergence. Therefore, Bassi et al. (2005) suggest an approach first introduced by Ilinca and Pelletier (1998) in the context of an FEM (Finite Element Method) implementation of the k-ε-model. The main idea is that instead of ω, an equation for $\tilde{\omega} = \ln \omega$ is solved. Since this means that $\omega = \exp \tilde{\omega}$, it is ensured that ω is always strictly positive, regardless of the value of $\tilde{\omega}$. The resulting equation for $\tilde{\omega}$ is structurally similar to the ω-equation (3.119) and reads

$$\frac{D\tilde{\omega}}{Dt} = -\frac{\alpha}{k}\tilde{R}_{ij}\frac{\partial \bar{U}_i}{\partial x_j} - \beta e^{\tilde{\omega}} + (\nu + \nu_t \sigma)\frac{\partial \tilde{\omega}}{\partial x_j}\frac{\partial \tilde{\omega}}{\partial x_j} + \frac{\partial}{\partial x_j}\left((\nu + \nu_t \sigma)\frac{\partial \tilde{\omega}}{\partial x_j}\right). \tag{3.143}$$

Additionally, Bassi et al. (2005) advocate for the use of realizability conditions to impose a stronger lower bound for ω, which improves numerical stability even more. In concrete terms, the realizability conditions (Lumley, 1979) for the modeled Reynolds stress tensor are $\tilde{R}_{ij}$

$$\tilde{R}_{[ii]} \geq 0 \ \ \forall i = 1, 2, 3; \tag{3.144}$$

$$\frac{\tilde{R}^2_{[ij]}}{\tilde{R}_{[ii]}\ \tilde{R}_{[jj]}} \leq 1 \ \ \forall i, j = 1, 2, 3, \tag{3.145}$$

which follow from the fact that squares of real numbers cannot be negative, and the Cauchy–Schwarz inequality, respectively. The Boussinesq approximation (3.106) with (3.117), however, does not guarantee that (3.144) and (3.145) are fulfilled in general. It turns out that inserting the Boussinesq approximation into the realizability conditions (3.144) and (3.145) gives rise to constraints on the lower bound ω_{min} which read

$$\omega_{\text{min}} - S_{ii} = 0 \;\; \forall i = 1, 2, 3, \tag{3.146}$$

$$\omega_{\text{min}}^2 - 3\left(S_{ii} + S_{jj}\right)\omega_{\text{min}} + 9\left(S_{ii}S_{jj} - S_{ij}S_{ij}\right) = 0 \;\; \forall i, j = 1, 2, 3; i \neq j, \tag{3.147}$$

where S_{ij} represents the symmetric part of the velocity gradient as defined by Eq. (3.121). For k, a simple limiting in the form $k' = \max(0, k)$ can be used, because in the k-ω-model, k never appears in the denominator.

As a final remark, the use of DG and other high-order methods for turbulence models is often criticized on the grounds that the model error dominates the numerical error anyway, so that the increased complexity and effort associated with a more sophisticated numerical scheme cannot be justified. However, the discussion in this section shows that making the numerical issues of turbulence models visible by using more sensitive schemes can lead to these issues being addressed. In turn, the modifications discussed here are also advantageous in the context of classical FVM schemes, even though they might not be as crucial. Therefore, it is difficult to dispute the usefulness of high-order methods for model development, even if the resulting model might be better solved using more traditional numerical schemes.

3.4.2. Reynolds Stress Models

Instead of inserting modeling assumptions for R_{ij} directly into Eq. (1.6), it is also possible to only introduce such approximations one level higher, i.e. in Eq. (3.3). This naturally leads to a more general model into which more physical effects can be incorporated, though this comes at the cost of an increased model complexity, because (3.3) alone consists of six independent equation components. This approach was pioneered by Rotta (1951), who, without the ability to perform numerical simulations, managed to develop closure relations that still form the basis of modern RSMs. Interestingly, some of the most important ideas to improve upon these early models include invariant modeling (Donaldson and Rosenbaum, 1968), which has already been discussed in Chapter 1, and realizability (Lumley, 1979) as mentioned in Section 3.4.1. Both of these concepts fundamentally rely on the insight that properties of the exact equations—be it invariance properties or the positive definiteness of the Reynolds stress tensor—must be preserved by the model, which is very much in the spirit of the present work, although we also seek to take into account additional constraints that have not been considered before. Today, some of the most widely used RSMs include those of Launder et al. (1975) and Speziale et al. (1991). More details on the main ideas behind these models can be found in the textbooks by Pope (2000) and Wilcox (1994) as well as the review article by Leschziner and Drikakis (2002), on which the following discussion is based.

In (3.3), the unknown terms to be modeled are the pressure-strain correlation

$$\Pi_{ij} = \overline{p\left(\frac{\partial u_i}{\partial x_j} + \frac{\partial u_j}{\partial x_i}\right)},$$

the dissipation

$$\varepsilon_{ij} = 2\nu\overline{\frac{\partial u_i}{\partial x_k}\frac{\partial u_j}{\partial x_k}},$$

and the diffusion terms

$$D_{ijk} = \left(R_{ijk} + \overline{(\delta_{jk}u_i + \delta_{ik}u_j)p}\right).$$

We discuss the most common modeling ideas for these terms in the following.

Pressure-Strain Correlation

Generally speaking, the pressure-strain correlation is probably the most important unknown term, because it is this term that is primarily responsible for the redistribution between the different components of R_{ij}. In terms of its magnitude, it is also comparable to the production term in many engineering applications. Motivated by the finding of Chou (1945) that Π_{ij} can be expressed exactly in terms of two-point velocity correlations, Π_{ij} is usually split into a slow part $\Pi_{ij}^{(\mathrm{s})}$ and a rapid part $\Pi_{ij}^{(\mathrm{r})}$. This terminology stems from the idea that the rapid part is directly affected by the mean velocity gradient, whereas the slow part is not.

In homogeneous anisotropic decaying turbulence, the rapid part vanishes, and the slow part is responsible for the return to isotropy that is observed in such a flow. The simplest model for this was proposed by Rotta (1951), who suggested

$$\Pi_{ij}^{(\mathrm{s})} = -C_R \frac{\varepsilon}{k}\left(R_{ij} - \frac{2}{3}k\delta_{ij}\right), \tag{3.148}$$

where the appearing constant C_R is named after him. However, it later turned out that the true behavior is more complicated, and that (3.148) should be generalized. The theory of tensor invariants together with dimensional analysis and invoking Galilean invariance allow narrowing down this general form to

$$\frac{\Pi_{ij}^{(\mathrm{s})}}{\varepsilon} = \sum_n f_n T_{ij}^{(n)}, \tag{3.149}$$

where $T_{ij}^{(n)}$ are the symmetric deviatoric tensors that can be formed from the normalized anisotropy tensor

$$b_{ij} = \frac{R_{ij}}{R_{kk}} - \frac{1}{3}\delta_{ij}, \tag{3.150}$$

and the free functions f_n determine the precise form of the model. They can be found in the respective publications and in the textbook by Pope (2000). Within this framework, more sophisticated models were suggested by Sarkar and Speziale (1990) and Chung and Kim (1995).

The rapid part $\Pi_{ij}^{(\mathrm{r})}$ is usually investigated using RDT (rapid distortion theory), which considers the limit of high mean velocity gradients. In this regime, the rapid term dominates, allowing one to investigate its effect in isolation. The simplest model for the rapid term is given by the linear relation due to Gibson and Launder (1978)

$$\Pi_{ij}^{(\mathrm{r})} = -C_2\left(\Gamma_{ij} - \frac{1}{3}\Gamma_{kk}\delta_{ij}\right), \tag{3.151}$$

where

$$\Gamma_{ij} = -R_{ik}\frac{\partial \bar{U}_j}{\partial x_k} - R_{jk}\frac{\partial \bar{U}_i}{\partial x_k}$$

denotes the production term, and C_2 is another empirical constant.

In between the two extreme states of vanishing velocity gradients as described by homogeneous turbulence and large velocity gradients as described by RDT, a basic model (Launder et al., 1975) is given by

$$\Pi_{ij} = -C_R \frac{\varepsilon}{k} \left(R_{ij} - \frac{2}{3} k \delta_{ij} \right) - C_2 \left(\Gamma_{ij} - \frac{1}{3} \Gamma_{kk} \delta_{ij} \right), \tag{3.152}$$

where the first term is Rotta's model given by Eq. (3.148), and the second term corresponds to Eq. (3.151). Many generalizations exist, and most pressure-rate-of-strain models can be represented using the form

$$\frac{\Pi_{ij}}{\varepsilon} = \sum_n f_n \tilde{T}_{ij}^{(n)}, \tag{3.153}$$

where the $\tilde{T}_{ij}^{(n)}$, similar to $T_{ij}^{(n)}$ in (3.149), represent symmetric deviatoric tensors that include b_{ij}, but, additionally, also include the symmetric and asymmetric velocity gradients S_{ij} and W_{ij}, which are normalized using the turbulent timescale k/ε. The most prominent models in this framework probably include two variants of the LRR model (Launder et al., 1975) and the SSG model (Speziale et al., 1991).

Dissipation

For the dissipation, most models invoke the hypothesis of local isotropy (Kolmogorov, 1941), leading to

$$\varepsilon_{ij} = \frac{2}{3} \varepsilon \delta_{ij}. \tag{3.154}$$

Having thus reduced the six unknown components of the dissipation to the scalar ε, an equation analogous to that used in two-equation models such as Eq. (3.116) is formulated,

$$\frac{D\varepsilon}{Dt} = -C_{\varepsilon,1} \frac{\varepsilon}{k} R_{ij} \frac{\partial \bar{U}_i}{\partial x_j} - C_{\varepsilon,2} \frac{\varepsilon^2}{k} + \frac{\partial}{\partial x_j} \left(C_\varepsilon \frac{k}{\varepsilon} R_{ij} \frac{\partial \varepsilon}{\partial x_i} \right), \tag{3.155}$$

though note that the availability of the full Reynolds stress tensor allows formulating the production term and the diffusion term sensitive to anisotropy. Obviously, it is also possible to use an equation for a different variable, such as ω, and infer ε from that.

Even though the hypothesis of local isotropy is usually reasonable, it is violated in the vicinity of solid walls. In the limit of low local Reynolds numbers, Rotta (1951) assumed that the energy-containing motion given by R_{ij} and the dissipation motion characterized by ε_{ij} overlap, leading to the approximation

$$\varepsilon_{ij} = \varepsilon \frac{R_{ij}}{2k/3}. \tag{3.156}$$

Therefore, Hanjalić and Launder (1976) use as a general expression

$$\varepsilon_{ij} = \frac{2}{3} \varepsilon \left((1 - f_s) \delta_{ij} + \frac{R_{ij}}{2k/3} f_s, \right) \tag{3.157}$$

where f_s, a function of the turbulent Reynolds number $k^2/(\nu\varepsilon)$ whose values range from zero to unity, blends between the two regimes characterized by Eq. (3.154) and Eq. (3.156). As better numerical results became available in the late 1980s and 1990s, Hanjalić and Jakirlić (1993) and Jakirlić and Hanjalić (2002) developed complicated extensions to (3.157), the precise form of which is beyond the scope of this review.

Diffusion

The remaining unclosed terms D_{ijk} can be interpreted as diffusion terms, and have received relatively little attention. Models for them are generally based on simple arguments relating to dimensional and tensorial correctness, where it must be noted that D_{ijk} is symmetric in the indices i and j, but not in k. Based on these considerations, the simplest model was suggested by Shir (1973) and reads

$$D_{ijk} = -\frac{2}{3} C_s \frac{k^2}{\varepsilon} \frac{\partial R_{ij}}{\partial x_k}, \tag{3.158}$$

whereas the slightly more complicated model by Daly and Harlow (1970)

$$D_{ijk} = -C_s \frac{k}{\varepsilon} R_{km} \frac{\partial R_{ij}}{\partial x_m} \tag{3.159}$$

is used more widely.

Some authors model R_{ijk} separately, in which case (3.158) and (3.159) have to be extended in such a way that the resulting expression is symmetric in all three indices. Extending (3.158), Donaldson (1972) and Mellor and Herring (1973) postulate

$$R_{ijk} = -\frac{2}{3} C_s \frac{k^2}{\varepsilon} \left(\frac{\partial R_{jk}}{\partial x_i} + \frac{\partial R_{ik}}{\partial x_j} + \frac{\partial R_{ij}}{\partial x_k} \right). \tag{3.160}$$

Hanjalić and Launder (1972) also suggest an alternative approximation of the form

$$R_{ijk} = -C_s \frac{k}{\varepsilon} \left(R_{im} \frac{\partial R_{jk}}{\partial x_m} + R_{jm} \frac{\partial R_{ik}}{\partial x_m} + R_{km} \frac{\partial R_{ij}}{\partial x_m} \right), \tag{3.161}$$

which is based on Eq. (3.159). In Eqs. (3.158)–(3.161), C_s denotes an empirical constant whose numerical value differs between models.

3.4.3. Explicit Algebraic Reynolds Stress Models

The numerical difficulties associated with solving the equations of RSMs have given rise to EARSMs, a class of models that can be viewed as a compromise between EVMs and RSMs. As mentioned in Section 3.4.1, these models are structurally similar to NLEVMs, but they are derived in a very different way, namely by inserting simplifying assumptions into RSMs.

In particular, in the transport equation for R_{ij} (3.3), convective and diffusive stress transport are modeled algebraically using (Rodi, 1976)

$$\frac{dR_{ij}}{dt} - \frac{\partial D_{ijk}}{\partial x_k} \approx \frac{R_{ij}}{k} \left(\frac{dk}{dt} - \frac{\partial D_{llk}}{\partial x_k} \right) = \frac{R_{ij}}{k} \left(\Gamma_{kk} - \varepsilon \right), \tag{3.162}$$

If Γ_{kk} and ε are known from the equations of a classical two-equation model such as the k-ε-model, the latter equality in (3.162) is an algebraic relation for the stresses. As shown by Pope (1975), inserting this relation into the model LRR-model (Launder et al., 1975) gives rise to an equation of the form (3.120).

This concludes our discussion of the main ideas in turbulence modeling.

3.5. Simplifications for Free Shear Flows

An important class of flows to study in the context of turbulence modeling is that of free shear flows, in which similarity solutions greatly simplify the numerical calculation. At the same time, unlike e.g. in parallel shear flows, all important terms, including the convective term, are present. Examples for free shear flows include the plane and round jet, the far wake and the mixing layer. Following Wilcox (1994), the starting point for this investigation are Eqs. (1.3) and (3.105) with the standard boundary layer type simplifications,

$$\frac{\partial \bar{U}_1}{\partial x_1} + \frac{\partial \bar{U}_2}{\partial x_2} = 0, \tag{3.163}$$

$$\bar{U}_1 \frac{\partial \bar{U}_1}{\partial x_1} + \bar{U}_2 \frac{\partial \bar{U}_1}{\partial x_2} = -\frac{\partial \tilde{R}_{12}}{\partial x_2}, \tag{3.164}$$

where

$$\tilde{R}_{12} = -\nu_t \frac{\partial \bar{U}_1}{\partial x_2}, \tag{3.165}$$

and we are assuming Cartesian coordinates, though analogous arguments can be made for rotationally symmetric flows using cylindrical coordinates. Similar simplifications also apply to the equations of the turbulence model, and, for example, the equations of the k-ε-model (3.115) and (3.116) simplify to

$$\bar{U}_1 \frac{\partial k}{\partial x_1} + \bar{U}_2 \frac{\partial k}{\partial x_2} = -\tilde{R}_{12} \frac{\partial \bar{U}_1}{\partial x_2} - \varepsilon + \frac{\partial}{\partial x_2}\left(\frac{\nu_t}{\sigma_k} \frac{\partial k}{\partial x_2} \right), \tag{3.166}$$

$$\bar{U}_1 \frac{\partial \varepsilon}{\partial x_1} + \bar{U}_2 \frac{\partial \varepsilon}{\partial x_2} = -C_{\varepsilon,1} \frac{\varepsilon}{k} \tilde{R}_{12} \frac{\partial \bar{U}_1}{\partial x_2} - C_{\varepsilon,2} \frac{\varepsilon^2}{k} + \frac{\partial}{\partial x_2}\left(\frac{\nu_t}{\sigma_\varepsilon} \frac{\partial \varepsilon}{\partial x_2} \right). \tag{3.167}$$

At this point, a crucial simplification can be made by introducing similarity variables. This relies on the key insight that beyond a developing region, the shape of the velocity profiles does not change, so that a single function, if scaled appropriately, can represent the entire two-dimensional velocity field. We assume here that this self-similarity is also observed for the other turbulent quantities appearing in the model. The form of the similarity variables differs between the types of free shear flows. For the plane jet, experimental evidence shows that it spreads linearly, so that the similarity variable

$$\eta = \frac{x_2}{x_1} \tag{3.168}$$

can be introduced. Further, we assume

$$\bar{U}_1 = \frac{\tilde{u}(\eta)}{x_1^{n_u}}, \quad \bar{U}_2 = \frac{\tilde{v}(\eta)}{x_1^{n_u}}, \quad k = \frac{\tilde{k}(\eta)}{x_1^{n_k}}, \quad \varepsilon = \frac{\tilde{\varepsilon}(\eta)}{x_1^{n_\varepsilon}}. \tag{3.169}$$

Note that this similarity ansatz can also be obtained as an invariant solution using symmetries, which is shown in Section 3.3. As discussed in textbooks (e.g. Pope, 2000), n_u can be constrained by integrating (3.164) from $-\infty$ to ∞, leading to

$$\frac{d}{dx_1}\int_{-\infty}^{\infty} \bar{U}_1^2 dx_2 = 0, \tag{3.170}$$

because $\bar{U}_1$ and $\tilde{R}_{12}$ vanish as the absolute value of x_2 tends to infinity. Inserting (3.168) and (3.169), one obtains

$$\frac{d}{dx_1}\int_{-\infty}^{\infty} \left(\frac{\tilde{u}(\eta)^2}{x_1^{2n_u}} x_1\right) d\eta = 0. \tag{3.171}$$

Since $\tilde{u}(\eta)$ does not depend on x_1, this can only be fulfilled if x_1 cancels in the integrand, i.e. $n_u = 1/2$. Then, in order for Eqs. (3.163)–(3.167) to be self-similar, it is necessary that $n_k = 1$ and $n_\varepsilon = 5/2$, in which case they become independent of x_1 and reduce to an ODE system. In order to simplify the notation slightly, it makes sense to introduce the velocity-like function $\tilde{V}(\eta)$ defined as

$$\tilde{V}(\eta) = \tilde{v}(\eta) - \eta\tilde{u}(\eta). \tag{3.172}$$

Then, (3.163)–(3.167) can be written as

$$\tilde{V}(\eta) = -\int_0^\eta \frac{1}{2}\tilde{u}(\hat{\eta})d\hat{\eta}, \tag{3.173}$$

$$\tilde{V}(\eta)\tilde{u}'(\eta) - \frac{1}{2}\tilde{u}(\eta)^2 = C_\mu \left(\frac{\tilde{k}(\eta)^2}{\tilde{\varepsilon}(\eta)}\tilde{u}'(\eta)\right)', \tag{3.174}$$

$$\begin{aligned}\tilde{V}(\eta)\tilde{k}'(\eta) - \tilde{u}(\eta)\tilde{k}(\eta) &= C_\mu \frac{\tilde{k}(\eta)^2}{\tilde{\varepsilon}(\eta)}\tilde{u}'(\eta)^2 \\ &\quad - \tilde{\varepsilon}(\eta) + \frac{C_\mu}{\sigma_k}\left(\frac{\tilde{k}(\eta)^2}{\tilde{\varepsilon}(\eta)}\tilde{k}'(\eta)\right)',\end{aligned} \tag{3.175}$$

$$\begin{aligned}\tilde{V}(\eta)\tilde{\varepsilon}'(\eta) - \frac{5}{2}\tilde{u}(\eta)\tilde{\varepsilon}(\eta) &= C_\mu C_{\varepsilon,1}\tilde{k}(\eta)\tilde{u}'(\eta)^2 \\ &\quad - C_{\varepsilon,2}\frac{\tilde{\varepsilon}(\eta)\tilde{\varepsilon}(\eta)}{\tilde{k}(\eta)} + \frac{C_\mu}{\sigma_\varepsilon}\left(\frac{\tilde{k}(\eta)^2}{\tilde{\varepsilon}(\eta)}\tilde{\varepsilon}'(\eta)\right)',\end{aligned} \tag{3.176}$$

where primes denote derivation with respect to η. Note that (3.173) is written in integral form to reduce the effort needed to calculate $\tilde{V}(\eta)$, and also because using it in differential form was found to lead to numerical instabilities. For the plane jet, the boundary conditions are

$$\tilde{u}(\eta \to \infty) = \tilde{k}(\eta \to \infty) = \tilde{\varepsilon}(\eta \to \infty) = 0, \tag{3.177}$$

$$\tilde{u}'(\eta = 0) = \tilde{k}'(\eta = 0) = \tilde{\varepsilon}'(\eta = 0) = 0, \tag{3.178}$$

though note that in practice, one would use small nonzero values in (3.177) for those variables that appear in the denominator. These boundary conditions have the flaw that they do not prevent the trivial solution of all variables becoming zero everywhere. Therefore, some symmetry-breaking constraint such as

$$\tilde{u}(\eta = 0) = 1 \tag{3.179}$$

has to also be enforced. The resulting BVP (boundary value problem) can be solved numerically with relatively little effort compared to a full two-dimensional PDE solution, which makes it feasible to use such flows for model calibration, as is done in Section 5.3.1.

Note that the numerical solution of this system can still be a bit difficult because the outer region of the jet, where the mean velocity tends to zero, is of course laminar. Due to the appearance of k in the denominator in some terms, laminar flow areas, where k is zero, can be a source of instability for two-equation models. The numerics become much more stable when a transformation first suggested by Rubel and Melnik (1984) is introduced, which reads

$$d\eta = C_\mu \frac{\tilde{k}^2}{\tilde{\varepsilon}} d\xi. \tag{3.180}$$

Its effect is to map the turbulent-nonturbulent interface to infinite values of ξ. In the ξ-domain, Eqs. (3.173)–(3.176) become

$$\tilde{V}(\xi) = -\int_0^\xi \frac{1}{2}\tilde{u}(\hat{\xi}) C_\mu \frac{\tilde{k}(\xi)^2}{\tilde{\varepsilon}(\xi)} d\hat{\xi}, \tag{3.181}$$

$$\tilde{V}(\xi)\tilde{u}'(\xi) - \frac{1}{2}\tilde{u}(\xi)^2 C_\mu \frac{\tilde{k}(\xi)^2}{\tilde{\varepsilon}(\xi)} = \tilde{u}''(\xi), \tag{3.182}$$

$$\tilde{V}(\xi)\tilde{k}'(\xi) - \tilde{u}(\xi)\tilde{k}(\xi) C_\mu \frac{\tilde{k}(\xi)^2}{\tilde{\varepsilon}(\xi)} = \tilde{u}'(\xi)^2 - \tilde{k}(\xi)^2 + \frac{1}{\sigma_k}\tilde{k}''(\xi), \tag{3.183}$$

$$\begin{aligned} \tilde{V}(\xi)\tilde{\varepsilon}'(\xi) - \frac{5}{2}\tilde{u}(\xi)\tilde{\varepsilon}(\xi) C_\mu \frac{\tilde{k}(\xi)^2}{\tilde{\varepsilon}(\xi)} &= C_{\varepsilon,1}\frac{\tilde{\varepsilon}(\xi)}{\tilde{k}(\xi)}\tilde{u}'(\xi)^2 - C_{\varepsilon,2}\tilde{\varepsilon}(\xi)\tilde{k}(\xi) \\ &+ \frac{1}{\sigma_\varepsilon}\tilde{\varepsilon}''(\xi), \end{aligned} \tag{3.184}$$

where primes now denote derivation with respect to ξ. The only drawback of this formulation is that it is unclear how far the numerical domain should extend in ξ-direction. For the plane jet, a value of $\xi_{\text{max}} = 150$ was found to work well. Results of the system (3.181)–(3.184) using the numerical scheme discussed in Section 4.4 are presented in Section 5.3.1.

This concludes the discussion of the theoretical background from turbulence research. In particular, the review of turbulence models in light of Lie symmetries lays an important foundation for the developments in Chapter 5. Before that, the necessary numerical aspects are discussed in the next chapter.

4. Numerical Aspects

The main purpose of turbulence models is to facilitate the numerical simulation of turbulent flows. Therefore, it is necessary to discretize their equations and implement them into a numerical solver. The background needed to understand the work done to this end is discussed in this chapter.

4.1. The Discontinuous Galerkin Method

For the numerical implementation of the classical k-ω-model discussed in Section 3.4.1, we use the solver framework BoSSS (Kummer and Oberlack, 2013), which employs a DG discretization. Since the use of DG is not yet widespread, we give a brief introduction into the method in the following.

In recent years, the DG method has attracted growing interest because it can be seen as a generalization of both FVM and FEM, thus combining the advantages of these two methods. Like FVM, but unlike FEM, it allows for a conservative discretization, which guarantees that locally, numerical errors can never lead to a violation of the conservation laws underlying the equations being solved. In the present context of an incompressible flow solver, this means that mass and momentum conservation are locally ensured. Since numerical errors are inevitable and could otherwise accumulate in long-running simulations to render the results physically unreasonable, this property is crucial in the context of CFD (computational fluid dynamics). At the same time, an attractive property of FEM—arbitrarily high convergence order without increasing the stencil—is also present in DG. In contrast to FVM, this allows for high-order accuracy on unstructured grids and with minimal communication overhead across cells. This latter aspect is particularly relevant in parallel calculations.

Several introductions into DG exist, including Cockburn (2003) and the textbook by Hesthaven and Warburton (2008). To illustrate the method, we loosely follow Bassi et al. (2005) and consider the general transport equation for a scalar quantity ϕ

$$\frac{\partial \phi}{\partial t} + \frac{\partial (\phi U_j)}{\partial x_j} - S = 0, \tag{4.1}$$

in which U_i is the convection velocity and S represents a general source term. Using the divergence-free property of the velocity (1.1), Eq. (4.1) could represent e.g. Eqs. (3.115) and (3.116) or any component of Eq. (1.6) with vanishing viscosity. The goal is to find a function ϕ_h that approximates the solution ϕ of Eq. (4.1). Since ϕ_h does not solve Eq. (4.1) exactly, inserting it into Eq. (4.1) leads to the residual

$$r = \frac{\partial \phi_h}{\partial t} + \frac{\partial(\phi_h U_{h;j})}{\partial x_j} - S, \tag{4.2}$$

where $U_{h;i}$ is an approximation for the velocity. In order to minimize this residual, the Galerkin orthogonality condition is invoked. In concrete terms, r is required to be orthogonal to the space of test functions v in the domain Ω_h, leading to the weak form of Eq. (4.1)

$$\int_{\Omega_h} rv dV = \int_{\Omega_h} \left(v\frac{\partial \phi_h}{\partial t} + v\frac{\partial(\phi_h U_{h;j})}{\partial x_j} - vS \right) dV = 0. \tag{4.3}$$

It is understood that (4.3) must hold for arbitrary v. Using integration by parts and Stokes's theorem, we can rewrite the convective term into a volume integral and a surface integral, yielding

$$\int_{\Omega_h} v\frac{\partial \phi_h}{\partial t} dV + \int_{\partial\Omega_h} v\phi_h U_{h;j} n_j dS - \int_{\Omega_h} \frac{\partial v}{\partial x_j}\phi_h U_{h;j} dV - \int_{\Omega_h} vS dV = 0, \tag{4.4}$$

where $\partial\Omega_h$ denotes the boundary of the domain Ω_h and n_i is the normal vector pointing outward from the domain. The next step is the actual discretization, i.e. we divide Ω_h into non-overlapping subdomains (or cells) Ω_k,

$$\begin{aligned} &\sum_k \int_{\Omega_k} v_k \frac{\partial \phi_k}{\partial t} dV + \sum_k \int_{\partial\Omega_k} v_k \phi_k U_{k;j} n_{k;j} dS - \sum_k \int_{\Omega_k} \frac{\partial v_k}{\partial x_j} U_{k;j} \phi_k dV \\ &- \sum_k \int_{\Omega_k} v_k S dV = 0, \end{aligned} \tag{4.5}$$

where the approximate solution ϕ_k, the approximate velocity $U_{k;i}$, the test function v_k and the outward-pointing normal vector $n_{k;i}$ are now specific to each cell. Here, we restrict ϕ_k and v_k to be piecewise polynomials inside a cell Ω_k. Crucially, this means that we do not enforce continuity across cell boundaries, which forces us to pay special attention to the surface integral, because at the interior edges of the domain, ϕ_k is double-valued. In order to ensure that the expression inside the surface integral in (4.5) is meaningful, we introduce the numerical flux

$$f_c(\phi_k^{\text{in}}, \phi_k^{\text{out}}, n_{\Gamma;i}) \approx \phi_k U_{k;j} n_{k;j}, \tag{4.6}$$

which not only depends on ϕ_k^{in}, i.e. the edge value when approaching an edge from the inside of the kth cell, but also on ϕ_k^{out}, which denotes the value on the edge when approaching an edge from the outside of the cell. Here, $n_{\Gamma;i}$ denotes a normal field that uniquely assigns a normal vector to each edge. On boundary edges, $n_{\Gamma;i}$ is chosen such that it points outward. The precise form of f_c is addressed later, though we note here that any suitable flux function must fulfill the symmetry condition $f_c(\phi_k^{\text{in}}, \phi_k^{\text{out}}, n_{\Gamma;i}) = -f_c(\phi_k^{\text{out}}, \phi_k^{\text{in}}, -n_{\Gamma;i})$. Also note that f_c is responsible for the coupling between cells, which is obviously a prerequisite for a meaningful discretization.

A natural question at this stage is why one would allow discontinuities when the exact solution for ϕ can be expected to be continuous. The answer is that allowing for discontinuities introduces additional freedom that can be used to ensure that the conservation laws are locally fulfilled. As has been alluded to at the beginning of this section, any numerical and discretization error will not lead to a violation of conservation laws, but instead cause discontinuities at cell boundaries. This is preferable because this kind of error does not accumulate over time, and, furthermore, is obviously visible in the numerical solution. The additional freedom also helps with ensuring the stability of the discretization.

Equation (4.5) can be written in a global form. First, the sums of the volume integrals over cells Ω_k are written as integrals over the entire discretized domain Ω_h. Second, if we distinguish between inner edges Σ_h and boundary edges Γ_h, the sum of the surface integrals can be rewritten, leading to

$$\begin{aligned}&\int_{\Omega_h} v\frac{\partial \phi_h}{\partial t}dV + \int_{\Sigma_h}(v^{\text{in}} - v^{\text{out}})f_c(\phi_h^{\text{in}}, \phi_h^{\text{out}}, n_{\Gamma;i}))dS + \int_{\Gamma_h} v^{\text{in}} f_c(\phi_h^{\text{in}}, \phi_h^{*}, n_{\Gamma,i})dS\\ &-\int_{\Omega_h}\frac{\partial v}{\partial x_j}\phi_h U_{h;j}dV - \int_{\Omega_h} vSdV = 0.\end{aligned} \tag{4.7}$$

The state ϕ_h^* is used to weakly prescribe boundary conditions. At the inflow, where Dirichlet boundary conditions are enforced, ϕ_h^* is set to the boundary value, and at the outflow, it is set equal to the inner value at the respective edge ϕ_h^{in}. A more general discussion about the implementation of boundary conditions is found in Hesthaven and Warburton (2008).

We now address the choice of the numerical flux function f_c, which serves to reconcile the two values of ϕ_h at inner edges, where discontinuities are allowed. In addition to the symmetry condition already mentioned above, the numerical flux function f_c also has to fulfill the consistency condition

$$f_c(\phi_h, \phi_h, n_i) = \phi_h U_{h;j} n_j, \tag{4.8}$$

and, furthermore, it must be Lipschitz continuous (Pietro and Ern, 2012). The simplest choice is an upwind flux, i.e. we select one of the two values depending on the local direction of the flow velocity, leading to

$$f_c(\phi_h^{\text{in}}, \phi_h^{\text{out}}, n_j) = \begin{cases}\phi_h^{\text{in}} U_{h;j}^{\text{in}} n_j & \text{for } U_{h;j}n_j > 0\\ \phi_h^{\text{out}} U_{h;j}^{\text{out}} n_j & \text{for } U_{h;j}n_j < 0.\end{cases} \tag{4.9}$$

The main disadvantage is that the upwind flux has a high numerical diffusion, though this leads to a very stable discretization. By contrast, the perhaps most straightforward idea of taking the average of both values leads to the central flux

$$f_c(\phi_h^{\text{in}}, \phi_h^{\text{out}}, n_j) = \left(\frac{\phi_h^{\text{in}} U_{h;j}^{\text{in}} + \phi_h^{\text{out}} U_{h;j}^{\text{out}}}{2}\right) n_j, \tag{4.10}$$

which has no numerical diffusion, rendering it unstable in many cases. However, for some terms, like the pressure gradient, using the central flux does not cause instability, in which case it makes sense to use it. For other terms where this is not the case, a compromise between lower numerical diffusivity and stability can be achieved by extending (4.10) such that discontinuities are penalized. This is known as the Lax–Friedrichs flux, which reads

$$f_c(\phi_h^{\text{in}}, \phi_h^{\text{out}}, n_j) = \left(\frac{\phi_h^{\text{in}} U_{h;j}^{\text{in}} + \phi_h^{\text{out}} U_{h;j}^{\text{out}}}{2}\right) n_j + C(\phi_h^{\text{in}} U_{h;j}^{\text{in}} - \phi_h^{\text{out}} U_{h;j}^{\text{out}}) n_j, \tag{4.11}$$

where the factor C can be chosen large enough to ensure stability, but not so large as to introduce excessive numerical diffusivity. This is generally used in BoSSS for convective terms, and C is chosen locally in each cell.

Some discussion is also necessary for the treatment of diffusion terms. Considering a pure diffusion equation with diffusion coefficient ν

$$\frac{\partial}{\partial x_j}\left(\nu \frac{\partial \phi}{\partial x_j}\right) = 0, \tag{4.12}$$

we again approximate ϕ with ϕ_h. The same arguments as before give rise to the weak form

$$\int_{\partial\Omega_h} v\left(\nu \frac{\partial \phi_h}{\partial x_j}\right) n_j dS - \int_{\Omega_h} \frac{\partial v}{\partial x_j}\left(\nu \frac{\partial \phi_h}{\partial x_j}\right) dV = 0. \tag{4.13}$$

On the discretized domain, the global form of Eq. (4.13) reads

$$\int_{\Gamma_h \cup \Sigma_h} f_d(\phi_h^{\text{in}}, \phi_h^{\text{out}}, n_{\Gamma;i})(v^{\text{in}} - v^{\text{out}}) dS - \int_{\Omega_h} \frac{\partial v}{\partial x_j}\left(\nu \frac{\partial \phi_h}{\partial x_j}\right) dV = 0. \tag{4.14}$$

Note that we again have to introduce a flux function f_d to ensure a reasonable expression despite the discontinuous nature of ϕ_h and v. Similarly to what we observe in the context of the convective term, the most straightforward idea

$$f_d(\phi_h^{\text{in}}, \phi_h^{\text{out}}, n_j)(v^{\text{in}} - v^{\text{out}}) = \frac{1}{2}\left(\left(\frac{\partial \phi_h}{\partial x_j}\right)^{\text{in}} + \left(\frac{\partial \phi_h}{\partial x_j}\right)^{\text{out}}\right) n_j (v^{\text{in}} - v^{\text{out}}) \tag{4.15}$$

fails to adequately penalize jumps across cells, which can again lead to instability. Therefore, BoSSS instead uses the SIP (symmetric interior penalty) flux, which reads (Shahbazi, 2005)

$$\begin{aligned} f_d(\phi_h^{\text{in}}, \phi_h^{\text{out}}, n_j)(v^{\text{in}} - v^{\text{out}}) = {} & \frac{1}{2}\left(\left(\frac{\partial \phi_h}{\partial x_j}\right)^{\text{in}} + \left(\frac{\partial \phi_h}{\partial x_j}\right)^{\text{out}}\right) n_j (v^{\text{in}} - v^{\text{out}}) \\ & + \frac{1}{2}\left(\left(\frac{\partial v}{\partial x_j}\right)^{\text{in}} + \left(\frac{\partial v}{\partial x_j}\right)^{\text{out}}\right) n_j (\phi_h^{\text{in}} - \phi_h^{\text{out}}) \\ & - C_\eta (\phi_h^{\text{in}} - \phi_h^{\text{out}})(v^{\text{in}} - v^{\text{out}}). \end{aligned} \tag{4.16}$$

Here, the last term serves to penalize jumps across cells, and C_η must be again chosen large enough to ensure stability, but too large a value would introduce unnecessary numerical diffusion. The optimal value varies across cells and is heuristically calculated in BoSSS. The first term is known as the consistency term, and the second term, or symmetry term, ensures that the expression does not change when exchanging ϕ_h and v, which is also true for the original weak formulation of (4.12).

The last question to be addressed concerns the choice of the trial function ϕ_h and the test function v. For ϕ_h, cell-local polynomials are used, i.e. for the cell with index k,

$$\phi_k(\boldsymbol{x}, t) = \sum_{i=0}^{N_k} \hat{\phi}_{k;i}(t) \psi_{k;i}(\boldsymbol{x}), \tag{4.17}$$

where $\psi_{k;i}(\boldsymbol{x})$ is the polynomial basis, and $\hat{\phi}_{k;i}$ are the degrees of freedom in the cell. In the one-dimensional case, one might e.g. choose monomials, i.e. $\psi_{k;i} = x^i$. While the choice of the polynomial basis does not affect the final solution, it does have an influence on the properties of the numerical method, e.g. in terms of stability and efficiency. BoSSS uses modal polynomials as a basis. Note that by definition, $\psi_{k;i}$ is zero everywhere outside the cell k. The global solution ϕ_h is then given by the sum of all ϕ_k. The characteristic feature of a Galerkin method is that the same basis functions are used for the test function v as for the trial function ϕ_h,

$$v_{k;i}(\boldsymbol{x}) = \psi_{k;i}(\boldsymbol{x}). \tag{4.18}$$

Inserting (4.17) and (4.18) into (4.7) or (4.14) (or a combination of both) while using appropriate flux functions then leads to an algebraic equation system which has to be solved for the $\hat{\phi}_{k;i}$ using a suitable numerical algorithm. Note that we can essentially recover an FVM discretization by restricting ourselves to zero-degree polynomials in (4.17) and (4.18). On the other hand, an FEM-like discretization would have emerged if we had excluded the possibility of discontinuities early in the derivation.

4.2. Temporal Discretization

Having discussed the spatial discretization, we now briefly demonstrate the temporal discretization following Ferziger et al. (2020). To this end, we write (4.1) as

$$\frac{d\phi_h}{dt} = F(t, \phi_h), \tag{4.19}$$

where we assume that ϕ_h is already spatially discretized, either using the DG discretization shown in Section 4.1 or another discretization technique such as FVM or FDS. Integration of Eq. (4.19) with respect to time leads to

$$\phi_h^{n+1} = \phi_h^n + \int_t^{t+\Delta t} F(\tau, \phi_h) d\tau, \tag{4.20}$$

where Δt is the time step size, ϕ_h^n represents the solution of the nth time step, which we assume to be the current time step, and ϕ_h^{n+1} is the solution of the next time step. Different approximations for this integral then lead to various time discretization schemes with different properties. The simplest idea is to use the current values of t and ϕ_h to approximate the entire interval, i.e.

$$\int_t^{t+\Delta t} F(\tau, \phi_h) d\tau \approx F(t, \phi_h^n)\Delta t, \tag{4.21}$$

which leads to the explicit Euler scheme. Notably, as is the defining feature of explicit methods, Eq. (4.21) together with Eq. (4.20) allows calculating the solution of the new time step based entirely on information of the current time step, which makes obtaining ϕ_h^{n+1} simple to implement and computationally inexpensive. However, explicit methods have the drawback that for too large a time step, they become unstable. The largest stable time step size is constrained by the CFL-condition (Courant et al., 1928), which can often lead to prohibitively small required time steps. Moreover, in the context of incompressible flows, since the continuity equation (1.1) does not contain a temporal derivative, the resulting spatially discretized system is a DAE (differential-algebraic equation) problem. For such stiff systems, implicit schemes are necessary (e.g. Hairer and Wanner, 1996). The simplest implicit method is the implicit Euler scheme, which is given by

$$\int_t^{t+\Delta t} F(\tau, \phi_h) d\tau \approx F(t + \Delta t, \phi_h^{n+1}) \Delta t, \tag{4.22}$$

where the right-hand side of (4.22) contains the unknown solution of the new time step, so that (4.20) with (4.22) inserted must be solved using either a nonlinear solver or, if F is linear or has been linearized, a linear solver. However, this additional effort compared to using (4.21) is often compensated by the possibility to use larger time steps, because the implicit Euler method is stable for arbitrarily large time steps. Of course, if an accurate resolution of transient effects is desired, this does introduce a constraint on the time step. An improvement over the first-order accurate implicit Euler method is provided by the second-order accurate Crank–Nicolson method given by

$$\int_t^{t+\Delta t} F(\tau, \phi_h) d\tau \approx \frac{F(t, \phi_h^n) + F(t + \Delta t, \phi_h^{n+1})}{2} \Delta t, \tag{4.23}$$

which we use for the pseudo-time stepping solution of the system discussed in Section 5.3.1.

All of these methods shown up to here fall into the category of two-level methods, because only information at the nth and the $(n + 1)$st time step are taken into account. In the solver implemented in BoSSS, implicit BDF (backward differentiation formula) schemes are used. The main idea is to increase the accuracy by using information of the k last time steps. Their general form reads

$$\phi_h^{n+1} - \Delta t a_0 F(t + \Delta t, \phi_h^{n+1}) = \sum_{j=1}^{k} a_j \phi_h^{n+1-j}, \tag{4.24}$$

where the coefficients a_j are given up to $k = 4$ in Table 4.1. Note that for $k = 1$, the implicit Euler method given by (4.22) is recovered.

k	a_0	a_1	a_2	a_3	a_4
1	1	1			
2	2/3	4/3	−1/3		
3	6/11	18/11	−9/11	2/11	
4	12/25	48/25	−36/25	16/25	−3/25

Table 4.1.: The values of the coefficients appearing in Eq. (4.24) for up to $k = 4$.

4.3. Implementation of the Classical k-ω-Model in BoSSS

The implementation of classical turbulence models such as the k-ω-model is intended to be an intermediate step toward using BoSSS as a testing ground for novel turbulence models, whose development is discussed in Chapter 5. However, this goal proved to be more ambitious than originally anticipated, because (i) even well-established models require significant effort to run reliably in DG, and (ii) the novel turbulence models proved even more numerically difficult. Therefore, a better path for the present purposes turned out to be to implement the new models for simple flows, in which the governing equations can be reduced to ODEs, and to discretize these equations using very simple numerical schemes to be discussed in Section 4.4. This special-purpose implementation is presented in Section 5.3.1. In conclusion, it should be kept in mind that the focus of the present section does not lie on reproducing experimental results with the k-ω-model, but rather to obtain qualitatively reasonable results in a robust way.

Solving two-equation RANS turbulence models using a DG discretization introduces an array of issues not as prominently encountered in a typical FVM context. A major challenge arises from the nonlinearity of the model equations, which obviously also carries over to the discretized system. Its solution, therefore, requires a nonlinear solver, which is always a potential point of failure, because no existing algorithm is guaranteed to converge to the correct solution. In fact, it is not even generally clear if a unique solution exists at all. This issue is neither specific to DG nor turbulence model calculations, because even a simple laminar Navier–Stokes FVM calculation requires some nonlinear solution algorithm due to the nonlinearity in the convective term of Eq. (1.2). However, convergence issues of the nonlinear solver are usually less pronounced for such relatively simple equations and diffusive schemes. On the other hand, in DG, more care must often be taken to prevent convergence issues, especially in the context of RANS calculations, but also in viscoelastic flows (Kikker and Kummer, 2018) or combustion calculations (Gutiérrez-Jorquera and Kummer, 2021).

For any incompressible flow solver, an issue that has to be addressed is that of velocity-pressure coupling. In BoSSS, the straightforward approach of solving the entire set of equations in a coupled way is employed. Care must be taken to prevent physically unreasonable fluctuations of the pressure, i.e. the analog of the checkerboard instability observed in many numerical methods for incompressible flows (Schäfer, 2006). To this end, a mixed-order discretization is used, in which the polynomial degree of the pressure field is chosen to be smaller by one than the polynomial degree of the velocity and the other variables. This is intended to ensure that the Ladyženskaja-Babuška-Brezzi condition (Babuška, 1973; Brezzi, 1974) is fulfilled, even though, strictly speaking, no rigorous proof for this in the general setting discussed here exists. Note that this fully-coupled solution approach, while conceptually simple, is very demanding of the nonlinear solver, and can easily lead to convergence issues. We discuss some measures that address these challenges in Sections 4.3.2–4.3.4.

In the context of the k-ω-model, care must also be taken with respect to the boundary conditions for ω. In theory, ω has the disadvantageous property of becoming infinitely large at solid walls. Numerical codes employ heuristics to obtain suitable wall boundary conditions ω^{wall}, however, these heuristics must be adapted for DG codes, because the appropriate value of ω^{wall} depends on the degree m of the polynomial used to approximate the solution for ω. Following Schoenawa (2014), we use

$$\omega^{\text{wall}} = \frac{6\nu}{\beta^*(a_m x^{\text{wall}})^2}, \tag{4.25}$$

where x^{wall} denotes the distance of the wall-adjacent cell center from the wall, and the factors a_m can be calculated using a recursion formula. We give values for up to $m = 3$ in Table 4.2, and values for up to $m = 10$ as well as details on their calculation can be found in Schoenawa (2014).

DG-degree m	a_m
0	0.37
1	0.0821
2	0.0357
3	0.0199

Table 4.2.: The parameter a_m appearing in Eq. (4.25).

In the following, we first present a boundary layer test case in Section 4.3.1. Since this test case is particularly difficult in terms of convergence, it serves as a case study with which the various measures to support the convergence of the nonlinear solver can be presented. These measures are discussed in Sections 4.3.2–4.3.4. A preliminary solver validation is discussed in Appendix A.2.

4.3.1. Results for a Boundary Layer Test Case

Since the implementation of the classical k-ω-model is an intermediate step on the path to implementing one of the new models discussed in Chapter 5, relatively few calculations were performed with it. Here, we present the results of a simple boundary layer flow. The primary purpose of this calculation was not to obtain accurate results, but to act as a proof of concept for a turbulence model in BoSSS. The simulation of the boundary layer, in particular, proved difficult, and, therefore, requires numerous tweaks to the solution algorithm, which are discussed in Sections 4.3.2–4.3.4. More information on these modifications can also be found in Gutiérrez-Jorquera and Kummer (2021), who discuss them in the context of combustion simulations.

The boundary layer test case consists of a rectangular domain with an impermeable, no-slip wall at the bottom, a velocity inlet on the left, and pressure outlets at the top and on the right. A schematic view is shown in Fig. 4.1. An important observation is that we cannot simply

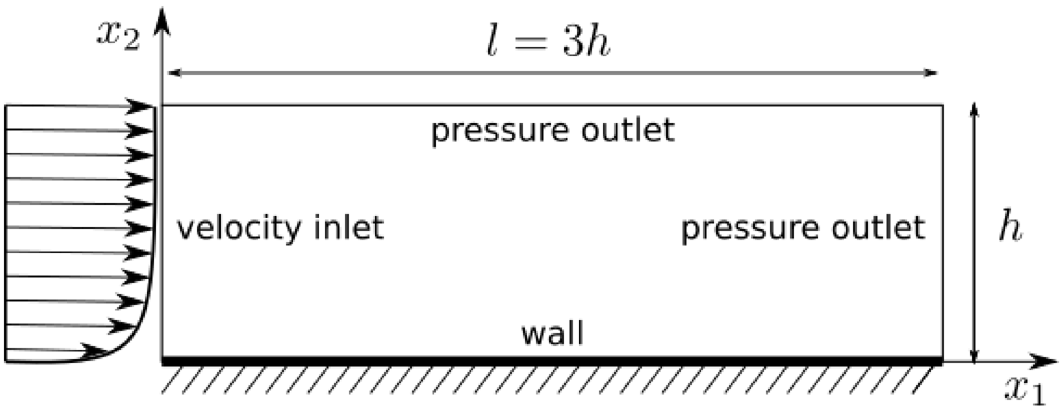

Figure 4.1.: Schematic view of the boundary layer setup.

impose a block profile for the velocity at the inlet, because this would lead to a contradiction in the lower left corner, where the velocity inlet meets the wall. Whereas more diffusive numerical methods might be able to smooth out such a singular point and obtain good results in the rest of the domain, high-order discretization schemes such as DG tend to be very sensitive to such points. Therefore, we have to impose an inlet velocity profile that qualitatively already resembles a very thin boundary layer profile. It is given by the function

$$\bar{U}_1^{\text{inlet}}(x_2) = \bar{U}_1^0 \left(1 - e^{x_2/\lambda}\right), \tag{4.26}$$

where $\bar{U}_1^0$ denotes the characteristic velocity, and for the length scale λ a value of $0.001h$ is chosen. Similarly, for k and $\tilde{\omega}$, the functions

$$k^{\text{inlet}}(x_2) = \left(k^0 - k^{\text{wall}}\right)\left(1 - e^{x_2/\lambda}\right) + k^{\text{wall}}, \tag{4.27}$$

$$\tilde{\omega}^{\text{inlet}}(x_2) = \left(\tilde{\omega}^0 - \tilde{\omega}^{\text{wall}}\right)\left(1 - e^{x_2/\lambda}\right) + \tilde{\omega}^{\text{wall}} \tag{4.28}$$

are used, where the characteristic values k^0 and $\tilde{\omega}^0$ are difficult to estimate directly, and are hence calculated from estimates for the turbulent intensity I and the turbulent length scale L using

$$k^0 = \frac{3}{2}\left(\bar{U}_1^0 I\right)^2, \tag{4.29}$$

$$\tilde{\omega}^0 = \frac{k^0}{\sqrt[4]{0.09}L}. \tag{4.30}$$

Here, the turbulent intensity I is chosen to be 10^{-4} and the length scale L is assumed to be $0.1h$. At the wall, the velocity has to be zero. The turbulent kinetic energy k also becomes zero at the wall, however, for numerical reasons, we assume a small nonzero value of 10^{-9} here. For the transformed turbulent dissipation rate $\tilde{\omega}$, we use Eq. (4.25) to calculate an appropriate wall value. At the pressure outlet, homogeneous Neumann boundary conditions for k and $\tilde{\omega}$ are assumed. The molecular viscosity is chosen to be 10^{-4}. All variables are nondimensionalized using the domain height h and the characteristic velocity $\bar{U}_1^0$.

The numerical mesh is shown in Fig. 4.2. Obviously, the resolution is much finer close to the wall, where we expect the highest gradients, and the expectation that gradients in x_2-direction are higher than in x_1-direction leads to the rectangular shape of the cells. Note that we use a simple hanging-node refinement, which makes it straightforward to ensure a similar aspect ratio in all cells. The ability of DG to work with such grids is one of its most prominent advantages (Cockburn, 2003). For the mean velocity $\bar{U}_i$, the turbulent kinetic energy k and the transformed specific turbulent dissipation rate $\tilde{\omega}$, we use a DG-degree of two, and a DG-degree of one is used for the pressure $\bar{P}$. This leads to a third-order discretization in $\bar{U}_i, k$ and $\tilde{\omega}$ and second-order discretization in $\bar{P}$.

The results for all quantities are shown in Fig. 4.3. For the mean velocity, the typical boundary layer profile can be observed. Note that close to the outlet, results for the turbulent kinetic energy k show a peak near the wall, which is expected and can be explained by the high velocity gradients causing turbulent production in this area. The turbulent dissipation rate ω becomes very large in a thin area close to the wall, so that it is better visualized using the transformed $\tilde{\omega}$. In a post-processing step, the original ω was also calculated, and a close-up of the lower right corner is shown in Fig. 4.4. We stress again that these results were only obtained as a proof of concept for a converging solver, and no claims to quantitative accuracy are made. The calculations were in part performed on the Lichtenberg high performance computer, which is

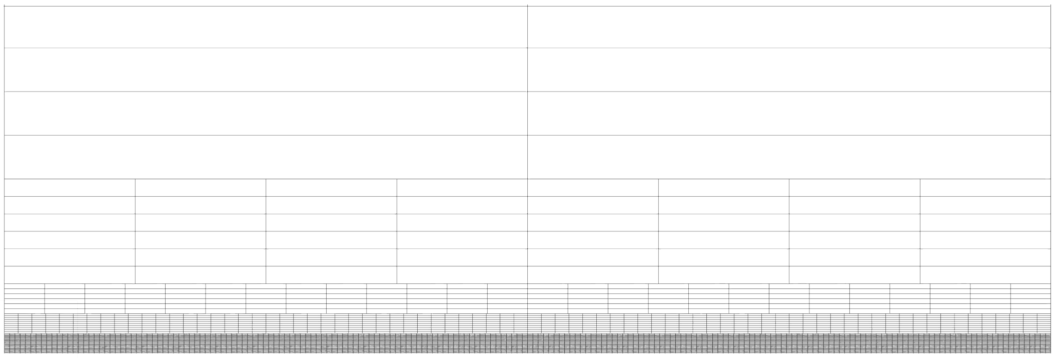

Figure 4.2.: The numerical mesh used for the boundary layer calculation.

funded by the Federal Ministry of Education and Research (BMBF) and the state of Hesse as part of the NHR Program.

Apart from the modifications to the implemented equations discussed in Section 3.4.1, BoSSS also features a number of important tweaks at a lower level, e.g. the nonlinear solver. We discuss these aspects in the following.

4.3.2. Globalization for the Nonlinear Solver

Evidently, the nonlinear nature of the governing equations requires some iterative solution approach for the discretized system. In principle, for stationary calculations, it would be possible to use a pseudo-time stepping approach, i.e. to treat the problem as time-dependent and apply one of the time discretization methods discussed in Section 4.2 until a stationary state is reached. In each time step, an ad-hoc linearization using values from the previous pseudo-time step can then be used. This technique was found to be very robust in the context of the FDS calculations of the self-similar turbulent plane jet to be discussed in Sections 4.4 and 5.3. However, another possibility is to use a Newton-type nonlinear solver. Note that such solvers do not always perform well when applied to numerically problematic equations such as those of two-equation turbulence models. The nonlinear solver implemented in BoSSS employs a globalization method to be described in this section, making its use feasible in this context. A thorough treatise of this subject is found in Pawlowski et al. (2006) and Deuflhard (2011).

The fundamental idea of Newton-type solvers for nonlinear equations is to find the roots of the equation through iteratively improved guesses while using gradient information to speed up convergence. In turn, this can also be applied to optimization problems, in which case we can use the Newton method to find local minima or maxima, i.e. roots of the first derivative. Note that in the following, we assume that we are interested in finding minima. In concrete terms, given a possibly nonlinear function $f(x)$, finding its minimum x^* is equivalent to finding the root of its derivative, i.e. $f'(x^*) = 0$. For some point x_n, which we can interpret as our current guess for x^*, we express $f'(x^*)$ using its Taylor expansion

$$f'(x^*) = f'(x_n) + f''(x_n)(x^* - x_n) + O(x^{*2}) = 0, \tag{4.31}$$

where we have used the fact that $f'(x^*)$ is zero, because x^* is a local minimum. We also assume that f is sufficiently smooth, so that this Taylor expansion is valid. Neglecting second-order

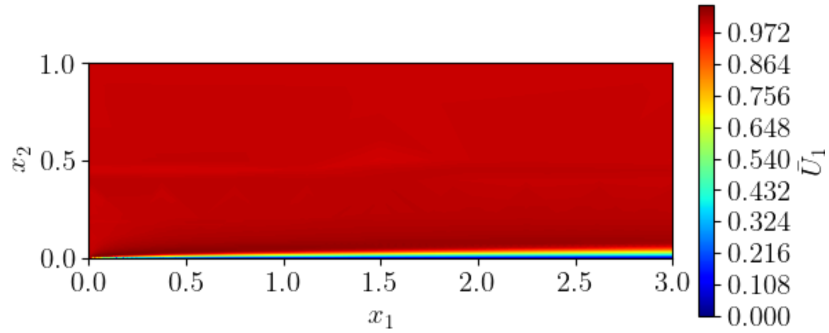

(a) Mean velocity $\bar{U}_1$.

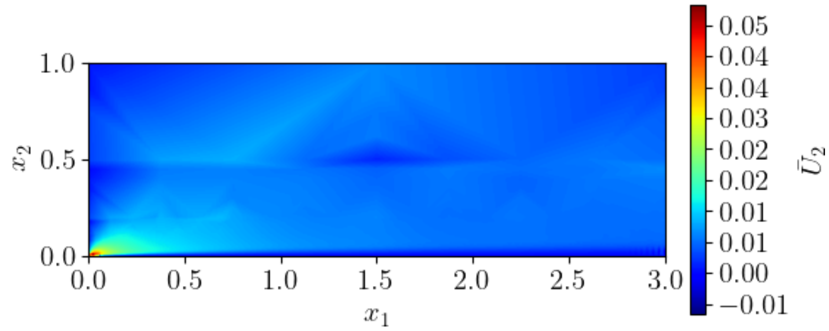

(b) Mean velocity $\bar{U}_2$.

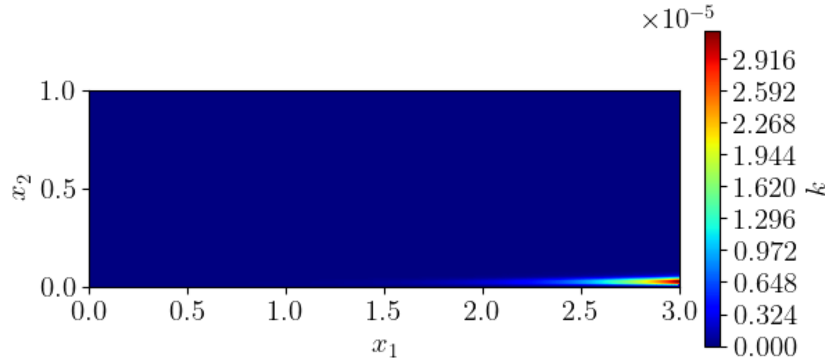

(c) Turbulent kinetic energy k.

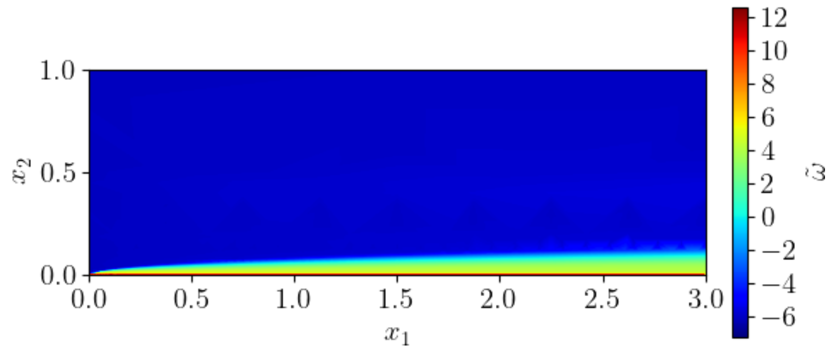

(d) Transformed turbulent dissipation rate $\tilde{\omega}$.

Figure 4.3.: Boundary layer results for the classical k-ω-model.

terms in (4.31) and solving for x^* then leads to

$$x^* \approx x_n - f''(x_n)^{-1} f'(x_n), \tag{4.32}$$

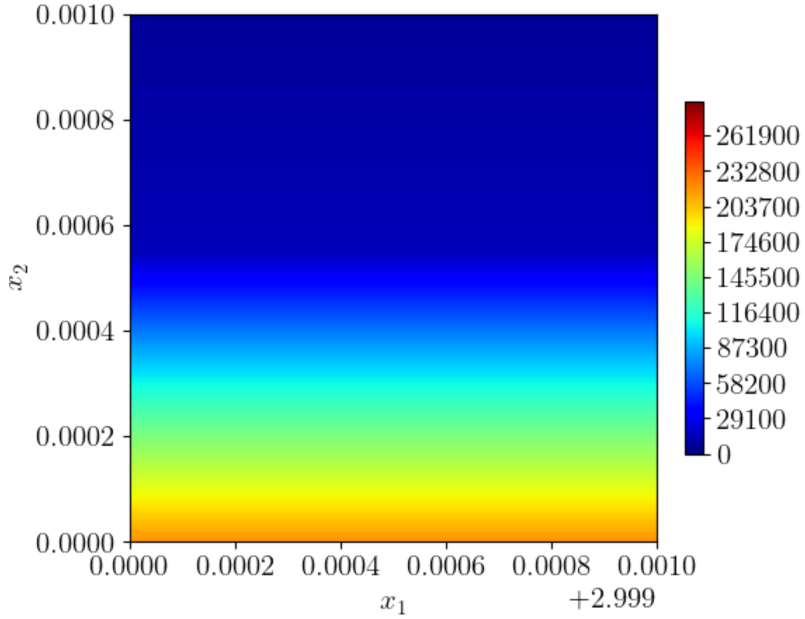

Figure 4.4.: Turbulent dissipation rate ω (close-up of the lower right corner).

where we cannot use an equal sign because we are dealing with an approximation. However, assuming that the error is small, we can interpret the right-hand side of (4.32) as an improved guess for x^*, leading to the recursion formula

$$x_{n+1} = x_n - f''(x_n)^{-1} f'(x_n). \tag{4.33}$$

This can be generalized to equation systems by understanding that f' then refers to the Jacobian matrix of f, f'' to its Hessian matrix and the operation $()^{-1}$ to matrix inversion.

Clearly, the success of this method hinges on whether the linear approximation given by (4.32) is sufficiently accurate. Roughly speaking, if the current guess x_n is already close to the correct minimum x^*, this approximation is reasonable, and a fast convergence can be achieved. However, far away from the correct minimum x^*, this linear approximation should not be trusted. In its classical form, the Newton algorithm includes no such notion of trust and always directly descends to approximated minimum x_{n+1}, which can cause seemingly random behavior under some circumstances. In other words, the classical Newton method has poor global convergence properties.

Note that there is not always a need to solve (4.33) exactly, especially in the early steps of the iteration, when the guess x_{n+1} is probably far from the correct minimum x^* anyway. Methods that only use an approximation for (4.33) are known as inexact Newton methods.

For guesses x_n far away from the correct minimum x^*, a more reasonable approach would be to descend along the direction of the steepest descent, but only as far as we can trust the linear approximation. This is precisely the idea behind gradient descent methods, which can be expressed by the recursion formula

$$x_{n+1} = x_n - \delta f'(x_n), \tag{4.34}$$

where δ determines the step size. The main challenge of these algorithms is to select an appropriate value for δ. If it is too large, the same issues as those observed with the Newton method can arise, but too small a value leads to unnecessarily slow convergence. Note that in the one-dimensional case, as a comparison of Eq. (4.34) and Eq. (4.33) reveals, the Newton method for optimization can be viewed as the special case of a gradient descend method in which the step size is determined using curvature information, i.e. f''.

In BoSSS, where we deal with high-dimensional equation systems, the nonlinear solution algorithm that proved to work best for the k-ω-model is the so-called Dogleg method (Powell, 1970), which falls into the category of trust region methods. Since it improves the global convergence properties of the Newton algorithm, the Dogleg method and similar algorithms are known in the literature as globalization methods. Apart from the current guess $\boldsymbol{x}_n$ (now typeset in bold because we are dealing with vectors) and the new, possibly inexact Newton guess $\boldsymbol{x}_{n+1}^N$ given by (4.33), this method also takes into account the so called Cauchy point $\boldsymbol{x}_{n+1}^C$, which is defined to be the point where $|\boldsymbol{f}|$ has its local minimum along the direction of steepest descent. We also assume that in a region of radius Δ around $\boldsymbol{x}_n$, the approximation of $\boldsymbol{f}$ can be trusted. The choice of the next guess $\boldsymbol{x}_{n+1}$ depends on the location of $\boldsymbol{x}_{n+1}^N$ and $\boldsymbol{x}_{n+1}^C$. Three cases can be distinguished:

(i) If the Newton guess $\boldsymbol{x}_{n+1}^N$ lies inside the trust region, we accept it as the next guess, i.e.

$$\boldsymbol{x}_{n+1} = \boldsymbol{x}_{n+1}^N.$$

(ii) If the Newton guess $\boldsymbol{x}_{n+1}^N$ and the Cauchy point $\boldsymbol{x}_{n+1}^C$ both lie outside the trust region, we go toward the Cauchy point until the edge of the trust region, i.e.

$$\boldsymbol{x}_{n+1} = \boldsymbol{x}_n + \frac{\Delta}{|\boldsymbol{x}_{n+1}^C - \boldsymbol{x}_n|}\left(\boldsymbol{x}_{n+1}^C - \boldsymbol{x}_n\right).$$

(iii) Otherwise, i.e. if the Newton guess $\boldsymbol{x}_{n+1}^N$ lies outside the trust region, but the Cauchy point $\boldsymbol{x}_{n+1}^C$ lies inside the trust region, we take as the new guess the point where the line from $\boldsymbol{x}_{n+1}^C$ to $\boldsymbol{x}_{n+1}^N$ intersects the boundary of the trust region. We can write this as

$$\boldsymbol{x}_{n+1} = \boldsymbol{x}_n + (1-\tau)\left(\boldsymbol{x}_{n+1}^C - \boldsymbol{x}_n\right) + \tau\left(\boldsymbol{x}_{n+1}^N - \boldsymbol{x}_n\right),$$

where τ is chosen such that $|\boldsymbol{x}_{n+1} - \boldsymbol{x}_n| = \Delta$.

These three cases are illustrated for the two-dimensional case in Fig. 4.5. Note that this method behaves like the classical Newton method close to the correct minimum $\boldsymbol{x}^*$, where, provided that the trust region is suitably chosen, case (i) will be invoked. On the other hand, far away from the correct minimum, case (ii) will occur, making the algorithm behave like a gradient descent method, with the step size given by the trust region radius Δ. Also note that in each iteration, measures are taken to ensure that the trust region radius Δ is not too large. This is accomplished by comparing the approximation for $\boldsymbol{f}(\boldsymbol{x}_{n+1})$ with its correct value. If the discrepancy is too large, instead of accepting $\boldsymbol{x}_{n+1}$ as the new guess, the iteration is repeated using a smaller trust region. For details on the heuristics used for the choice and the adaptation of the trust region, we refer to Pawlowski et al. (2006).

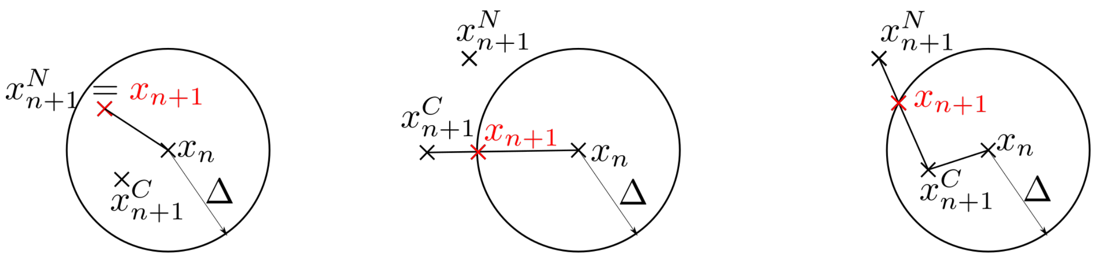

(a) Case (i) (b) Case (ii) (c) Case (iii)

Figure 4.5.: The three possible cases of the trust region algorithm. The selected next step x_{n+1} is highlighted in red.

4.3.3. Homotopy Approach to Improve the Initial Guess

In cases where the above modifications still do not lead to convergence, it may be helpful to improve the initial guess for the nonlinear solver. An obvious way of accomplishing this is by using one's intuition, or, if available, an analytical solution for a similar setup, to initialize the calculation in a reasonable way. However, this only works for relatively simple setups. More generally, one may employ homotopy methods, in which one first solves a simplified equation system for which the solver will converge even with a poor initial guess, and then gradually fades to the full equation system. In the case of the k-ω-model, one could set all model constants to zero. This relatively simple system, which essentially consists of the laminar Navier–Stokes equations coupled with two scalar convection-diffusion equations, is likely to converge in most cases. If necessary, one could also raise the molecular viscosity for this early step, thus further increasing the numerical stability. Of course, the molecular viscosity would have to be decreased to its target value throughout the following homotopy steps. This was, however, not found to be needed for the boundary layer test case. The solution of such a simplified equation system, while quantitatively quite different from the result of the full system, can nonetheless be used as a reasonable initial guess for the full system. If necessary, intermediate steps, in which the aforementioned terms are scaled down by some factor, can be taken.

Such a homotopy method has been implemented and successfully applied to a turbulent boundary layer case, the details of which are discussed in Section 4.3.1. It was found that this test case does not converge if a solution of the full model equations given by (1.3), (3.105), (3.106), (3.117), (3.118) and (3.143) is attempted directly. If, instead, the homotopy path whose steps are shown in Table 4.3 is followed, the solver converges successfully. The rationale for this particular homotopy path is that the first step, which consists of a weakly-coupled system of the Navier–Stokes equations and two scalar convection-diffusion equations, is likely to converge without problems for most test cases. The subsequent activation of the turbulent viscosity in all equations by setting C_ω, σ and σ^* to unity increases the coupling, but, due to its diffusive nature, is also unlikely to cause major convergence issues. However, switching on the production and dissipation terms by increasing α, α^*, β and β^* can quickly lead to convergence issues and, therefore, these terms are faded in slowly. The intermediate results for $\bar{U}_1$ and k in the various homotopy steps are shown in Figs. 4.6 and 4.7. It is clear that whereas the changes of the mean velocity are hardly visible, the effects of the turbulence source terms on k are drastic, to the point where we even have to adapt the color map for the different k-plots. Note that the convergence criterion for the intermediate steps need not be too strict, which manifests itself in the visible artifacts in the intermediate solutions for k. Clearly, the final result for k is very different from the initial guess, which helps explain the observed convergence issues when not using the homotopy approach described here.

As an alternative to this manual homotopy mode, in which the user has to specify each of the homotopy steps taken, an automatic mode, which is less flexible, but requires no configuration by the user, is also available. The latter mode tightly integrates with the nonlinear solver algorithm discussed in Section 4.3.2, and aims to move along the homotopy path sufficiently slowly that the Newton step never lies outside the trust region. Preliminary tests indicate that the manual homotopy mode works more reliably for this test case.

homotopy step i	$\alpha_i^*/\alpha_{\text{end}}^*$	$\beta_i^*/\beta_{\text{end}}^*$	$\sigma_i^*/\sigma_{\text{end}}^*$	$\alpha_i/\alpha_{\text{end}}$	$\beta_i/\beta_{\text{end}}$	$\sigma_i/\sigma_{\text{end}}$	$C_{\omega,i}/C_{\omega,\text{end}}$
1	0	0	0	0	0	0	0
2	0.001	0.001	1	0.001	0.001	1	1
3	0.1	0.1	1	0.1	0.1	1	1
4	0.5	0.5	1	0.5	0.5	1	1
5	0.8	0.8	1	0.8	0.8	1	1
6	1	1	1	1	1	1	1

Table 4.3.: Homotopy steps for the calculation of a turbulent boundary layer.

4.3.4. Adaptive Mesh Refinement

The fact that we have to limit k and $\tilde{\omega}$ to physically reasonable values is usually due to poor local spatial resolution of the numerical grid. Therefore, in addition to applying the limiting as described in Section 3.4.1, it is sensible to also dynamically refine the mesh in these areas. For the numerical test case of the boundary layer presented in Section 4.3.1, AMR (adaptive mesh refinement) proved pivotal to achieve convergence, even though the initial mesh was already finer close to the wall. In combination with the homotopy method discussed in Section 4.3.3, it is particularly powerful, because problematic areas emerge slowly in early homotopy steps, where they are less likely to cause serious issues, and AMR ensures a suitable grid for the later homotopy steps, where the grid quality becomes more critical. AMR is already available in BoSSS, and we only have to specify the refinement criterion. Early tests using physically impossible (i.e. negative) values for k as a refinement criterion have been quite successful, though we note that other criteria, such as the local condition number of the matrix, may alternatively be considered.

As an example, Fig. 4.8 shows a close-up of the near-wall region of the boundary layer calculation discussed in Section 4.3.1, which makes visible the effect of AMR.

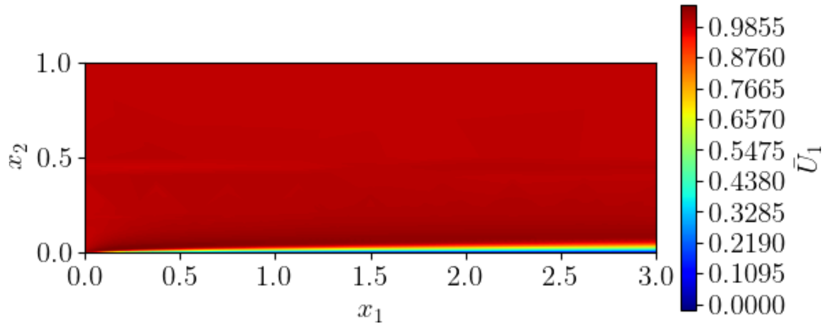

(a) Mean velocity $\bar{U}_i$, 1st homotopy step $i = 1$.

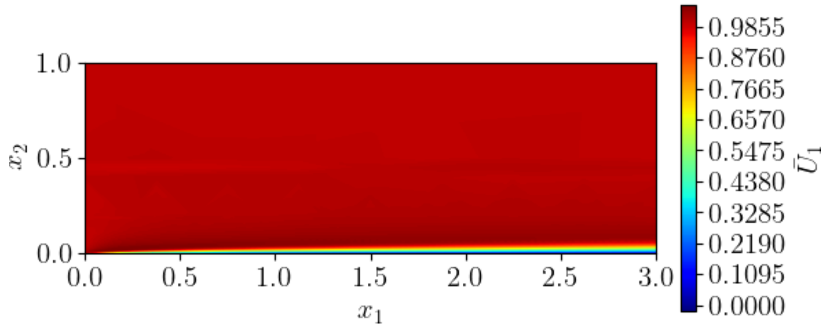

(b) Mean velocity $\bar{U}_i$, 3rd homotopy step $i = 3$.

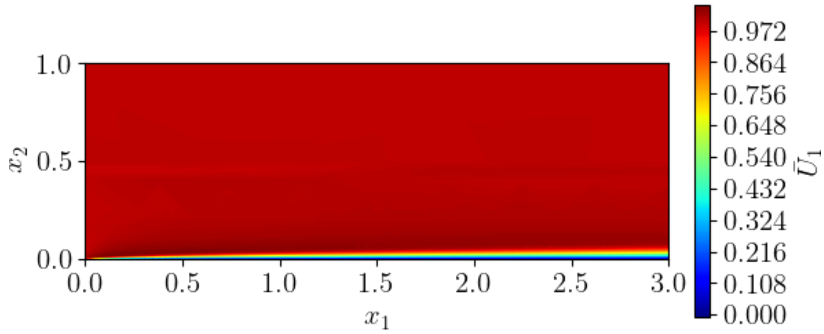

(c) Mean velocity $\bar{U}_i$, 4th homotopy step $i = 4$.

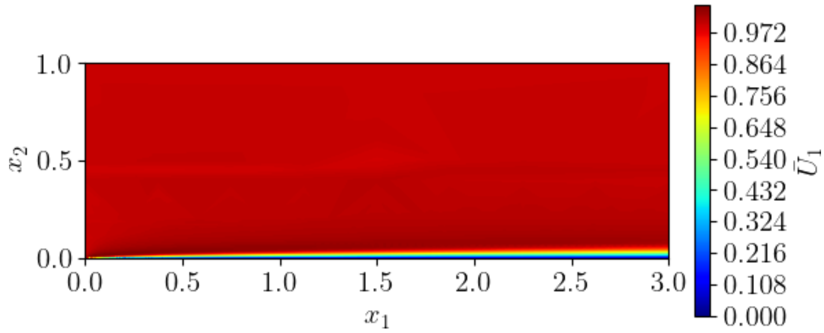

(d) Mean velocity $\bar{U}_i$, 5th homotopy step $i = 5$.

Figure 4.6.: Boundary layer: Results for $\bar{U}_1$ from intermediate homotopy steps. The final result is shown in Fig. 4.3.

4.4. Approaches for the Numerical Solution of One-Dimensional Boundary-Value Problems

As discussed in Section 3.5, for many flows of intermediate complexity, the governing equations can be simplified to ODEs. The numerical solution of these ODE systems offers a robust and efficient alternative to full calculations as presented in the preceding sections. For the new models developed in Section 5.2.1, a full solution is difficult, whereas an ODE solution is feasible. More details on these calculations are found in Section 5.3. In the following, we discuss the necessary background from a numerics point of view.

Depending on the nature of their boundary conditions, ODEs can be distinguished into IVPs (initial value problems), where all boundary conditions are specified on one side of the domain, and BVPs, where there is a mix between conditions given on one side and conditions given on the other side. Generally speaking, BVPs require more computational effort to solve numerically than IVPs. Examples for flows that can be simplified to BVPs include self-similar flows such as the boundary layer and free shear flows such as the jet, wake or mixing layer. For the purpose of this section, we consider a FDS discretization.

A very simple idea to solve BVPs is the shooting method, which relies on treating the problem as an IVP, and adjusting the missing initial conditions in an iterative process until the solution matches the boundary condition on the other side. The term “shooting method” derives from the idea that one repeatedly “aims” by adjusting the initial conditions until the target end conditions are hit. However, in the present context, this turned out to work poorly, probably because of the complexity of the considered ODE systems.

The straightforward approach of discretizing the ODE system in space and using a nonlinear solver to find the solution works to some degree, however, the complexity of the equations makes the convergence of the nonlinear solver somewhat difficult. The convergence of the classical models is unreliable and requires some sophistication such as a suitable initial guess, but for the modified models, convergence issues are even more pronounced.

Therefore, the much more robust method of pseudo-time stepping is used to obtain the results shown in Section 5.2.1, and we describe the method in more detail here. For a deeper introduction into the subject, the reader is referred to Olver (2013).

In the following, we consider the second-order ODE system

$$\boldsymbol{F}(x, \boldsymbol{u}, \boldsymbol{u}', \boldsymbol{u}'') = 0, \tag{4.35}$$

where x is the independent variable, $\boldsymbol{u}$ the vector of N dependent variable and primes denote derivatives with respect to x subject to the general boundary conditions

$$\begin{aligned} \boldsymbol{C}_{\text{min},1}\boldsymbol{u}(x_{\text{min}}) + \boldsymbol{C}_{\text{min},2}\boldsymbol{u}'(x_{\text{min}}) &= \boldsymbol{a}_{\text{min}}, \\ \boldsymbol{C}_{\text{max},1}\boldsymbol{u}(x_{\text{max}}) + \boldsymbol{C}_{\text{max},2}\boldsymbol{u}'(x_{\text{max}}) &= \boldsymbol{a}_{\text{max}}, \end{aligned} \tag{4.36}$$

where the domain extends from x_{min} to x_{max}. In (4.36), the $\boldsymbol{C}$ are $N \times N$-matrices and the $\boldsymbol{a}$ are N-dimensional vectors. In practice, the boundary conditions are often simple and can be written as

$$\begin{aligned} \boldsymbol{u}(x_{\text{min}}) &= \boldsymbol{u}_{\text{min}}, \ \text{ or } \ \boldsymbol{u}'(x_{\text{min}}) = \boldsymbol{u}'_{\text{min}}, \\ \boldsymbol{u}(x_{\text{max}}) &= \boldsymbol{u}_{\text{max}}, \ \text{ or } \ \boldsymbol{u}'(x_{\text{max}}) = \boldsymbol{u}'_{\text{max}}. \end{aligned} \tag{4.37}$$

Note that we need two boundary conditions for each component of $\boldsymbol{u}$ in order for the problem to be well-posed. If, as in (4.37), boundary conditions on both sides of the domain are given, the problem is referred to as a BVP. On the other hand, if only conditions on one side (typically x_{min}) are provided, this leads to an IVP. Generally speaking, IVPs are easier to solve, because starting from the known initial state at x_{min}, the solution can be evolved forward in x using a time-stepping scheme as discussed in Section 4.2. In a BVP, this is not possible, because the initial state is not fully known. For its solution, a numerical grid which places n nodes in the domain $[x_{\text{min}}, x_{\text{max}}]$ has to be introduced. Instead of looking for a continuous solution $\boldsymbol{u}$, we now solve for the discrete values of $\boldsymbol{u}$ at each node. Derivatives can then be approximated using finite differences between the nodal values. For example, a simple idea to approximate the first derivative at the ith node $\boldsymbol{u}_i'$ would be to use the backward difference formula

$$\boldsymbol{u}_i' = \frac{\boldsymbol{u}_i - \boldsymbol{u}_{i-1}}{h}. \tag{4.38}$$

As a Taylor expansion reveals, this is first-order accurate with the grid spacing $h = x_i - x_{i-1}$, i.e. a grid twice as fine will lead to a halving of the discretization error. This can be improved by using the central difference, which, assuming an equidistant grid, reads

$$\boldsymbol{u}_i' = \frac{\boldsymbol{u}_{i+1} - \boldsymbol{u}_{i-1}}{2h}. \tag{4.39}$$

This approximation is second-order accurate, so that doubling the number of grid points leads to a quartering of the discretization error. However, depending on the ODE, such a discretization can become unstable. In the context of solving the self-similar flows discussed in Section 5.3.1, the second-order backward difference formula

$$\boldsymbol{u}_i' = \frac{\boldsymbol{u}_{i-2} - 4\boldsymbol{u}_{i-1} + 3\boldsymbol{u}_i}{2h} \tag{4.40}$$

was found to yield better results. In the first interior node close to the left edge, where no $\boldsymbol{u}_{i-2}$ exists, the first-order backward difference formula (4.38) is instead used. Second derivatives are approximated using the second-order accurate central difference formula

$$\boldsymbol{u}_i'' = \frac{\boldsymbol{u}_{i+1} - 2\boldsymbol{u}_i + \boldsymbol{u}_{i-1}}{h^2}. \tag{4.41}$$

Inserting these approximations into (4.35) for each interior node turns the differential equation system into an algebraic equation system, which we can write

$$\boldsymbol{F}_{\text{disc}}(x_i, \boldsymbol{u}_i) = 0. \tag{4.42}$$

In general, $\boldsymbol{F}_{\text{disc}}$ can be nonlinear, as is the case for the equations considered in Section 5.3.1. A common method for solving such nonlinear equation systems are Newton methods, which are used in the context of the DG solver and are discussed in more detail in Section 4.3.2. While Newton-type methods work well for a large class of problems, they can exhibit convergence issues when applied to the complicated equation systems arising from discretized turbulence model equations. In this context, a more robust approach is often that of pseudo-time stepping, which exploits the physical structure of the underlying ODE. If we assume that the system (4.35) was obtained by simplifying a PDE that contains time as one of its independent variables, pseudo-time stepping relies on reintroducing the temporal derivatives that were originally cancelled by assuming a stationary solution, leading to

$$\boldsymbol{F}(x, \boldsymbol{u}, \boldsymbol{u}', \boldsymbol{u}'') = \frac{\partial \boldsymbol{u}}{\partial t}. \tag{4.43}$$

Both sides of this equation are then discretized in space, and, starting from some initial guess, the solution is evolved forward in time until a steady state is reached. This problem is already easier to solve for a nonlinear solver, because convergence issues can be mitigated by decreasing the time step, thus also decreasing the difference between the current state, which can be used as the initial guess, and the target solution, i.e. the state in the next pseudo-time step. Moreover, one can eliminate the need for a nonlinear solver altogether by linearizing the equation system using values from the previous time step. Obviously, the closer one approaches the steady-state solution, the smaller the error introduced by this linearization becomes.

In order to evolve the solution forward in time, a temporal discretization as discussed in Section 4.2 has to be introduced.

Having discussed the numerical aspects relevant for the present work, we now turn to the question of symmetry-based turbulence modeling.

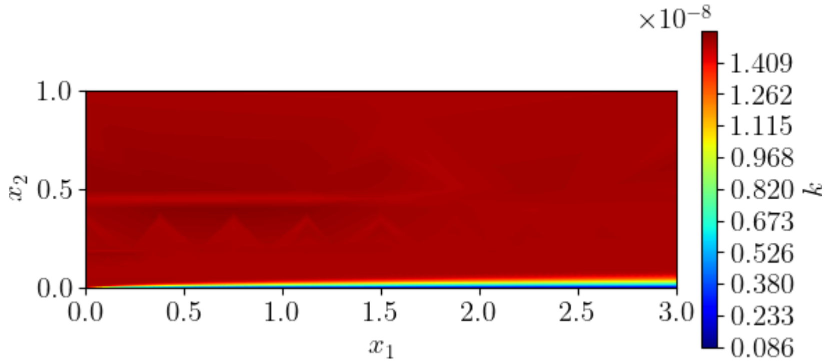

(a) Turb. kin. energy k, 1st homotopy step $i = 1$.

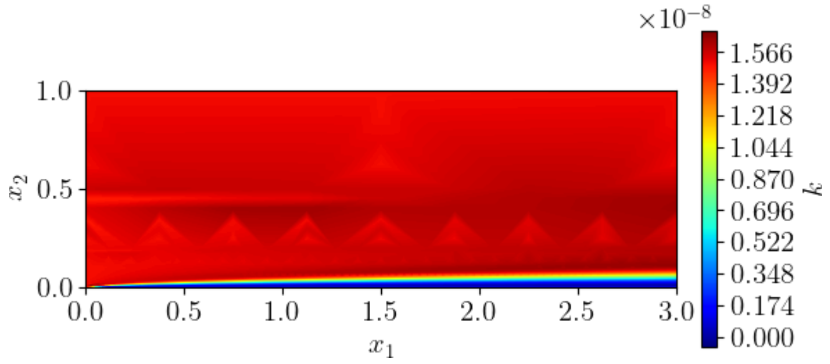

(b) Turb. kin. energy k, 3rd homotopy step $i = 3$.

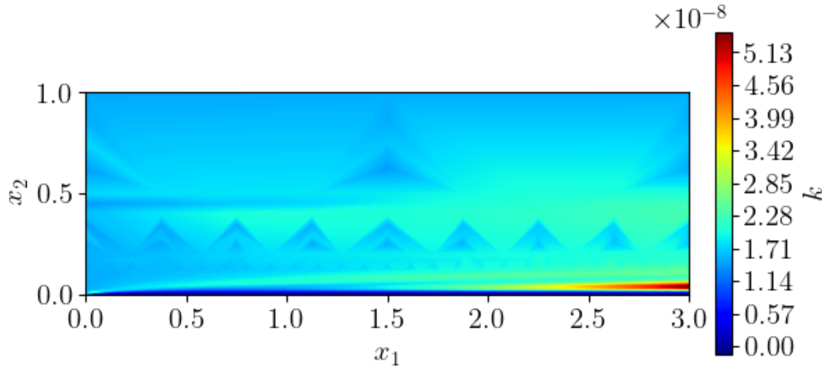

(c) Turb. kin. energy k, 4th homotopy step $i = 4$.

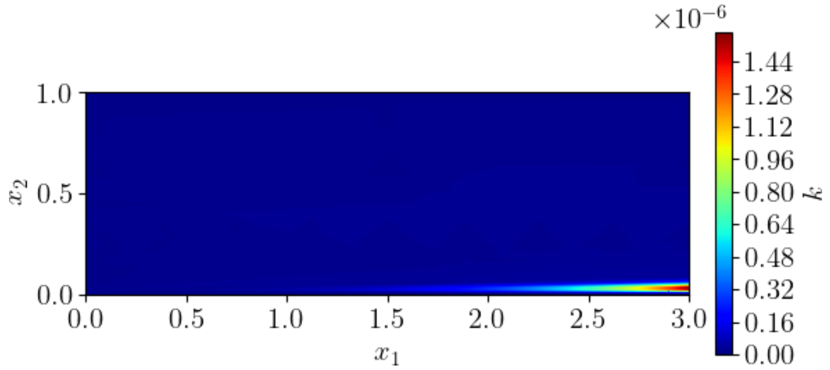

(d) Turb. kin. energy k, 5th homotopy step $i = 5$.

Figure 4.7.: Boundary layer: Results for k from intermediate homotopy steps. Note the different color ranges, which are needed for visibility. The final result is shown in Fig. 4.3.

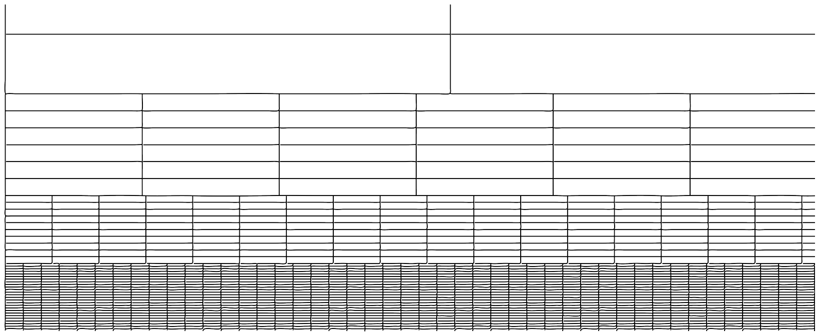

(a) Original grid.

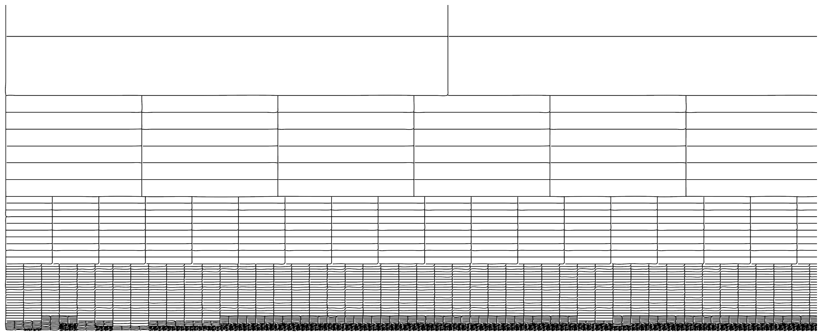

(b) Grid after AMR.

Figure 4.8.: Boundary layer: numerical grid showing the effect of AMR (adaptive mesh refinement), close-up view of the near-wall region close to the inlet.

5. Symmetry-Based Turbulence Modeling

In this section, the main results of the present work are discussed. The key question to be addressed is how to develop turbulence models that are not only invariant under the classical symmetries (3.27)–(3.32) (with the last two combining to (3.33) in the viscous case), but also under the statistical symmetries (3.55)–(3.58). In the following, we refer to such models as statistically invariant for short. Whereas the classical symmetries have generally been incorporated into two-equation models and more complicated ones, the statistical symmetries have only been taken into account as recently as Klingenberg et al. (2020) and Klingenberg and Oberlack (2022). Formulating reasonable model equations that fulfill this requirement turns out to be difficult. Therefore, to gain a general idea of what such a model could look like, we first employ an algorithmic modeling approach to develop a model skeleton in Section 5.1. Using the insights obtained there, we then turn to a more conventional modeling strategy in Section 5.2 to develop full turbulence models based on existing modeling ideas. One representative of these newly developed models is applied to some simple flow cases. Due to their relative simplicity, we mostly focus on EVMs, in particular the k-ε-model and the k-ω-model, but some ideas how to formulate statistically invariant RSMs are also developed. Note that early results on this subject already appear in the present author's Master's thesis (Klingenberg, 2017).

5.1. Constructing Model Equations from Symmetries

As has been discussed in Chapter 2, the perhaps most typical usage of Lie theory is to find the symmetries of a given equation system. However, in the context of modeling challenges, the inverse problem is often of interest, i.e. finding equations that are invariant under a given set of symmetries. The key idea is to use the symmetries one would like to embed into the model as the starting point, and to construct model equations that are invariant under these symmetries. In the context of turbulence modeling, the symmetries that should be present in a model are those of the RANS system given by (1.3) and (1.4) and an infinite hierarchy of equations for higher moments. These symmetries were already discussed in Section 3.2 and are given by (3.27)–(3.32) and (3.55)–(3.58), where (3.31) and (3.32) combine to (3.33) in the viscous case. Popovich and Bihlo (2012) employ this so-called inverse problem of group classification to constrain turbulence models for atmospheric calculations, although only the classical symmetries were taken into account in this work. As an alternative to the algorithm used in the present work, we note that there is the equivalent method of equivariant moving frames developed by Olver (2000), which Bihlo et al. (2014) applied to turbulence modeling. The developments discussed in this section is one of the main contributions of Klingenberg et al. (2020), and, to the best of the author's knowledge, are the first example of using statistical symmetry constraints for turbulence models.

Developing new model equations from symmetries follows a similar logic as creating symmetry invariant solutions, which is discussed in Section 3.3. In both cases, invariant functions are calculated, although when deriving equations, we also include physical derivatives as possible variables.

5.1.1. Introductory Example: Constructing the Euler Equations from Their Symmetries

A simple example that not only illustrates the method, but also gives rise to an interesting result is found in the Euler equations, which are given by (1.1) and (1.2) with $\nu = 0$. Supposing for the purpose of this demonstration that we did not know the form of the Euler equations, but we did know their symmetries and the variables appearing in them, we write them as the general function

$$\boldsymbol{F}\left(t; x_i; U_i; P; \frac{\partial U_i}{\partial t}; \frac{\partial U_i}{\partial x_j}; \frac{\partial P}{\partial t}; \frac{\partial P}{\partial x_i}\right) = 0, \tag{5.1}$$

or, using jet notation,

$$\boldsymbol{F}\left(t; x_i; U_i; P; U_{i,t}; U_{i,x_j}; P_{,t}; P_{,x_i}\right) = 0. \tag{5.2}$$

This switch to jet notation is not purely intended to be more compact, but is also meant to indicate that the physical derivatives appearing in $\boldsymbol{F}$ are treated just like the other, non-derivative variables. A similar shift in perspective has also been discussed in Chapter 2, and, here, it reverts the present problem to the problem of finding invariant solutions.

As a side comment, even though the assumption that we know the Euler symmetries but not the Euler equations may seem a bit contrived, note that all classical Euler symmetries are connected to fundamental physical principles. Therefore, it is not that unreasonable to envision a scenario in which someone correctly postulates all Euler symmetries without knowing the equations themselves.

One might also object that the decision to only include first derivatives in (5.2) requires a priori knowledge of the result by invoking the only slightly different Navier–Stokes case, in which the second spatial velocity derivative appears. However, it makes more sense to think of the Navier–Stokes equations as a first-order system consisting of mass and momentum conservation and a material law. Then, extending the Euler case to the Navier–Stokes case can be achieved by adding the molecular stress tensor and its first derivatives to the list of variables, which directly corresponds to the additional physics encoded by the Navier–Stokes equations and is not as arbitrary as increasing the order of derivatives to two. This approach is also necessary because the symmetries to be fulfilled by a material law are different from those of momentum conservation. For example, a material law has to be invariant under time-dependent rotation—a principle referred to as objectivity in material modeling—whereas the momentum equation, in which inertial effects are important, must not have this particular symmetry. We may, therefore, conclude that first derivatives in the argument list of $\boldsymbol{F}$ in (5.2) should always suffice, and note that the choice of variables impacts the physical effects that the resulting equations can represent.

After this preliminary discussion, we can start with the derivation of the Euler equations. Since we are considering the unaveraged system, only the classical symmetries and no statistical symmetries are taken into account. In concrete terms, using the invariant surface condition (2.9), demanding invariance of $\boldsymbol{F}$ with respect to (3.18)–(3.23) gives rise to the PDE system

$$X_t^{(1)}\boldsymbol{F}|_{\boldsymbol{F}=0} = 0 \wedge X_{x_i}^{(1)}\boldsymbol{F}|_{\boldsymbol{F}=0} = 0 \wedge \cdots \wedge X_{\mathrm{Sc},II}^{(1)}\boldsymbol{F}|_{\boldsymbol{F}=0} = 0, \tag{5.3}$$

the solution of which is a constrained form of $\boldsymbol{F}$ which is guaranteed to be invariant under all considered symmetries. Note that we omit the arguments of $\boldsymbol{F}(t; x_i; U_i; P; U_{i,t}; U_{i,x_j}; P_{,t}; P_{,x_i})$ for the sake of brevity. Since $\boldsymbol{F}$ contains first derivatives as its arguments, the first prolongations of all symmetries have to be calculated using Eqs. (2.17) and (2.18) to account for their action on these first derivatives.

Instead of treating (5.3) as a coupled system, it is possible to apply the symmetries one by one and see the effect of each individual symmetry, which makes for a simpler and more insightful discussion. Note that this is generally not possible when using the moving frames method, which operates on the level of global transformations and, hence, gives rise to a generally nonlinear algebraic coupled equation system instead of a linear PDE system. It is sensible to start with the arguably simpler symmetries, therefore, we begin with the time translation symmetry given by Eq. (3.18). As can be seen by invoking Eq. (2.17) with (2.18), its first prolongation is trivial, leading to

$$X_t^{(1)}\boldsymbol{F} = X_t\boldsymbol{F} = \frac{\partial \boldsymbol{F}}{\partial t} = 0. \tag{5.4}$$

Equation (5.4) can only be fulfilled if $\boldsymbol{F}$ does not depend on t explicitly, which implies that t has to be removed from the list of possible arguments. Hence, the form of the Euler equations has been constrained to

$$\boldsymbol{F}\left(x_i; U_i; P; U_{i,t}; U_{i,x_j}; P_{,t}; P_{,x_i}\right) = 0. \tag{5.5}$$

Here, we may point out the distinction we intend to highlight with the use of jet notation: Only t, but not the temporal derivatives, are affected by X_t, which is indeed correct. The next symmetry to consider is the similarly simple translation symmetry in space, i.e. (3.20) with $f_{\mathrm{Gal}_i}(t) =$ const. Note that the free function $f_{\mathrm{Gal}_i}(t)$ is arbitrary, so that we can simplify the application of the symmetry (3.20) by first setting $f_{\mathrm{Gal}_i}(t)$ to a constant before turning to the general case later. This leads to

$$X_{x_i}^{(1)}\boldsymbol{F} = X_{x_i}\boldsymbol{F} = \frac{\partial \boldsymbol{F}}{\partial x_i} = 0, \tag{5.6}$$

implying that x_i also has to be removed as a possible variable. An analogous conclusion can be obtained from the pressure translation symmetry (3.21), whose first prolongation reads

$$X_P^{(1)} = f_P(t)\frac{\partial}{\partial P} + f_P'(t)\frac{\partial}{\partial P_{,t}}. \tag{5.7}$$

We note again that the free function is arbitrary, so we can simplify the discussion by first setting $f_P(t) = a_P =$ constant. Then, in analogy to the two previously invoked symmetries, this leads to

$$X_{P;f_P(t)=a_P}^{(1)}\boldsymbol{F} = a_P\frac{\partial \boldsymbol{F}}{\partial P} = 0, \tag{5.8}$$

eliminating P from the list of variables,

$$\boldsymbol{F}\left(U_i; U_{i,t}; U_{i,x_j}; P_{,t}; P_{,x_i}\right) = 0. \tag{5.9}$$

Now, we set $f'_P(t) = a_P^{(1)} = $ constant. Equation (5.9) implies $\partial \boldsymbol{F}/\partial P = 0$, so that

$$X^{(1)}_{P;f'_P(t)=a_P^{(1)}} \boldsymbol{F} = a_P^{(1)} \frac{\partial \boldsymbol{F}}{\partial P_{,t}} = 0. \tag{5.10}$$

This is again a symmetry as simple as the ones invoked before, and we can conclude that $P_{,t}$ has to be eliminated from the list of possible arguments. Note that by considering higher prolongations and carrying on in this way, all temporal derivatives of P could successively be eliminated, but we only assumed first derivatives anyway. Clearly, spatial derivatives of the pressure can never be affected by this symmetry.

At this point, we have applied all translation symmetries, and the form of the Euler equations is narrowed down to

$$\boldsymbol{F}\left(U_i; U_{i,t}; U_{i,x_j}; P_{,x_i}\right) = 0. \tag{5.11}$$

In concrete terms, any equation containing only expressions of these variables automatically fulfills the symmetries considered so far. Having thus simplified the problem, we can apply the significantly more complicated generalized Galilean symmetry (3.20) with arbitrary $f_{\mathrm{Gal}_i}(t)$. Unlike the simple translation symmetries considered above, the Galilean symmetry has a nontrivial first prolongation, which is calculated according to Eq. (2.17). The resulting system

$$X^{(1)}_{\mathrm{Gal}} \boldsymbol{F} = f'_{\mathrm{Gal}_i}(t) \frac{\partial \boldsymbol{F}}{\partial U_i} + (f''_{\mathrm{Gal}_i}(t) - U_{i,x_j} f'_{\mathrm{Gal}_j}(t)) \frac{\partial \boldsymbol{F}}{\partial U_{i,t}} - f''_{\mathrm{Gal}_i}(t) \frac{\partial \boldsymbol{F}}{\partial P_{,x_i}} = 0 \tag{5.12}$$

is solved using the method of characteristics, an introduction to which can be found in the textbook by John (1978). The fundamental idea of this method is that the PDE (5.12) can be written as an ODE system in the characteristic variables τ and s, which, in this case, reads

$$\frac{d\boldsymbol{F}}{d\tau} = 0, \tag{5.13}$$

$$\frac{dU_i}{d\tau} = f'_{\mathrm{Gal}_i}(t), \tag{5.14}$$

$$\frac{dU_{i,t}}{d\tau} = f''_{\mathrm{Gal}_i}(t) - U_{i,x_j} f'_{\mathrm{Gal}_j}(t), \tag{5.15}$$

$$\frac{dU_{i,x_j}}{d\tau} = 0, \tag{5.16}$$

$$\frac{dP_{,x_i}}{d\tau} = -f''_{\mathrm{Gal}_i}(t). \tag{5.17}$$

Equation (5.13) can directly be integrated to yield $\boldsymbol{F} = c_1(s)$, and Eq. (5.16), which essentially states that U_{i,x_j} is Galilean invariant, yields $U_{i,x_j} = c_{2_{ij}}(s)$. Equations (5.14), (5.15) and (5.17) can be combined to

$$\frac{dU_{i,t}}{d\tau} + \frac{dU_j}{d\tau} U_{i,x_j} + \frac{dP_{,x_i}}{d\tau} = 0, \tag{5.18}$$

which is integrated to

$$U_{i,t} + U_j U_{i,x_j} + P_{,x_i} = c_{3_i}(s). \tag{5.19}$$

Note that U_{i,x_j} does not depend on τ, making this integration very simple. Since all constants of integration c_1, $c_{2_{ij}}$ and c_{3_i} depend only on s, we can equivalently write c_1 (i.e. $\boldsymbol{F}$) as a function of $c_{2_{ij}}$ and c_{3_i}. In other words, we have further reduced the form of $\boldsymbol{F}$ to

$$\boldsymbol{F}\left(U_{i,x_j}; U_{i,t} + U_j U_{i,x_j} + P_{,x_i}\right) = 0. \tag{5.20}$$

Interestingly, the form (5.20) already resembles the final Euler equations closely. A final constraint is found in the rotational symmetry (3.19), leading to

$$U_{i,t} + U_j U_{i,x_j} + P_{,x_i} = 0, \tag{5.21}$$

$$\boldsymbol{F}\left(U_{i,x_i}; U_{i,x_j} U_{j,x_i}; U_{i,x_j} U_{j,x_k} U_{k,x_i}\right) = 0. \tag{5.22}$$

At this point, no further symmetry constraints can be made use of. Evidently, the reason why only the first invariant of the velocity gradient U_{i,x_i} appears in the final form cannot be explained by symmetries alone. Nevertheless, this analysis clearly demonstrates how tightly the symmetries constrain the Euler equations, and, in other words, how much of the physics expressed by the Euler equations apparently are encoded in its symmetries. This result, therefore, further motivates the use of symmetry-based modeling approaches.

5.1.2. Application to Turbulence Modeling

Adapting the rationale demonstrated in the previous section to the challenge of developing a turbulence model is straightforward. We start with the infinite hierarchy of moment equations and their symmetries, which can be calculated algorithmically and are already known, as discussed in Chapter 2 and Section 3.2. They are given by Eqs. (3.34)–(3.39) and (3.59)–(3.62), with (3.38) and (3.39) combining to (3.40) in the viscous case. Additionally, we select a finite set of model variables that the final model may depend on. Then, following the steps shown in the previous section, we can derive the general possible form of the model equations. In this framework, most of the freedom one has as a modeler lies in the step of selecting possible model variables, after which the process is mostly algorithmic. Therefore, the process does not lead to one particular new model, but to a new class of models.

To a certain degree, existing turbulence models already follow this logic. A selection of variables is made based on physical arguments, and the form of the equations is then constrained using, among other things, the arguments of invariant modeling. However, the process through which the invariance constraints are invoked is not rigorous, which might work for the relatively simple classical symmetries, but does not remain feasible once the statistical symmetries are taken into account. This motivates the developments of the present work, where we extend the invariant modeling approach in two crucial ways: First, by also taking into account the statistical symmetries (3.59)–(3.62) and, second, by following an algorithmic approach to generate possible model equations.

An important resulting feature of this approach is that instead of starting with an equation system in which only a few unclosed terms have to be modeled, we start with a completely general equation form, rendering the distinction between the closed and the unclosed part obsolete. Therefore, in the present context, the term turbulence model refers to the full set of model equations, not only the unclosed part. This approach is made necessary by the fact that the closed part of the RANS equations, i.e. (1.3) and (1.6) without the Reynolds stress tensor R_{ij}, by itself, does not fulfill the statistical symmetries (3.59)–(3.62). Therefore, it is not enough to ensure that any closure relations fulfill all symmetries, and instead, the whole equation has to be taken into consideration. The situation is different when only considers the classical symmetries, because those the closed part does fulfill by itself. The same arguments analogously also hold for RSMs.

Failure of the Algorithm with No Additional Model Variables

In this section, we investigate what the symmetry constraints resulting from classical and statistical symmetries imply if we do not introduce any additional model variables. As can be seen, the symmetries reduce the possible form of the model equations to a point where no meaningful model is possible.

Eddy-Viscosity Model We first discuss what happens when we try to develop an EVM that is invariant under the classical symmetries given by Eqs. (3.34)–(3.40) and the first statistical translation symmetry given by Eq. (3.60). Note that the latter symmetry expresses that without the presence of the Reynolds stress tensor, the mean velocity $\bar{U}_i$ cannot appear explicitly, Its derivatives, however, are allowed to appear. The exact, unclosed RANS equation (1.6) obviously fulfills this symmetry, which is mainly because of the quite complicated transformation of the Reynolds stress tensor given by (3.72), while invariance is better observed in the equations of the instantaneous approach defined by (1.3) and (1.4). However, as soon as the Reynolds stress tensor is replaced by a turbulence model, i.e. some function of the mean velocities, the nonlinear term inevitably breaks the translation symmetry due to the explicitly appearing mean velocity. This complicated situation motivates the idea to start with a completely generic equation of the form

$$\boldsymbol{F}\left(t; x_i; \bar{U}_i; \bar{P}; \bar{U}_{i,t}; \bar{U}_{i,x_j}; \bar{P}_{,t}; \bar{P}_{,x_i}\right) = 0. \tag{5.23}$$

For this analysis, we ignore viscous effects and hence omit the molecular stress tensor. According to Eq. (2.9), $\boldsymbol{F}$ is invariant under a set of symmetries if the condition

$$X_t^{(1)}\boldsymbol{F}|_{\boldsymbol{F}=0} = 0 \wedge X_{\text{Gal}_i}^{(1)}\boldsymbol{F}|_{\boldsymbol{F}=0} = 0 \wedge \cdots \wedge X_{\text{Sc,stat}}^{(1)}\boldsymbol{F}|_{\boldsymbol{F}=0} = 0, \tag{5.24}$$

holds, where the $X_i^{(1)}$ refer to the first prolongations of the considered symmetries in infinitesimal form given by Eqs. (3.34)–(3.39), (3.59) and (3.60). Equation (5.24) is a system of partial differential equations that can be solved using the method of characteristics, the result of which is a reduced set of variables. These variables are invariant under the employed symmetries.

To illustrate the implication of each symmetry, we apply them one at a time. As derivatives appear in the general form (5.23), we have to compute the prolongations of all symmetries using Eq. (2.17). These prolongations yield the effect of the respective symmetry on derivatives. In the case of translation symmetries without free functions, the prolongations are equal to the non-prolonged symmetries. The time translation symmetry (3.34), the translation symmetry in space given by the Galilean symmetry (3.36) with $f'_{\text{Gal}_i}(t) = 0$, the statistical translation symmetry (3.60) and the translation symmetry of pressure given by Eq. (3.37) have an analogous effect as in Section 5.1.1, eliminating respectively $t, x_i, \bar{U}_i, \bar{P}$ and $\bar{P}_{,t}$, and, thus, reducing $\boldsymbol{F}$ to

$$\boldsymbol{F}\left(\bar{U}_{i,t}; \bar{U}_{i,x_j}; \bar{P}_{,x_i}\right) = 0. \tag{5.25}$$

Note that due to the statistical symmetry (3.60), the mean velocity $\bar{U}_i$ is removed from the list of arguments, creating a different situation compared to the derivation of the non-averaged Euler equations shown in Section 5.1.1, where the statistical symmetries did not play any role.

At this point, we invoke the Galilean symmetry given by Eq. (3.36) with no restrictions on the free function. This symmetry also has a nontrivial prolongation, which reads

$$\begin{aligned} X_{\mathrm{Gal}}^{(1)} &= f_{\mathrm{Gal}_i}(t)\frac{\partial}{\partial x_i} + f'_{\mathrm{Gal}_i}(t)\frac{\partial}{\partial \bar{U}_i} - x_i f''_{\mathrm{Gal}_i}(t)\frac{\partial}{\partial \bar{P}} \\ &+ (f''_{\mathrm{Gal}_i}(t) - \bar{U}_{i,x_j} f'_{\mathrm{Gal}_j}(t))\frac{\partial}{\partial \bar{U}_{i,t}} - f''_{\mathrm{Gal}_i}(t)\frac{\partial}{\partial \bar{P}_{,x_i}}. \end{aligned} \tag{5.26}$$

Applying this operator to the reduced form of the equation $\boldsymbol{F}$ given by Eq. (5.25), we obtain

$$X_{\mathrm{Gal}}^{(1)}\boldsymbol{F} = (f''_{\mathrm{Gal}_i}(t) - \bar{U}_{i,x_j} f'_{\mathrm{Gal}_j}(t))\frac{\partial \boldsymbol{F}}{\partial \bar{U}_{i,t}} - f''_{\mathrm{Gal}_i}(t)\frac{\partial \boldsymbol{F}}{\partial \bar{P}_{,x_i}} = 0. \tag{5.27}$$

Since this must hold for any $f_{\mathrm{Gal}_i}(t)$, we may simplify the solution process by first considering the special case $f''_{\mathrm{Gal}_i}(t) = 0$, for which (5.27) reduces to

$$\frac{\partial \boldsymbol{F}}{\partial \bar{U}_{j,t}} = 0. \tag{5.28}$$

The time derivative of the velocity thus also has to vanish, leaving only

$$\boldsymbol{F}\left(\bar{U}_{i,x_j}, \bar{P}_{,x_i}\right) = 0. \tag{5.29}$$

Applying the prolonged Galilean symmetry generator (5.26) with no restrictions on the free function to the reduced form (5.29) then leads to

$$X_{\mathrm{Gal}}^{(1)}\boldsymbol{F} = -f''_{\mathrm{Gal}_i}(t)\frac{\partial \boldsymbol{F}}{\partial \bar{P}_{,x_i}} = 0, \tag{5.30}$$

eliminating the pressure gradient from the list of possible variables. In conclusion, this means that in order for an equation of the assumed form (5.23) to fulfill the classical and statistical symmetries at the same time, it can only contain the velocity gradient. Obviously, there is no hope that any meaningful set of equations generally describing turbulent flows can be built on that basis. Note that without the statistical translation symmetry (3.60), which eliminates the mean velocity from the generic form, these problems would not exist. With the velocity still present, the Galilean symmetry would have allowed the generic form

$$\boldsymbol{F}\left(\bar{U}_{i,x_j}; \bar{U}_{i,t} + \bar{U}_j \bar{U}_{i,x_j} + \bar{P}_{,x_i}\right) = 0, \tag{5.31}$$

in which the averaged Navier–Stokes equations (1.3) and (1.6) with vanishing viscosity and $R_{ij} = 0$ can be found. If the statistical symmetries are also included, however, the above procedure proves that the assumed form (5.23) is too restrictive, and some additional freedom is needed.

Reynolds Stress Model Before exploring which model variables to introduce in order to gain such additional freedom, we first attempt to derive an RSM that is invariant under the classical symmetries (3.34)–(3.39), where (3.38) and (3.39) combine to (3.40) in the viscous case, and the statistical symmetries (3.59)–(3.62). The generic equation form this time also contains second moments, leading to

$$\boldsymbol{F}\left(t; x_i; \bar{U}_i; \bar{P}; \bar{U}_{i,t}; \bar{U}_{i,x_j}; \bar{P}_{,t}; \bar{P}_{,x_i}; H_{ij}; H_{ij,t}; H_{ij,x_k}; \overline{U_i P_{,x_j}}; \overline{U_i P_{,x_j},t}; \overline{U_i P_{,x_j,x_k}}\right) = 0. \tag{5.32}$$

The list of arguments is almost equivalent to the set of closed variables present in the first and second moment equations, i.e. (1.4) and (3.4), though it turns out that $\overline{U_i P_{,x_j}}$ and its derivatives are also needed. Viscous effects are still excluded for simplicity. Following the same steps as before, the classical and statistical translation symmetries (3.34), (3.37) and (3.56)–(3.58) as well as (3.36) with $f'_{\mathrm{Gal}_i}(t) = 0$ reduce the possible form of the model to

$$\boldsymbol{F}\left(\bar{U}_{i,t}; \bar{U}_{i,x_j}; \bar{P}_{,x_i}; H_{ij,t}; H_{ij,x_k}; \overline{U_i P_{,x_j}}; \overline{U_i P_{,x_j,x_k}}\right) = 0. \tag{5.33}$$

This time, the action of the Galilean symmetry (3.36) also has to be extended to the second moments and their derivatives. The first prolongation of its infinitesimal generator then reads

$$\begin{aligned}
X^{(1)}_{\mathrm{Gal}} = {} & f_{\mathrm{Gal}_i}(t)\frac{\partial}{\partial x_i} + f'_{\mathrm{Gal}_i}(t)\frac{\partial}{\partial \bar{U}_i} + \left(f'_{\mathrm{Gal}_i}(t)\bar{U}_j + f'_{\mathrm{Gal}_j}(t)\bar{U}_i\right)\frac{\partial}{\partial H_{ij}} \\
& - x_i f''_{\mathrm{Gal}_i}(t)\frac{\partial}{\partial \bar{P}} + \left(f'_{\mathrm{Gal}_i}(t)\bar{P} - \bar{U}_i x_j f''_{\mathrm{Gal}_j}(t)\right)\frac{\partial}{\partial \overline{PU_i}}, \\
& + \left(f''_{\mathrm{Gal}_i}(t) - \bar{U}_{i,x_j} f'_{\mathrm{Gal}_j}(t)\right)\frac{\partial}{\partial \bar{U}_{i,t}} \\
& - f''_{\mathrm{Gal}_i}(t)\frac{\partial}{\partial \bar{P}_{,x_i}} \\
& + \left(\bar{U}_{i,t} f'_{\mathrm{Gal}_j}(t) + \bar{U}_{j,t} f'_{\mathrm{Gal}_i}(t) + \bar{U}_i f''_{\mathrm{Gal}_j}(t) + \bar{U}_j f''_{\mathrm{Gal}_i}(t) - H_{ij,x_k} f'_{\mathrm{Gal}_k}(t)\right)\frac{\partial}{\partial H_{ij,t}} \\
& + \left(\bar{U}_{i,x_k} f'_{\mathrm{Gal}_j}(t) + \bar{U}_{j,x_k} f'_{\mathrm{Gal}_i}(t)\right)\frac{\partial}{\partial H_{ij,x_k}} \\
& + \left(\bar{P}_{,x_j} f'_{\mathrm{Gal}_i}(t) - \bar{U}_i f''_{\mathrm{Gal}_j}(t)\right)\frac{\partial}{\partial \overline{U_i P_{,x_j}}} \\
& + \left(\bar{P}_{,x_j x_k} f'_{\mathrm{Gal}_i}(t) - \bar{U}_{i,x_k} f''_{\mathrm{Gal}_j}(t)\right)\frac{\partial}{\partial \overline{U_i P_{,x_j,x_k}}}.
\end{aligned} \tag{5.34}$$

Inserting (5.34) and (5.33) into the invariant surface condition (2.9) then leads to the complicated PDE system

$$\begin{aligned}
X^{(1)}_{\mathrm{Gal}}\boldsymbol{F} = {} & \left(f''_{\mathrm{Gal}_i}(t) - \bar{U}_{i,x_j} f'_{\mathrm{Gal}_j}(t)\right)\frac{\partial F}{\partial \bar{U}_{i,t}} - f''_{\mathrm{Gal}_i}(t)\frac{\partial F}{\partial \bar{P}_{,x_i}} \\
& + \left(\bar{U}_{i,t} f'_{\mathrm{Gal}_j}(t) + \bar{U}_{j,t} f'_{\mathrm{Gal}_i}(t) + \bar{U}_i f''_{\mathrm{Gal}_j}(t) + \bar{U}_j f''_{\mathrm{Gal}_i}(t) - H_{ij,x_k} f'_{\mathrm{Gal}_k}(t)\right)\frac{\partial F}{\partial H_{ij,t}} \\
& + \left(\bar{U}_{i,x_k} f'_{\mathrm{Gal}_j}(t) + \bar{U}_{j,x_k} f'_{\mathrm{Gal}_i}(t)\right)\frac{\partial F}{\partial H_{ij,x_k}} \\
& + \left(\bar{P}_{,x_j} f'_{\mathrm{Gal}_i}(t) - \bar{U}_i f''_{\mathrm{Gal}_j}(t)\right)\frac{\partial F}{\partial \overline{U_i P_{,x_j}}} \\
& + \left(\bar{P}_{,x_j x_k} f'_{\mathrm{Gal}_i}(t) - \bar{U}_{i,x_k} f''_{\mathrm{Gal}_j}(t)\right)\frac{\partial F}{\partial \overline{U_i P_{,x_j,x_k}}} = 0.
\end{aligned} \tag{5.35}$$

The details of the solution, which was initially performed using the CAS Maple (Waterloo Maple Inc., 2017) and subsequently verified manually using the method of characteristics, are given in Appendix A.3.1. Due to its complexity, care must be taken not to overlook any of the solutions of this system. The full solution reads

$$\boldsymbol{F}\left(\bar{U}_{i,t} + H_{ij,x_j} + \bar{P}_{,x_i}; \bar{U}_{i,x_j}; H_{ij,t} + H_{ij,x_k}\gamma_k + \overline{U_i P_{,x_j}} + \overline{U_j P_{,x_i}}\right) = 0, \tag{5.36}$$

where γ_i is implicitly defined by

$$\bar{U}_{i,t} + \bar{U}_{i,x_j}\gamma_j + \bar{P}_{,x_i} = 0. \tag{5.37}$$

At first glance, it looks like we have enough variables to construct meaningful equations for the considered first and the second moments. Unsurprisingly, the exact RANS momentum equation (1.4) (with $\nu = 0$) and continuity equation (1.3) can be constructed from the first two variables in (5.36). Moreover, it seems like a model equation for H_{ij} could be built from the last variable in (5.36). This expression resembles a material derivative, though in place of the mean velocity, the variable γ_i appears. However, this variable is defined by (5.37), which is only unique if the velocity gradient can be inverted. Since this is generally not the case, the whole result is not physically meaningful, and we again have to conclude that (5.32) is too narrow a form to fulfill all classical and statistical symmetries in the final model. However, the result is still interesting because it offers an insight into how to remedy this problem. The main question arising after the application of the statistical translation symmetry (3.60) is how to formulate the convective term of the model equation. The exact equations in instantaneous formulation (3.4) offer no insight here, because in them, the convective term is not closed. In a sense, our algorithm circumvents this issue by introducing the expression γ_i to replace the mean velocity in the convective term. Using (5.37) to determine the behavior of γ_i under the considered symmetries, it can be seen that it behaves like the mean velocity $\bar{U}_i$ under all classical symmetries (3.34)–(3.40), but unlike $\bar{U}_i$, it is invariant under the statistical symmetries (3.59) and (3.60). In other words, its symmetry behavior is similar enough to that of the mean velocity that γ_i can appear in the material derivative without violating any classical symmetries, but crucially differs in its behavior under the statistical symmetries such that its appearance does not break them. Evidently, from the list of variables included in (5.32), only the physically dubious and mathematically problematic variable γ_i can be formed with this particular symmetry behavior. However, since we are completely free to add additional model variables to (5.32), this issue can be addressed by introducing a variable with the symmetry behavior of γ_i as a new model variable. In the next section, the algorithm presented here is repeated with such an additional model variable.

5.1.3. Successful New Invariant Modeling Approach with Additional Model Variables

To summarize, we have gained two important insights from the failed attempts in Section 5.1.2: First, when trying to construct EVMs or RSMs, the form (5.23) or, respectively, (5.32), is not general enough to allow for meaningful equations subject to all invoked symmetry constraints. Second, this can be rectified by introducing an additional model variable that behaves like the mean velocity under all classical symmetries (3.34)–(3.40), while being invariant under the statistical symmetries (3.59)–(3.62).

At this point, an analogy to the step from classical one-equation models to two-equation models as discussed in Section 3.4.1 can be made. With too few model variables to form a dimensionally correct expression for the turbulent viscosity ν_t, or, in other words, to fulfill the classical scaling symmetries, an additional scale-providing variable such as ε is introduced to ensure the necessary freedom. In the present context, as suggested by γ_i in (5.37), we extend the generic form assumed in Eq. (5.23) by a new model variable denoted here with $\hat{U}_i$, and a corresponding pressure $\hat{P}$, which respectively transform like $\bar{U}_i$ and $\bar{P}$ under all classical symmetries (3.34)–(3.40), but are invariant under the statistical symmetries (3.59)–(3.62). In concrete terms, the classical symmetries (3.34)–(3.40) extended with $\hat{U}_i$ and $\hat{P}$ read in infinitesimal form

$$X_t = \frac{\partial}{\partial t}, \tag{5.38}$$

$$\begin{aligned} X_{\mathrm{rot}_\alpha} = {}& \epsilon_{jk\alpha} x_j \frac{\partial}{\partial x_k} + \epsilon_{jk\alpha} \bar{U}_j \frac{\partial}{\partial \bar{U}_k} + \epsilon_{jk\alpha} \hat{U}_j \frac{\partial}{\partial \hat{U}_k} \\ & + (\epsilon_{ki\alpha} H_{kj} + \epsilon_{kj\alpha} H_{ik}) \frac{\partial}{\partial H_{ij}} + \epsilon_{jk\alpha} \overline{PU_j} \frac{\partial}{\partial \overline{PU_k}}, \end{aligned} \tag{5.39}$$

$$\begin{aligned} X_{\mathrm{Gal}} = {}& f_{\mathrm{Gal}_i}(t) \frac{\partial}{\partial x_i} + f'_{\mathrm{Gal}_i}(t) \frac{\partial}{\partial \bar{U}_i} + f'_{\mathrm{Gal}_i}(t) \frac{\partial}{\partial \hat{U}_i} \\ & - x_i f''_{\mathrm{Gal}_i}(t) \frac{\partial}{\partial \bar{P}} - x_i f''_{\mathrm{Gal}_i}(t) \frac{\partial}{\partial \hat{P}} \\ & + \left(f'_{\mathrm{Gal}_i}(t) \bar{U}_j + f'_{\mathrm{Gal}_j}(t) \bar{U}_i \right) \frac{\partial}{\partial H_{ij}} \\ & + \left(f'_{\mathrm{Gal}_i}(t) \bar{P} - \bar{U}_i x_j f''_{\mathrm{Gal}_j}(t) \right) \frac{\partial}{\partial \overline{PU_i}}, \end{aligned} \tag{5.40}$$

$$X_P = f_P(t) \frac{\partial}{\partial \bar{P}} + f_{\hat{P}}(t) \frac{\partial}{\partial \hat{P}} + f_P(t) \bar{U}_i \frac{\partial}{\partial \overline{PU_i}}, \tag{5.41}$$

$$\begin{aligned} X_{\mathrm{Sc},I} = {}& x_i \frac{\partial}{\partial x_i} + \bar{U}_i \frac{\partial}{\partial \bar{U}_i} + \hat{U}_i \frac{\partial}{\partial \hat{U}_i} + 2\bar{P} \frac{\partial}{\partial \bar{P}} + 2\hat{P} \frac{\partial}{\partial \hat{P}} \\ & + 2H_{ij} \frac{\partial}{\partial H_{ij}} + 3\overline{PU_i} \frac{\partial}{\partial \overline{PU_i}}, \end{aligned} \tag{5.42}$$

$$\begin{aligned} X_{\mathrm{Sc},II} = {}& t \frac{\partial}{\partial t} - \bar{U}_i \frac{\partial}{\partial \bar{U}_i} - \hat{U}_i \frac{\partial}{\partial \hat{U}_i} - 2\bar{P} \frac{\partial}{\partial \bar{P}} - 2\hat{P} \frac{\partial}{\partial \hat{P}} \\ & - 2H_{ij} \frac{\partial}{\partial H_{ij}} - 3\overline{PU_i} \frac{\partial}{\partial \overline{PU_i}}, \end{aligned} \tag{5.43}$$

$$\begin{aligned} X_{\mathrm{Sc,ns}} = {}& 2t \frac{\partial}{\partial t} + x_i \frac{\partial}{\partial x_i} - \bar{U}_i \frac{\partial}{\partial \bar{U}_i} - \hat{U}_i \frac{\partial}{\partial \hat{U}_i} - 2\bar{P} \frac{\partial}{\partial \bar{P}} - 2\hat{P} \frac{\partial}{\partial \hat{P}} \\ & - 2H_{ij} \frac{\partial}{\partial H_{ij}} - 3\overline{PU_i} \frac{\partial}{\partial \overline{PU_i}}. \end{aligned} \tag{5.44}$$

Since $\hat{U}_i$ and $\hat{P}$ are invariant under the statistical symmetries, we can still use (3.59)–(3.62). The symmetries (5.38)–(5.44) in global form are given by Eqs. (A.42)–(A.52).

Eddy-Viscosity Model

Turning first to the question of how to make use of these additional model variables in order to construct a statistically invariant EVM, we assume as the general form

$$\boldsymbol{F}\left(t; x_i; \bar{U}_i; \hat{U}_i; \bar{P}; \hat{P}; \bar{U}_{i,t}; \bar{U}_{i,x_j}; \hat{U}_{i,t}; \hat{U}_{i,x_j}; \bar{P}_{,t}; \bar{P}_{,x_i}; \hat{P}_{,t}; \hat{P}_{,x_i}\right) = 0. \tag{5.45}$$

It is a remarkable feature of the modeling algorithm that it is not necessary to specify anything about these new variables apart from their behavior under the symmetry transformations we are going to use. The application of the translation symmetries, i.e. (3.60), (5.38) and (5.41) as well as (5.40) with $f'_{\mathrm{Gal}_i}(t) = 0$, is as straightforward as before, reducing Eq. (5.45) to

$$\boldsymbol{F}\left(\hat{U}_i; \bar{U}_{i,t}; \bar{U}_{i,x_j}; \hat{U}_{i,t}; \hat{U}_{i,x_j}; \bar{P}_{,x_i}; \hat{P}_{,x_i}\right) = 0. \tag{5.46}$$

Unlike $\bar{U}_i$, $\hat{U}_i$ is not affected by the statistical translation symmetry (3.60) and, therefore, remains in (5.46) after the application of these symmetries. Similar to the discussion in the previous sections, we now apply the Galilean symmetry (5.40), whose first prolongation is

$$\begin{aligned} X^{(1)}_{\mathrm{Gal}} = {} & f_{\mathrm{Gal}_i}(t)\frac{\partial}{\partial x_i} + f'_{\mathrm{Gal}_i}(t)\frac{\partial}{\partial \bar{U}_i} + f'_{\mathrm{Gal}_i}(t)\frac{\partial}{\partial \hat{U}_i} \\ & + (f''_{\mathrm{Gal}_i}(t) - \bar{U}_{i,x_j} f'_{\mathrm{Gal}_j}(t))\frac{\partial}{\partial \bar{U}_{i,t}} + (f''_{\mathrm{Gal}_i}(t) - \hat{U}_{i,x_j} f'_{\mathrm{Gal}_j}(t))\frac{\partial}{\partial \hat{U}_{i,t}} \\ & - x_i f''_{\mathrm{Gal}_i}(t)\frac{\partial}{\partial \bar{P}} - x_i f''_{\mathrm{Gal}_i}(t)\frac{\partial}{\partial \hat{P}} - f''_{\mathrm{Gal}_i}(t)\frac{\partial}{\partial \bar{P}_{,x_i}} - f''_{\mathrm{Gal}_i}(t)\frac{\partial}{\partial \hat{P}_{,x_i}}, \end{aligned} \tag{5.47}$$

where we restrict ourselves to derivatives appearing in (5.46). Applying (5.47) to (5.46) yields the invariant surface condition

$$\begin{aligned} X^{(1)}_{\mathrm{Gal}}\boldsymbol{F} = {} & f'_{\mathrm{Gal}_i}(t)\frac{\partial \boldsymbol{F}}{\partial \hat{U}_i} + (f''_{\mathrm{Gal}_i}(t) - \bar{U}_{i,x_j} f'_{\mathrm{Gal}_j}(t))\frac{\partial \boldsymbol{F}}{\partial \bar{U}_{i,t}} + (f''_{\mathrm{Gal}_i}(t) - \hat{U}_{i,x_j} f'_{\mathrm{Gal}_j}(t))\frac{\partial \boldsymbol{F}}{\partial \hat{U}_{i,t}} \\ & - f''_{\mathrm{Gal}_i}(t)\frac{\partial \boldsymbol{F}}{\partial \bar{P}_{,x_i}} - f''_{\mathrm{Gal}_i}(t)\frac{\partial \boldsymbol{F}}{\partial \hat{P}_{,x_i}} = 0, \end{aligned} \tag{5.48}$$

resulting in the characteristic system

$$\frac{d\boldsymbol{F}}{d\tau} = 0, \tag{5.49}$$

$$\frac{d\hat{U}_i}{d\tau} = f'_{\mathrm{Gal}_i}(t), \tag{5.50}$$

$$\frac{d\bar{U}_{i,t}}{d\tau} = f''_{\mathrm{Gal}_i}(t) - \bar{U}_{i,x_j} f'_{\mathrm{Gal}_j}(t), \tag{5.51}$$

$$\frac{d\hat{U}_{i,t}}{d\tau} = f''_{\mathrm{Gal}_i}(t) - \hat{U}_{i,x_j} f'_{\mathrm{Gal}_j}(t), \tag{5.52}$$

$$\frac{d\bar{U}_{i,x_j}}{d\tau} = 0, \tag{5.53}$$

$$\frac{d\hat{U}_{i,x_j}}{d\tau} = 0, \tag{5.54}$$

$$\frac{d\bar{P}_{,x_i}}{d\tau} = -f''_{\mathrm{Gal}_i}(t), \tag{5.55}$$

$$\frac{d\hat{P}_{,x_i}}{d\tau} = -f''_{\mathrm{Gal}_i}(t). \tag{5.56}$$

Eqs. (5.49), (5.53) and (5.54) are integrated directly, yielding $\boldsymbol{F} = c_1(s)$, $\bar{U}_{i,x_j} = c_{2_{ij}}(s)$ and $\hat{U}_{i,x_j} = c_{3_{ij}}(s)$, respectively. Combining (5.50), (5.51) and (5.55) to

$$\frac{d\bar{U}_{i,t}}{d\tau} + \frac{d\hat{U}_j}{d\tau}\bar{U}_{i,x_j} + \frac{d\bar{P}_{,x_i}}{d\tau} = 0,$$

and integrating leads to

$$\bar{U}_{i,t} + \hat{U}_j\bar{U}_{i,x_j} + \bar{P}_{,x_i} = c_{4_i}(s),$$

where we have again used the result that $\bar{U}_{i,x_j}$ is constant in τ, as implied by (5.53). Similarly, Eqs. (5.50), (5.52) and (5.56) can be combined to

$$\frac{d\hat{U}_{i,t}}{d\tau} + \frac{d\hat{U}_j}{d\tau}\hat{U}_{i,x_j} + \frac{d\hat{P}_{,x_i}}{d\tau} = 0,$$

which, when integrated, gives rise to

$$\hat{U}_{i,t} + \hat{U}_j\hat{U}_{i,x_j} + \hat{P}_{,x_i} = c_{5_i}(s).$$

As has been discussed in Section 5.1.1, saying that all of these constants of integration depend on s is the same as stating that one constant of integration depends on all the others. Expressing the dependency as $c_1 = c_1(c_{2_{ij}}, c_{3_{ij}}, c_{4_i}, c_{5_i})$ is then equivalent to

$$\boldsymbol{F}\left(\bar{U}_{i,x_j}; \hat{U}_{i,x_j}; \bar{U}_{i,t} + \hat{U}_j\bar{U}_{i,x_j} + \bar{P}_{,x_j}; \hat{U}_{i,t} + \hat{U}_j\hat{U}_{i,x_j} + \hat{P}_{,x_j}\right) = 0. \tag{5.57}$$

Next, the rotational symmetries (3.35) are invoked. The invariance condition

$$X^{(1)}_{\mathrm{rot}_\alpha}\boldsymbol{F} = 0 \tag{5.58}$$

is fulfilled if

$$\bar{U}_{i,t} + \hat{U}_j\bar{U}_{i,x_j} + \bar{P}_{,x_i} = 0, \tag{5.59}$$

$$\hat{U}_{i,t} + \hat{U}_j\hat{U}_{i,x_j} + \hat{P}_{,x_i} = 0, \tag{5.60}$$

$$\boldsymbol{F}\left(\bar{U}_{i,x_i}; \hat{U}_{i,x_i}; \bar{U}_{i,x_j}\bar{U}_{j,x_i}; \hat{U}_{i,x_j}\hat{U}_{j,x_i}; \bar{U}_{i,x_j}\bar{U}_{j,x_k}\bar{U}_{k,x_i}; \hat{U}_{i,x_j}\hat{U}_{j,x_k}\hat{U}_{k,x_i}\right) = 0. \tag{5.61}$$

If we disregard the second and third tensor invariants of $\bar{U}_{i,x_j}$ and $\hat{U}_{i,x_j}$, i.e. variables three to six, the scaling symmetries uniquely yield

$$\bar{U}_{i,x_i} = 0, \tag{5.62}$$

$$\hat{U}_{i,x_i} + S_{\mathrm{conti}} = 0, \tag{5.63}$$

where a source term S_{conti} could, in principle, appear in (5.63). As far as symmetry constraints are concerned, a source term could also appear in (5.62), however, we dismiss this possibility on physical grounds, i.e. we obviously expect the mean velocity field to be divergence-free because of mass conservation. The system (5.59), (5.60), (5.62) and (5.63) is apparently closed and invariant under all classical and statistical symmetries.

From a theoretical point of view, we have now solved the problem that this section is concerned with. However, in practice, it seems unlikely that Eqs. (5.59), (5.60), (5.62) and (5.63) can actually predict turbulent flows accurately, but this is only due to the minimalistic form of the assumed general form (5.45). Nevertheless, this rigorous algorithmic approach has put us in a position more similar to classical turbulence modeling, in which we can and must rely on heuristic arguments to evolve (5.59), (5.60), (5.62) and (5.63) into a proper turbulence model. Introducing $\hat{U}_i$ and $\hat{P}$ increases the solution space, i.e. it now becomes possible to formulate numerous terms that are invariant under all considered symmetries, especially if additional model variables such as k and ε are introduced. The resulting combinatorial explosion of possible model equations renders the algorithmic approach used up to here highly inefficient. For the task of developing a practically useful statistically invariant turbulence model, it is, therefore, easier to disregard the rigorous approach used up to this point and instead focus on formulating equations that intuitively appear sensible and resemble existing models.

From experience, we can formulate a number of expectations that the new model equations should fulfill. First, viscous effects need to be incorporated into the equations if near-wall effects are to be considered. This could be done rigorously by including the molecular stress tensor and the viscosity in the generic form (5.45) and then repeating the process, or simply by adding viscous terms to Eqs. (5.59) and (5.60), yielding

$$\frac{\partial \bar{U}_i}{\partial t} + \hat{U}_j \frac{\partial \bar{U}_i}{\partial x_j} + \frac{\partial \bar{P}}{\partial x_i} - \nu \frac{\partial^2 \bar{U}_i}{\partial x_j \partial x_j} = 0, \tag{5.64}$$

$$\frac{\partial \hat{U}_i}{\partial t} + \hat{U}_j \frac{\partial \hat{U}_i}{\partial x_j} + \frac{\partial \hat{P}}{\partial x_i} - \nu \frac{\partial^2 \hat{U}_i}{\partial x_j \partial x_j} = 0. \tag{5.65}$$

Note that the inclusion of viscous terms does not break any symmetries, except that the two scaling symmetries (5.42) and (5.43) combine to (5.44), which is expected. Second, as in every classical turbulence model, we would expect a term accounting for the effect of the turbulent stresses on the mean velocity. Again, at least two possibilities for incorporating such a term into Eqs. (5.64) and (5.65) exist. The more general one would be to (i) select additional model variables such as k, ε, etc., (ii) propose how they transform under the above given symmetries and (iii) repeat the process starting at Eq. (5.45) with these additional variables. The simpler one is to append an additional source term, which represents closure relations to be specified later, to Eqs. (5.64) and (5.65), leading to

$$\frac{\partial \bar{U}_i}{\partial t} + \hat{U}_j \frac{\partial \bar{U}_i}{\partial x_j} + \frac{\partial \bar{P}}{\partial x_i} - \nu \frac{\partial^2 \bar{U}_i}{\partial x_j \partial x_j} + \frac{\partial \tilde{R}_{ij}}{\partial x_j} = 0, \tag{5.66}$$

$$\frac{\partial \hat{U}_i}{\partial t} + \hat{U}_j \frac{\partial \hat{U}_i}{\partial x_j} + \frac{\partial \hat{P}}{\partial x_i} - \nu \frac{\partial^2 \hat{U}_i}{\partial x_j \partial x_j} - S_{\mathrm{mom},i} = 0. \tag{5.67}$$

The closed part of the system (5.62), (5.63), (5.66) and (5.67), which consists of all terms except $\tilde{R}_{ij}$, $S_{\mathrm{mom},i}$ and S_{conti}, fulfills the classical symmetries (5.38)–(5.43), where the last two combine to (5.44) in the viscous case, and the statistical symmetries (3.59)–(3.62). This allows us to focus on finding a model for the unclosed part $\tilde{R}_{ij}$ and $S_{\mathrm{mom},i}$, which is further addressed in Section 5.2.1.

Reynolds Stress Model

Similar steps can also be followed to obtain a statistically invariant RSM. We again extend the generic form assumed in Eq. (5.32) by $\hat{U}_i$, $\hat{P}$, and their derivatives, which respectively transform like $\bar{U}_i$ and $\bar{P}$ under all classical symmetries (5.38)–(5.44), but are invariant under the statistical symmetries (3.59)–(3.62). In concrete terms, our starting point is

$$\boldsymbol{F}(x_i, t, \bar{U}_i, \bar{P}, H_{ij}, \hat{U}_i, \hat{P}, \bar{U}_{i,x_j}, \bar{U}_{i,t}, \bar{P}_{,x_i}, \bar{P}_{,t}, \hat{U}_{i,x_j}, \hat{U}_{i,t}, \hat{P}_{,x_j}, \hat{P}_{,t},$$
$$H_{ij,x_k}, H_{ij,t}, \overline{U_i P_{,x_j}}, \overline{U_i P_{,x_j,x_k}}, \overline{U_i P_{,x_j,t}}) = 0. \tag{5.68}$$

As we have already seen in the previous sections, the first step is to invoke the classical and statistical translation symmetries, i.e. (3.56)–(3.58), (5.38) and (5.41) as well as (5.40) with $f'_{\mathrm{Gal}_i}(t) = 0$, narrowing down the form of $\boldsymbol{F}$ to

$$\boldsymbol{F}(\hat{U}_i, \bar{U}_{i,x_j}, \bar{U}_{i,t}, \bar{P}_{,x_i}, \hat{U}_{i,x_j}, \hat{U}_{i,t}, \hat{P}_{,x_j}, H_{ij,x_k}, H_{ij,t}, \overline{U_i P_{,x_j}}, \overline{U_i P_{,x_j,x_k}}) = 0. \tag{5.69}$$

Like before, a crucial part in the derivation is demanding invariance with respect to the Galilean symmetry (5.40), which now reads in prolonged form

$$\begin{aligned}
X_{\mathrm{Gal}}^{(1)} &= f_{\mathrm{Gal}_i}(t)\frac{\partial}{\partial x_i} + f'_{\mathrm{Gal}_i}(t)\frac{\partial}{\partial \bar{U}_i} + f'_{\mathrm{Gal}_i}(t)\frac{\partial}{\partial \hat{U}_i} + \left(f'_{\mathrm{Gal}_i}(t)\bar{U}_j + f'_{\mathrm{Gal}_j}(t)\bar{U}_i\right)\frac{\partial}{\partial H_{ij}} \\
&\quad - x_i f''_{\mathrm{Gal}_i}(t)\frac{\partial}{\partial \bar{P}} - x_i f''_{\mathrm{Gal}_i}(t)\frac{\partial}{\partial \hat{P}} + \left(f'_{\mathrm{Gal}_i}(t)\bar{P} - \bar{U}_i x_j f''_{\mathrm{Gal}_j}(t)\right)\frac{\partial}{\partial \overline{PU_i}}, \\
&\quad + (f''_{\mathrm{Gal}_i}(t) - \bar{U}_{i,x_j} f'_{\mathrm{Gal}_j}(t))\frac{\partial}{\partial \bar{U}_{i,t}} + (f''_{\mathrm{Gal}_i}(t) - \hat{U}_{i,x_j} f'_{\mathrm{Gal}_j}(t))\frac{\partial}{\partial \hat{U}_{i,t}} \\
&\quad - f''_{\mathrm{Gal}_i}(t)\frac{\partial}{\partial \bar{P}_{,x_i}} - f''_{\mathrm{Gal}_i}(t)\frac{\partial}{\partial \hat{P}_{,x_i}} \\
&\quad + \left(\bar{U}_{i,t} f'_{\mathrm{Gal}_j}(t) + \bar{U}_{j,t} f'_{\mathrm{Gal}_i}(t) + \bar{U}_i f''_{\mathrm{Gal}_j}(t) + \bar{U}_j f''_{\mathrm{Gal}_i}(t) - H_{ij,x_k} f'_{\mathrm{Gal}_k}(t)\right)\frac{\partial}{\partial H_{ij,t}} \\
&\quad + (\bar{U}_{i,x_k} f'_{\mathrm{Gal}_j}(t) + \bar{U}_{j,x_k} f'_{\mathrm{Gal}_i}(t))\frac{\partial}{\partial H_{ij,x_k}} + (\bar{P}_{,x_j} f'_{\mathrm{Gal}_i}(t) - \bar{U}_i f''_{\mathrm{Gal}_j}(t))\frac{\partial}{\partial \overline{U_i P_{,x_j}}} \\
&\quad + (\bar{P}_{,x_j x_k} f'_{\mathrm{Gal}_i}(t) - \bar{U}_{i,x_k} f''_{\mathrm{Gal}_j}(t))\frac{\partial}{\partial \overline{U_i P_{,x_j,x_k}}}.
\end{aligned} \tag{5.70}$$

Solving the equation arising from inserting (5.69) and (5.70) into the invariant surface condition (2.9), i.e.

$$\begin{aligned}
X_{\mathrm{Gal}}^{(1)}\boldsymbol{F} &= f'_{\mathrm{Gal}_i}(t)\frac{\partial \boldsymbol{F}}{\partial \hat{U}_i} + (f''_{\mathrm{Gal}_i}(t) - \bar{U}_{i,x_j} f'_{\mathrm{Gal}_j}(t))\frac{\partial \boldsymbol{F}}{\partial \bar{U}_{i,t}} + (f''_{\mathrm{Gal}_i}(t) - \hat{U}_{i,x_j} f'_{\mathrm{Gal}_j}(t))\frac{\partial \boldsymbol{F}}{\partial \hat{U}_{i,t}} \\
&\quad - f''_{\mathrm{Gal}_i}(t)\frac{\partial \boldsymbol{F}}{\partial \bar{P}_{,x_i}} - f''_{\mathrm{Gal}_i}(t)\frac{\partial \boldsymbol{F}}{\partial \hat{P}_{,x_i}} \\
&\quad + \left(\bar{U}_{i,t} f'_{\mathrm{Gal}_j}(t) + \bar{U}_{j,t} f'_{\mathrm{Gal}_i}(t) + \bar{U}_i f''_{\mathrm{Gal}_j}(t) + \bar{U}_j f''_{\mathrm{Gal}_i}(t) - H_{ij,x_k} f'_{\mathrm{Gal}_k}(t)\right)\frac{\partial \boldsymbol{F}}{\partial H_{ij,t}} \\
&\quad + (\bar{U}_{i,x_k} f'_{\mathrm{Gal}_j}(t) + \bar{U}_{j,x_k} f'_{\mathrm{Gal}_i}(t))\frac{\partial \boldsymbol{F}}{\partial H_{ij,x_k}} + (\bar{P}_{,x_j} f'_{\mathrm{Gal}_i}(t) - \bar{U}_i f''_{\mathrm{Gal}_j}(t))\frac{\partial \boldsymbol{F}}{\partial \overline{U_i P_{,x_j}}}
\end{aligned}$$

$$+ (\bar{P}_{,x_j x_k} f'_{\mathrm{Gal}_i}(t) - \bar{U}_{i,x_k} f''_{\mathrm{Gal}_j}(t)) \frac{\partial \boldsymbol{F}}{\partial \overline{U_i P_{,x_j,x_k}}} = 0, \tag{5.71}$$

again requires a somewhat lengthy calculation, which is detailed in Appendix A.3.2. Unsurprisingly, Eqs. (1.3) and (1.4) without the viscous term can again be obtained. Furthermore, we now also need to find equations for the newly introduced model variables $\hat{U}_i$ and $\hat{P}$. From the results of (5.71), we can, like in Section 5.1.3, construct (5.60) and (5.63). This time, unlike in Section 5.1.2, we are also able to find a meaningful transport equation for the second velocity moment, which reads

$$\begin{aligned}\frac{\partial H_{ij}}{\partial t} + \hat{U}_k \frac{\partial H_{ij}}{\partial x_k} + \overline{U_i P_{,x_j}} + \overline{U_j P_{,x_i}} \\ + \hat{U}_i \frac{\partial H_{jk}}{\partial x_k} + \hat{U}_j \frac{\partial H_{ik}}{\partial x_k} - \frac{\partial \bar{U}_i}{\partial x_k} \hat{U}_j \hat{U}_k - \frac{\partial \bar{U}_j}{\partial x_k} \hat{U}_i \hat{U}_k = 0.\end{aligned} \tag{5.72}$$

Interestingly enough, an independent equation for the velocity-pressure-gradient terms can also be obtained and reads

$$\frac{\partial \overline{U_i P_{,x_j}}}{\partial x_k} - \hat{U}_i \frac{\partial^2 \bar{P}}{\partial x_j \partial x_k} - \frac{\partial \hat{P}}{\partial x_j} \frac{\partial \bar{U}_i}{\partial x_k} = 0. \tag{5.73}$$

In summary, Eqs. (1.3), (1.4), (5.60), (5.63), (5.72) and (5.73) form a closed system that fulfills all considered classical and statistical symmetries, which successfully concludes the discussion in this section. Nevertheless, it must be strongly emphasized that these equations only constitute a minimal model, and that additional terms are needed to develop a practically useful model. The most obvious example are the viscous terms, but also effects like turbulent dissipation and redistribution are not yet adequately accounted for. Crucially, however, many of the terms corresponding to these effects have a relatively simple behavior under all considered symmetries, which makes it possible to use Eqs. (1.3), (1.4), (5.60), (5.63), (5.72) and (5.73) as a foundation to which more terms can be added. We further explore this path in Section 5.2.2.

As a prerequisite, it makes sense to rewrite (5.72) in the more common fluctuation formulation, which turns it into a model equation for the Reynolds stress tensor,

$$\begin{aligned}\frac{\partial R_{ij}}{\partial t} + \hat{U}_k \frac{\partial R_{ij}}{\partial x_k} = \frac{\partial \bar{U}_j}{\partial x_k} (\bar{U}_i - \hat{U}_i)(\bar{U}_k - \hat{U}_k) + \frac{\partial \bar{U}_i}{\partial x_k} (\bar{U}_j - \hat{U}_j)(\bar{U}_k - \hat{U}_k) \\ + \frac{\partial R_{ik}}{\partial x_k} (\bar{U}_j - \hat{U}_j) + \frac{\partial R_{jk}}{\partial x_k} (\bar{U}_i - \hat{U}_i) - \overline{u_i \frac{\partial p}{\partial x_j}} - \overline{u_j \frac{\partial p}{\partial x_i}}.\end{aligned} \tag{5.74}$$

Note that unlike in (3.3), we do not use the decomposition

$$\overline{u_i \frac{\partial p}{\partial x_j}} + \overline{u_j \frac{\partial p}{\partial x_i}} = \frac{\partial \overline{(\delta_{jk} u_i + \delta_{ik} u_j) p}}{\partial x_k} - \overline{p \left(\frac{\partial u_i}{\partial x_j} + \frac{\partial u_j}{\partial x_i} \right)},$$

with which the last two terms of (5.74) could be written differently. Again, we can see the recurring theme of $\hat{U}_i$ replacing $\bar{U}_i$ in the convective term. Interestingly, the first right-hand side terms loosely resemble the production terms of the exact equation given by (3.3). Finally, Eq. (5.73) in fluctuation variables reads

$$\frac{\partial}{\partial x_k} \left(\overline{u_i \frac{\partial p}{\partial x_j}} \right) + \frac{\partial^2 \bar{P}}{\partial x_j \partial x_k} (\bar{U}_i - \hat{U}_i) + \frac{\partial \bar{U}_i}{\partial x_k} \left(\frac{\partial \bar{P}}{\partial x_j} - \frac{\partial \hat{P}}{\partial x_j} \right) = 0. \tag{5.75}$$

A major question remaining is that concerning the physical interpretation of the new model variables $\hat{U}_i$ and $\hat{P}$. Unfortunately, the mathematical formalism cannot shed much light on this question. To the best of our knowledge, no model with the exact form developed here has so far been suggested. However, looking at the literature, at least two ideas have led to similar modifications of the convective term. The first example is the Navier–Stokes-α model (Foias et al., 2001), which deviates from the classical derivation leading to the RANS equations (1.3) and (1.6) by performing the averaging on the level of Lagrangian trajectories and only then shifting into the Eulerian picture. Perhaps unsurprisingly, this order of steps leads to final equations with a different-looking convective term than the one appearing in (1.6). Second, ideas developed by Libby (1975) and Byggstoyl and Kollmann (1986), who proposed a conditional averaging of turbulent and laminar flow fields to better predict the otherwise complicated statistics of intermittent flow, lead to a second velocity field and a modified convective term. Two interesting connections from their work to the present investigation can be made. Firstly, the idea of the second velocity field corresponding to a laminar flow field is congruent with the symmetry behavior of transforming like a velocity under all classical symmetries while being invariant under the statistical symmetries. Similarly, the auxiliary velocity field $\hat{U}_i$ appearing in our models could also be interpreted as the most likely value of the velocity, which would usually be equal to the mean velocity, but correspond to the laminar velocity in an intermittent region. Secondly, their focus on intermittent flow links back to the discovery of Waclawczyk et al. (2014), who establish a connection between the statistical scaling symmetry (3.55) and intermittency. Unfortunately, however, the equations of Libby (1975) and Byggstoyl and Kollmann (1986) do not agree with the statistical symmetries, which makes it difficult to develop the analogy any further. A different, more practical interpretation could be to interpret $\hat{U}_i$ and $\hat{P}$ as the results of some classical turbulence model, which would fulfill with the classical symmetries (3.27)–(3.33) while violating the statistical symmetries (3.55)–(3.58). Note that this would be consistent with the assertion that $\hat{U}_i$ and $\hat{P}$ behave like their classical counterparts $\bar{U}_i$ and $\bar{P}$ under all classical symmetries while being invariant under the statistical symmetries. In turn, the newly developed models could then be viewed as a correction algorithm that, if necessary, accounts for the effects of the statistical symmetries. However, we conclude that in order to further improve our understanding of these variables, numerical tests of the model equations are necessary, which we discuss in Sections 5.2.1 and 5.3.

5.2. Modifying existing turbulence models

In principle, we could take the approach developed in Section 5.1 even further and employ it for constructing not only model skeletons, but full-fledged models. This could be accomplished by further adding model variables such as k or ε to the general form of the model, for example (5.45). However, the formalism works best in situations with strong constraints and little modeling freedom, as was the case in Section 5.1.2. After introducing $\hat{U}_i$, $\hat{P}$ and possibly further model variables, it again becomes feasible to follow a more traditional modeling approach and build upon existing models. The formalism, on the other hand, becomes intractable due to numerous possible terms remaining even after all symmetry constraints are invoked. Many of these terms do not make sense in a model for reasons unrelated to invariance considerations, e.g. simply because they do not correspond to a physical effect that is observed in practice.

5.2.1. Eddy-Viscosity Models

When developing new statistically invariant models based on existing ones, a sensible minimal requirement for the base model is that it already fulfills all classical symmetries (3.27)–(3.32), the last two of which combine to (3.33) in the viscous case, so that we only have to introduce modifications addressed at fulfilling constraints resulting from the statistical symmetries (3.55)–(3.57). The simplest class of models to fulfill this requirement is that of two-equation models, which motivates our choice of considering the k-ε-model and the k-ω-model. Clearly, the modified models should be expected to inherit some of the flaws found in the base models, but any observed improvements can more clearly highlight the benefits of considering the statistical symmetries in turbulence modeling.

Development of the Model Equations

Let us first consider the classical k-ε-model (Jones and Launder, 1972; Launder and Sharma, 1974), which already has the desired behavior under all classical symmetries in the sense that it fulfills (3.27)–(3.32) in the limit $\nu = 0$, with the last two symmetries (3.31) and (3.32) combining to (3.33) when $\nu \neq 0$. At the same time, it violates the statistical symmetries (3.55)–(3.57) in two ways.

Firstly, the issue thoroughly discussed in Section 5.1.2 of the explicitly appearing mean velocity in the convective term is clearly evident in the model equations (3.115) and (3.116). In Section 5.1.3, we have already shown that this can be addressed by introducing auxiliary velocity and pressure fields, for example using (5.63) and (5.67). It is not clear what the best choice of the model term appearing in these equations is, but the general assumption that $\hat{U}_i$ should behave similarly to $\bar{U}_i$ leads to $S_{\text{conti}} = 0$ and

$$S_{\text{mom},i} = \frac{\partial}{\partial x_j}\left(\iota\nu_t\left(\frac{\partial \hat{U}_i}{\partial x_j} + \frac{\partial \hat{U}_j}{\partial x_i}\right)\right) - \frac{2}{3}\iota\frac{\hat{\varepsilon}}{\varepsilon}\frac{\partial k}{\partial x_i}, \tag{5.76}$$

where ι is a model constant to be determined by calibration of canonical flows, and $\hat{\varepsilon}$ is an auxiliary model variable to be discussed later. This velocity field can in turn be used to define a material derivative that is invariant under all statistical symmetries and reads

$$\frac{\hat{D}}{\hat{D}t} = \frac{\partial}{\partial t} + \hat{U}_j\frac{\partial}{\partial x_j}. \tag{5.77}$$

Note that a comparison between the model equation for the mean velocity given by (5.66) and the exact equation given by (1.6) reveals that (5.66) effectively implies a non-symmetric model for the Reynolds stress tensor. However, since the rotational symmetries are fulfilled by the equations, we do not expect this to be a problem in practice. If one intends to rectify this, the only possibility seems to be to use

$$\frac{\hat{D}\bar{U}_i}{\hat{D}t} = \frac{\partial \bar{U}_i}{\partial t} + \hat{U}_j\frac{\partial \bar{U}_i}{\partial x_j} + \bar{U}_j\frac{\partial \hat{U}_i}{\partial x_j} \tag{5.78}$$

as the material derivative in (5.66). This form is closer to the Navier–Stokes–α model (Foias et al., 2001) and the models developed by Libby (1975) and Byggstoyl and Kollmann (1986), which, as discussed in Section 5.1.3, resemble the present model because they also contain an additional velocity field. However, the explicit appearance of the mean velocity in the last term of (5.78) breaks the statistical translation symmetry (3.56), though the other statistical symmetries (3.55) and (3.57) can still be fulfilled. Nonetheless, in an effort to include the statistical symmetry (3.56), we do not use (5.78) in the present work.

Secondly, the scaling of some of the source terms in (3.115) and (3.116) cannot be reconciled with the statistical scaling symmetry (3.55). To overcome this, a third scale-providing variable can be introduced. Before developing these ideas any further, however, a comment must be made about the behavior of k and ε under the statistical symmetries (3.55)–(3.57). In classical modeling, the line between model variables (such as k) and the properties they are originally based on (the turbulent kinetic energy), is often blurred. However, in the present context, this leads to problems, because the exact k and ε fields that could be measured in a real flow have very complicated symmetry transformations under all statistical symmetries we cannot attempt to fulfill in a turbulence model. Therefore, we realize that the primary purpose of the model variables k and ε is not to reproduce the exact fields in the most precise possible way, but rather to enter the Boussinesq approximation (3.106) such that the mean velocity is predicted as accurately as possible. This perspective makes it obvious that we have the freedom to assign to k and ε any behavior under the symmetries, as long as the model equations reflect this behavior adequately. There is no good reason to change the behavior of k and ε under any of the classical symmetries, but we assume that they are invariant under the statistical translation symmetries (3.56) and (3.57), and that they scale under the statistical scaling symmetry (3.55) in such a way that a correct scaling of the Boussinesq approximation (3.106) is ensured. In order to see what this means in concrete terms, we extend (3.55) with the general ansatz

$$\begin{aligned} T_{\text{Sc,stat}}:\ & t^* = t,\ \ x_i^* = x_i,\ \ \bar{U}_i^* = \bar{U}_i e^{a_{\text{Sc,stat}}},\ \ \hat{U}_i^* = \hat{U}_i,\ \ \bar{P}^* = \bar{P} e^{a_{\text{Sc,stat}}},\ \ \hat{P}^* = \hat{P}, \\ & \tilde{R}_{ij}^* = \tilde{R}_{ij} e^{a_R},\ \ k^* = k e^{a_k},\ \ \varepsilon^* = \varepsilon e^{a_\varepsilon}. \end{aligned} \tag{5.79}$$

Inserting this into Eq. (5.66) yields

$$\begin{aligned} & \frac{\partial \bar{U}_i^*}{\partial t^*} e^{-a_{\text{Sc,stat}}} + \hat{U}_j^* \frac{\partial \bar{U}_i^*}{\partial x_j^*} e^{-a_{\text{Sc,stat}}} \\ & = -\frac{\partial \bar{P}^*}{\partial x_i^*} e^{-a_{\text{Sc,stat}}} + \nu \frac{\partial^2 \bar{U}_i^*}{\partial x_j^* \partial x_j^*} e^{-a_{\text{Sc,stat}}} - \frac{\partial \tilde{R}_{ij}^*}{\partial x_j^*} e^{-a_R}. \end{aligned} \tag{5.80}$$

It is apparent that all terms whose scaling behavior we know scale with $e^{-a_{\text{Sc,stat}}}$. This implies that the model for the Reynolds stress tensor, $\tilde{R}_{ij}$, also has to scale linearly, i.e. $a_R = a_{\text{Sc,stat}}$. Similarly, we infer the behavior of k and ε by insertion of (5.79) into the Boussinesq approximation (3.106), which leads to

$$\begin{aligned} \tilde{R}_{ij}^* e^{-a_R} & = \tilde{R}_{ij}^* e^{-a_{\text{Sc,stat}}} \\ & = -C_\mu \frac{k^{*2}}{\varepsilon^*} \left(\frac{\partial \bar{U}_i^*}{\partial x_j^*} + \frac{\partial \bar{U}_j^*}{\partial x_i^*} \right) e^{-a_{\text{Sc,stat}} - 2a_k + a_\varepsilon} + \frac{2}{3} k^* \delta_{ij} e^{-a_k}. \end{aligned} \tag{5.81}$$

In order for (5.81) to fulfill the statistical scaling symmetry, all e^{a_i}-terms have to cancel. This allows us to infer that k must scale linearly, i.e. $a_k = a_{\text{Sc,stat}}$, and ε scales quadratically, i.e. $a_\varepsilon = 2a_{\text{Sc,stat}}$.

After this prerequisite discussion, we may now take a closer look at the production and dissipation terms in (3.115) and (3.116). Inserting the statistical scaling symmetry (5.79) using a_R, a_k and a_ε as determined above into (3.115) and (3.116) with the material derivative modified according to the preceding discussion yields

$$\begin{aligned}\frac{\hat{D}k^*}{\hat{D}t^*}e^{-a_{\text{Sc,stat}}} &= -\tilde{R}^*_{ij}\frac{\partial \bar{U}^*_i}{\partial x^*_j}e^{-2a_{\text{Sc,stat}}} - \varepsilon^* e^{-2a_{\text{Sc,stat}}} \\ &\quad + \frac{\partial}{\partial x^*_j}\left(\left(\nu + \frac{C_\mu}{\sigma_k}\frac{k^{*2}}{\varepsilon^*}\right)\frac{\partial k^*}{\partial x^*_j}\right)e^{-a_{\text{Sc,stat}}}, \end{aligned} \tag{5.82}$$

$$\begin{aligned}\frac{\hat{D}\varepsilon^*}{\hat{D}t^*}e^{-2a_{\text{Sc,stat}}} &= -C_{\varepsilon,1}\frac{\varepsilon^*}{k^*}\tilde{R}^*_{ij}\frac{\partial \bar{U}^*_i}{\partial x^*_j}e^{-3a_{\text{Sc,stat}}} - C_{\varepsilon,2}\frac{\varepsilon^{*2}}{k^*}e^{-3a_{\text{Sc,stat}}} \\ &\quad + \frac{\partial}{\partial x^*_j}\left(\left(\nu + \frac{C_\mu}{\sigma_\varepsilon}\frac{k^{*2}}{\varepsilon^*}\right)\frac{\partial \varepsilon^*}{\partial x^*_j}\right)e^{-2a_{\text{Sc,stat}}}. \end{aligned} \tag{5.83}$$

Clearly, the scaling behavior of the production and dissipation terms under the statistical scaling symmetry (5.79) is different from the other terms in the equation. In order to remedy this issue while still keeping in mind the classical scaling symmetries (3.31) and (3.32), which effectively enforce dimensional correctness, we introduce a third scale-providing variable we call $\hat{\varepsilon}$. By assumption, this variable transforms just like ε under all classical symmetries, is also invariant under the statistical translation symmetries, but scales linearly (rather than quadratically) under the statistical scaling symmetry. This then allows using the dimensionless expression $\hat{\varepsilon}/\varepsilon$ to correct the scaling behavior of any given term. In summary, the symmetries (3.31), (3.32) and (3.55) taking into account these new model variables now read

$$\begin{aligned} T_{\text{Sc},I}:\ & t^* = t,\ \ x^*_i = x_i e^{a_{\text{Sc},I}}, \\ & \bar{U}^*_i = \bar{U}_i e^{a_{\text{Sc},I}},\ \ \bar{P}^* = \bar{P}e^{2a_{\text{Sc},I}}, \\ & k^* = ke^{2a_{\text{Sc},I}},\ \ \varepsilon^* = \varepsilon e^{2a_{\text{Sc},I}},\ \ \hat{\varepsilon}^* = \hat{\varepsilon}e^{2a_{\text{Sc},I}}; \end{aligned} \tag{5.84}$$

$$\begin{aligned} T_{\text{Sc},II}:\ & t^* = te^{a_{\text{Sc},II}},\ \ x^*_i = x_i, \\ & \bar{U}^*_i = \bar{U}_i e^{-a_{\text{Sc},II}},\ \ \bar{P}^* = \bar{P}e^{-2a_{\text{Sc},II}}, \\ & k^* = ke^{2a_{\text{Sc},II}},\ \ \varepsilon^* = \varepsilon e^{3a_{\text{Sc},II}},\ \ \hat{\varepsilon}^* = \hat{\varepsilon}e^{3a_{\text{Sc},II}}; \end{aligned} \tag{5.85}$$

$$\begin{aligned} T_{\text{Sc,stat}}:\ & t^* = t,\ \ x^*_i = x_i,\ \ \bar{U}^*_i = \bar{U}_i e^{a_{\text{Sc,stat}}},\ \ \bar{P}^* = \bar{P}e^{a_{\text{Sc,stat}}}, \\ & k^* = ke^{a_{\text{Sc,stat}}},\ \ \varepsilon^* = \varepsilon e^{2a_{\text{Sc,stat}}},\ \ \hat{\varepsilon}^* = \hat{\varepsilon}e^{a_{\text{Sc,stat}}}. \end{aligned} \tag{5.86}$$

All other symmetries (3.27)–(3.30), (3.56) and (3.57) are not repeated here because k, ε and $\hat{\varepsilon}$ are invariant under them.

As a side note, the above discussion is predicated on the modeling decision not to alter the Boussinesq approximation (3.106). We make this decision only because we do not see a reason to change the form of Eq. (3.106), and note that in principle, altering Eq. (3.106) would be perfectly valid. For example, if we had a reason to prefer, say, ε scaling linearly and $\hat{\varepsilon}$ being invariant under (3.55), we could accommodate this by modifying the definition of the turbulent viscosity appearing in the Boussinesq approximation (3.106) to $\nu_t = C_\mu k^2\hat{\varepsilon}/\varepsilon^2$.

For the newly introduced variable $\hat{\varepsilon}$, a transport equation has to be defined. Similar to the construction of the ε-equation (3.116) in the classical k-ε-model, for which Jones and Launder

(1972) essentially used the k-equation (3.115) as a template, we propose an equation with the same structure that reads

$$\frac{\hat{D}\hat{\varepsilon}}{\hat{D}t} = -\hat{C}_{\varepsilon,1}\left(\frac{\hat{\varepsilon}^2}{k\varepsilon}\tilde{R}_{ij}\frac{\partial \bar{U}_i}{\partial x_j} + \gamma\frac{\varepsilon}{k}\hat{R}_{ij}\frac{\partial \hat{U}_i}{\partial x_j}\right) - \hat{C}_{\varepsilon,2}\frac{\hat{\varepsilon}^2}{k} + \frac{\partial}{\partial x_j}\left(\left(\nu + \frac{\nu_t}{\hat{\sigma}_\varepsilon}\right)\frac{\partial \hat{\varepsilon}}{\partial x_j}\right), \tag{5.87}$$

where the additional model parameters $\hat{C}_{\varepsilon,1}, \gamma, \hat{C}_{\varepsilon,2}$ and $\hat{\sigma}_\varepsilon$ arise, and

$$\hat{R}_{ij} = -\nu_t\left(\frac{\partial \hat{U}_i}{\partial x_j} + \frac{\partial \hat{U}_j}{\partial x_i}\right). \tag{5.88}$$

Note that unlike in Eq. (3.106), we do not require a δ_{ij}-term in (5.88) because $\hat{R}_{ij}$ only appears in the production term of Eq. (5.87) where such a δ_{ij}-term would vanish anyway due to the multiplication with the divergence-free $\partial \hat{U}_i/\partial x_j$. The γ-term was found to significantly improve the numerical properties of the model, because all other production and dissipation terms contain $\hat{\varepsilon}$. This leads to the possibility that areas with low values of $\hat{\varepsilon}$ expand due to a lack of production of all turbulent scalars. Even with small values for γ, this can be prevented. The new model variable $\hat{\varepsilon}$ now introduces enough freedom to make the equations for the other two variables k and ε invariant under the statistical scaling symmetry (3.55), leading to

$$\frac{\hat{D}k}{\hat{D}t} = -\frac{\hat{\varepsilon}}{\varepsilon}\tilde{R}_{ij}\frac{\partial \bar{U}_i}{\partial x_j} - \hat{\varepsilon} + \frac{\partial}{\partial x_j}\left(\left(\nu + \frac{\nu_t}{\sigma_k}\right)\frac{\partial k}{\partial x_j}\right), \tag{5.89}$$

$$\frac{\hat{D}\varepsilon}{\hat{D}t} = -C_{\varepsilon,1}\frac{\hat{\varepsilon}}{k}\tilde{R}_{ij}\frac{\partial \bar{U}_i}{\partial x_j} - C_{\varepsilon,2}\frac{\varepsilon\hat{\varepsilon}}{k} + \frac{\partial}{\partial x_j}\left(\left(\nu + \frac{\nu_t}{\sigma_\varepsilon}\right)\frac{\partial \varepsilon}{\partial x_j}\right). \tag{5.90}$$

Note that $\hat{\varepsilon}$ never appears in the denominator, which is advantageous from a numerical point of view. The modified k-ε-model consisting of Eqs. (3.106), (3.114), (5.62), (5.63), (5.66), (5.67) and (5.87)–(5.90) is invariant under not only the classical symmetries (3.27)–(3.33), but also the statistical symmetries (3.55)–(3.57). The only remaining question is which values to choose for the model parameters ι, C_μ, σ_k, $C_{\varepsilon,1}$, $C_{\varepsilon,2}$, σ_ε, $\hat{C}_{\varepsilon,1}$, γ, $\hat{C}_{\varepsilon,2}$ and $\hat{\sigma}_\varepsilon$. Constraints on these parameters are found by applying the model to canonical flows, as is discussed in detail in the next section.

In order to show the general applicability of the steps followed above, we now discuss another widely used turbulence model, the k-ω-model (Wilcox, 1988) introduced in Section 3.4.1, which is given by Eqs. (1.3), (3.105), (3.106) and (3.117)–(3.119).

Again, the first step is to determine the scaling behavior of k and ω under the statistical scaling symmetry (3.55). To this end, we make the general ansatz

$$\begin{aligned} T_{\text{Sc,stat}}:\ & t^* = t,\ \ x_i^* = x_i,\ \ \bar{U}_i^* = \bar{U}_i e^{a_{\text{Sc,stat}}},\ \ \hat{U}_i^* = \hat{U}_i,\ \ \bar{P}^* = \bar{P}e^{a_{\text{Sc,stat}}},\ \ \hat{P}^* = \hat{P}, \\ & \tilde{R}_{ij}^* = \tilde{R}_{ij}e^{a_R},\ \ k^* = ke^{a_k},\ \ \omega^* = \omega e^{a_\omega}. \end{aligned} \tag{5.91}$$

Equation (5.66) is the same as for the k-ε-model, so the conclusion $a_R = a_{\text{Sc,stat}}$ still holds. However, the definition of the turbulent viscosity ν_t in the Boussinesq assumption (3.106) is different, so that inserting (5.91) into (3.106) with (3.117) now yields

$$\begin{aligned} \tilde{R}_{ij}^* e^{-a_R} &= \tilde{R}_{ij}^* e^{-a_{\text{Sc,stat}}} \\ &= -C_\omega\frac{k^*}{\omega^*}\left(\frac{\partial \bar{U}_i^*}{\partial x_j^*} + \frac{\partial \bar{U}_j}{\partial x_i}\right)e^{-a_{\text{Sc,stat}}-a_k+a_\omega} + \frac{2}{3}k^*\delta_{ij}e^{-a_k}. \end{aligned} \tag{5.92}$$

Clearly, in order for all e^{a_i}-terms to cancel, k still has to scale linearly, i.e. $a_k = a_{\text{Sc,stat}}$, and ω also has to scale linearly, i.e. $a_\omega = a_{\text{Sc,stat}}$. Using these insights, we next turn to the equations for k and ω. If (5.91) is inserted into Eqs. (3.118) and (3.119) with the modified material derivative (5.77), they become

$$\begin{aligned}\frac{\hat{D}k^*}{\hat{D}t^*}e^{-a_{\text{Sc,stat}}} &= -\alpha^*\tilde{R}^*_{ij}\frac{\partial \bar{U}^*_i}{\partial x^*_j}e^{-2a_{\text{Sc,stat}}} - \beta^* k^*\omega^* e^{-2a_{\text{Sc,stat}}} \\ &\quad + \frac{\partial}{\partial x^*_j}\left(\left(\nu + C_\omega\sigma^*\frac{k^*}{\omega^*}\right)\frac{\partial k^*}{\partial x^*_j}\right)e^{-a_{\text{Sc,stat}}}, \end{aligned} \tag{5.93}$$

$$\begin{aligned}\frac{D\omega^*}{Dt^*}e^{-a_{\text{Sc,stat}}} &= -\alpha\frac{\omega^*}{k^*}\tilde{R}^*_{ij}\frac{\partial \bar{U}^*_i}{\partial x^*_j}e^{-2a_{\text{Sc,stat}}} - \beta{\omega^*}^2 e^{-2a_{\text{Sc,stat}}} \\ &\quad + \frac{\partial}{\partial x^*_j}\left(\left(\nu + C_\omega\sigma\frac{k^*}{\omega^*}\right)\frac{\partial \omega^*}{\partial x^*_j}\right)e^{-a_{\text{Sc,stat}}}. \end{aligned} \tag{5.94}$$

As an inspection of the production and dissipation terms in (5.93) and (5.94) reveals, they break the statistical scaling symmetry (5.91). In order to make possible the necessary modifications, we again introduce a third variable denoted with $\hat{\omega}$, which, by assumption, has the same dimensional units as ω, thus ensuring that it behaves like ω under the classical scaling symmetries (3.31) and (3.32), but is invariant under the statistical scaling symmetry (5.91). This choice allows using the dimensionless ratio $\hat{\omega}/\omega$ to adequately modify the source terms of the model equations. We summarize the above discussion by giving (3.31), (3.32) and (3.55) while including the model variables,

$$\begin{aligned} T_{\text{Sc},I}: \;& t^* = t,\;\; x^*_i = x_i e^{a_{\text{Sc},I}}, \\ & \bar{U}^*_i = \bar{U}_i e^{a_{\text{Sc},I}},\;\; \bar{P}^* = \bar{P}e^{2a_{\text{Sc},I}}, \\ & k^* = k e^{2a_{\text{Sc},I}},\;\; \omega^* = \omega,\;\; \hat{\omega}^* = \hat{\omega}; \end{aligned} \tag{5.95}$$

$$\begin{aligned} T_{\text{Sc},II}: \;& t^* = t e^{a_{\text{Sc},II}},\;\; x^*_i = x_i, \\ & \bar{U}^*_i = \bar{U}_i e^{-a_{\text{Sc},II}},\;\; \bar{P}^* = \bar{P}e^{-2a_{\text{Sc},II}}, \\ & k^* = k e^{2a_{\text{Sc},II}},\;\; \omega^* = \omega e^{-a_{\text{Sc},II}},\;\; \hat{\omega}^* = \hat{\omega}e^{-a_{\text{Sc},II}}; \end{aligned} \tag{5.96}$$

$$\begin{aligned} T_{\text{Sc,stat}}: \;& t^* = t,\;\; x^*_i = x_i,\;\; \bar{U}^*_i = \bar{U}_i e^{a_{\text{Sc,stat}}},\;\; \bar{P}^* = \bar{P}e^{a_{\text{Sc,stat}}}, \\ & k^* = k e^{a_{\text{Sc,stat}}},\;\; \omega^* = \omega e^{a_{\text{Sc,stat}}},\;\; \hat{\omega}^* = \hat{\omega}. \end{aligned} \tag{5.97}$$

Note that k, ω and $\hat{\omega}$ are invariant under the other symmetries (3.27)–(3.30), (3.56) and (3.57).

The model equation for $\hat{\omega}$ is again formulated in analogy to the ω-equation. Taking into account the statistical scaling behavior of $\hat{\omega}$, a simple form of the three scale-providing equations reads

$$\frac{\hat{D}k}{\hat{D}t} = -\,\alpha^*\frac{\hat{\omega}}{\omega}\tilde{R}_{ij}\frac{\partial \bar{U}_i}{\partial x_j} - \beta^* k\hat{\omega} + \frac{\partial}{\partial x_j}\left((\nu + \sigma^*\nu_t)\frac{\partial k}{\partial x_j}\right), \tag{5.98}$$

$$\frac{\hat{D}\omega}{\hat{D}t} = -\,\alpha\frac{\hat{\omega}}{k}\tilde{R}_{ij}\frac{\partial \bar{U}_i}{\partial x_j} - \beta\omega\hat{\omega} + \frac{\partial}{\partial x_j}\left((\nu + \sigma\nu_t)\frac{\partial \omega}{\partial x_j}\right), \tag{5.99}$$

$$\frac{\hat{D}\hat{\omega}}{\hat{D}t} = -\,\alpha^{**}\left(\frac{\hat{\omega}^2}{\omega k}\tilde{R}_{ij}\frac{\partial \bar{U}_i}{\partial x_j} + \gamma^*\frac{\omega}{k}\hat{R}_{ij}\frac{\partial \hat{U}_i}{\partial x_j}\right) - \beta^{**}\hat{\omega}^2 + \frac{\partial}{\partial x_j}\left((\nu + \sigma^{**}\nu_t)\frac{\partial \hat{\omega}}{\partial x_j}\right), \tag{5.100}$$

where we have again introduced an additional small production term in (5.100).

Note that for both the modified k-ε-model and the modified k-ω-model shown here, it could make sense to include additional source terms in the equations. Cross-diffusion terms, like in classical two-equation models, could be especially sensible, because we introduce three instead of only two scale-providing variables here, and the decision which particular scale-providing variables to select is always associated with a certain arbitrariness. Apart from the diffusion terms, this decision does not really matter, because e.g. ω can be expressed in terms of k and ε, and, therefore, it is possible to transform e.g. the ω-equation (5.99) into a transport equation for ε, which differs from Eq. (5.90) only by additional terms arising from the diffusion term. In turn, one can use the model parameters to blend between k-ε-model and k-ω-model behavior, which is the main idea of Menter's SST model as discussed in Section 3.4.1. Therefore, cross-diffusion terms, in some sense, allow postponing the decision in which turbulent variables we formulate our model until the parameter calibration phase.

Model Calibration

In the following, we apply the modified k-ε-model developed in the previous section, which is given by (3.106), (3.114), (5.62), (5.63), (5.66), (5.67), (5.87), (5.89) and (5.90), to a number of canonical flows. The purpose of this is twofold: First, it allows us to demonstrate that this model is able to incorporate a wide variety of physical effects because it can make reasonable predictions for a broad range of flow types. To some degree, this is to be expected simply because the modified model contains more free parameters than the original one, but the increased generality can also be explained by the additional symmetries built into it. This latter aspect becomes important when the model is applied to flows that it was not calibrated against. Clearly, not all shortcomings of the classical k-ε-model are related to the statistical symmetries, so that some are also inherited by the modified model. Second, it enables inferring appropriate values for the model parameters. The selection of flows to be considered here is guided by the arguments used for classical models (see Section 3.4.1), though, as it turns out, we are able to incorporate additional flows here.

Homogeneous Turbulence Like in Section 3.4.1, we start with the perhaps simplest possible test case, namely that of homogeneous turbulence. As the term implies, all spatial gradients vanish, so that the scale-providing equations (5.87), (5.89) and (5.90) reduce to

$$\frac{\partial k}{\partial t} = \frac{dk}{dt} = -\hat{\varepsilon}, \tag{5.101}$$

$$\frac{\partial \varepsilon}{\partial t} = \frac{d\varepsilon}{dt} = -C_{\varepsilon,2}\frac{\varepsilon\hat{\varepsilon}}{k}, \tag{5.102}$$

$$\frac{\partial \hat{\varepsilon}}{\partial t} = \frac{d\hat{\varepsilon}}{dt} = -\hat{C}_{\varepsilon,2}\frac{\hat{\varepsilon}^2}{k}. \tag{5.103}$$

The solution to this system is given by the power law

$$k(t) \propto t^{\frac{1}{1-\hat{C}_{\varepsilon,2}}}, \quad \varepsilon(t) \propto t^{\frac{C_{\varepsilon,2}}{1-\hat{C}_{\varepsilon,2}}}, \quad \hat{\varepsilon}(t) \propto t^{\frac{\hat{C}_{\varepsilon,2}}{1-\hat{C}_{\varepsilon,2}}}. \tag{5.104}$$

Evidently, the evolution for k is analogous to that in the classical model given by (3.125), except $\hat{C}_{\varepsilon,2}$ appears in the exponent instead of $C_{\varepsilon,2}$. This leads to the choice of $\hat{C}_{\varepsilon,2} = 1.92$. In order to also predict the classical evolution of ε given by Eq. (3.125), we select $C_{\varepsilon,2} = \hat{C}_{\varepsilon,2} = 1.92$.

Homogeneous Shear Turbulence Having thus established the contribution of dissipation, the next step is to investigate that of production by considering homogeneous shear turbulence. Again, the spatial gradients of the scalars vanish, but one component of the velocity gradient takes a nonvanishing value, $\partial \bar{U}_1/\partial x_2 = 2S_{12}$. If we assume that $\hat{U}_i$ behaves analogously, and all components except for $\partial \hat{U}_1/\partial x_2 = 2\hat{S}_{12}$ vanish, this leads to

$$\frac{\partial k}{\partial t} = \frac{dk}{dt} = 4C_\mu S_{12}^2 \frac{k^2 \hat{\varepsilon}}{\varepsilon^2} - \hat{\varepsilon}, \tag{5.105}$$

$$\frac{\partial \varepsilon}{\partial t} = \frac{d\varepsilon}{dt} = 4C_{\varepsilon,1} C_\mu S_{12}^2 \frac{k\hat{\varepsilon}}{\varepsilon} - C_{\varepsilon,2}\frac{\varepsilon\hat{\varepsilon}}{k}, \tag{5.106}$$

$$\frac{\partial \hat{\varepsilon}}{\partial t} = \frac{d\hat{\varepsilon}}{dt} = 4\hat{C}_{\varepsilon,1} C_\mu \left(S_{12}^2 \frac{k\hat{\varepsilon}^2}{\varepsilon^2} + \gamma \hat{S}_{12}^2 k \right) - \hat{C}_{\varepsilon,2}\frac{\hat{\varepsilon}^2}{k}. \tag{5.107}$$

Experimental evidence shows that k and ε grow approximately exponentially. Inserting the corresponding ansatz

$$k = k_0 e^{\lambda_k t}, \tag{5.108}$$

$$\varepsilon = \varepsilon_0 e^{\lambda_\varepsilon t}, \tag{5.109}$$

$$\hat{\varepsilon} = \hat{\varepsilon}_0 e^{\hat{\lambda}_\varepsilon t}, \tag{5.110}$$

into (5.105)–(5.107) leads to the relation (3.131), which was already observed for the classical model. However, unlike the classical model, the eigenvalue $\lambda = \lambda_k = \lambda_\varepsilon = \hat{\lambda}_\varepsilon$ is given by

$$\lambda = \hat{S}_{12} \sqrt{\frac{\gamma C_\mu}{C_{\varepsilon,1} - \hat{C}_{\varepsilon,1}} \frac{C_{\varepsilon,1} - 1}{C_{\varepsilon,2} - 1}}. \tag{5.111}$$

For the limit of large times, the effect of the initial conditions becomes negligible, and the ratio of k/ε approaches an equilibrium value (Pope, 2000). From (5.105) and (5.106), it follows that

$$\frac{d}{dt}\left(\frac{k}{\varepsilon}\right) = \frac{dk}{dt}\frac{1}{\varepsilon} - \frac{d\varepsilon}{dt}\frac{k}{\varepsilon^2} = 4C_\mu S_{12}^2 \frac{k^2}{\varepsilon^2}(1 - C_{\varepsilon,1}) - (1 - C_{\varepsilon,2}) = 0, \tag{5.112}$$

where, notably, $\hat{\varepsilon}$ cancels out, so that (5.107) does not enter this part of the discussion at all. Thus, Eq. (5.112) is the same as the equation arising for the classical model (3.128), so that the following arguments carry over directly. The ratio of production to dissipation $4C_\mu S_{12}^2 k^2/\varepsilon^2$ in (5.112) can be measured experimentally to be around 1.8, introducing a constraint on $C_{\varepsilon,1}$ and $C_{\varepsilon,2}$. Though this is not required, using the same values as in the classical k-ε-model of $C_{\varepsilon,1} = 1.44$ and $C_{\varepsilon,2} = 1.92$ was found to produce reasonable results. Note, however, that like for the classical model, this choice leads to a slightly too high $C_\mu S_{12}^2 k^2/\varepsilon^2$ of around 2.1.

The Log Region Further constraints can be inferred from the logarithmic law of the wall. Inserting the famous log law for the velocity, assuming a vanishing pressure gradient and making a power-law ansatz for the scalar quantities, i.e.

$$\begin{aligned}\bar{U}_1 &= \frac{u_\tau}{\kappa}\log x_{2+} + B,\ \ \hat{U}_1 = \hat{C}_1 u_\tau \log x_{2+} + \hat{B},\\ k &= C_k {u_\tau}^2 x_{2+}^{n_k},\ \ \varepsilon = C_\varepsilon \frac{{u_\tau}^4}{\nu} x_{2+}^{n_\varepsilon},\ \ \hat{\varepsilon} = \hat{C}_\varepsilon \frac{{u_\tau}^4}{\nu} x_{2+}^{\hat{n}_\varepsilon},\end{aligned} \tag{5.113}$$

greatly simplifies the model equations (5.66), (5.87), (5.89) and (5.90), leading to

$$0 = \frac{d}{dx_{2+}}\left(C_\mu \frac{C_k^2}{C_\varepsilon}\frac{1}{\kappa} x_{2+}^{2n_k - n_\varepsilon - 1}\right), \tag{5.114}$$

$$\begin{aligned}0 &= C_\mu \frac{C_k^2 \hat{C}_\varepsilon}{C_\varepsilon^2}\frac{1}{\kappa^2} x_{2+}^{2n_k+\hat{n}_\varepsilon-2n_\varepsilon-2} - \hat{C}_\varepsilon x_{2+}^{\hat{n}_\varepsilon}\\ &\quad + \frac{C_\mu}{\sigma_k}\frac{C_k^3}{C_\varepsilon} n_k(3n_k - n_\varepsilon - 1) x_{2+}^{3n_k - n_\varepsilon - 2},\end{aligned} \tag{5.115}$$

$$\begin{aligned}0 &= C_\mu C_{\varepsilon,1}\frac{C_k \hat{C}_\varepsilon}{C_\varepsilon}\frac{1}{\kappa^2} x_{2+}^{n_k+\hat{n}_\varepsilon-n_\varepsilon-2} - C_{\varepsilon,2}\frac{C_\varepsilon \hat{C}_\varepsilon}{C_k} x_{2+}^{n_\varepsilon+\hat{n}_\varepsilon-n_k}\\ &\quad + \frac{C_\mu}{\sigma_\varepsilon} C_k^2 n_\varepsilon (2n_k - 1) x_{2+}^{2n_k-2},\end{aligned} \tag{5.116}$$

$$\begin{aligned}0 &= C_\mu \hat{C}_{\varepsilon,1}\left(\frac{C_k \hat{C}_\varepsilon^2}{C_\varepsilon^2}\frac{1}{\kappa^2} x_{2+}^{n_k+\hat{n}_\varepsilon-n_\varepsilon-2} + \gamma C_k \hat{C}_1^2 x_{2+}^{n_k-2}\right) - \hat{C}_{\varepsilon,2}\frac{\hat{C}_\varepsilon^2}{C_k} x_{2+}^{2\hat{n}_\varepsilon - n_k}\\ &\quad + \frac{C_\mu}{\hat{\sigma}_\varepsilon}\frac{C_k^2 \hat{C}_\varepsilon}{C_\varepsilon} n_\varepsilon (2n_k + \hat{n}_\varepsilon - n_\varepsilon - 1) x_{2+}^{2n_k+\hat{n}_\varepsilon-n_\varepsilon-2}.\end{aligned} \tag{5.117}$$

From Eq. (5.114), since the coefficient cannot reasonably vanish, we infer that the exponent $2n_k - n_\varepsilon - 1$ must be equal to zero. Further constraints on the exponents can be inferred from the requirement that the x_2-factors must cancel in Eqs. (5.115)–(5.117), leading to

$$2n_k - 2n_\varepsilon - 2 = 0, \tag{5.118}$$

$$3n_k - n_\varepsilon - \hat{n}_\varepsilon - 2 = 0, \tag{5.119}$$

from which it follows that $n_k = 0,\ \ n_\varepsilon = \hat{n}_\varepsilon = -1$, similar to the classical k-ε-model. This leads to the vanishing of the diffusion term in (5.115), and, thus, the constraint

$$\frac{C_\varepsilon}{C_k} = \frac{\sqrt{C_\mu}}{\kappa}. \tag{5.120}$$

Note that in analogy to the classical model, Eq. (5.115) also implies $\hat{C}_\varepsilon = 1/\kappa$, which, together with (5.120), yields

$$C_k = \frac{1}{\kappa}\sqrt{\frac{1}{\sqrt{C_\mu}}(C_{\varepsilon,2} - C_{\varepsilon,1})},\ \ C_\varepsilon = \frac{1}{\kappa^2}\sqrt{\frac{1}{\sqrt{C_\mu}}(C_{\varepsilon,2} - C_{\varepsilon,1})}. \tag{5.121}$$

In turn, two model parameter constraints can be inferred from this: First, k is constant in the log layer, and its ratio to the Reynolds stress component $\tilde{R}_{12}$ is determined by C_μ. Comparison to experimental data leads to the choice $C_\mu = 0.09$, like in the classical model. Second, and in contrast to the classical model, instead of a concrete value for σ_ε, inserting (5.120) into (5.116) and (5.117) only yields a relation between σ_ε, $\hat{\sigma}_\varepsilon$ and other model parameters, which, if we neglect the contribution from the γ-term, reads

$$\frac{C_{\varepsilon,1} - C_{\varepsilon,2}}{\hat{C}_{\varepsilon,1} - \hat{C}_{\varepsilon,2}} = \frac{\hat{\sigma}_\varepsilon}{\sigma_\varepsilon}, \tag{5.122}$$

providing additional freedom compared to the classical model. Evidently, if we do not neglect the γ-term, the assumed solution (5.113) still works, but the slightly more complicated form of (5.117) prevents us from obtaining a simple constraint on the model parameters.

Core-Region Deficit Law At this point, we deviate from the classical model calibration procedure for the first time by considering a test case not usually taken into account, the core region scaling law recently discovered by Oberlack et al. (2022). It appears in the central region of channel and pipe flow, and spans a significantly larger area than the log law. The fact that it results from an invariant solution is convenient, because we can extend the invariant surface condition (3.82) to also include the model variables, leading to

$$\begin{aligned}
\frac{dx_2}{a_{\text{Sc},I}x_2} &= \frac{d\bar{U}_1}{(a_{\text{Sc},I} - a_{\text{Sc},II} + a_{\text{Sc,stat}})\bar{U}_1 + a_{\text{Tr,stat},I,1}} \\
&= \frac{d\hat{U}_1}{(a_{\text{Sc},I} - a_{\text{Sc},II})\hat{U}_1} = \frac{dk}{(2(a_{\text{Sc},I} - a_{\text{Sc},II}) + a_{\text{Sc,stat}})k} \\
&= \frac{d\varepsilon}{(2a_{\text{Sc},I} - 3a_{\text{Sc},II} + 2a_{\text{Sc,stat}})\varepsilon} = \frac{d\hat{\varepsilon}}{(2a_{\text{Sc},I} - 3a_{\text{Sc},II} + a_{\text{Sc,stat}})\hat{\varepsilon}}.
\end{aligned} \tag{5.123}$$

This implies the result that they also follow a power law, which we write in compact form by renaming the appearing integration constants and group parameters, yielding

$$\hat{U}_1 = \hat{C}_1 x_2^{\hat{\sigma}_1}, \;\; \bar{U}_1 = C_1 x_2^{\sigma_1} + C, \;\; k = C_k x_2^{n_k}, \;\; \varepsilon = C_\varepsilon x_2^{n_\varepsilon}, \;\; \hat{\varepsilon} = \hat{C}_\varepsilon x_2^{\hat{n}_\varepsilon}. \tag{5.124}$$

Note that the C_i and n_i appearing here are different from the coefficients and exponents appearing in (5.113).

Since this is not one of the classical test cases discussed in Section 3.4.1, we first examine what the classical k-ε-model predicts here. Inserting (5.124) into its model equations (3.105), (3.115) and (3.116) yields

$$0 = -\frac{\partial \bar{P}}{\partial x_1} + \frac{d}{dx_2}\left(C_\mu \frac{C_k^2}{C_\varepsilon} C_1 \sigma_1 x_2^{2n_k - n_\varepsilon + \sigma_1 - 1}\right), \tag{5.125}$$

$$\begin{aligned}
0 &= C_\mu \frac{C_k^2 \sigma_1^2}{C_\varepsilon} C_1^2 x_2^{2n_k - n_\varepsilon + 2\sigma_1 - 2} - C_\varepsilon x_2^{n_\varepsilon} \\
&\quad + \frac{C_\mu}{\sigma_k} \frac{C_k^3}{C_\varepsilon} n_k (3n_k - n_\varepsilon - 1) x_2^{3n_k - n_\varepsilon - 2},
\end{aligned} \tag{5.126}$$

$$\begin{aligned}
0 &= C_\mu C_{\varepsilon,1} C_k \sigma_1^2 C_1^2 x_2^{n_k + 2\sigma_1 - 2} - C_{\varepsilon,2} \frac{C_\varepsilon^2}{C_k} x_2^{2n_\varepsilon - n_k} \\
&\quad + \frac{C_\mu}{\sigma_\varepsilon} C_k^2 n_\varepsilon (2n_k - 1) x_2^{2n_k - 2}.
\end{aligned} \tag{5.127}$$

The pressure gradient $\partial\bar{P}/\partial x_1$ is constant and nonzero, so that (5.125) implies $2n_k - n_\varepsilon + \sigma_1 = 2$. Then, the requirement that x_2 must cancel out in (5.126) and (5.127) yields

$$2n_k - 2n_\varepsilon + 2\sigma_1 - 2 = 0, \tag{5.128}$$
$$3n_k - 2n_\varepsilon - 2 = 0, \tag{5.129}$$

resulting in $n_k = 1$, $n_\varepsilon = \sigma_1$, and, further, $\sigma_1 = 1/2$. However, this is quite far off from experimental and numerical data (Oberlack et al., 2022), which indicates $\sigma_1 \approx 1.95$. As a side note, the classical k-ω-model does a better job by predicting $\sigma_1 = 2$, which is more accurate and has, moreover, been conjectured to be the asymptotic value for infinite Reynolds number. However, the modified model is far more flexible, allowing for arbitrary values of σ_1, depending on the choice of model parameters.

We show this by inserting (5.124) into the modified model equations (5.66), (5.67), (5.87), (5.89) and (5.90), leading to

$$0 = -\frac{\partial\hat{P}}{\partial x_1} + \frac{d}{dx_2}\left(\iota C_\mu \frac{C_k^2}{C_\varepsilon}\hat{C}_1\hat{\sigma}_1 x_2^{2n_k - n_\varepsilon + \hat{\sigma}_1 - 1}\right), \tag{5.130}$$

$$0 = -\frac{\partial\bar{P}}{\partial x_1} + \frac{d}{dx_2}\left(C_\mu \frac{C_k^2}{C_\varepsilon} C_1\sigma_1 x_2^{2n_k - n_\varepsilon + \sigma_1 - 1}\right), \tag{5.131}$$

$$\begin{aligned} 0 = {} & C_\mu \frac{C_k^2\hat{C}_\varepsilon\sigma_1^2}{C_\varepsilon^2} C_1^2 x_2^{2n_k + \hat{n}_\varepsilon - 2n_\varepsilon + 2\sigma_1 - 2} - \hat{C}_\varepsilon x_2^{\hat{n}_\varepsilon} \\ & + \frac{C_\mu}{\sigma_k}\frac{C_k^3}{C_\varepsilon} n_k(3n_k - n_\varepsilon - 1)x_2^{3n_k - n_\varepsilon + 2\sigma_1 - 2}, \end{aligned} \tag{5.132}$$

$$\begin{aligned} 0 = {} & C_\mu C_{\varepsilon,1}\frac{C_k\hat{C}_\varepsilon\sigma_1^2}{C_\varepsilon} C_1^2 x_2^{n_k + \hat{n}_\varepsilon + 2\sigma_1 - n_\varepsilon - 2} - C_{\varepsilon,2}\frac{C_\varepsilon\hat{C}_\varepsilon}{C_k} x_2^{n_\varepsilon + \hat{n}_\varepsilon - n_k} \\ & + \frac{C_\mu}{\sigma_\varepsilon} C_k^2 n_\varepsilon(2n_k - 1)x_2^{2n_k - 2}, \end{aligned} \tag{5.133}$$

$$\begin{aligned} 0 = {} & C_\mu\hat{C}_{\varepsilon,1}\left(\frac{C_k\hat{C}_\varepsilon^2}{C_\varepsilon^2\sigma_1^2} C_1^2 x_2^{n_k + \hat{n}_\varepsilon - n_\varepsilon + 2\sigma_1 - 2} + \gamma C_k\hat{C}_1^2\hat{\sigma}_1^2 x_2^{n_k + 2\hat{\sigma}_1 - 2}\right) - \hat{C}_{\varepsilon,2}\frac{\hat{C}_\varepsilon^2}{C_k} x_2^{2\hat{n}_\varepsilon - n_k} \\ & + \frac{C_\mu}{\hat{\sigma}_\varepsilon}\frac{C_k^2\hat{C}_\varepsilon}{C_\varepsilon} n_\varepsilon(2n_k + \hat{n}_\varepsilon - n_\varepsilon - 1)x_2^{2n_k + \hat{n}_\varepsilon - n_\varepsilon - 2}. \end{aligned} \tag{5.134}$$

Again, (5.131) implies $2n_k - n_\varepsilon + \sigma_1 = 2$, and comparison of the x_2-exponents in (5.132)–(5.134) yields

$$2n_k - 2n_\varepsilon + 2\sigma_1 - 2 = 0, \tag{5.135}$$
$$3n_k - n_\varepsilon - \hat{n}_\varepsilon + 2\sigma_1 - 2 = 0, \tag{5.136}$$

so that $n_k = 1$, $n_\varepsilon = \sigma_1$, and $\hat{n}_\varepsilon = -\sigma_1 + 1$. For $\hat{\sigma}_1$, (5.134) only leaves two options: Either, $\hat{\sigma}_1 = -\sigma_1 + 1$, or $\hat{\sigma}_1 = 0$. In the latter case, the γ-term would simply vanish. Only this second option is compatible with (5.130), from which, in turn, we can infer that the gradient $\partial\hat{P}/\partial x_1$ must vanish. Note that thanks to the additional scaling symmetry (3.59) present in the model, the concrete value for σ_1 does not follow from comparison of the exponents, but is instead determined by the model parameters. Assuming the conjectured exact value of $\sigma_1 = 2$ again leads to a vanishing diffusion term in the k-equation (5.132), though, in contrast to the log layer, this is because $3n_k - n_\varepsilon - 1 = 0$, not because k is constant. In any event, this yields

$$\frac{C_\mu C_k C_1 \sigma_1}{C_\varepsilon} = 1, \tag{5.137}$$

which greatly simplifies (5.133) and (5.134). In fact, these two equations again lead to the constraint that already arose from the log layer, Eq. (5.122). The fact that no additional constraint arises from this test case clearly exemplifies the superior ability of the modified model to generalize to flows against which it is not originally calibrated. We attribute this to the additional symmetries (3.59) and (3.60) built into the model, because both the log law and the core region scaling law, when obtained as an invariant solution as discussed in Section 3.3, result from the statistical symmetries. Therefore, our new model only has to be calibrated against one to automatically also predict the other one accurately. A minor weakness observed for this test case is that the exponents for k and $\hat{\varepsilon}$ do not make sense on the centerline position, so that we have to exclude this point from the range of validity. In practice, we do not expect this to cause any problems because of the regularizing effect of viscosity.

Shear-Free One-Dimensional Turbulence Next, we consider a test case that is also not part of the traditional model calibration as discussed in Section 3.4.1, but that is nonetheless theoretically interesting and practically relevant. Shear-free one-dimensional turbulence occurs when velocity gradients vanish, but the turbulent scalars do have a gradient in one direction. Then, the model equations (5.87), (5.89) and (5.90) simplify to

$$0 = -\hat{\varepsilon} + \frac{\partial}{\partial x_1}\left(\frac{\nu_t}{\sigma_k}\frac{\partial k}{\partial x_1}\right), \tag{5.138}$$

$$0 = -C_{\varepsilon,2}\frac{\varepsilon\hat{\varepsilon}}{k} + \frac{\partial}{\partial x_1}\left(\frac{\nu_t}{\sigma_\varepsilon}\frac{\partial \varepsilon}{\partial x_1}\right), \tag{5.139}$$

$$0 = -\hat{C}_{\varepsilon,2}\frac{\hat{\varepsilon}^2}{k} + \frac{\partial}{\partial x_1}\left(\frac{\nu_t}{\hat{\sigma}_\varepsilon}\frac{\partial \hat{\varepsilon}}{\partial x_1}\right). \tag{5.140}$$

From a theoretical point of view, this setting allows one to study the model for a balance of dissipation and diffusion, which nicely complements the study for a balance of production and dissipation in the context of homogeneous shear. Moreover, this flow is also practically relevant in the context of oceanography, where it serves as a simple model for turbulence in resting bodies of water into which turbulent energy is injected by surface waves (Umlauf et al., 2003).

Numerical tests (Umlauf et al., 2003) in the context of classical two-equation models suggest a power law for the scalar quantities, which we also extend to $\hat{\varepsilon}$, i.e.

$$k = C_k x_2^{n_k}, \quad \varepsilon = C_\varepsilon x_2^{n_\varepsilon}, \quad \hat{\varepsilon} = \hat{C}_\varepsilon x_2^{\hat{n}_\varepsilon}, \tag{5.141}$$

leading to the system of nonlinear algebraic equations

$$3n_k - n_\varepsilon - \hat{n}_\varepsilon = 2, \tag{5.142}$$

$$\frac{\sigma_k}{\sigma_\varepsilon C_{\varepsilon,2}} = \frac{n_k(3n_k - n_\varepsilon - 1)}{n_\varepsilon(2n_k - 1)}, \tag{5.143}$$

$$\frac{\sigma_k}{\hat{\sigma}_\varepsilon \hat{C}_{\varepsilon,2}} = \frac{n_k(3n_k - n_\varepsilon - 1)}{\hat{n}_\varepsilon(2n_k + \hat{n}_\varepsilon - n_\varepsilon - 1)}. \tag{5.144}$$

The solution of (5.142)–(5.144) is so complicated that it is better to solve it numerically. The choice of model parameters that works well for all considered flows and is summarized in Eq. (5.197) predicts a decay exponent for k of -3.7, a value reasonably close to the measured range of $-1.7\ldots-3$ (Nokes, 1988). By contrast, inserting (5.141) into the classical k-ε-model leads to

$$3n_k - 2n_\varepsilon = 2, \tag{5.145}$$

$$\frac{\sigma_k}{\sigma_\varepsilon C_{\varepsilon,2}} = \frac{n_k(3n_k - n_\varepsilon - 1)}{n_\varepsilon(2n_k - 1)}, \tag{5.146}$$

which can be solved for n_k to yield

$$n_k = -\frac{7\sigma_k}{6(\sigma_\varepsilon - 2\sigma_k)} - \sqrt{\frac{49{\sigma_k}^2}{36(\sigma_\varepsilon - 2\sigma_k)^2} + \frac{2\sigma_k}{3(\sigma_\varepsilon - 2\sigma_k)}}. \tag{5.147}$$

For standard model parameters, this leads to -4.97, which is quite far from the observed range. Changing σ_ε in order to achieve a better value is possible, but this comes at the expense of no longer being able to predict the log region accurately. On the other hand, the modified model is capable of accommodating both test cases. Note that a different problematic property of the k-ε-model, namely that the exponent n_k is very sensitive to the choice of model parameters, is inherited and even somewhat amplified by the modified model. However, for a fixed set of model parameters, this is not an issue. Also, other choices of scale-providing variables could likely mitigate this drawback (Umlauf, 2001).

Unlike the classical k-ε-model, the modified model can be calibrated in such a way as to correctly predict all flows considered in this section. However, so far, no constraints on the parameters γ and ι could be inferred. This also means that the auxiliary velocity field $\hat{U}_i$ has not entered the discussion so far. To investigate these aspects further and to test the model in a slightly more complicated setting, we have to take into account flows such as the plane jet. The numerical investigation of this flow is discussed in Section 5.3.1.

5.2.2. Reynolds Stress Models

The results in this section have largely been obtained in collaboration with Nils Benedikt, who discusses them in his Bachelor's thesis (Benedikt, 2022). Even though developing a statistically invariant RSM is considerably more complicated than the modeling ideas presented in Section 5.2.1, early steps toward extending the model framework presented in Section 5.1.3, which gives rise to the simplistic model given by Eqs. (1.3), (1.4), (5.60), (5.63), (5.72) and (5.73), to a physically reasonable and statistically invariant RSM have been taken as part of the present work. The central challenge is introduced by the complicated transformation behavior of the Reynolds stresses under the statistical symmetries (3.59)–(3.61), which makes it difficult to make use of existing modeling ideas as discussed in Section 3.4.2. In many cases, it is possible to circumvent these difficulties by using instantaneous moments instead of fluctuating ones, however, since they are not Galilean invariant, in the present context, one would only trade complications associated with the statistical symmetries with complications arising from the Galilean symmetry (3.36). Therefore, a crucial idea developed in Benedikt (2022) is the introduction of an additional Reynolds stress tensor-like variable we call $\hat{R}_{ij}$, which, in analogy to $\hat{U}_i$, transforms like R_{ij} under all classical symmetries (3.41)–(3.47), but has a simple behavior under the statistical symmetries (3.68)–(3.70). Thanks to the assumed simple behavior of $\hat{R}_{ij}$ under the statistical symmetries, which is given by Eqs. (5.159)–(5.162), we can easily adapt any classical RSM or EARSM to define it. Benedikt (2022) uses Eqs. (3.148), (3.151), (3.154) and (3.159) to suggest

$$\begin{aligned}\frac{\hat{D}\hat{R}_{ij}}{\hat{D}t} &= -\hat{R}_{ik}\frac{\partial \hat{U}_j}{\partial x_k} - \hat{R}_{jk}\frac{\partial \hat{U}_i}{\partial x_k} - C_1\frac{\hat{\varepsilon}}{\hat{k}}\left(\hat{R}_{ij} - \frac{1}{3}\hat{R}_{kk}\delta_{ij}\right) \\ &\quad + C_2\left(\hat{R}_{ik}\frac{\partial \hat{U}_j}{\partial x_k} + \hat{R}_{jk}\frac{\partial \hat{U}_i}{\partial x_k} - \frac{2}{3}\hat{R}_{lk}\frac{\partial \hat{U}_l}{\partial x_k}\delta_{ij}\right) - \frac{2}{3}\hat{\varepsilon}\delta_{ij} \\ &\quad + \frac{\partial}{\partial x_k}\left(\hat{c}_R\hat{R}_{lk}\frac{\hat{k}}{\hat{\varepsilon}}\frac{\partial \hat{R}_{ij}}{\partial x_l}\right),\end{aligned} \tag{5.148}$$

where, analogous to the definition of k, $\hat{k} = \hat{R}_{kk}/2$. Note that the introduction of $\hat{R}_{ij}$ directly suggests using it in (5.67), which would lead to

$$S_{\mathrm{mom},i} = \frac{\partial \hat{R}_{ij}}{\partial x_j}. \tag{5.149}$$

Like with classical RSMs, it is also useful to introduce an equation for the scalar dissipation ε,

$$\frac{\hat{D}\varepsilon}{\hat{D}t} = -C_{\varepsilon,1}\frac{\hat{\varepsilon}}{\hat{k}}\hat{R}_{ij}\frac{\partial \bar{U}_i}{\partial x_j} - C_{\varepsilon,2}\frac{\varepsilon\hat{\varepsilon}}{\hat{k}} + \frac{\partial}{\partial x_l}\left(c_\varepsilon\hat{R}_{lk}\frac{\hat{k}}{\hat{\varepsilon}}\frac{\partial \varepsilon}{\partial x_k}\right). \tag{5.150}$$

Furthermore, in order to be able to adapt the statistical scaling behavior of model terms as needed, a statistically invariant version $\hat{\varepsilon}$ is also introduced, similarly to the EVMs discussed in Section 5.2.1. By adapting Eq. (5.150), a possible equation for $\hat{\varepsilon}$ is

$$\frac{\hat{D}\hat{\varepsilon}}{\hat{D}t} = -\hat{C}_{\varepsilon,1}\frac{\hat{\varepsilon}}{\hat{k}}\hat{R}_{ij}\frac{\partial \hat{U}_i}{\partial x_j} - \hat{C}_{\varepsilon,2}\frac{\hat{\varepsilon}^2}{\hat{k}} + \frac{\partial}{\partial x_l}\left(\hat{c}_\varepsilon\hat{R}_{lk}\frac{\hat{k}}{\hat{\varepsilon}}\frac{\partial \hat{\varepsilon}}{\partial x_k}\right). \tag{5.151}$$

With these newly introduced variables, the classical and statistical symmetries (3.27)–(3.33) and (3.55)–(3.58) then become

$$\begin{aligned}T_t:\ & t^* = t + a_T,\ x_i^* = x_i,\ \bar{U}_i^* = \bar{U}_i,\ \hat{U}_i^* = \hat{U}_i,\ ,\ \bar{P}^* = \bar{P},\ \hat{P}^* = \hat{P} \\ & R_{ij}^* = R_{ij},\ \hat{R}_{ij}^* = \hat{R}_{ij},\ \overline{pu_i}^* = \overline{pu_i},\ \varepsilon^* = \varepsilon,\ \hat{\varepsilon}^* = \hat{\varepsilon}; \qquad (5.152)\\ T_{\mathrm{rot}_\alpha}:\ & t^* = t,\ x_i^* = x_jQ_{ij}^{[\alpha]},\ \bar{U}_i^* = \bar{U}_jQ_{ij}^{[\alpha]},\ \hat{U}_i^* = \hat{U}_jQ_{ij}^{[\alpha]}, \\ & \bar{P}^* = \bar{P},\ \hat{P}^* = \hat{P},\ R_{ij}^* = R_{kl}Q_{ik}^{[\alpha]}Q_{jl}^{[\alpha]},\ \hat{R}_{ij}^* = \hat{R}_{kl}Q_{ik}^{[\alpha]}Q_{jl}^{[\alpha]}, \\ & \overline{pu_i}^* = \overline{pu_j}Q_{ij}^{[\alpha]},\ \varepsilon^* = \varepsilon,\ \hat{\varepsilon}^* = \hat{\varepsilon}; \qquad (5.153)\\ T_{\mathrm{Gal}_i}:\ & t^* = t,\ x_i^* = x_i + f_{\mathrm{Gal}_i}(t),\ \bar{U}_i^* = \bar{U}_i + f'_{\mathrm{Gal}_i}(t),\ \hat{U}_i^* = \hat{U}_i + f'_{\mathrm{Gal}_i}(t), \\ & \bar{P}^* = \bar{P} - x_jf''_{\mathrm{Gal}_j}(t),\ \hat{P}^* = \hat{P} - x_jf''_{\mathrm{Gal}_j}(t),\ R_{ij}^* = R_{ij},\ \hat{R}_{ij}^* = \hat{R}_{ij}, \\ & \overline{pu_i}^* = \overline{pu_i},\ \varepsilon^* = \varepsilon,\ \hat{\varepsilon}^* = \hat{\varepsilon}; \qquad (5.154)\\ T_P:\ & t^* = t,\ x_i^* = x_i,\ \bar{U}_i^* = \bar{U}_i,\ \hat{U}_i^* = \hat{U}_i,\ \bar{P}^* = \bar{P} + f_P(t),\ \hat{P}^* = \hat{P} + f_P(t), \\ & R_{ij}^* = R_{ij},\ \hat{R}_{ij}^* = \hat{R}_{ij},\ \overline{pu_i}^* = \overline{pu_i},\ \varepsilon^* = \varepsilon,\ \hat{\varepsilon}^* = \hat{\varepsilon}; \qquad (5.155)\end{aligned}$$

$$
\begin{aligned}
T_{\mathrm{Sc},I}:\ & t^* = t,\ \ x_i^* = x_i e^{a_{\mathrm{Sc},I}},\ \ \bar{U}_i^* = \bar{U}_i e^{a_{\mathrm{Sc},I}},\ \ \hat{U}_i^* = \hat{U}_i e^{a_{\mathrm{Sc},I}},\\
& \bar{P}^* = \bar{P} e^{2a_{\mathrm{Sc},I}},\ \ \hat{P}^* = \hat{P} e^{2a_{\mathrm{Sc},I}},\ \ R_{ij}^* = R_{ij} e^{2a_{\mathrm{Sc},I}},\ \ \hat{R}_{ij}^* = \hat{R}_{ij} e^{2a_{\mathrm{Sc},I}},\\
& \overline{pu_{ij}}^* = \overline{pu_{ij}} e^{3a_{\mathrm{Sc},I}},\ \ \varepsilon^* = \varepsilon e^{2a_{\mathrm{Sc},I}},\ \ \hat{\varepsilon}^* = \hat{\varepsilon} e^{2a_{\mathrm{Sc},I}}; && (5.156)\\
T_{\mathrm{Sc},II}:\ & t^* = t e^{a_{\mathrm{Sc},II}},\ \ x_i^* = x_i,\ \ \bar{U}_i^* = \bar{U}_i e^{-a_{\mathrm{Sc},II}},\ \ \hat{U}_i^* = \hat{U}_i e^{-a_{\mathrm{Sc},II}},\\
& \bar{P}^* = \bar{P} e^{-2a_{\mathrm{Sc},II}},\ \ \hat{P}^* = \hat{P} e^{-2a_{\mathrm{Sc},II}},\ \ R_{ij}^* = R_{ij} e^{-2a_{\mathrm{Sc},II}},\ \ \hat{R}_{ij}^* = \hat{R}_{ij} e^{-2a_{\mathrm{Sc},II}},\\
& \overline{pu_i}^* = \overline{pu_i} e^{-3a_{\mathrm{Sc},II}},\ \ \varepsilon^* = \varepsilon e^{-3a_{\mathrm{Sc},II}},\ \ \hat{\varepsilon}^* = \hat{\varepsilon} e^{-3a_{\mathrm{Sc},II}}; && (5.157)
\end{aligned}
$$

$$
\begin{aligned}
T_{\mathrm{Sc,ns}}:\ & t^* = t e^{2a_{\mathrm{Sc,ns}}},\ \ x_i^* = x_i e^{a_{\mathrm{Sc,ns}}},\ \ \bar{U}_i^* = \bar{U}_i e^{-a_{\mathrm{Sc,ns}}},\ \ \hat{U}_i^* = \hat{U}_i e^{-a_{\mathrm{Sc,ns}}},\\
& \bar{P}^* = \bar{P} e^{-2a_{\mathrm{Sc,ns}}},\ \ \hat{P}^* = \hat{P} e^{-2a_{\mathrm{Sc,ns}}},\ \ R_{ij}^* = R_{ij} e^{-2a_{\mathrm{Sc,ns}}},\ \ \hat{R}_{ij}^* = \hat{R}_{ij} e^{-2a_{\mathrm{Sc,ns}}},\\
& \overline{pu_i}^* = \overline{pu_i} e^{-3a_{\mathrm{Sc,ns}}},\ \ \varepsilon^* = \varepsilon e^{-4a_{\mathrm{Sc,ns}}},\ \ \hat{\varepsilon}^* = \hat{\varepsilon} e^{-4a_{\mathrm{Sc,ns}}}; && (5.158)\\
T_{\mathrm{Sc,stat}}:\ & t^* = t,\ \ x_i^* = x_i,\ \ \bar{U}_i^* = \bar{U}_i e^{a_{\mathrm{Sc,stat}}},\ \ \hat{U}_i^* = \hat{U}_i,\\
& R_{ij}^* = (R_{ij} + \bar{U}_i\bar{U}_j) e^{a_{\mathrm{Sc,stat}}} - \bar{U}_i\bar{U}_j e^{2a_{\mathrm{Sc,stat}}},\ \ \hat{R}_{ij}^* = \hat{R}_{ij},\ \ \bar{P}^* = \bar{P} e^{a_{\mathrm{Sc,stat}}},\ \ \hat{P}^* = \hat{P},\\
& \overline{u_i p}^* = (\overline{u_i p} + \bar{U}_i\bar{P}) e^{a_{\mathrm{Sc,stat}}} - \bar{U}_i\bar{P} e^{2a_{\mathrm{Sc,stat}}},\ \ \varepsilon^* = \varepsilon e^{a_{\mathrm{Sc,stat}}},\ \ \hat{\varepsilon}^* = \hat{\varepsilon}; && (5.159)\\
T_{\mathrm{Tr,stat,1}}:\ & t^* = t,\ \ x_i^* = x_i,\ \ \bar{U}_i^* = \bar{U}_i + a_{\mathrm{Tr,stat},I,i},\ \ \hat{U}_i^* = \hat{U}_i,\ \ \bar{P}^* = \bar{P},\ \ \hat{P}^* = \hat{P},\\
& R_{ij}^* = R_{ij} - \bar{U}_i a_{\mathrm{Tr,stat},I,j} - \bar{U}_j a_{\mathrm{Tr,stat},I,i} - a_{\mathrm{Tr,stat},I,i} a_{\mathrm{Tr,stat},I,j},\\
& \hat{R}_{ij}^* = \hat{R}_{ij},\ \ \overline{u_i p}^* = \overline{u_i p} - \bar{P} a_{\mathrm{Tr,stat},I,i},\ \ \varepsilon^* = \varepsilon,\ \ \hat{\varepsilon}^* = \hat{\varepsilon}; && (5.160)\\
T_{\mathrm{Tr,stat,2}}:\ & t^* = t,\ \ x_i^* = x_i,\ \ \bar{U}_i^* = \bar{U}_i, \hat{U}_i^* = \hat{U}_i, \bar{P}^* = \bar{P},\ \ \hat{P}^* = \hat{P},\\
& R_{ij}^* = R_{ij} + a_{\mathrm{Tr,stat},II,ij},\ \ \hat{R}_{ij}^* = \hat{R}_{ij},\ \ \overline{pu_i}^* = \overline{pu_i},\\
& \varepsilon^* = \varepsilon,\ \ \hat{\varepsilon}^* = \hat{\varepsilon}; && (5.161)\\
T_{\mathrm{Tr,stat,3}}:\ & t^* = t,\ \ x_i^* = x_i,\ \ \bar{U}_i^* = \bar{U}_i,\ \ \hat{U}_i^* = \hat{U}_i,\ \ \bar{P}^* = \bar{P},\ \ \hat{P}^* = \hat{P},\\
& R_{ij}^* = R_{ij},\ \ \hat{R}_{ij}^* = \hat{R}_{ij},\ \ \overline{pu_i}^* = \overline{pu_i} + a_{\mathrm{Tr,stat},III,i},\\
& \varepsilon^* = \varepsilon,\ \ \hat{\varepsilon}^* = \hat{\varepsilon}, && (5.162)
\end{aligned}
$$

or, in infinitesimal form,

$$
X_t = \frac{\partial}{\partial t}, \tag{5.163}
$$

$$
\begin{aligned}
X_{\mathrm{rot}_\alpha} = {} & \epsilon_{jk\alpha} x_j \frac{\partial}{\partial x_k} + \epsilon_{jk\alpha}\bar{U}_j \frac{\partial}{\partial \bar{U}_k} + \epsilon_{jk\alpha}\hat{U}_j \frac{\partial}{\partial \hat{U}_k}\\
& + (\epsilon_{ki\alpha} R_{kj} + \epsilon_{kj\alpha} R_{ik}) \frac{\partial}{\partial R_{ij}} + (\epsilon_{ki\alpha}\hat{R}_{kj} + \epsilon_{kj\alpha}\hat{R}_{ik}) \frac{\partial}{\partial \hat{R}_{ij}}\\
& + \epsilon_{jk\alpha}\overline{pu_j} \frac{\partial}{\partial \overline{pu_k}},
\end{aligned} \tag{5.164}
$$

$$
\begin{aligned}
X_{\mathrm{Gal}} = {} & f_{\mathrm{Gal}_i}(t) \frac{\partial}{\partial x_i} + f'_{\mathrm{Gal}_i}(t) \frac{\partial}{\partial \bar{U}_i} + f'_{\mathrm{Gal}_i}(t) \frac{\partial}{\partial \hat{U}_i}\\
& - x_i f''_{\mathrm{Gal}_i}(t) \frac{\partial}{\partial \bar{P}} - x_i f''_{\mathrm{Gal}_i}(t) \frac{\partial}{\partial \hat{P}}
\end{aligned} \tag{5.165}
$$

$$
X_P = f_P(t) \frac{\partial}{\partial \bar{P}} + f_{\hat{P}}(t) \frac{\partial}{\partial \hat{P}}, \tag{5.166}
$$

$$X_{\text{Sc},I} = x_i \frac{\partial}{\partial x_i} + \bar{U}_i \frac{\partial}{\partial \bar{U}_i} + \hat{U}_i \frac{\partial}{\partial \hat{U}_i} + 2\bar{P} \frac{\partial}{\partial \bar{P}} + 2\hat{P} \frac{\partial}{\partial \hat{P}}$$

$$+ 2R_{ij} \frac{\partial}{\partial R_{ij}} + 2\hat{R}_{ij} \frac{\partial}{\partial \hat{R}_{ij}} + 3\overline{pu_i} \frac{\partial}{\partial \overline{pu_i}} + 2\varepsilon \frac{\partial}{\partial \varepsilon} + 2\hat{\varepsilon} \frac{\partial}{\partial \hat{\varepsilon}}, \tag{5.167}$$

$$X_{\text{Sc},II} = t \frac{\partial}{\partial t} - \bar{U}_i \frac{\partial}{\partial \bar{U}_i} - \hat{U}_i \frac{\partial}{\partial \hat{U}_i} - 2\bar{P} \frac{\partial}{\partial \bar{P}} - 2\hat{P} \frac{\partial}{\partial \hat{P}}$$

$$- 2R_{ij} \frac{\partial}{\partial R_{ij}} - 2\hat{R}_{ij} \frac{\partial}{\partial \hat{R}_{ij}} - 3\overline{pu_i} \frac{\partial}{\partial \overline{pu_i}} - 3\varepsilon \frac{\partial}{\partial \varepsilon} - 3\hat{\varepsilon} \frac{\partial}{\partial \hat{\varepsilon}}, \tag{5.168}$$

$$X_{\text{Sc,ns}} = 2t \frac{\partial}{\partial t} + x_i \frac{\partial}{\partial x_i} - \bar{U}_i \frac{\partial}{\partial \bar{U}_i} - \hat{U}_i \frac{\partial}{\partial \hat{U}_i} - 2\bar{P} \frac{\partial}{\partial \bar{P}} - 2\hat{P} \frac{\partial}{\partial \hat{P}}$$

$$- 2R_{ij} \frac{\partial}{\partial R_{ij}} - 2\hat{R}_{ij} \frac{\partial}{\partial \hat{R}_{ij}} - 3\overline{pu_i} \frac{\partial}{\partial \overline{pu_i}} - 4\varepsilon \frac{\partial}{\partial \varepsilon} - 4\hat{\varepsilon} \frac{\partial}{\partial \hat{\varepsilon}}, \tag{5.169}$$

$$X_{\text{Sc,stat}} = \bar{U}_i \frac{\partial}{\partial \bar{U}_i} + \bar{P} \frac{\partial}{\partial \bar{P}} + \left(R_{ij} - \bar{U}_i \bar{U}_j\right) \frac{\partial}{\partial R_{ij}} + \left(\overline{pu_i} - \bar{U}_i \bar{P}\right) \frac{\partial}{\partial \overline{pu_i}} + \varepsilon \frac{\partial}{\partial \varepsilon}, \tag{5.170}$$

$$X_{\text{Tr,stat,1}} = \frac{\partial}{\partial \bar{U}_i} - \left(\delta_{ij} \bar{U}_k + \delta_{ik} \bar{U}_j\right) \frac{\partial}{\partial R_{jk}} - \bar{P} \frac{\partial}{\partial \overline{pu_i}}, \tag{5.171}$$

$$X_{\text{Tr,stat,2}} = \frac{\partial}{\partial R_{ij}}, \tag{5.172}$$

$$X_{\text{Tr,stat,3}} = \frac{\partial}{\partial \overline{pu_i}}. \tag{5.173}$$

It is difficult to rigorously prove that the addition of all of these model variables is mathematically necessary. The main reason for this is that it is not possible to encode the requirement for the model to be physically accurate in a mathematical language that would allow for such a proof. However, Benedikt (2022) motivates this decision by considering very simple canonical flows such as homogeneous turbulence and homogeneous shear. In both cases, unsurprisingly, the model skeleton presented in Section 5.1.3 simplifies so much as to no longer allow for the inclusion of very basic physical effects, such as the decay of the turbulent kinetic energy due to dissipation and the return to isotropy of the Reynolds stress tensor. Moreover, due to the absence of gradients in these test cases, it can clearly be shown that from the available variables, no terms capable of accounting for these effects can be formed. This justifies the introduction of the new model variables, which is also supported by an investigation carried out by Schäfer (2021), who investigated the usefulness of including second derivatives in order to gain more freedom for formulating an RSM.

Having introduced the previously discussed model variables then allows formulating the statistically invariant RSM given by Eqs. (5.148), (5.150) and (5.151) together with (1.3) and (1.6), the transport equation for R_{ij}, which is an extended version of Eq. (5.74) and reads

$$\begin{aligned}
\frac{\partial R_{ij}}{\partial t} + \hat{U}_k \frac{\partial R_{ij}}{\partial x_k} = & \frac{\partial \bar{U}_j}{\partial x_k}(\bar{U}_i - \hat{U}_i)(\bar{U}_k - \hat{U}_k) + \frac{\partial \bar{U}_i}{\partial x_k}(\bar{U}_j - \hat{U}_j)(\bar{U}_k - \hat{U}_k) \\
& + \frac{\partial R_{ik}}{\partial x_k}(\bar{U}_j - \hat{U}_j) + \frac{\partial R_{jk}}{\partial x_k}(\bar{U}_i - \hat{U}_i) - \overline{u_i \frac{\partial p}{\partial x_j}} - \overline{u_j \frac{\partial p}{\partial x_i}} \\
& + \nu \left(\frac{\partial^2 R_{ij}}{\partial x_k \partial x_k} + \bar{U}_i \frac{\partial^2 \bar{U}_j}{\partial x_k \partial x_k} + \bar{U}_j \frac{\partial^2 \bar{U}_i}{\partial x_k \partial x_k} + 2 \frac{\partial \bar{U}_i}{\partial x_k} \frac{\partial \bar{U}_j}{\partial x_k} \right) \\
& + 2\nu C_1 \left(\frac{\partial \bar{U}_i}{\partial x_k} \frac{\partial \hat{U}_j}{\partial x_k} + \frac{\partial \hat{U}_i}{\partial x_k} \frac{\partial \bar{U}_j}{\partial x_k} \right),
\end{aligned} \tag{5.174}$$

and an extended version of Eq. (5.75) given by

$$\begin{aligned}
\frac{\partial}{\partial x_k} \left(\overline{u_i \frac{\partial p}{\partial x_j}} \right) + \frac{\partial^2 \bar{P}}{\partial x_j \partial x_k}(\bar{U}_i - \hat{U}_i) + \frac{\partial \bar{U}_j}{\partial x_k} \left(\frac{\partial \bar{P}}{\partial x_j} - \frac{\partial \hat{P}}{\partial x_j} \right) & \\
= \frac{\partial \hat{U}_i}{\partial x_k} \left(C_2 \left(\left(\bar{U}_l - \hat{U}_l \right) \frac{\partial \bar{U}_j}{\partial x_l} + \frac{\partial R_{ij}}{\partial x_l} \right) - C_3 \nu \frac{\partial^2 \bar{U}_j}{\partial x_l \partial x_l} \right). &
\end{aligned} \tag{5.175}$$

This model is able to represent the decay of turbulent kinetic energy in homogeneous turbulence, however, more work is needed to properly accommodate the return to isotropy and the model performance in homogeneous shear.

Evidently, due to the considerable model complexity, the numerical implementation and the calibration for more complicated flows remains an open challenge to be addressed in future work. It is reasonable to assume that a further development of simpler models, such as those discussed in Section 5.2.1, which could yield deeper insights into the physical interpretation of $\hat{U}_i$ and $\hat{P}$, is a prerequisite before one can address the further development of such complicated models as presented in this section.

As a final note, even though the modifications leading to the models developed in this work lead to a considerable increase in equations, the structure of the equation systems suggests some potential for optimizations. In particular, the observation that the equations for $\bar{U}_i$ and $\hat{U}_i$, like the equations for R_{ij} and $\hat{R}_{ij}$, have the same general structure, hints at solving one first and then using the results as an initial guess for the other one. This could vastly improve the convergence of the numerical solver. At the same time, from a theoretical point of view, this suggests an interpretation of the model modifications as an improvement algorithm. If $\hat{U}_i$ and $\hat{R}_{ij}$ are viewed as the results of a classical model, then the equations leading to $\bar{U}_i$ and R_{ij} can be interpreted as a correction algorithm accounting for the statistical symmetries.

5.3. Numerical Implementation

Due to the convergence issues of the classical k-ω-model discussed in Section 4.3, the modified k-ε-model was first implemented for the special case of self-similar flows, where the model equations can be simplified to an ODE. The resulting BVP is then solved using very simple and well-established numerical schemes discussed in Section 4.4 and further detailed in the following.

5.3.1. Finite-Difference Implementation for Self-Similar Flow

An important class of flows to consider for model calibration is that of free shear flows, such as the plane jet, the round jet, the wake and the mixing layer. These flows are two-dimensional in space and, therefore, unlike parallel shear flows, contain nonvanishing convective terms. However, through the introduction of a suitable similarity variable, the equations can be reduced to an ODE. This makes them suitable for understanding the modifications to the convective terms discussed in Section 5.1.3 and Section 5.2.1, because they are complex enough to contain the relevant convective terms, but still simple enough to allow for a relatively cheap and robust numerical solution.

In the following, we consider the plane jet. Adapting the line of argumentation presented in Wilcox (1994) to the modified model, we make the classical similarity ansatz

$$\bar{U}_1 = \frac{\tilde{u}(\eta)}{x_1^{n_u}}, \;\; \hat{U}_1 = \frac{\tilde{\hat{u}}(\eta)}{x_1^{\hat{n}_u}}, \;\; \hat{U}_2 = \frac{\tilde{\hat{v}}(\eta)}{x_1^{\hat{n}_u}}, \;\; k = \frac{\tilde{k}(\eta)}{x_1^{n_k}}, \;\; \varepsilon = \frac{\tilde{\varepsilon}(\eta)}{x_1^{n_\varepsilon}}, \;\; \hat{\varepsilon} = \frac{\tilde{\hat{\varepsilon}}(\eta)}{x_1^{\hat{n}_\varepsilon}}, \tag{5.176}$$

where the similarity variables denoted with a tilde only depend on the similarity coordinate

$$\eta = \frac{x_2}{x_1}. \tag{5.177}$$

Classical scaling arguments as discussed in Sections 3.3 and 3.5 lead to

$$n_u = \hat{n}_u = \frac{1}{2}, \;\; n_k = 1, \;\; n_\varepsilon = \hat{n}_\varepsilon = \frac{5}{2}. \tag{5.178}$$

Note that the modified model, unlike the original model, can also accommodate the more general scaling behavior developed in Section 3.3. However, we restrict ourselves to the classical jet here. Then, the model equations (5.62), (5.63), (5.66), (5.67), (5.87), (5.89) and (5.90) become

$$\tilde{\hat{V}}(\eta) = -\int_0^\eta \frac{1}{2}\tilde{\hat{u}}(\hat{\eta})d\hat{\eta}, \tag{5.179}$$

$$\tilde{\hat{V}}(\eta)\tilde{\hat{u}}'(\eta) - \frac{1}{2}\tilde{\hat{u}}(\eta)^2 = \iota C_\mu \left(\frac{\tilde{k}(\eta)^2}{\tilde{\varepsilon}(\eta)}\tilde{\hat{u}}'(\eta)\right)', \tag{5.180}$$

$$\tilde{\hat{V}}(\eta)\tilde{u}'(\eta) - \frac{1}{2}\tilde{\hat{u}}(\eta)\tilde{u}(\eta) = C_\mu \left(\frac{\tilde{k}(\eta)^2}{\tilde{\varepsilon}(\eta)}\tilde{u}'(\eta)\right)', \tag{5.181}$$

$$\begin{aligned}\tilde{\hat{V}}(\eta)\tilde{k}'(\eta) - \tilde{\hat{u}}(\eta)\tilde{k}(\eta) = {} & C_\mu \frac{\tilde{k}(\eta)^2\tilde{\hat{\varepsilon}}(\eta)}{\tilde{\varepsilon}(\eta)^2}\tilde{u}'(\eta)^2 \\ & - \tilde{\hat{\varepsilon}}(\eta) + \frac{C_\mu}{\sigma_k}\left(\frac{\tilde{k}(\eta)^2}{\tilde{\varepsilon}(\eta)}\tilde{k}'(\eta)\right)',\end{aligned} \tag{5.182}$$

$$\begin{aligned}\tilde{\hat{V}}(\eta)\tilde{\varepsilon}'(\eta) - \frac{5}{2}\tilde{\hat{u}}(\eta)\tilde{\varepsilon}(\eta) = {} & C_\mu C_{\varepsilon,1}\frac{\tilde{k}(\eta)\tilde{\hat{\varepsilon}}(\eta)}{\tilde{\varepsilon}(\eta)}\tilde{u}'(\eta)^2 \\ & - C_{\varepsilon,2}\frac{\tilde{\varepsilon}(\eta)\tilde{\hat{\varepsilon}}(\eta)}{\tilde{k}(\eta)} + \frac{C_\mu}{\sigma_\varepsilon}\left(\frac{\tilde{k}(\eta)^2}{\tilde{\varepsilon}(\eta)}\tilde{\varepsilon}'(\eta)\right)',\end{aligned} \tag{5.183}$$

$$\tilde{\tilde{V}}(\eta)\tilde{\tilde{\varepsilon}}'(\eta) - \frac{5}{2}\tilde{\tilde{u}}(\eta)\tilde{\tilde{\varepsilon}}(\eta) = C_\mu \hat{C}_{\varepsilon,1}\left(\frac{\tilde{k}(\eta)\tilde{\tilde{\varepsilon}}(\eta)^2}{\tilde{\varepsilon}(\eta)^2}\tilde{u}'(\eta)^2 + \gamma\tilde{k}(\eta)\tilde{\tilde{u}}'(\eta)^2\right)$$
$$- \hat{C}_{\varepsilon,2}\frac{\tilde{\tilde{\varepsilon}}(\eta)^2}{\tilde{k}(\eta)} + \frac{C_\mu}{\hat{\sigma}_\varepsilon}\left(\frac{\tilde{k}(\eta)^2}{\tilde{\varepsilon}(\eta)}\tilde{\tilde{\varepsilon}}'(\eta)\right)', \tag{5.184}$$

where primes denote derivation with respect to η, and the normal velocity-like function $\tilde{\tilde{V}}(\eta)$ is defined as

$$\tilde{\tilde{V}}(\eta) = \tilde{\tilde{v}}(\eta) - \eta\tilde{\tilde{u}}(\eta). \tag{5.185}$$

$\tilde{\tilde{V}}(\eta)$ is calculated in every time step using the integral relation (5.179), which is derived from the continuity equation (5.63) with $S_{\text{conti}} = 0$. Note that using this relation in differential form was found to lead to numerical instabilities, probably not dissimilar to the issues related to pressure-velocity coupling in full Navier–Stokes solvers. Since $\tilde{\tilde{V}}(\eta)$ is calculated from an integral relation, no boundary conditions have to be specified for it, though note that Eq. (5.179) obviously implies $\tilde{\tilde{V}}(\eta = 0) = 0$. For the other variables, we impose that they approach zero as $\eta \to \infty$, and that their gradients vanish at the centerline, i.e.

$$\begin{aligned}\tilde{\tilde{u}}(\eta \to \infty) = \tilde{u}(\eta \to \infty) = \tilde{k}(\eta \to \infty) = \tilde{\varepsilon}(\eta \to \infty) = \tilde{\tilde{\varepsilon}}(\eta \to \infty) = 0,\\ \tilde{\tilde{u}}'(\eta = 0) = \tilde{u}'(\eta = 0) = \tilde{k}'(\eta = 0) = \tilde{\varepsilon}'(\eta = 0) = \tilde{\tilde{\varepsilon}}(\eta = 0) = 0.\end{aligned} \tag{5.186}$$

Since these boundary conditions are fully homogeneous, the trivial solution of all variables becoming zero globally is still possible, which is a commonly encountered issue of such self-similar jet simulations. This can be addressed by imposing an additional symmetry-breaking constraint such as

$$\tilde{u}(\eta = 0) = 1, \tag{5.187}$$

which breaks the scaling symmetry in time given by Eq. (5.96). Note that the scaling symmetry in space (5.95) is already broken by the similarity ansatz (5.176). In the modified model, we have the additional statistical scaling symmetry (5.97), so that we require a second constraint, for which we select

$$\tilde{\tilde{u}}(\eta = 0) = 1. \tag{5.188}$$

It is important to note that the constraints (5.187) and (5.188) are arbitrary, and do not affect the final result beyond a normalization factor.

For improved numerical stability, it was found helpful to use the transformation (3.180) proposed by Rubel and Melnik (1984) and already discussed in Section 3.5, which effectively moves the turbulent-nonturbulent interface to infinity in the ξ-domain. Equations (5.179)–

(5.184) then become

$$\tilde{\hat{V}}(\xi) = -\int_0^{\xi} \frac{1}{2}\tilde{\hat{u}}(\hat{\xi}) C_\mu \frac{\tilde{k}(\xi)^2}{\tilde{\varepsilon}(\xi)} d\hat{\xi}, \tag{5.189}$$

$$\tilde{\hat{V}}(\xi)\tilde{\hat{u}}'(\xi) - \frac{1}{2}\tilde{\hat{u}}(\xi)^2 C_\mu \frac{\tilde{k}(\xi)^2}{\tilde{\varepsilon}(\xi)} = \iota \tilde{\hat{u}}''(\xi), \tag{5.190}$$

$$\tilde{\hat{V}}(\xi)\tilde{u}'(\xi) - \frac{1}{2}\tilde{\hat{u}}(\xi)\tilde{u}(\xi) C_\mu \frac{\tilde{k}(\xi)^2}{\tilde{\varepsilon}(\xi)} = \tilde{u}''(\xi), \tag{5.191}$$

$$\begin{aligned}\tilde{\hat{V}}(\xi)\tilde{k}'(\xi) - \tilde{\hat{u}}(\xi)\tilde{k}(\xi) C_\mu \frac{\tilde{k}(\xi)^2}{\tilde{\varepsilon}(\xi)} &= \frac{\tilde{\hat{\varepsilon}}(\xi)}{\tilde{\varepsilon}(\xi)} \tilde{u}'(\xi)^2 \\ &\quad - C_\mu \frac{\tilde{k}(\xi)^2}{\tilde{\varepsilon}(\xi)} \tilde{\hat{\varepsilon}}(\xi) + \frac{1}{\sigma_k}\tilde{k}''(\xi),\end{aligned} \tag{5.192}$$

$$\begin{aligned}\tilde{\hat{V}}(\xi)\tilde{\varepsilon}'(\xi) - \frac{5}{2}\tilde{\hat{u}}(\xi)\tilde{\varepsilon}(\xi) C_\mu \frac{\tilde{k}(\xi)^2}{\tilde{\varepsilon}(\xi)} &= C_{\varepsilon,1} \frac{\tilde{\hat{\varepsilon}}(\xi)}{\tilde{k}(\xi)} \tilde{u}'(\xi)^2 \\ &\quad - C_\mu C_{\varepsilon,2} \tilde{k}(\xi) \tilde{\hat{\varepsilon}}(\xi) + \frac{1}{\sigma_\varepsilon}\tilde{\varepsilon}''(\xi),\end{aligned} \tag{5.193}$$

$$\begin{aligned}\tilde{\hat{V}}(\xi)\tilde{\hat{\varepsilon}}'(\xi) - \frac{5}{2}\tilde{\hat{u}}(\xi)\tilde{\hat{\varepsilon}}(\xi) C_\mu \frac{\tilde{k}(\xi)^2}{\tilde{\varepsilon}(\xi)} &= \hat{C}_{\varepsilon,1} \left(\frac{\tilde{\hat{\varepsilon}}(\xi)^2}{\tilde{\varepsilon}(\xi)\tilde{k}(\xi)} \tilde{u}'(\xi)^2 + \gamma \frac{\tilde{\varepsilon}(\xi)}{\tilde{k}(\xi)} \tilde{\hat{u}}'(\xi)^2 \right) \\ &\quad - C_\mu \hat{C}_{\varepsilon,2} \frac{\tilde{k}(\xi)\tilde{\hat{\varepsilon}}(\xi)^2}{\tilde{\varepsilon}(\xi)} + \frac{1}{\hat{\sigma}_\varepsilon}\tilde{\hat{\varepsilon}}''(\xi),\end{aligned} \tag{5.194}$$

where primes now denote derivation with respect to ξ, and η is calculated using the integral form of (3.180),

$$\eta(\xi) = \int_0^{\xi} C_\mu \frac{\tilde{k}(\hat{\xi})^2}{\tilde{\varepsilon}(\hat{\xi})} d\hat{\xi}. \tag{5.195}$$

This BVP is solved using a finite-difference discretization in space as discussed in Section 4.4. First spatial derivatives are discretized using the second-order accurate backward difference formula (4.40), and second spatial derivatives are discretized with second-order accurate central differences as given by (4.41). Due to the complicated source terms, the resulting discretized system proved difficult to solve using a nonlinear solver. Therefore, following Wilcox (1994), a pseudo-time stepping approach, which has already been discussed in Section 4.4, is employed. To this end, the temporal terms that were eliminated from (5.190)–(5.194) because of assumed stationarity are added back in, allowing the system to be evolved in time until a steady state is reached. For the temporal discretization, we use the Crank–Nicolson scheme shown in Section 4.2. In each pseudo-time step, the equations can then be linearized by using the state of the previous pseudo-time step. A numerically disadvantageous property in some of the source terms of the k and ε equations (5.192) and (5.193) is that they do not contain k and ε, respectively. This negatively impacts the diagonal dominance of the resulting matrix, or, in other words, its condition number. A remedy for this is to multiply these source terms with the ratios $\tilde{k}(\xi)^n/\tilde{k}(\xi)^{n-1}$ or, respectively, $\tilde{\varepsilon}(\xi)^n/\tilde{\varepsilon}(\xi)^{n-1}$, where we denote values of the current nth time step with the superscript n, and values of the previous time step with the superscript

$n-1$. In concrete terms, e.g. the time-discretized k-equation (5.192) then reads

$$\begin{aligned} &\frac{\tilde{k}(\xi)^n-\tilde{k}(\xi)^{n-1}}{\Delta t}+\tilde{\hat{V}}(\xi)^{n-1}\tilde{k}'(\xi)^n-\tilde{\hat{u}}(\xi)^{n-1}\tilde{k}(\xi)^n C_\mu\frac{\left(\tilde{k}(\xi)^{n-1}\right)^2}{\tilde{\varepsilon}(\xi)^{n-1}} \\ &=\frac{\tilde{\hat{\varepsilon}}(\xi)^{n-1}}{\tilde{\varepsilon}(\xi)^{n-1}}\frac{\tilde{k}(\xi)^n}{\tilde{k}(\xi)^{n-1}}\left(\tilde{u}'(\xi)^{n-1}\right)^2-C_\mu\frac{\tilde{k}(\xi)^{n-1}\tilde{k}(\xi)^n}{\tilde{\varepsilon}(\xi)^{n-1}}\tilde{\hat{\varepsilon}}(\xi)^{n-1}+\frac{1}{\sigma_k}\tilde{k}''(\xi)^n, \end{aligned} \tag{5.196}$$

where the production and dissipation terms have been multiplied with $\tilde{k}(\xi)^n/\tilde{k}(\xi)^{n-1}$. Evidently, this does not affect the converged solution. The numerical solver is implemented in the free and open-source programming language Python (Python Software Foundation, 2016), and its source code has been published to `www.gitlab.com/dakling/python-k-eps-jet-fds`. In order to validate the solver, the results for the classical k-ε-model found in Wilcox (1994) were successfully reproduced.

As model parameters for the modified k-ε-model, the choice

$$\begin{aligned} \sigma_k &= 0.91, \quad \iota = 2.0 \\ C_{\varepsilon,1} &= 1.44, \quad C_{\varepsilon,2} = 1.92, \quad \sigma_\varepsilon = 1.3, \\ \hat{C}_{\varepsilon,1} &= 1.42, \quad \gamma = 0.05, \quad \hat{C}_{\varepsilon,2} = 1.92, \quad \hat{\sigma}_\varepsilon = 1.25 \end{aligned} \tag{5.197}$$

not only fulfills all constraints derived in Section 5.2.1, but also provides excellent agreement for the plane jet, as is shown in Fig. 5.1. For completeness, the profiles of the other model variables are also shown in Fig. 5.2, even though no reference against which to reasonably compare them to is available. Interestingly, the performance at the intermittent edge of the jet is slightly superior to the classical k-ε-model. There could be a link between this observation and the fulfilling of the statistical scaling symmetry (3.55), which, as mentioned in Section 3.2, has also been linked to intermittency. However, more research is needed before such a conclusion can be drawn with confidence.

This concludes the presentation of the main developments in this work. It is important to emphasize that this discussion should not be reduced to the resulting model, but that the rationale presented here gives rise to an entire class of models.

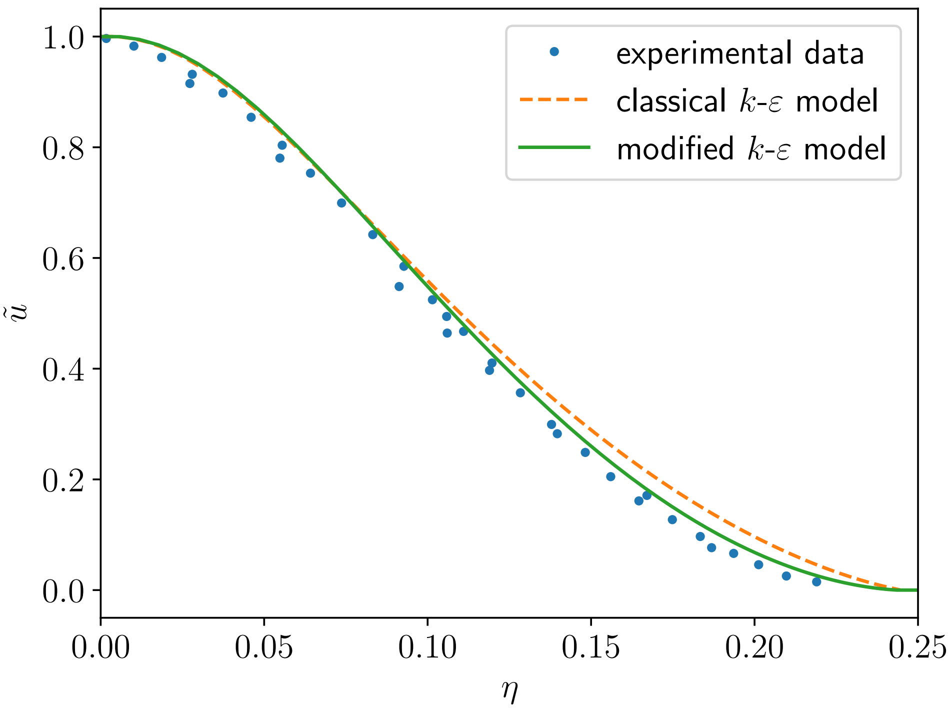

Figure 5.1.: Plane jet experimental data (Wygnanski and Fiedler, 1969) compared with classical and modified, statistically invariant k-ε-model

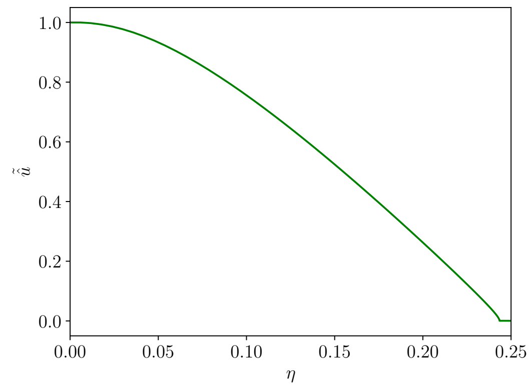

(a) Auxiliary velocity field $\tilde{\tilde{u}}(\xi)$.

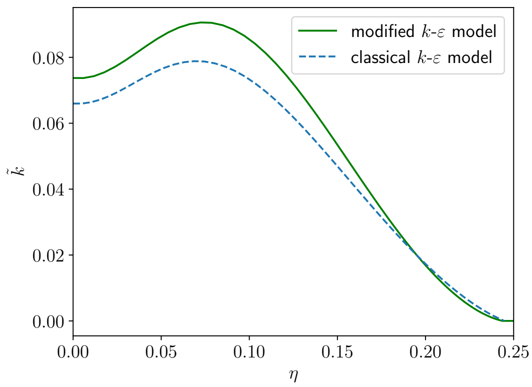

(b) Turbulent kinetic energy $\tilde{k}(\xi)$.

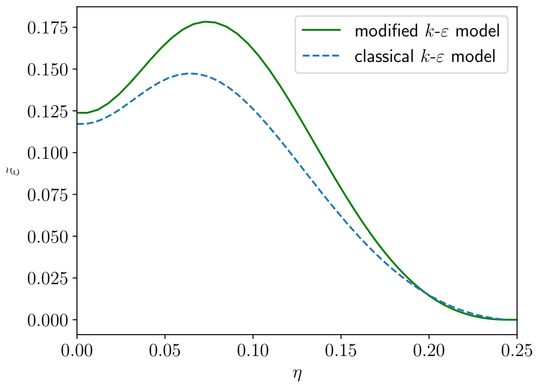

(c) Turbulent dissipation $\tilde{\varepsilon}(\xi)$.

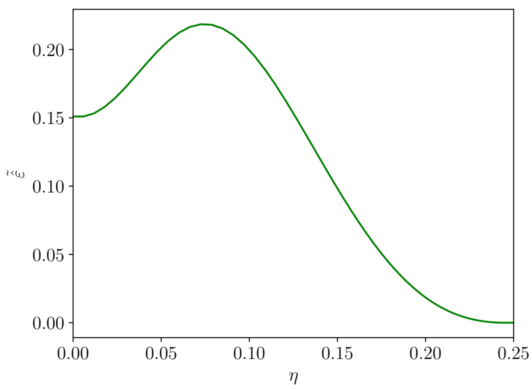

(d) Additional turbulent dissipation field $\tilde{\hat{\varepsilon}}(\xi)$.

Figure 5.2.: Results for the other fields.

6. Conclusion

In this work, the concept of Lie symmetries is applied to the problem of turbulence modeling. After introducing symmetries and exact statistical descriptions of turbulence in a general way, turbulence is analyzed through the lens of symmetries. Subsequently, existing RANS (Reynolds-Averaged Navier–Stokes) modeling approaches are presented and examined with regard to their symmetries. This discussion reveals a number of shortcomings of existing models, which we seek to overcome by developing a completely novel class of statistically invariant turbulence models with enhanced symmetry properties. The development of these models and the calibration and numerical implementation of a specific representative, a modified k-ε-model, is the main contribution of this work.

Furthermore, the present work contains a discussion of the numerical implementation of existing and novel turbulence models as well as the theoretical background underlying these implementations. In particular, the implementation of the classical k-ω-model in the DG (Discontinuous Galerkin) solver framework BoSSS (Bounded Support Spectral Solver) is presented. Results for a boundary layer flow are shown, though the focus of the discussion lies on the measures needed to obtain a numerically robust solver. For the classical k-ε-model and a statistically invariant version of it, we also discuss a special-purpose FDS (Finite Differencing Scheme) solver that efficiently performs calculations of certain simple flows. Such a lightweight solver is crucial when optimizing model parameters, because this requires many successive numerical calculations.

As a formal model development algorithm presented in this work reveals, a key ingredient necessary for formulating statistically invariant models are auxiliary velocity-like and pressure-like fields. Furthermore, depending on the model type, the introduction of additional auxiliary fields is required. Even though some existing turbulence models introduce additional velocity fields, the statistically invariant models developed in this work differ significantly from any existing turbulence model. This both represents a challenge and an opportunity: On the one hand, it is more difficult to incorporate well-established aspects of existing models and to interpret the auxiliary variables physically, but, on the other hand, the symmetry arguments presented in this work lead to a completely new class of models with tremendous potential. Among other things, these new models offer the possibility to naturally incorporate more physical effects of turbulence, such as intermittency and non-Gaussianity.

Among all statistically invariant models presented in this work, the one whose development has been taken the furthest is a modified k-ε-model. Even though this new model is still in an early development stage, its performance for canonical flows already shows great promise. It is clear that the new model is more general, because it can be calibrated against a broader range of flows when compared to the classical k-ε-model. In conjunction with its enhanced symmetry properties, this leads to the expectation that it can also more reliably be applied to flows it was not calibrated against, which is something classical two-equation models tend to struggle with. In the future, now that reasonable values for the parameters of the model are known, the implementation of the full model in BoSSS or a similar solver framework should be revisited.

The modified k-ε-model is intended to be a relatively simple representative of the class of statistically invariant turbulence models, and, therefore, inherits some limitations of the classical k-ε-model. Most notably, we cannot expect it to perform well in rotating flows or flows with high streamline curvature due to the incorrect invariance of the Boussinesq approximation under time-dependent rotation. In order to overcome this issue, future modeling efforts could be directed at extending the Boussinesq approximation with additional rotation-sensitive terms, which is the idea behind NLEVMs (nonlinear Eddy-viscosity models) and EARSMs (explicit algebraic Reynolds stress models). To include even more of the physics of turbulence, the class of statistically invariant RSMs (Reynolds stress models) could be developed further. Additionally, the symmetry-based modeling approach presented here could be further enhanced by allowing it to algorithmically incorporate constraints arising from conservation laws or other constraints such as the condition of realizability.

However, another important question that should possibly be addressed prior to those developments concerns the physical interpretation of the newly introduced model variables. The symmetry-based modeling strategy has the unusual feature that auxiliary model variables for which we do not yet have a physical intuition can be built into the model. Since we can derive a general form of possible model equations for these variables, which we can in turn calibrate against canonical flows, this is less of an issue than one might expect. Nonetheless, this becomes increasingly problematic as the model complexity grows, which is the primary reason why we have mostly focused on the development of relatively simple linear EVMs (Eddy-viscosity models). We expect that from these simple models, further insights into the physical significance of the auxiliary velocity and pressure fields can be extracted by applying them to an even broader range of flows, especially to more complicated ones.

Bibliography

Babuška, I. (1973). “The Finite Element Method With Lagrangian Multipliers”. In: *Numerische Mathematik* 20.3, pp. 179–192. DOI: 10.1007/bf01436561.

Baldwin, B. and Lomax, H. (1978). “Thin-layer approximation and algebraic model for separated turbulentflows”. In: *16th Aerospace Sciences Meeting*. DOI: 10.2514/6.1978-257.

Barenblatt, G. I. (1993). “Scaling Laws for Fully Developed Turbulent Shear Flows. Part 1. Basic Hypotheses and Analysis”. In: *Journal of Fluid Mechanics* 248, pp. 513–520. DOI: 10.1017/s0022112093000874.

Barenblatt, G. I., Chorin, A. J., and Prostokishin, V. M. (2014). “Turbulent Flows At Very Large Reynolds Numbers: New Lessons Learned”. In: *Physics-Uspekhi* 57.3, pp. 250–256. DOI: 10.3367/ufne.0184.201403d.0265.

Barenblatt, G. I. and Prostokishin, V. M. (1993). “Scaling Laws for Fully Developed Turbulent Shear Flows. Part 2. Processing of Experimental Data”. In: *Journal of Fluid Mechanics* 248, pp. 521–529. DOI: 10.1017/s0022112093000886.

Bassi, F., Ghidoni, A., Perbellini, A., Rebay, S., Crivellini, A., Franchina, N., and Savini, M. (2014). “A high-order Discontinuous Galerkin solver for the incompressible RANS and k–ω turbulence model equations”. In: *Computers & Fluids* 98, pp. 54–68. ISSN: 0045-7930. DOI: 10.1016/j.compfluid.2014.02.028.

Bassi, F., Crivellini, A., Rebay, S., and Savini, M. (2005). “Discontinuous Galerkin solution of the Reynolds-averaged Navier–Stokes and k–ω turbulence model equations”. In: *Computers & Fluids* 34.4. Residual Distribution Schemes, Discontinuous Galerkin Schemes and Adaptation, pp. 507–540. ISSN: 0045-7930. DOI: https://doi.org/10.1016/j.compfluid.2003.08.004.

Benedikt, N. (2022). “Development of a Reynolds Stress Turbulence Model Subject to Statistical Symmetry Constraints”. Bachelor’s Thesis. Technical University Darmstadt.

Bihlo, A. and Bluman, G. (2013). “Conservative parametrization schemes”. In: *Journal of Mathematical Physics* 54, pp. 08313-1 –08313-24. DOI: 10.1063/1.4816123.

Bihlo, A., Cardoso-Bihlo, E. D. S., and Popovych, R. O. (2014). “Invariant Parameterization and Turbulence Modeling on the Beta-Plane”. In: *Physica D: Nonlinear Phenomena* 269, pp. 48–62. DOI: 10.1016/j.physd.2013.11.010.

Bluman, G., Cheviakov, A., and Anco, S. (2010). *Applications of Symmetry Methods to Partial Differential Equations*. Applied Mathematical Sciences. Springer New York. ISBN: 9780387680286.

Bluman, G. and Anco, S. (2002). *Symmetry and Integration Methods for Differential Equations*. Applied Mathematical Sciences. Springer New York. DOI: 10.1007/b97380.

Boussinesq, J. (1877). “Essai sur la théorie des eaux courantes”. In: *Mémoires présentés par divers savants à l’Académie des Sciences* XXIII, 1, pp. 1–680.

Brezzi, F. (1974). “On the existence, uniqueness and approximation of saddle-point problems arising from lagrangian multipliers”. eng. In: *ESAIM: Mathematical Modelling and Numerical Analysis - Modélisation Mathématique et Analyse Numérique* 8.R2, pp. 129–151.

Byggstoyl, S. and Kollmann, W. (1986). “Stress Transport in the Rotational and Irrotational Zones of Turbulent Shear Flows”. In: *Physics of Fluids* 29.5, p. 1423. DOI: 10.1063/1.865659.

Bytev, V. O. (1972). “Group properties of the Navier-Stokes equations”. In: *Chislennye metody mehaniki sploshnoy sredy* 3, pp. 13–17.

Chou, P. (1945). “On velocity correlations and the solutions of the equations of turbulent flucuation”. In: *Quarterly of Applied Mathematics* 3.1, pp. 38–54.

Chung, M. K. and Kim, S. K. (1995). “A Nonlinear Return-to-isotropy Model With Reynolds Number and Anisotropy Dependency”. In: *Physics of Fluids* 7.6, pp. 1425–1437. DOI: 10.1063/1.868760.

Cockburn, B. (2003). “Discontinuous Galerkin Methods”. In: *ZAMM* 83.11, pp. 731–754. DOI: 10.1002/zamm.200310088.

Courant, R., Friedrichs, K., and Lewy, H. (1928). “Über Die Partiellen Differenzengleichungen Der Mathematischen Physik”. In: *Mathematische Annalen* 100.1, pp. 32–74. DOI: 10.1007/bf01448839.

Craft, T., Launder, B., and Suga, K. (1996). “Development and Application of a Cubic Eddy-Viscosity Model of Turbulence”. In: *International Journal of Heat and Fluid Flow* 17.2, pp. 108–115. DOI: 10.1016/0142-727x(95)00079-6.

Daly, B. J. and Harlow, F. H. (1970). “Transport Equations in Turbulence”. In: *Physics of Fluids* 13.11, p. 2634. DOI: 10.1063/1.1692845.

Deuflhard, P. (2011). *Newton Methods for Nonlinear Problems*. Springer Series in Computational Mathematics. Springer Berlin Heidelberg. DOI: 10.1007/978-3-642-23899-4.

Donaldson, C. d. (1972). “Construction of a Dynamic Model of the Production of Athmospheric Pollutants”. In: *Aeronaut. Res. Assoc. Princeton* 175.

Donaldson, C. d. and Rosenbaum, H. (1968). “Calculation Of The Turbulent Shear Flows Through Closure Of The Reynolds Equations By Invariant Modeling”. In: *Aeronaut. Res. Assoc. Princeton* 127.

Ferziger, J. H., Perić, M., and Street, R. L. (2020). *Numerische Strömungsmechanik*. [] Springer Berlin Heidelberg. DOI: 10.1007/978-3-662-46544-8.

Foias, C., Holm, D. D., and Titi, E. S. (2001). “The Navier-Stokes-alpha model of fluid turbulence”. In: *Physica D: Nonlinear Phenomena* 152-153, pp. 505–519. ISSN: 0167-2789. DOI: https://doi.org/10.1016/S0167-2789(01)00191-9.

Gatski, T. B. and Speziale, C. G. (1993). “On Explicit Algebraic Stress Models for Complex Turbulent Flows”. In: *Journal of Fluid Mechanics* 254.-1, p. 59. DOI: 10.1017/s0022112093002034.

Geisenhofer, M., Kummer, F., and Müller, B. (2019). “A Discontinuous Galerkin Immersed Boundary Solver for Compressible Flows: Adaptive Local Time Stepping for Artificial Viscosity-Based Shock-capturing on Cut Cells”. In: *International Journal for Numerical Methods in Fluids* 91.9, pp. 448–472. DOI: 10.1002/fld.4761.

George, W. K. (1989). “The Self-Preservation of Turbulent Flows and Its Relation to Initial Conditions and Coherent Structures”. In.

Gibson, M. M. and Launder, B. E. (1978). “Ground Effects on Pressure Fluctuations in the Atmospheric Boundary Layer”. In: *Journal of Fluid Mechanics* 86.3, pp. 491–511. DOI: 10.1017/s0022112078001251.

Gründing, D., Smuda, M., Antritter, T., Fricke, M., Rettenmaier, D., Kummer, F., Stephan, P., Marschall, H., and Bothe, D. (2020). “A Comparative Study of Transient Capillary Rise Using

Direct Numerical Simulations". In: *Applied Mathematical Modelling* 86, pp. 142–165. DOI: 10.1016/j.apm.2020.04.020.
Gutiérrez-Jorquera, J. and Kummer, F. (2021). "A Fully Coupled High-order Discontinuous Galerkin Method for Diffusion Flames in a Low-mach Number Framework". In: *International Journal for Numerical Methods in Fluids* 94.4, pp. 316–345. DOI: 10.1002/fld.5056.
Hairer, E. and Wanner, G. (1996). *Solving Ordinary Differential Equations II*. Springer Series in Computational Mathematics. Springer Berlin Heidelberg. DOI: 10.1007/978-3-642-05221-7.
Hanjalić, K. and Jakirlić, S. (1993). "A Model of Stress Dissipation in Second-Moment Closures". In: *Advances in Turbulence IV*. Advances in Turbulence IV. Springer Netherlands, pp. 513–518. DOI: 10.1007/978-94-011-1689-3_80.
Hanjalić, K. and Launder, B. E. (1972). "Fully Developed Asymmetric Flow in a Plane Channel". In: *Journal of Fluid Mechanics* 51.2, pp. 301–335. DOI: 10.1017/s0022112072001211.
Hanjalić, K. and Launder, B. E. (1976). "Contribution Towards a Reynolds-Stress Closure for Low-Reynolds-Number Turbulence". In: *Journal of Fluid Mechanics* 74.4, pp. 593–610. DOI: 10.1017/s0022112076001961.
Hesthaven, J. S. and Warburton, T. (2008). *Nodal Discontinuous Galerkin Methods*. Texts in Applied Mathematics. Springer New York. DOI: 10.1007/978-0-387-72067-8.
Hirai, S., Takagi, T., and Matsumoto, M. (1988). "Predictions of the Laminarization Phenomena in an Axially Rotating Pipe Flow". In: *Journal of Fluids Engineering* 110.4, p. 424. DOI: 10.1115/1.3243573.
Hopf, E. (1952). "Statistical hydromechanics and functional calculus". In: *Journal of rational Mechanics and Analysis* 1, pp. 87–123.
Hoyas, S., Oberlack, M., Alcántara-Ávila, F., Kraheberger, S. V., and Laux, J. (2022). "Wall turbulence at high friction Reynolds numbers". In: *Phys. Rev. Fluids* 7 (1), p. 014602. DOI: 10.1103/PhysRevFluids.7.014602.
Hunter, J. D. (2007). "Matplotlib: A 2D graphics environment". In: *Computing In Science & Engineering* 9.3, pp. 90–95. DOI: 10.1109/MCSE.2007.55.
Ilinca, F. and Pelletier, D. (1998). "Positivity Preservation and Adaptive Solution for the k-ε Model of Turbulence". In: *AIAA Journal* 36.1, pp. 44–50. DOI: 10.2514/2.350.
Jakirlić, S. and Hanjalić, K. (2002). "A New Approach To Modelling Near-Wall Turbulence Energy and Stress Dissipation". In: *Journal of Fluid Mechanics* 459, pp. 139–166. DOI: 10.1017/s0022112002007905.
Johansson, P. B. V., George, W. K., and Gourlay, M. J. (2003). "Equilibrium similarity, effects of initial conditions and local Reynolds number on the axisymmetric wake". In: *Physics of Fluids* 15.3, pp. 603–617. ISSN: 1070-6631. DOI: 10.1063/1.1536976.
John, F. (1978). *Partial Differential Equations*. Applied Mathematical Sciences. Springer US. DOI: 10.1007/978-1-4684-0059-5.
Jones, W. and Launder, B. (1972). "The Prediction Of Laminarization With A Two-Equation Model Of Turbulence". In: *Int. J. Heat Mass Transfer* 15, pp. 301–314.
Kármán, T. von (1930). "Mechanische Ähnlichkeit und Turbulenz". In: *Nachrichten von der Gesellschaft der Wissenschaften zu Göttingen*, pp. 58–76.
Kikker, A. and Kummer, F. (2018). "A High-Order Local Discontinuous Galerkin Scheme for Viscoelastic Fluid Flow". In: *Lecture Notes in Computational Science and Engineering*. Lecture Notes in Computational Science and Engineering. Springer International Publishing, pp. 51–61. DOI: 10.1007/978-3-319-93891-2_4.

Klein, B., Kummer, F., Keil, M., and Oberlack, M. (2015). “An Extension of the Simple Based Discontinuous Galerkin Solver To Unsteady Incompressible Flows”. In: *International Journal for Numerical Methods in Fluids* 77.10, pp. 571–589. DOI: 10.1002/fld.3994.

Klein, B., Kummer, F., and Oberlack, M. (2013). “A Simple Based Discontinuous Galerkin Solver for Steady Incompressible Flows”. In: *Journal of Computational Physics* 237, pp. 235–250. DOI: 10.1016/j.jcp.2012.11.051.

Klingenberg, D. (2017). “Statistical One-Point Turbulence Modelling Using Symmetries”. Master’s Thesis. Technical University Darmstadt.

Klingenberg, D. S. and Oberlack, M. (2022). “Statistically Invariant Eddy Viscosity Models”. In: *Physics of Fluids*. DOI: 10.1063/5.0090988.

Klingenberg, D. S., Oberlack, M., and Pluemacher, D. (2020). “Symmetries and turbulence modeling”. In: *Physics of Fluids* 32.2. ISSN: 1089-7666. DOI: 10.1063/1.5141165.

Kolmogorov, A. N. (1941). “The Local Structure of Turbulence in Incompressible Viscous Fluid for Very Large Reynolds Numbers”. In: *Doklady Akademii Nauk SSSR* 30, pp. 299–303.

Kolmogorov, A. N. (1942). “Equations of Turbulent Motion of an Incompressible Fluid”. In: *Ivzestia Academy of Sciences*.

Kummer, F. and Oberlack, M. (2013). “An Extension of the Discontinuous Galerkin Method for the singular Poisson equation”. In: *SIAM Journal on Scientific Computing* 35.2, A603–A622. ISSN: 1064-8275.

Kummer, F. (2016). “Extended Discontinuous Galerkin Methods for Two-Phase Flows: the Spatial Discretization”. In: *International Journal for Numerical Methods in Engineering* 109.2, pp. 259–289. DOI: 10.1002/nme.5288.

Launder, B., Reece, G., and Rodi, W. (1975). “Progress in the Development of a Reynolds-Stress Turbulent Closure”. In: *Journal of Fluid Mechanics* 269, pp. 143–168.

Launder, B. and Sharma, B. (1974). “Application of the Energy-Dissipation Model of Turbulence To the Calculation of Flow Near a Spinning Disc”. In: *Letters in Heat and Mass Transfer* 1.2, pp. 131–137. DOI: 10.1016/0094-4548(74)90150-7.

Launder, B. E. and Spalding, D. B. (1972). “Mathematical Models of Turbulence”. In: *Academic Press*.

Laux, J. (2020). “Validation and assessment of symmetry-induced turbulent scaling laws using experimental and numerical data”. Bachelor’s Thesis. Technical University Darmstadt.

Leschziner, M. and Drikakis, D. (2002). “Turbulence Modeling And Turbulent-Flow Computation in Aeronautics”. In: *The Aeronautic Journal*, pp. 363–383.

Libby, P. A. (1975). “On the Prediction of Intermittent Turbulent Flows”. In: *Journal of Fluid Mechanics* 68.02, p. 273. DOI: 10.1017/s0022112075000808.

Lumley, J. L. (1979). “Computational Modeling of Turbulent Flows”. In: *Advances in Applied Mechanics*. Advances in Applied Mechanics. Elsevier, pp. 123–176. DOI: 10.1016/s0065-2156(08)70266-7.

Lundgren, T. S. (1967). “Distribution Functions in the Statistical Theory of Turbulence”. In: *Physics of Fluids* 10.5, p. 969. DOI: 10.1063/1.1762249.

Mach, E. (1883). *Die mechanik in ihrer entwickelung*. Die mechanik in ihrer entwickelung. F.A. Brockhaus.

Marusic, I., Monty, J. P., Hultmark, M., and Smits, A. J. (2013). “On the logarithmic region in wall turbulence”. In: *Journal of Fluid Mechanics* 716, R3. DOI: 10.1017/jfm.2012.511.

Mellor, G. L. and Herring, H. J. (1973). “A Survey of the Mean Turbulent Field Closure Models.” In: *AIAA Journal* 11.5, pp. 590–599. DOI: 10.2514/3.6803.

Menter, F. R. (1994). "Two-Equation Eddy-Viscosity Turbulence Models for Engineering Applications". In: *AIAA Journal* 32.8, pp. 1598–1605. DOI: 10.2514/3.12149.

Moin, P. and Kim, J. (1997). "Tackling Turbulence With Supercomputers". In: *Scientific American*, pp. 62–68.

Müller, B., Krämer-Eis, S., Kummer, F., and Oberlack, M. (2016). "A High-Order Discontinuous Galerkin Method for Compressible Flows With Immersed Boundaries". In: *International Journal for Numerical Methods in Engineering* 110.1, pp. 3–30. DOI: 10.1002/nme.5343.

Noether, E. (1918). "Invariante Variationsprobleme". ger. In: *Nachrichten von der Gesellschaft der Wissenschaften zu Göttingen, Mathematisch-Physikalische Klasse* 1918, pp. 235–257.

Nokes, R. I. (1988). "On the Entrainment Rate Across a Density Interface". In: *Journal of Fluid Mechanics* 188, pp. 185–204. DOI: 10.1017/s0022112088000692.

Oberlack, M. (1997). "Invariant modeling in large-eddy simulation of turbulence". In: *Center for Turbulence Research Annual Research Briefs*, pp. 3–22.

Oberlack, M. and Peters, N. (1993). "Closure of the Two-Point Correlation Equation As a Basis for Reynolds Stress Models". In: *Applied Scientific Research* 51.1-2, pp. 533–538. DOI: 10.1007/bf01082587.

Oberlack, M. and Rosteck, A. (2010). "New Statistical Symmetries Of The Multi-Point Equations And Its Importance For Turbulent Scaling Laws". In: *Discrete and Continuous Dynamical System Series S* 3.3.

Oberlack, M. (2000). "Symmetrie, Invarianz und Selbstähnlichkeit in der Turbulenz". Habilitation thesis. Rheinisch-Westfälische Hochschule Aachen.

Oberlack, M. (2001). "A Unified Approach for Symmetries in Plane Parallel Turbulent Shear Flows". In: *Journal of Fluid Mechanics* 427, pp. 299–328.

Oberlack, M., Hoyas, S., Kraheberger, S. V., Alcántara-Ávila, F., and Laux, J. (2022). "Turbulence Statistics of Arbitrary Moments of Wall-Bounded Shear Flows: A Symmetry Approach". In: *Phys. Rev. Lett.* 128 (2), p. 024502. DOI: 10.1103/PhysRevLett.128.024502.

Olver, P. (2000). *Applications of Lie Groups to Differential Equations*. Applications of Lie Groups to Differential Equations. Springer New York. ISBN: 9780387950006.

Olver, P. J. (2013). "Finite Differences". In: *Introduction to Partial Differential Equations*. Introduction to Partial Differential Equations. Springer International Publishing, pp. 181–214. DOI: 10.1007/978-3-319-02099-0_5.

Pawlowski, R. P., Shadid, J. N., Simonis, J. P., and Walker, H. F. (2006). "Globalization Techniques for Newton–Krylov Methods and Applications to the Fully Coupled Solution of the Navier–Stokes Equations". In: *SIAM Review* 48 (4), pp. 700–721. DOI: 10.1137/S0036144504443511.

Pietrasanta, L., Zheng, S., Marinis, D. D., Hasler, D., and Obrist, D. (2022). "Characterization of Turbulent Flow Behind a Transcatheter Aortic Valve in Different Implantation Positions". In: *Frontiers in Cardiovascular Medicine* 8. DOI: 10.3389/fcvm.2021.804565.

Pietro, D. A. D. and Ern, A. (2012). *Mathematical Aspects of Discontinuous Galerkin Methods*. Mathématiques et Applications. Springer Berlin Heidelberg. DOI: 10.1007/978-3-642-22980-0.

Pope, S. B. (1994). "Lagrangian Pdf Methods for Turbulent Flows". In: *Annual Review of Fluid Mechanics* 26.1, pp. 23–63. DOI: 10.1146/annurev.fl.26.010194.000323.

Pope, S. B. (1975). "A More General Effective-Viscosity Hypothesis". In: *Journal of Fluid Mechanics* 72.02, p. 331. DOI: 10.1017/s0022112075003382.

Pope, S. B. (2000). *Turbulent Flows*. Cambridge University Press. ISBN: 9780521598866.

Pope, S. B. (2011). “Simple Models of Turbulent Flows”. In: *Physics of Fluids* 23.1, p. 011301. DOI: 10.1063/1.3531744.
Popovich, R. and Bihlo, A. (2012). “Symmetry preserving parametrization schemes”. In: *Journal of Mathematical Physics* 53, pp. 07312-1 –07312-36. DOI: 10.1063/1.4734344.
Powell, M. J. D. (1970). “A hybrid method for nonlinear equations”. In: *Numerical Methods for Nonlinear Algebraic Equations*.
Prandtl, L. (1925). “Über die Ausgebildete Turbulenz”. In: *Z. Angew. Math. Mech.* 5, pp. 136–139.
Python Software Foundation (2016). *Python*. Version 3.6.2.
Reynolds, O. (1883). “Iii. an Experimental Investigation of the Circumstances Which Determine Whether the Motion of Water Shall Be Direct Or Sinuous, and of the Law of Resistance in Parallel Channels”. In: *Proceedings of the Royal Society of London* 35.224-226, pp. 84–99. DOI: 10.1098/rspl.1883.0018.
Reynolds, O. (1895). “On the Dynamical Theory of Incompressible Viscous Fluids and the Determination of the Criterion”. In: *Philosophical Transactions of the Royal Society of London. A* 186, pp. 123–164. ISSN: 02643820.
Rodi, W. (1976). “A new algebraic relation for calculating the Reynolds stresses”. In: *Gesellschaft Angewandte Mathematik und Mechanik Workshop Paris France*. Vol. 56, p. 219.
Rosteck, A. and Oberlack, M. (2011). “Lie Algebra Of The Symmetries Of The Multi-Point Equations In Statistical Turbulence”. In: *Jounal of Nonlinear Mathematical Physics* 18.1.
Rosteck, A. (2013). “Scaling Laws In Turbulence - A Theoretical Approach Using Lie-Point Symmetries”. Dissertation. Technical University of Darmstadt.
Rotta, J. (1951). “Statistische Theorie nichthomogener Turbulenz”. In: *Zeitschrift fuer Physik* 129.6, pp. 537–566.
Rotta, J. C. (1975). *Prediction Methods For Turbulent Flows*.
Rubel, A. and Melnik, R. (1984). “Jet, wake and wall jet similarity solutions using a k-epsilon turbulence model”. In: *17th Fluid Dynamics, Plasma Dynamics, and Lasers Conference*. DOI: 10.2514/6.1984-1523.
Rubinstein, R. and Barton, J. M. (1990). “Nonlinear Reynolds Stress Models and the Renormalization Group”. In: *Physics of Fluids A: Fluid Dynamics* 2.8, pp. 1472–1476. DOI: 10.1063/1.857595.
Rubinstein, R. and Zhou, Y. (2004). “Turbulence Modeling for the Axially Rotating Pipe From the Viewpoint of Analytical Closures”. In: *Theoretical and Computational Fluid Dynamics* 17.5-6, pp. 299–312. DOI: 10.1007/s00162-004-0111-y.
Sadeghi, H., Oberlack, M., and Gauding, M. (2018). “On new scaling laws in a temporally evolving turbulent plane jet using Lie symmetry analysis and direct numerical simulation”. In: *Journal of Fluid Mechanics*.
Saffmann, P. G. (1970). “A Model for Inhomogeneous Turbulent Flow”. In: *Proceedings of the Royal Society of London. A. Mathematical and Physical Sciences* 317.1530, pp. 417–433. DOI: 10.1098/rspa.1970.0125.
Sarkar, S. and Speziale, C. G. (1990). “A Simple Nonlinear Model for the Return To Isotropy in Turbulence”. In: *Physics of Fluids A: Fluid Dynamics* 2.1, pp. 84–93. DOI: 10.1063/1.857694.
Schaefer-Rolffs, U. (2019). “The scale invariance criterion for geophysical fluids”. In: *European Journal of Mechanics - B/Fluids* 74, pp. 92–98. ISSN: 0997-7546. DOI: https://doi.org/10.1016/j.euromechflu.2018.11.005.

Schaefer-Rolffs, U., Knöpfel, R., and Becker, E. (2015). “A scale invariance criterion for LES parametrizations”. In: *Meteorologische Zeitschrift* 24.1, pp. 3–13. DOI: 10.1127/metz/2014/0623.

Schäfer, J. (2021). “Extension of Symmetry-Invariant Modeling Strategies to Novel Turbulence Models”. Master’s Thesis. Technical University Darmstadt.

Schäfer, M. (2006). *Computational Engineering - Introduction to Numerical Methods*. Springer-Verlag. DOI: 10.1007/3-540-30686-2.

Schoenawa, S. (2014). “Higher-order discontinuous Galerkin discretizations of two-Equation models of turbulence”. Dissertation. Technische Universitaet Carolo-Wilhemina zu Braunschweig.

Shahbazi, K. (2005). “An explicit expression for the penalty parameter of the interior penalty method”. In: *Journal of Computational Physics* 205.2, pp. 401–407. DOI: 10.1016/j.jcp.2004.11.017.

Shih, T.-H. and Zhu, J. (1993). “A Realizable Reynolds Stress Algebraic Equation Model”. In: *NASA Technical Memorandum* 105993, p. 38.

Shir, C. C. (1973). “A Preliminary Numerical Study of Atmospheric Turbulent Flows in the Idealized Planetary Boundary Layer”. In: *Journal of the Atmospheric Sciences* 30.7, pp. 1327–1339. DOI: 10.1175/1520-0469(1973)030<1327:apnsoa>2.0.co;2.

Smith, A. and Cebeci, T. (1967). *Numerical solution of the turbulent-boundary-layer equations*. Tech. rep. Douglas Aircraft CO Long Beach CA Aircraft Div.

Spalart, P. and Allmaras, S. (1992). “A one-equation turbulence model for aerodynamic flows”. In: *30th Aerospace Sciences Meeting and Exhibit*. DOI: 10.2514/6.1992-439.

Speziale, C. G., Sarkar, S., and Gatski, T. B. (1991). “Modelling the pressure-strain correlation of turbulence: an invariant dynamical systems approach”. In: *Journal of Fluid Mechanics* 227, pp. 245–272. DOI: 10.1017/S0022112091000101.

Tiberga, M., Hennink, A., Kloosterman, J. L., and Lathouwers, D. (2020). “A High-Order Discontinuous Galerkin Solver for the Incompressible Rans Equations Coupled To The $k - \varepsilon$ turbulence Model”. In: *Computers & Fluids* 212, p. 104710. DOI: 10.1016/j.compfluid.2020.104710.

Uddin, M. and Pollard, A. (2007). “Self-similarity of coflowing jets: The virtual origin”. In: *Physics of Fluids* 19.6, p. 068103. ISSN: 1070-6631. DOI: 10.1063/1.2740709.

Umlauf, L., Burchard, H., and Hutter, K. (2003). “Extending the k–ω turbulence model towards oceanic applications”. In: *Ocean Modelling* 5.3, pp. 195–218. ISSN: 1463-5003. DOI: https://doi.org/10.1016/S1463-5003(02)00039-2.

Umlauf, L. (2001). “Turbulence parameterisation in hydrobiological models for natural waters”. Dissertation. Technical University of Darmstadt.

Waclawczyk, M., Staffolani, N., Oberlack, M., Rosteck, A., Wilczek, M., and Friedrich, R. (2014). “Statistical symmetries of the Lundgren-Monin-Novikov hierarchy”. In: *Physical Review* 90, pp. 1–11.

Wallin, S. and Johansson, A. V. (2000). “An Explicit Algebraic Reynolds Stress Model for Incompressible and Compressible Turbulent Flows”. In: *Journal of Fluid Mechanics* 403, pp. 89–132. DOI: 10.1017/s0022112099007004.

Waterloo Maple Inc. (2017). *Maple*. Version 2016.2.

Wilcox, D. C. (1994). *Turbulence Modeling for CFD*. DCW Industries, Incorporated. ISBN: 9780963605108.

Wilcox, D. C. (2007). “AIAA Formulation of the k-omega Turbulence Model Revisited”. In: *45th AIAA Aerospace Sciences*.

Wilcox, D. C. (1988). "Reassessment of the scale-determining equation for advanced turbulence models". In: *AIAA Journal* 26.11, pp. 1299–1310. ISSN: 0001-1452. DOI: 10.2514/3.10041.
Wygnanski, I. and Fiedler, H. (1969). "Some Measurements in the Self-Preserving Jet". In: *Journal of Fluid Mechanics* 38.3, pp. 577–612. DOI: 10.1017/s0022112069000358.
Yoshizawa, A. (1984). "Statistical Analysis of the Deviation of the Reynolds Stress From Its Eddy-Viscosity Representation". In: *Physics of Fluids* 27.6, p. 1377. DOI: 10.1063/1.864780.

A. Appendix

A.1. Definitions of Groups and Lie Groups

The content of this section is discussed in more detail in Bluman and Anco (2002).

Groups are formed by a set G and a binary operation $f(x, y)$ provided that the following four properties are met:

1. G is closed with respect to $f(x, y)$, i.e. if $x, y \in G$, then $f(x, y) \in G$ holds as well.
2. f is associative, i.e. $f(f(x, y), z) = f(x, f(y, z))$,
3. G contains an identity element e such that $f(x, e) = x$, and
4. for every $x \in G$, there exists an inverse element x^{-1} such that $f(x, x^{-1}) = f(x^{-1}, x) = e$.

Symmetries are variable transformations that, when inserted into an equation, leave the equation form invariant. Given a set of variables $\boldsymbol{x}$, the transformation

$$\boldsymbol{x}^* = \boldsymbol{\phi}(\boldsymbol{x}, a), \tag{A.1}$$

$$\tag{A.2}$$

is called a symmetry of equation $F(\boldsymbol{x}) = 0$ if

$$F(\boldsymbol{x}) = 0 \quad \Leftrightarrow \quad F(\boldsymbol{x}^*) = 0, \tag{A.3}$$

where a is an arbitrary constant referred to as the group parameter.

Groups and symmetry transformations are intimately connected, because if we consider the variable space the transformation acts on as the set G and the subsequent application of the transformation, possibly with different values for a, as the operation f, transformations admit group properties in the following sense: Given $\boldsymbol{x} = (x_1, x_2, \cdots, x_n) \in G \subset \mathbb{R}^n$, $a \in S \subset \mathbb{R}$, and a law of composition $f(a_1, a_2)$ (where $a_1, a_2 \in S$), the transformation (A.1) is a one-parameter group of transformations if

1. all $\boldsymbol{x}^*$ lie in G,
2. S with the law of composition $f(a_1, a_2)$ forms a group as defined above,
3. there exists an identity element e such that for all $\boldsymbol{x} \in G$, $\boldsymbol{x}^* = \boldsymbol{\phi}(\boldsymbol{x}, e) = \boldsymbol{x}$, and
4. the repeated application of the transformation can be expressed using the law of composition, i.e. $\phi(\phi(\boldsymbol{x}, a_1), a_2) = \phi(\boldsymbol{x}, f(a_1, a_2))$.

In order for a symmetry to form a one-parameter Lie group of transformations, three additional conditions have to be met:

5. a is a continuous parameter,
6. ϕ and ψ are indefinitely often differentiable, and
7. the concatenation operation f is an analytical function.

A.2. Validation of the BoSSS Implementation of the Classical k-ω-Model

The implementation of the classical k-ω-model in BoSSS is validated by repeatedly solving the same problem on different meshes with increasing resolution and for different DG-degrees. Then, by using the finest solution as a reference, the cumulative error of each of the coarser solutions is computed using the L_2-norm. For a DG-degree m, a convergence order of $m+1$ can be expected. Note that due to the mixed-order discretization, the polynomial degree used for the pressure is smaller by one than that for the other fields. As a result, the convergence order expected for the pressure is also smaller by one compared to the other fields.

Since the grid resolution has to span a sufficiently wide range in order for the results to be meaningful, a test case that converges quickly and robustly on both coarse and fine grids should be chosen. For the k-ω-model, it turns out to be somewhat challenging to find a test case that fulfills these requirements, because even the simplest canonical flows are quite unreliable in their convergence, as is further discussed in Section 4.3.1. Here, we make use of a setting consisting of a rectangular domain on $[0,l] \times [0,l]$, which is discretized using equally spaced $n \times n$ grids. Dirichlet boundary conditions for the velocity fields are imposed on all four sides. The functions used read

$$\bar{U}_1^{\text{inlet}} = \bar{U}^0 \sin\left(\frac{x_2 \pi}{2l}\right), \tag{A.4}$$

$$\bar{U}_2^{\text{inlet}} = \bar{U}^0 \sin\left(\frac{x_1 \pi}{2l}\right), \tag{A.5}$$

where $\bar{U}^0$ is the reference velocity. The nonpolynomial functions for $\bar{U}_1^{\text{inlet}}$ and $\bar{U}_2^{\text{inlet}}$ are intended to make the velocity fields sufficiently complicated, because too simple a velocity field could potentially already be represented accurately using a coarse grid, which would make it impossible to observe improvements upon grid refinement. For k and $\tilde{\omega}$, the solutions are sufficiently complicated anyway, so that simple Dirichlet boundary conditions with constant values of $k^{\text{inlet}} = 1.35 \cdot 10^{-3}$ and $\tilde{\omega}^{\text{inlet}} = -0.399$ can be prescribed on the left and the bottom side of the domain. These values roughly correspond to a turbulent intensity of 10^{-2} for the parameters of this setup. On the other two sides, we use homogeneous Neumann conditions. It was found that if Dirichlet conditions for k and ω are enforced on all four sides, convergence is negatively affected, especially on coarser grids. The setup is shown in Fig. A.1. Note that these boundary conditions do not set a reference value for the pressure, so that some arbitrariness associated with the pressure translation symmetry (3.30) remains. In such cases, BoSSS automatically takes care to set a pressure reference value in order to ensure a stable computation, however, this reference value may vary across calculations. Therefore, when

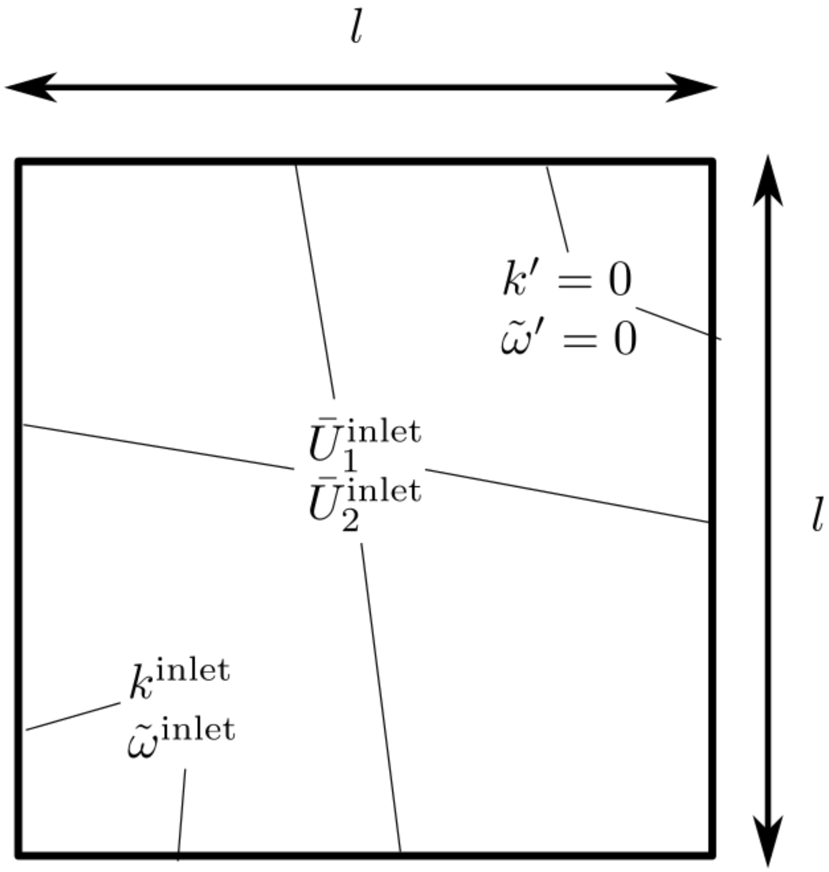

Figure A.1.: Schematic view of the validation case setup.

calculating the pressure field errors, each pressure field must be shifted in order to ensure that all pressure fields have the same reference value.

An important measure to improve convergence is to set the production and dissipation terms in (3.118) and (3.119) to one tenth their usual value. The fact that this produces physically inaccurate results is not important in the present context, because we are only interested in the validation of the numerical method. If any of the terms was implemented incorrectly, this would still be visible in the final result. The viscosity is chosen to be 10^{-4}. Note that all variables are nondimensionalized using the domain size l and the maximum velocity $\bar{U}^0$.

To give an impression of the setup, the numerical solution obtained with a resolution of 96×96 cells and $m = 2$ is shown in Fig. A.2.

Figure A.3 shows the errors plotted against the grid spacing for $m = 1, 2$, and the orders of convergence are summarized in Table A.1. Note that since the coarser grids clearly lie outside the range of convergence, we only include the three finest grids (with the finest one serving as the reference) in the calculation of the EOC (experimental order of convergence) in Table A.1. Since we restrict ourselves to calculations with $m = 2$ in Section 4.3.1, and calculations with higher polynomial degrees become increasingly computationally expensive, no higher polynomial degrees are considered. The coarsest grid consists of 12×12 cells. The finest grid for $m = 1$ contains 768×768 cells, while the finest grid for $m = 2$ consists of 96×96 cells. It can be seen that whereas the results for $m = 1$ exceed expectations, the resolutions

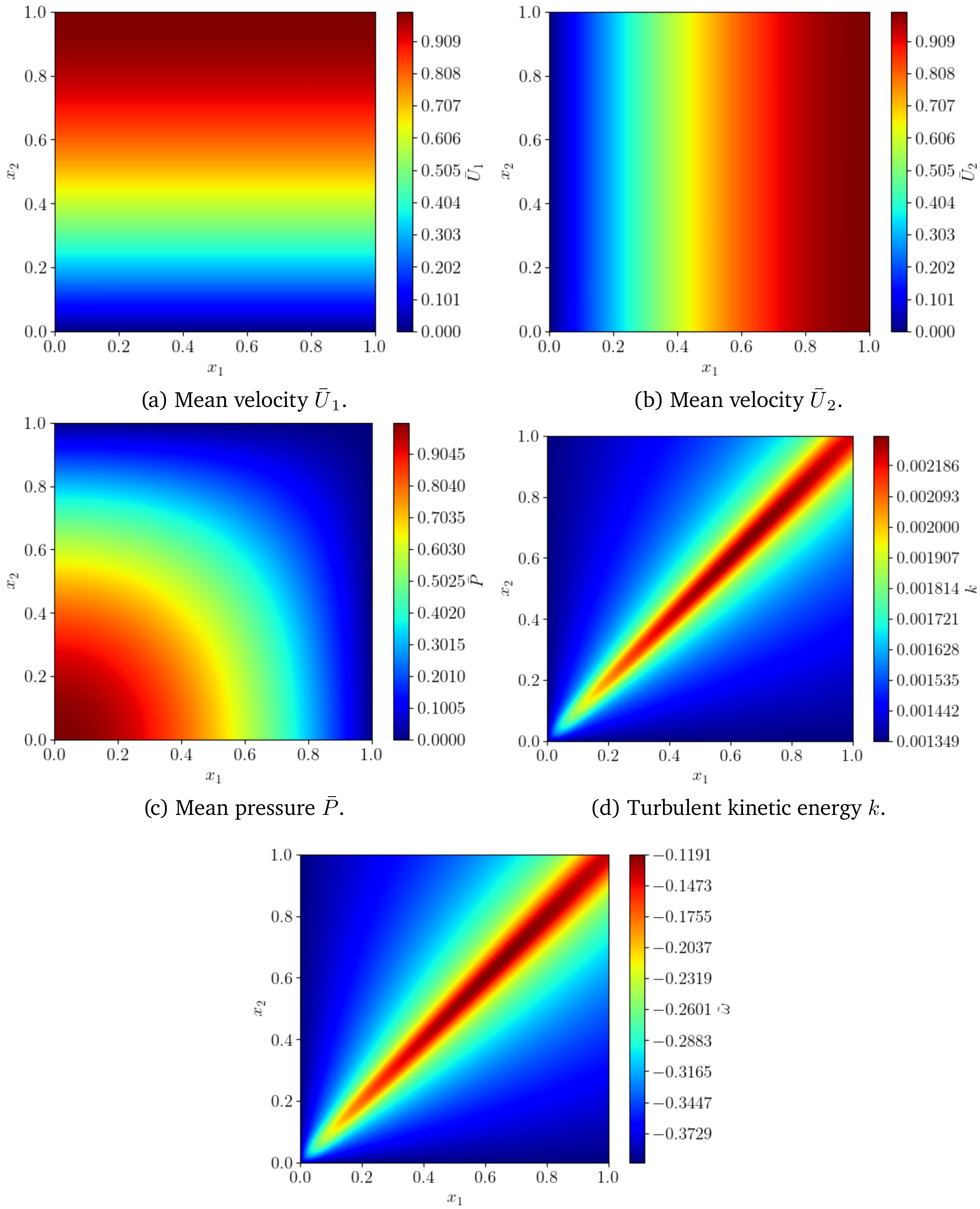

(a) Mean velocity $\bar{U}_1$.

(b) Mean velocity $\bar{U}_2$.

(c) Mean pressure $\bar{P}$.

(d) Turbulent kinetic energy k.

(e) Transformed turbulent dissipation rate $\tilde{\omega}$.

Figure A.2.: Numerical solutions for $\bar{U}_1$, $\bar{U}_2$, $\bar{P}$, k and $\tilde{\omega}$ in the setup used for the convergence study.

used for $m = 2$ lie somewhat outside the area of convergence, which is especially visible for the pressure. However, since the overall results are sufficient for this preliminary solver validation,

m	EOC				
	$\bar{U}_1$	$\bar{U}_2$	$\bar{P}$	k	$\tilde{\omega}$
1	2.33	2.33	1.13	2.17	2.17
2	2.72	2.72	0.59	2.56	2.49

Table A.1.: Experimental order of convergence for $\bar{U}_1$, $\bar{U}_2$, k and $\tilde{\omega}$ determined using only the three finest grids. Due to the mixed-order discretization, we expect a convergence order of m for the pressure $\bar{P}$, and for all other fields, we expect a convergence order of $m+1$.

it is decided not to carry out further calculations, which would be computationally expensive.

A.3. Deriving a Reynolds Stress Transport Model from Symmetries

In the following, we detail the derivation of a RSM from symmetries as discussed in Section 5.1.

A.3.1. Using No Additional Model Variables

First, we discuss the derivation shown in Section 5.1.2 in greater detail. We start by assuming the general form for the model equations to be

$$\begin{aligned}\boldsymbol{F}\big(&x_i, t, \bar{U}_i, \bar{P}, H_{ij}, \overline{U_i P_{,x_j}}, \bar{U}_{i,x_j}, \bar{U}_{i,t}, \bar{P}_{,x_i}, \bar{P}_{,t},\\ &H_{ij,x_k}, H_{ij,t}, \overline{U_i P_{,x_j,x_k}}, \overline{U_i P_{,x_j,t}}\big) = 0.\end{aligned} \tag{A.6}$$

We demand that this equation system remain invariant under all classical symmetries (3.34)–(3.39) and the statistical symmetries (3.59)–(3.61). As discussed in Chapter 2, this leads to the linear PDE (partial differential equation) system

$$X_t \boldsymbol{F}|_{\boldsymbol{F}=0} = 0 \wedge X_{\mathrm{rot}_\alpha} \boldsymbol{F}|_{\boldsymbol{F}=0} = 0 \wedge \cdots \wedge X_{\mathrm{Tr,stat},2} \boldsymbol{F}|_{\boldsymbol{F}=0} = 0. \tag{A.7}$$

Note that the system (A.7) does not need to be solved as a whole, but instead, we can make the solution procedure simpler to follow by invoking one symmetry at a time. If we start with the time translation symmetry (3.34), the corresponding constraint

$$X_t \boldsymbol{F} = \frac{\partial \boldsymbol{F}}{\partial t} = 0 \tag{A.8}$$

immediately eliminates t as a possible variable in (A.6), which is thus reduced to

$$\begin{aligned}\boldsymbol{F}\big(&x_i, \bar{U}_i, \bar{P}, H_{ij}, \overline{U_i P_{,x_j}}, \bar{U}_{i,x_j}, \bar{U}_{i,t}, \bar{P}_{,x_i}, \bar{P}_{,t},\\ &H_{ij,x_k}, H_{ij,t}, \overline{U_i P_{,x_j,x_k}}, \overline{U_i P_{,x_j,t}}\big) = 0.\end{aligned} \tag{A.9}$$

Analogous results are obtained from the other translation symmetries: The Galilean symmetry (3.36) with $f_{\mathrm{Gal}_i}(t) = \text{const.}$ i.e. translation invariance in space, eliminates x_i, the pressure translation symmetry (3.37) with $f_P(t) = \text{const.}$ eliminates $\bar{P}$, and the same symmetry with

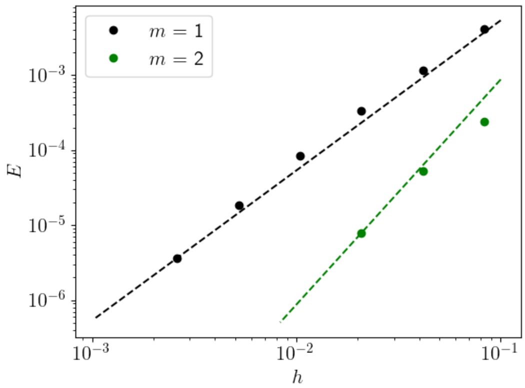

(a) Error of the mean velocity $\bar{U}_1$.

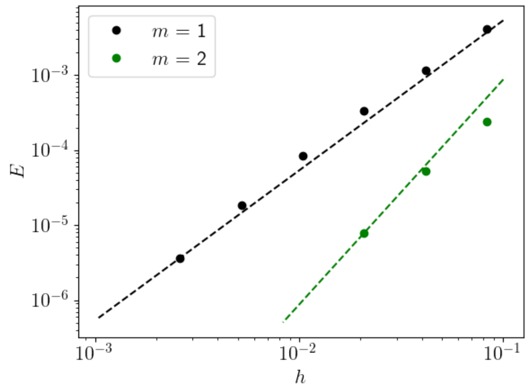

(b) Error of the mean velocity $\bar{U}_2$.

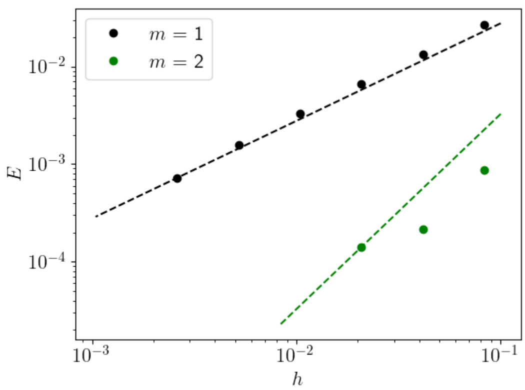

(c) Error of the mean pressure $\bar{P}$.

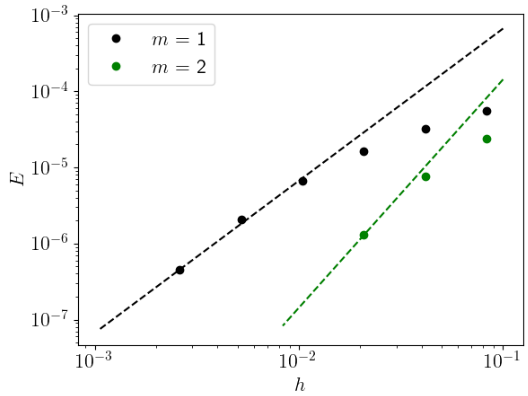

(d) Error of the turbulent kinetic energy k.

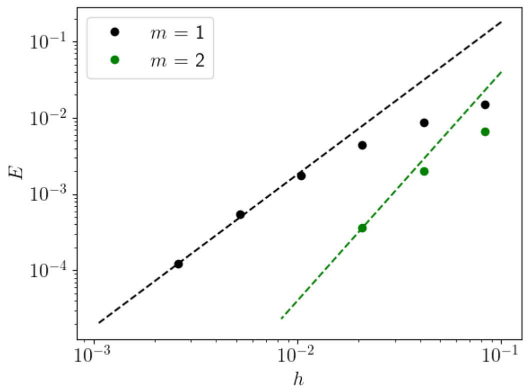

(e) Error of the transformed turbulent dissipation rate $\tilde{\omega}$.

Figure A.3.: Errors obtained by comparison with the finest grid results plotted against the grid spacing. For the pressure, a convergence order of m can be expected, whereas for the other fields, a convergence order of $m + 1$ can be expected.

$f'_P(t) =$ const. eliminates $\bar{P}_{,t}$ and $\overline{U_i P_{,x_j,t}}$. This is shown in more detail in Section 5.1.1. The statistical translation symmetries (3.60)–(3.62) eliminate $\bar{U}_i, H_{ij}$ and $\overline{U_i P_{,x_j}}$, respectively, leaving only

$$\boldsymbol{F}\left(\overline{U_i P_{,x_j}}, \bar{U}_{i,x_j}, \bar{U}_{i,t}, \bar{P}_{,x_i}, H_{ij,x_k}, H_{ij,t}, \overline{U_i P_{,x_j,x_k}}\right) = 0. \tag{A.10}$$

Having invoked all relatively simple symmetries, we now demand invariance with respect to the full Galilean symmetry (3.36) for arbitrary functions $f_{\mathrm{Gal}_i}(t)$. Its first prolongation reads

$$\begin{aligned}
X_{\mathrm{Gal}}^{(1)} = {} & (f''_{\mathrm{Gal}_i}(t) - \bar{U}_{i,x_j} f'_{\mathrm{Gal}_j}(t)) \frac{\partial}{\partial \bar{U}_{i,t}} - f''_{\mathrm{Gal}_i}(t) \frac{\partial}{\partial \bar{P}_{,x_i}} \\
& + \left(\bar{U}_{i,t} f'_{\mathrm{Gal}_j}(t) + \bar{U}_{j,t} f'_{\mathrm{Gal}_i}(t) + \bar{U}_i f''_{\mathrm{Gal}_j}(t) + \bar{U}_j f''_{\mathrm{Gal}_i}(t) - H_{ij,x_k} f'_{\mathrm{Gal}_k}(t)\right) \frac{\partial}{\partial H_{ij,t}} \\
& + (\bar{U}_{i,x_k} f'_{\mathrm{Gal}_j}(t) + \bar{U}_{j,x_k} f'_{\mathrm{Gal}_i}(t)) \frac{\partial}{\partial H_{ij,x_k}} \\
& + (\bar{P}_{,x_j} f'_{\mathrm{Gal}_i}(t) - \bar{U}_i f''_{\mathrm{Gal}_j}(t)) \frac{\partial}{\partial \overline{U_i P_{,x_j}}} \\
& + (\bar{P}_{,x_j x_k} f'_{\mathrm{Gal}_i}(t) - \bar{U}_{i,x_k} f''_{\mathrm{Gal}_j}(t)) \frac{\partial}{\partial \overline{U_i P_{,x_j,x_k}}},
\end{aligned} \tag{A.11}$$

where we omitted all terms acting on variables that have already been eliminated from the generic form of the equation, i.e. do not appear in (A.10). In turn, the invariance condition $X_{\mathrm{Gal}}^{(1)} \boldsymbol{F} = 0$ yields the scalar PDE

$$\begin{aligned}
X_{\mathrm{Gal}}^{(1)} \boldsymbol{F} = {} & (f''_{\mathrm{Gal}_i}(t) - \bar{U}_{i,x_j} f'_{\mathrm{Gal}_j}(t)) \frac{\partial \boldsymbol{F}}{\partial \bar{U}_{i,t}} - f''_{\mathrm{Gal}_i}(t) \frac{\partial \boldsymbol{F}}{\partial \bar{P}_{,x_i}} \\
& + \left(\bar{U}_{i,t} f'_{\mathrm{Gal}_j}(t) + \bar{U}_{j,t} f'_{\mathrm{Gal}_i}(t) + \bar{U}_i f''_{\mathrm{Gal}_j}(t) + \bar{U}_j f''_{\mathrm{Gal}_i}(t) - H_{ij,x_k} f'_{\mathrm{Gal}_k}(t)\right) \frac{\partial \boldsymbol{F}}{\partial H_{ij,t}} \\
& + (\bar{U}_{i,x_k} f'_{\mathrm{Gal}_j}(t) + \bar{U}_{j,x_k} f'_{\mathrm{Gal}_i}(t)) \frac{\partial \boldsymbol{F}}{\partial H_{ij,x_k}} \\
& + (\bar{P}_{,x_j} f'_{\mathrm{Gal}_i}(t) - \bar{U}_i f''_{\mathrm{Gal}_j}(t)) \frac{\partial \boldsymbol{F}}{\partial \overline{U_i P_{,x_j}}} \\
& + (\bar{P}_{,x_j x_k} f'_{\mathrm{Gal}_i}(t) - \bar{U}_{i,x_k} f''_{\mathrm{Gal}_j}(t)) \frac{\partial \boldsymbol{F}}{\partial \overline{U_i P_{,x_j,x_k}}} = 0.
\end{aligned} \tag{A.12}$$

Like shown in Section 5.1.1, we now apply the method of characteristics (for more background, we refer to the textbook by John, 1978) to obtain the ODE (ordinary differential equation) system

$$\frac{d\boldsymbol{F}}{d\tau} = 0, \tag{A.13}$$

$$\frac{d\bar{U}_{i,x_j}}{d\tau} = 0, \tag{A.14}$$

$$\frac{d\bar{U}_{i,t}}{d\tau} = f''_{\mathrm{Gal}_i}(t) - \bar{U}_{i,x_j} f'_{\mathrm{Gal}_j}(t), \tag{A.15}$$

$$\frac{d\bar{P}_{,x_i}}{d\tau} = -f''_{\mathrm{Gal}_i}(t), \tag{A.16}$$

$$\frac{dH_{ij,t}}{d\tau} = \bar{U}_{i,t} f'_{\mathrm{Gal}_j}(t) + \bar{U}_{j,t} f'_{\mathrm{Gal}_i}(t) + \bar{U}_i f''_{\mathrm{Gal}_j}(t) + \bar{U}_j f''_{\mathrm{Gal}_i}(t) - H_{ij,x_k} f'_{\mathrm{Gal}_k}(t), \tag{A.17}$$

$$\frac{dH_{ij,x_k}}{d\tau} = \bar{U}_{i,x_k} f'_{\mathrm{Gal}_j}(t) + \bar{U}_{j,x_k} f'_{\mathrm{Gal}_i}(t), \tag{A.18}$$

$$\frac{d\overline{U_i P_{,x_j}}}{d\tau} = \bar{P}_{,x_j} f'_{\mathrm{Gal}_i}(t) - \bar{U}_i f''_{\mathrm{Gal}_j}(t), \tag{A.19}$$

$$\frac{d\overline{U_i P_{,x_j,x_k}}}{d\tau} = \bar{P}_{,x_j x_k} f'_{\mathrm{Gal}_i}(t) - \bar{U}_{i,x_k} f''_{\mathrm{Gal}_j}(t). \tag{A.20}$$

Equations (A.13)–(A.16) and (A.18) can be integrated directly, yielding

$$\boldsymbol{F} = c_1(s), \tag{A.21}$$

$$\bar{U}_{i,x_j} = c_{2_{ij}}(s), \tag{A.22}$$

$$\bar{U}_{i,t} = f''_{\mathrm{Gal}_i}(t)\tau - \bar{U}_{i,x_j} f'_{\mathrm{Gal}_j}(t)\tau + c_{3_i}(s), \tag{A.23}$$

$$\bar{P}_{,x_i} = -f''_{\mathrm{Gal}_i}(t)\tau + c_{4_i}(s), \tag{A.24}$$

$$H_{ij,x_k} = \bar{U}_{i,x_k} f'_{\mathrm{Gal}_j}(t)\tau + \bar{U}_{j,x_k} f'_{\mathrm{Gal}_i}(t)\tau + c_{5_{ijk}}(s), \tag{A.25}$$

Here, all constants of integration may still depend on s, i.e. the other coordinate in the characteristic τ, s-system. The solution of Eq. (A.12) is found by eliminating τ, s and all constants of integration from the system (A.13)–(A.20). Note that in order to find a general solution, this must be accomplished without imposing any constraints on the constants of integration. We proceed by adding (A.23) and (A.24), which yields

$$\bar{U}_{i,t} + \bar{P}_{,x_i} = -\bar{U}_{i,x_j} f'_{\mathrm{Gal}_j}(t)\tau + c_{i_3}(s) + c_{i_4}(s). \tag{A.26}$$

Thus,

$$\bar{U}_{i,x_j} f'_{\mathrm{Gal}_j}(t)\tau = -\bar{U}_{i,t} - \bar{P}_{,x_i} + c_{i_3}(s) + c_{i_4}(s), \tag{A.27}$$

and, equivalently,

$$f'_{\mathrm{Gal}_i}(t)\tau = \bar{U}_{i,x_j}^{-1}(-\bar{U}_{j,t} - \bar{P}_{,x_j} + c_{j_3}(s) + c_{j_4}(s)). \tag{A.28}$$

Now, by contracting $j = k$ in (A.25) and using the divergence-free property of the velocity, i.e. $\bar{U}_{j,x_j} = 0$, we find

$$H_{ij,x_j} = \bar{U}_{i,x_j} f'_{\mathrm{Gal}_j}(t)\tau + c_{ijj_5}(s). \tag{A.29}$$

Then, adding Eqs. (A.27) and (A.29) leads to

$$\bar{U}_{i,t} + \bar{P}_{,x_i} + H_{ij,x_j} = c_{i_3}(s) + c_{i_4}(s) + c_{ijj_5}(s). \tag{A.30}$$

Recall that since by virtue of (A.21), $\boldsymbol{F}$ does not depend on τ, any expression constant in τ can appear as its argument. Clearly, since the right-hand side of (A.30) does not depend on τ, neither does the left-hand side. Therefore, we can conclude that $\bar{U}_{i,t} + \bar{P}_{,x_i} + H_{ij,x_j}$, which we recognize as one side of the inviscid momentum equation, i.e. Eq. (1.4) with $\nu = 0$, may appear as an argument of $\boldsymbol{F}$. In other words, and as expected, this expression is Galilean invariant.

While the preceding discussion nicely illustrates how the method works, in the context of turbulence modeling, we are obviously primarily interested in the equations that require closure assumptions, such as the transport equation for H_{ij}. To obtain it, we proceed by adding (A.17) and (A.19), thus eliminating $\bar{U}_i$ and $\bar{U}_j$. We then obtain

$$\frac{dH_{ij,t}}{d\tau}+\frac{d\overline{U_iP_{,x_j}}}{d\tau}+\frac{d\overline{U_jP_{,x_i}}}{d\tau}=\bar{U}_{i,t}f'_{\mathrm{Gal}_j}(t)+\bar{U}_{j,t}f'_{\mathrm{Gal}_i}(t)$$
$$+\bar{P}_{,x_j}f'_{\mathrm{Gal}_i}(t)+\bar{P}_{,x_i}f'_{\mathrm{Gal}_j}(t)-H_{ij,x_k}f'_{\mathrm{Gal}_k}(t). \tag{A.31}$$

Further, using (A.26), we find

$$\begin{aligned}&\frac{dH_{ij,t}}{d\tau}+\frac{d\overline{U_iP_{,x_j}}}{d\tau}+\frac{d\overline{U_jP_{,x_i}}}{d\tau}\\&=f'_{\mathrm{Gal}_i}(t)(-\bar{U}_{j,x_k}f'_{\mathrm{Gal}_k}(t)\tau+c_{j_3}(s)+c_{j_4}(s))\\&+f'_{\mathrm{Gal}_j}(t)(-\bar{U}_{i,x_k}f'_{\mathrm{Gal}_k}(t)\tau+c_{i_3}(s)+c_{i_4}(s))\\&-H_{ij,x_k}f'_{\mathrm{Gal}_k}(t).\end{aligned}\tag{A.32}$$

Before integrating this equation, we replace H_{ij,x_k} (which depends on τ) using (A.25), yielding

$$\begin{aligned}&\frac{dH_{ij,t}}{d\tau}+\frac{d\overline{U_iP_{,x_j}}}{d\tau}+\frac{d\overline{U_jP_{,x_i}}}{d\tau}\\&=f'_{\mathrm{Gal}_i}(t)(-\bar{U}_{j,x_k}f'_{\mathrm{Gal}_k}(t)\tau+c_{j_3}(s)+c_{j_4}(s))\\&+f'_{\mathrm{Gal}_j}(t)(-\bar{U}_{i,x_k}f'_{\mathrm{Gal}_k}(t)\tau+c_{i_3}(s)+c_{i_4}(s))\\&-\bar{U}_{i,x_k}f'_{\mathrm{Gal}_j}(t)\tau f'_{\mathrm{Gal}_k}(t)-\bar{U}_{j,x_k}f'_{\mathrm{Gal}_i}(t)\tau f'_{\mathrm{Gal}_k}(t)\\&-c_{ijk_5}(s)f'_{\mathrm{Gal}_k}(t)\\&=2f'_{\mathrm{Gal}_i}(t)(-\bar{U}_{j,x_k}f'_{\mathrm{Gal}_k}(t)\tau)+f'_{\mathrm{Gal}_i}(t)(c_{j_3}(s)+c_{j_4}(s))\\&+2f'_{\mathrm{Gal}_j}(t)(-\bar{U}_{i,x_k}f'_{\mathrm{Gal}_k}(t)\tau)+f'_{\mathrm{Gal}_j}(t)(c_{i_3}(s)+c_{i_4}(s))\\&-c_{ijk_5}(s)f'_{\mathrm{Gal}_k}(t).\end{aligned}\tag{A.33}$$

Carrying out the integration yields

$$\begin{aligned}&H_{ij,t}+\overline{U_iP_{,x_j}}+\overline{U_jP_{,x_i}}\\&=-f'_{\mathrm{Gal}_i}(t)\tau\bar{U}_{j,x_k}f'_{\mathrm{Gal}_k}(t)\tau+f'_{\mathrm{Gal}_i}(t)\tau(c_{j_3}(s)+c_{j_4}(s))\\&-f'_{\mathrm{Gal}_j}(t)\tau\bar{U}_{i,x_k}f'_{\mathrm{Gal}_k}(t)\tau+f'_{\mathrm{Gal}_j}(t)\tau(c_{i_3}(s)+c_{i_4}(s))\\&-c_{ijk_5}(s)f'_{\mathrm{Gal}_k}(t)\tau+c_{ij_6}(s).\end{aligned}\tag{A.34}$$

Some of the τ-terms still appearing here can be eliminated using Eq. (A.25). We also introduce as an abbreviation the constant $c_{i_7}(s)=c_{i_3}(s)+c_{i_4}(s)$. Then, we may use (A.27), or, where necessary, the inverse form (A.28) to eliminate the remaining $f'_{\mathrm{Gal}_i}(t)\tau$-terms, which results in

$$\begin{aligned}&H_{ij,t}+\overline{U_iP_{,x_j}}+\overline{U_jP_{,x_i}}\\&=-H_{ij,x_k}\bar{U}_{k,x_l}^{-1}(-\bar{U}_{n,t}-\bar{P}_{,x_l}+c_{l_7}(s))\\&-\bar{U}_{i,x_k}^{-1}(-\bar{U}_{k,t}-\bar{P}_{,x_k}+c_{k_7}(s))c_{j_7}(s)\\&-\bar{U}_{j,x_k}^{-1}(-\bar{U}_{k,t}-\bar{P}_{,x_k}+c_{k_7}(s))c_{i_7}(s)\\&+c_{ij_6}(s).\end{aligned}\tag{A.35}$$

At this stage, recognizing that the expression $\bar{U}_{i,x_k}^{-1}(-\bar{U}_{k,t} - \bar{P}_{,x_k})$ appears repeatedly, we introduce the abbreviation

$$\gamma_i = \bar{U}_{i,x_k}^{-1}(-\bar{U}_{k,t} - \bar{P}_{,x_k}). \tag{A.36}$$

From its definition, we can infer the interesting observation that γ_i transforms like $\bar{U}_i$ under all classical symmetries (3.34)–(3.39), but is invariant under all statistical symmetries (3.59)–(3.62).

Furthermore, using the momentum equation (1.4) to replace

$$\bar{U}_{i,t} + \bar{P}_{,x_i} = -H_{ik,x_k}, \tag{A.37}$$

we write (A.35) as

$$\begin{aligned} H_{ij,t} + H_{ij,x_k}\gamma_k + \overline{U_i P_{,x_j}} + \overline{U_j P_{,x_i}} \\ = -H_{ij,x_k}\bar{U}_{k,x_n}^{-1}c_{n_7}(s) \\ - \gamma_i c_{j_7}(s) - \gamma_j c_{i_7}(s) \\ + c_{ij_6}(s). \end{aligned} \tag{A.38}$$

Without any hope of simplifying the right-hand side any further, we observe that by setting $c_{i_7}(s) = 0$, the left-hand side of (A.38) becomes Galilean invariant. However, we must note that setting $c_{i_7}(s) = 0$ directly implies that

$$\bar{U}_{i,t} + \gamma_k \bar{U}_{i,x_k} + \bar{P}_{,x_i} = 0, \tag{A.39}$$

i.e. the definition of γ_i (A.36). This can cause problems if we attempt to define γ_i differently, e.g. by formulating a transport equation for it, which is further discussed in Appendix A.3.2. In the present context, however, we may conclude that

$$H_{ij,t} + H_{ij,x_k}\gamma_k + \overline{U_i P_{,x_j}} + \overline{U_j P_{,x_i}} = 0 \tag{A.40}$$

is a viable model equation for the second velocity moment. In principle, further invariants could be added to the right-hand side, and (A.40) should be understood to be a minimal form in a certain sense.

As a last step, we obtain an equation form $\overline{U_i P_{,x_j}}$ by integrating (A.20) and eliminating the τ-terms using (A.16) and (A.28), which yields

$$\frac{\partial \overline{U_i P_{,x_j}}}{\partial x_k} - \gamma_i \frac{\partial^2 \bar{P}}{\partial x_j \partial x_k} - \frac{\partial \bar{P}}{\partial x_j}\frac{\partial \bar{U}_i}{\partial x_k} = 0. \tag{A.41}$$

Note, however, that the last term violates the statistical scaling symmetry (3.59), which we have not invoked yet. There are other, even more severe practical problems with this model, in particular with the definition of γ_i (A.36), which are discussed in Section 5.1.2. The derivation of a model without such shortcomings is discussed next.

A.3.2. Using Auxiliary Velocity and Pressure Fields

The derivation in Appendix A.3.1 already shows the general structure of a statistically invariant RSM, but the resulting equations have a number of serious drawbacks. Most significantly, depending on the velocity gradient, Eq. (A.36) may not uniquely determine γ_i. Therefore, we conclude that it is necessary to obtain additional freedom by introducing a new model variable we denote $\hat{U}_i$, for which we also have to develop a transport equation. Like γ_i, this model velocity is defined to behave like $\bar{U}_i$ under all classical symmetries (3.34)–(3.40), while being invariant under the statistical symmetries (3.59)–(3.62). It turns out to be necessary to also introduce a corresponding pressure field $\hat{P}$. In analogy to $\hat{U}_i$, it behaves like $\bar{P}$ under the classical symmetries, but is also invariant under the statistical ones. In concrete terms, the symmetries (3.27)–(3.33) and (3.55)–(3.57) extended with $\hat{U}_i$ and $\hat{P}$ read

$$
\begin{aligned}
T_t: \ & t^* = t + a_T, \ \ x_i^* = x_i, \ \ \bar{U}_i^* = \bar{U}_i, \ \ \hat{U}_i^* = \hat{U}_i, \\
& \bar{P}^* = \bar{P}, \ \ \hat{P}^* = \hat{P}, \ \ H_{ij}^* = H_{ij}, \ \ \overline{PU_i}^* = \overline{PU_i}; && \text{(A.42)} \\
T_{\mathrm{rot}_\alpha}: \ & t^* = t, \ \ x_i^* = x_j Q_{ij}^{[\alpha]}, \ \ \bar{U}_i{}^* = \bar{U}_j Q_{ij}^{[\alpha]}, \ \ \hat{U}_i{}^* = \hat{U}_j Q_{ij}^{[\alpha]}, \\
& \bar{P}^* = \bar{P}, \ \ \hat{P}^* = \hat{P}, \ \ H_{ij}{}^* = H_{kl} Q_{ik}^{[\alpha]} Q_{jl}^{[\alpha]}, \ \ \overline{PU_i}^* = \overline{PU_j} Q_{ij}^{[\alpha]}; && \text{(A.43)} \\
T_{\mathrm{Gal}_i}: \ & t^* = t, \ \ x_i^* = x_i + f_{\mathrm{Gal}_i}(t), \ \ \bar{U}_i^* = \bar{U}_i + f'_{\mathrm{Gal}_i}(t), \ \ \hat{U}_i^* = \hat{U}_i + f'_{\mathrm{Gal}_i}(t), \\
& \bar{P}^* = \bar{P} - x_j f''_{\mathrm{Gal}_j}(t), \ \ \hat{P}^* = \hat{P} - x_j f''_{\mathrm{Gal}_j}(t), \\
& H_{ij}^* = H_{ij} + f'_{\mathrm{Gal}_i}(t)\bar{U}_j + f'_{\mathrm{Gal}_j}(t)\bar{U}_i + f'_{\mathrm{Gal}_i}(t) f'_{\mathrm{Gal}_j}(t), \\
& \overline{PU_i}^* = \overline{PU_i} + \bar{P} f'_{\mathrm{Gal}_i}(t) - \bar{U}_i x_j f''_{\mathrm{Gal}_j}(t) - f'_{\mathrm{Gal}_i}(t) x_j f''_{\mathrm{Gal}_j}(t); && \text{(A.44)} \\
T_P: \ & t^* = t, \ \ x_i^* = x_i, \ \ \bar{U}_i^* = \bar{U}_i, \ \ \hat{U}_i^* = \hat{U}_i, \ \ \bar{P}^* = \bar{P} + f_P(t), \ \ \hat{P}^* = \hat{P} + f_P(t), \\
& H_{ij}^* = H_{ij}, \ \ \overline{PU_i}^* = \overline{PU_i} + \bar{U}_i f_P(t); && \text{(A.45)} \\
T_{\mathrm{Sc},I}: \ & t^* = t, \ \ x_i^* = x_i e^{a_{\mathrm{Sc},I}}, \ \ \bar{U}_i^* = \bar{U}_i e^{a_{\mathrm{Sc},I}}, \ \ \hat{U}_i^* = \hat{U}_i e^{a_{\mathrm{Sc},I}}, \\
& \bar{P}^* = \bar{P} e^{2a_{\mathrm{Sc},I}}, \ \ \hat{P}^* = \hat{P} e^{2a_{\mathrm{Sc},I}}, \\
& H_{ij}^* = H_{ij} e^{2a_{\mathrm{Sc},I}}, \ \ \overline{PU_{ij}}^* = \overline{PU_{ij}} e^{3a_{\mathrm{Sc},I}}; && \text{(A.46)} \\
T_{\mathrm{Sc},II}: \ & t^* = t e^{a_{\mathrm{Sc},II}}, \ \ x_i^* = x_i, \ \ \bar{U}_i^* = \bar{U}_i e^{-a_{\mathrm{Sc},II}}, \ \ \hat{U}_i^* = \hat{U}_i e^{-a_{\mathrm{Sc},II}}, \\
& \bar{P}^* = \bar{P} e^{-2a_{\mathrm{Sc},II}}, \ \ \hat{P}^* = \hat{P} e^{-2a_{\mathrm{Sc},II}}, \\
& H_{ij}^* = H_{ij} e^{-2a_{\mathrm{Sc},II}}, \ \ \overline{PU_i}^* = \overline{PU_i} e^{-3a_{\mathrm{Sc},II}}, ; && \text{(A.47)} \\
T_{\mathrm{Sc,ns}}: \ & t^* = t e^{2a_{\mathrm{Sc,ns}}}, \ \ x_i^* = x_i e^{a_{\mathrm{Sc,ns}}}, \ \ \bar{U}_i^* = \bar{U}_i e^{-a_{\mathrm{Sc,ns}}}, \ \ \hat{U}_i^* = \hat{U}_i e^{-a_{\mathrm{Sc,ns}}}, \\
& \bar{P}^* = \bar{P} e^{-2a_{\mathrm{Sc,ns}}}, \ \ \hat{P}^* = \hat{P} e^{-2a_{\mathrm{Sc,ns}}}, \\
& H_{ij}^* = H_{ij} e^{-2a_{\mathrm{Sc,ns}}}, \ \ \overline{PU_i}^* = \overline{PU_i} e^{-3a_{\mathrm{Sc,ns}}}; && \text{(A.48)} \\
T_{\mathrm{Sc,stat}}: \ & t^* = t, \ \ x_i^* = x_i, \ \ \bar{U}_i^* = \bar{U}_i e^{a_{\mathrm{Sc,stat}}}, \ \ \hat{U}_i^* = \hat{U}_i, \\
& \bar{P}^* = \bar{P} e^{a_{\mathrm{Sc,stat}}}, \ \ \hat{P}^* = \hat{P}, \ \ H_{ij}^* = H_{ij} e^{a_{\mathrm{Sc,stat}}}, \ \ \overline{PU_i}^* = \overline{PU_i} e^{a_{\mathrm{Sc,stat}}}; && \text{(A.49)} \\
T_{\mathrm{Tr,stat},1}: \ & t^* = t, \ \ x_i^* = x_i, \ \ \bar{U}_i^* = \bar{U}_i + a_{\mathrm{Tr,stat},I,i}, \ \ \hat{U}_i^* = \hat{U}_i, \ \ \bar{P}^* = \bar{P}, \ \ \hat{P}^* = \hat{P}, \\
& H_{ij}^* = H_{ij}, \ \ \overline{PU_i}^* = \overline{PU_i}; && \text{(A.50)} \\
T_{\mathrm{Tr,stat},2}: \ & t^* = t, \ \ x_i^* = x_i, \ \ \bar{U}_i^* = \bar{U}_i, \hat{U}_i^* = \hat{U}_i, \bar{P}^* = \bar{P}, \ \ \hat{P}^* = \hat{P}, \\
& H_{ij}^* = H_{ij} + a_{\mathrm{Tr,stat},II,ij}, \ \ \overline{PU_i}^* = \overline{PU_i}; && \text{(A.51)}
\end{aligned}
$$

$$T_{\text{Tr,stat,3}}: \; t^* = t, \;\; x_i^* = x_i, \;\; \bar{U}_i^* = \bar{U}_i,$$
$$H_{ij}^* = H_{ij}, \;\; \overline{PU_i}^* = \overline{PU_i} + a_{\text{Tr,stat},III,i}, \tag{A.52}$$
$$\dots$$

We mostly need the infinitesimal form of (A.42)–(A.52), which reads

$$X_t = \frac{\partial}{\partial t}, \tag{A.53}$$

$$\begin{aligned} X_{\text{rot}_\alpha} &= \epsilon_{jk\alpha} x_j \frac{\partial}{\partial x_k} + \epsilon_{jk\alpha} \bar{U}_j \frac{\partial}{\partial \bar{U}_k} + \epsilon_{jk\alpha} \hat{U}_j \frac{\partial}{\partial \hat{U}_k} \\ &+ (\epsilon_{ki\alpha} H_{kj} + \epsilon_{kj\alpha} H_{ik}) \frac{\partial}{\partial H_{ij}} + \epsilon_{jk\alpha} \overline{PU_j} \frac{\partial}{\partial \overline{PU_k}}, \end{aligned} \tag{A.54}$$

$$\begin{aligned} X_{\text{Gal}} &= f_{\text{Gal}_i}(t) \frac{\partial}{\partial x_i} + f'_{\text{Gal}_i}(t) \frac{\partial}{\partial \bar{U}_i} + f'_{\text{Gal}_i}(t) \frac{\partial}{\partial \hat{U}_i} \\ &- x_i f''_{\text{Gal}_i}(t) \frac{\partial}{\partial \bar{P}} - x_i f''_{\text{Gal}_i}(t) \frac{\partial}{\partial \hat{P}} \\ &+ \left(f'_{\text{Gal}_i}(t) \bar{U}_j + f'_{\text{Gal}_j}(t) \bar{U}_i \right) \frac{\partial}{\partial H_{ij}}, \end{aligned}$$

$$X_P = f_P(t) \frac{\partial}{\partial \bar{P}} + f_{\hat{P}}(t) \frac{\partial}{\partial \hat{P}} + f_P(t) \bar{U}_i \frac{\partial}{\partial \overline{PU_i}}, \tag{A.55}$$

$$+ \left(f'_{\text{Gal}_i}(t) \bar{P} - \bar{U}_i x_j f''_{\text{Gal}_j}(t) \right) \frac{\partial}{\partial \overline{PU_i}}, \tag{A.56}$$

$$\begin{aligned} X_{\text{Sc},I} &= x_i \frac{\partial}{\partial x_i} + \bar{U}_i \frac{\partial}{\partial \bar{U}_i} + \hat{U}_i \frac{\partial}{\partial \hat{U}_i} + 2\bar{P} \frac{\partial}{\partial \bar{P}} + 2\hat{P} \frac{\partial}{\partial \hat{P}} \\ &+ 2H_{ij} \frac{\partial}{\partial H_{ij}} + 3\overline{PU_i} \frac{\partial}{\partial \overline{PU_i}}, \end{aligned} \tag{A.57}$$

$$\begin{aligned} X_{\text{Sc},II} &= t \frac{\partial}{\partial t} - \bar{U}_i \frac{\partial}{\partial \bar{U}_i} - \hat{U}_i \frac{\partial}{\partial \hat{U}_i} - 2\bar{P} \frac{\partial}{\partial \bar{P}} - 2\hat{P} \frac{\partial}{\partial \hat{P}} \\ &- 2H_{ij} \frac{\partial}{\partial H_{ij}} - 3\overline{PU_i} \frac{\partial}{\partial \overline{PU_i}}, \end{aligned} \tag{A.58}$$

$$\begin{aligned} X_{\text{Sc,ns}} &= 2t \frac{\partial}{\partial t} + x_i \frac{\partial}{\partial x_i} - \bar{U}_i \frac{\partial}{\partial \bar{U}_i} - \hat{U}_i \frac{\partial}{\partial \hat{U}_i} - 2\bar{P} \frac{\partial}{\partial \bar{P}} - 2\hat{P} \frac{\partial}{\partial \hat{P}} \\ &- 2H_{ij} \frac{\partial}{\partial H_{ij}} - 3\overline{PU_i} \frac{\partial}{\partial \overline{PU_i}}, \end{aligned} \tag{A.59}$$

$$X_{\text{Sc,stat}} = \bar{U}_i \frac{\partial}{\partial \bar{U}_i} + \bar{P} \frac{\partial}{\partial \bar{P}} + H_{ij} \frac{\partial}{\partial H_{ij}} + \overline{PU_i} \frac{\partial}{\partial \overline{PU_i}} + \cdots, \tag{A.60}$$

$$X_{\text{Tr,stat,1}} = \frac{\partial}{\partial \bar{U}_i}, \tag{A.61}$$

$$X_{\text{Tr,stat,2}} = \frac{\partial}{\partial H_{ij}}, \tag{A.62}$$

$$X_{\text{Tr,stat,3}} = \frac{\partial}{\partial \overline{PU_i}}, \;\; \cdots . \tag{A.63}$$

Returning now to the actual model development, we assume as the general form of the model

$$\boldsymbol{F}\Big(x_i, t, \bar{U}_i, \bar{P}, H_{ij}, \hat{U}_i, \hat{P}, \bar{U}_{i,x_j}, \bar{U}_{i,t}, \bar{P}_{,x_i}, \bar{P}_{,t}, \hat{U}_{i,x_j}, \hat{U}_{i,t}, \hat{P}_{,x_j}, \hat{P}_{,t},$$
$$H_{ij,x_k}, H_{ij,t}, \overline{U_i P_{,x_j}}, \overline{U_i P_{,x_j,x_k}}, \overline{U_i P_{,x_j,t}}\Big) = 0. \tag{A.64}$$

Invoking the translation symmetries (A.53), (A.56) with $f_{\mathrm{Gal}_=}(t)$const., (A.55) with $f_P(t) =$ const. and with $f'_P(t) =$ const., has a similar effect as in Appendix A.3.1 and reduces the possible form of the model to

$$\boldsymbol{F}\Big(\hat{U}_i, \bar{U}_{i,x_j}, \bar{U}_{i,t}, \bar{P}_{,x_i}, \hat{U}_{i,x_j}, \hat{U}_{i,t}, \hat{P}_{,x_j}, H_{ij,x_k}, H_{ij,t},$$
$$\overline{U_i P_{,x_j}}, \overline{U_i P_{,x_j,x_k}}\Big) = 0. \tag{A.65}$$

The most crucial part is again invoking the generalized Galilean symmetry, i.e. Eq. (A.53) with arbitrary $f_{\mathrm{Gal}_i}(t)$. Taking into account the new model variables $\hat{U}_i$ and $\hat{P}$, its first prolongation reads

$$\begin{aligned}
X^{(1)}_{\mathrm{Gal}} &= f'_{\mathrm{Gal}_i}(t)\frac{\partial}{\partial \hat{U}_i} + (f''_{\mathrm{Gal}_i}(t) - \bar{U}_{i,x_j} f'_{\mathrm{Gal}_j}(t))\frac{\partial}{\partial \bar{U}_{i,t}} \\
&+ (f''_{\mathrm{Gal}_i}(t) - \hat{U}_{i,x_j} f'_{\mathrm{Gal}_j}(t))\frac{\partial}{\partial \hat{U}_{i,t}} - f''_{\mathrm{Gal}_i}(t)\frac{\partial}{\partial \bar{P}_{,x_i}} - f''_{\mathrm{Gal}_i}(t)\frac{\partial}{\partial \hat{P}_{,x_i}} \\
&+ \Big(\bar{U}_{i,t} f'_{\mathrm{Gal}_j}(t) + \bar{U}_{j,t} f'_{\mathrm{Gal}_i}(t) + \bar{U}_i f''_{\mathrm{Gal}_j}(t) + \bar{U}_j f''_{\mathrm{Gal}_i}(t) - H_{ij,x_k} f'_{\mathrm{Gal}_k}(t)\Big)\frac{\partial}{\partial H_{ij,t}} \\
&+ (\bar{U}_{i,x_k} f'_{\mathrm{Gal}_j}(t) + \bar{U}_{j,x_k} f'_{\mathrm{Gal}_i}(t))\frac{\partial}{\partial H_{ij,x_k}} \\
&+ (\bar{P}_{,x_j} f'_{\mathrm{Gal}_i}(t) - \bar{U}_i f''_{\mathrm{Gal}_j}(t))\frac{\partial}{\partial \overline{U_i P_{,x_j}}} \\
&+ (\bar{P}_{,x_j x_k} f'_{\mathrm{Gal}_i}(t) - \bar{U}_{i,x_k} f''_{\mathrm{Gal}_j}(t))\frac{\partial}{\partial \overline{U_i P_{,x_j,x_k}}},
\end{aligned} \tag{A.66}$$

where we have again omitted its action on variables already eliminated from Eq. (A.65). Applying it to $\boldsymbol{F}$ yields the PDE

$$\begin{aligned}
X^{(1)}_{\mathrm{Gal}}\boldsymbol{F} &= f'_{\mathrm{Gal}_i}(t)\frac{\partial \boldsymbol{F}}{\partial \hat{U}_i} + (f''_{\mathrm{Gal}_i}(t) - \bar{U}_{i,x_j} f'_{\mathrm{Gal}_j}(t))\frac{\partial \boldsymbol{F}}{\partial \bar{U}_{i,t}} \\
&+ (f''_{\mathrm{Gal}_i}(t) - \hat{U}_{i,x_j} f'_{\mathrm{Gal}_j}(t))\frac{\partial \boldsymbol{F}}{\partial \hat{U}_{i,t}} - f''_{\mathrm{Gal}_i}(t)\frac{\partial \boldsymbol{F}}{\partial \bar{P}_{,x_i}} - f''_{\mathrm{Gal}_i}(t)\frac{\partial \boldsymbol{F}}{\partial \hat{P}_{,x_i}} \\
&+ \Big(\bar{U}_{i,t} f'_{\mathrm{Gal}_j}(t) + \bar{U}_{j,t} f'_{\mathrm{Gal}_i}(t) + \bar{U}_i f''_{\mathrm{Gal}_j}(t) + \bar{U}_j f''_{\mathrm{Gal}_i}(t) - H_{ij,x_k} f'_{\mathrm{Gal}_k}(t)\Big)\frac{\partial \boldsymbol{F}}{\partial H_{ij,t}} \\
&+ (\bar{U}_{i,x_k} f'_{\mathrm{Gal}_j}(t) + \bar{U}_{j,x_k} f'_{\mathrm{Gal}_i}(t))\frac{\partial \boldsymbol{F}}{\partial H_{ij,x_k}} \\
&+ (\bar{P}_{,x_j} f'_{\mathrm{Gal}_i}(t) - \bar{U}_i f''_{\mathrm{Gal}_j}(t))\frac{\partial \boldsymbol{F}}{\partial \overline{U_i P_{,x_j}}} \\
&+ (\bar{P}_{,x_j x_k} f'_{\mathrm{Gal}_i}(t) - \bar{U}_{i,x_k} f''_{\mathrm{Gal}_j}(t))\frac{\partial \boldsymbol{F}}{\partial \overline{U_i P_{,x_j,x_k}}} = 0,
\end{aligned} \tag{A.67}$$

whose characteristic system reads

$$\frac{d\boldsymbol{F}}{d\tau} = 0, \tag{A.68}$$

$$\frac{d\hat{U}_i}{d\tau} = f'_{\mathrm{Gal}_i}(t), \tag{A.69}$$

$$\frac{d\bar{U}_{i,x_j}}{d\tau} = 0, \tag{A.70}$$

$$\frac{d\hat{U}_{i,x_j}}{d\tau} = 0, \tag{A.71}$$

$$\frac{d\bar{U}_{i,t}}{d\tau} = f''_{\mathrm{Gal}_i}(t) - \bar{U}_{i,x_j} f'_{\mathrm{Gal}_j}(t), \tag{A.72}$$

$$\frac{d\hat{U}_{i,t}}{d\tau} = f''_{\mathrm{Gal}_i}(t) - \hat{U}_{i,x_j} f'_{\mathrm{Gal}_j}(t), \tag{A.73}$$

$$\frac{d\bar{P}_{,x_i}}{d\tau} = -f''_{\mathrm{Gal}_i}(t), \tag{A.74}$$

$$\frac{d\hat{P}_{,x_i}}{d\tau} = -f''_{\mathrm{Gal}_i}(t), \tag{A.75}$$

$$\begin{aligned}\frac{dH_{ij,t}}{d\tau} &= \bar{U}_{i,t} f'_{\mathrm{Gal}_j}(t) + \bar{U}_{j,t} f'_{\mathrm{Gal}_i}(t) \\ &+ \bar{U}_i f''_{\mathrm{Gal}_j}(t) + \bar{U}_j f''_{\mathrm{Gal}_i}(t) - H_{ij,x_k} f'_{\mathrm{Gal}_k}(t),\end{aligned} \tag{A.76}$$

$$\frac{dH_{ij,x_k}}{d\tau} = \bar{U}_{i,x_k} f'_{\mathrm{Gal}_j}(t) + \bar{U}_{j,x_k} f'_{\mathrm{Gal}_i}(t), \tag{A.77}$$

$$\frac{d\overline{U_i P_{,x_j}}}{d\tau} = \bar{P}_{,x_j} f'_{\mathrm{Gal}_i}(t) - \bar{U}_i f''_{\mathrm{Gal}_j}(t), \tag{A.78}$$

$$\frac{d\overline{U_i P_{,x_j,x_k}}}{d\tau} = \bar{P}_{,x_j x_k} f'_{\mathrm{Gal}_i}(t) - \bar{U}_{i,x_k} f''_{\mathrm{Gal}_j}(t). \tag{A.79}$$

Combining (A.69), (A.71), (A.73) and (A.75) yields the variable

$$c_{i_1}(s) = \frac{\partial \hat{U}_i}{\partial t} + \hat{U}_j \frac{\partial \hat{U}_i}{\partial x_j} + \frac{\partial \hat{P}}{\partial x_i}, \tag{A.80}$$

from which we can derive a transport equation for $\hat{U}_i$,

$$\frac{\partial \hat{U}_i}{\partial t} + \hat{U}_j \frac{\partial \hat{U}_i}{\partial x_j} + \frac{\partial \hat{P}}{\partial x_i} = 0. \tag{A.81}$$

We may now proceed in a similar way as in Appendix A.3.1 to integrate (A.76), again yielding

$$\begin{aligned}H_{ij,t} &+ \overline{U_i P_{,x_j}} + \overline{U_j P_{,x_i}} \\ &= -H_{ij} x_k f'_{\mathrm{Gal}_k}(t)\tau + f'_{\mathrm{Gal}_i}(t)\tau c_{j_7}(s) \\ &+ f'_{\mathrm{Gal}_j}(t)\tau c_{i_7}(s) \\ &+ c_{ij_6}(s),\end{aligned} \tag{A.82}$$

where we are using the same indices for integration constants as in Appendix A.3.1, which allows us to omit writing out steps that were already shown there. Next, we integrate (A.69) to obtain

$$\hat{U}_i = f'_{\mathrm{Gal}_i}(t)\tau + c_{i_8}(s). \tag{A.83}$$

Furthermore, it follows from (A.26) that

$$c_{i_7}(s) = \bar{U}_{i,t} + \bar{U}_{i,x_k} f'_{\mathrm{Gal}_k}(t)\tau + \bar{P}_{,x_i}. \tag{A.84}$$

Then, combining (A.82)–(A.84) yields

$$\begin{aligned} H_{ij,t} + \hat{U}_k H_{ij,x_k} &+ \overline{U_i P_{,x_j}} + \overline{U_j P_{,x_i}} \\ &+ \hat{U}_i H_{jk,x_k} + \hat{U}_j H_{ik,x_k} - \bar{U}_{i,x_k}\hat{U}_j\hat{U}_k - \bar{U}_{j,x_k}\hat{U}_i\hat{U}_k \\ &= H_{ij,x_k} c_{k_8}(s) + \hat{U}_i\bar{U}_{j,x_k} c_{k_8}(s) + \hat{U}_k\bar{U}_{j,x_k} c_{i_8}(s) + \hat{U}_k\bar{U}_{i,x_k} c_{j_8}(s) \\ &- H_{jk,x_k} c_{i_8}(s) - H_{ik,x_k} c_{j_8}(s) \\ &+ c_{i_8}(s) c_{k_8}(s)\bar{U}_{j,x_k} + c_{ij_6}(s) \end{aligned} \tag{A.85}$$

Note that unlike in the derivation in Appendix A.3.1, there is now no need to set $c_{i_7}(s) = 0$. Instead, we set $c_{i_8}(s) = 0$, which does not lead to any complications. A possible transport equation for H_{ij} is then given by the left-hand side of Eq. (A.85), i.e.

$$\begin{aligned} \frac{\partial H_{ij}}{\partial t} + \hat{U}_k \frac{\partial H_{ij}}{\partial x_k} + \overline{U_i P_{,x_j}} + \overline{U_j P_{,x_i}} \\ + \hat{U}_i \frac{\partial H_{jk}}{\partial x_k} + \hat{U}_j \frac{\partial H_{ik}}{\partial x_k} - \frac{\partial \bar{U}_i}{\partial x_k}\hat{U}_j\hat{U}_k - \frac{\partial \bar{U}_j}{\partial x_k}\hat{U}_i\hat{U}_k = 0. \end{aligned} \tag{A.86}$$

Note that the equation for the velocity-pressure term can now be constructed in such a way as to also fulfill the statistical scaling symmetry (A.53). To this end, we integrate (A.79) and eliminate the τ-terms using (A.28) and (A.75) to obtain

$$\frac{\partial \overline{U_i P_{,x_j}}}{\partial x_k} - \hat{U}_i \frac{\partial^2 \bar{P}}{\partial x_j \partial x_k} - \frac{\partial \hat{P}}{\partial x_j}\frac{\partial \bar{U}_i}{\partial x_k} = 0. \tag{A.87}$$

In conclusion, Eqs. (5.72), (5.73) and (A.81) in combination with continuity equations for the two velocity fields $\bar{U}_i$ and $\hat{U}_i$ and the classical momentum equation (A.30) constitute a closed set of model equations. This model fulfills all classical and statistical symmetries (A.53)–(A.63), allowing it to serve as a foundation for further modeling efforts. These are discussed in Sections 5.1.3 and 5.2.